MACQUARIE UNIVERSITY

**HIGHER DEGREE THESIS**
**AUTHOR'S CONSENT**
**DOCTORATE DEGREE**

This is to certify that I, Yogeshwar Ranga being a candidate for the degree of Doctor of Philosophy am aware of the policy of the University relating to the retention and use of higher degree theses as contained in the University's Higher Degree Research Thesis Preparation, Submission and Examination Policy.

In the light of this policy, I agree to allow a copy of my thesis to be deposited in the University Library for consultation, loan and photocopying forthwith.

.....
Signature of Candidate
Date: 14/11/11

.....
Full Name & Signature of Witness
Date: 14/11/11

MACQUARIE UNIVERSITY

The Academic Senate on 15 November 2011 resolved that Mr Yogeshwar Ranga had satisfied the requirements for admission to the degree of PhD.

This thesis represents a major part of the prescribed program of study.

1881267

Thesis
TK
7871
.67
.U45
R36
copy 1

# USE OF THESES

This volume is the property of Macquarie University, but the literary rights of the author must be respected. Passages must not be copied or closely paraphrased without the written consent of the author. If the reader obtains any assistance from this volume, he/she must give proper credit in his/her own work.

This thesis by .....Y. Ranga.....has been used by the following persons, whose signatures attest their acceptance of the above restrictions.

| NAME | DATE | NAME | DATE |
|---|---|---|---|
| | | | |

# ANTENNAS FOR ULTRA-WIDEBAND SYSTEMS

by

Yogeshwar Ranga


Dissertation submitted in fulfilment of the requirements

for the degree of

DOCTOR OF PHILOSOPHY

Department of Electronic Engineering
Faculty of Science
Macquarie University
Sydney, Australia

$12^{th}$ August, 2011

## ABSTRACT

Wide-band wireless systems are used in a wide range of applications including ground-penetrating radars, biomedical imaging systems, high-data-rate short range wireless local networks, communication systems and medium- and long-range military radars due to their high spatial and temporal resolution. As is the case in conventional wireless communication systems, an antenna plays a crucial role in wide-band systems. However, there are additional challenges when designing an antenna to operate over a wideband or an ultra-wide-band. In the recent past the interest of academia and industry developed in the Federal Communication Commission (FCC)-sanctioned UWB systems standard, which makes use of the spectrum from 3.1 GHz to 10.6 GHz. To utilise this spectrum fully, the challenges in designing a viable antenna are great. Antenna design involves achieving a 110% bandwidth, stable radiation patterns over the bandwidth, compact size and low manufacturing cost particularly for consumer electronics applications. In some important applications such as point-to-point high-speed data-communication systems, in addition to the above characteristics a small gain variation over the bandwidth may required. Several compact planar monopole antenna geometries have been investigated for such UWB applications. Most of these planar antennas have a significant gain variation (1 dBi to 5 dBi) at lower frequencies (3 GHz to 6 GHz) and then the gain becomes nearly constant. On the other hand some slot antennas have a relatively constant gain between 2 dBi and 3 dBi and only 1 dB variation in gain over the complete bandwidth. High-gain slot antennas have exhibited a stronger gain variation, between 2 dBi to 7 dBi. Indeed, gain enhancement is a challenging task for UWB systems where gain flatness across 3 GHz to 10 GHz is preferred.

In this work, efforts have been made for enhancing the gain, and the gain variation with frequency, of printed monopole antennas. Extensive investigations were also carried out on different types of concepts in enhancing the gain of UWB antennas. The types of antenna studied in this thesis are based on monopole and slot antennas. A concept of proximity coupling has been proposed for the printed monopoles and it has been demonstrated with practical implementation and testing. This concept helps to enhance the angular stability of the printed monopoles. Based on the understanding of UWB antennas, two more compact versions of TEM horns are proposed. Their integration with printed-circuit boards has been studied. Both of them are fed using printed monopoles; one fed by a circular monopole and the the other by a co-planar waveguide (CPW)-based semicircular monopole. Short horn antennas designed in this thesis are comparable to conformal or integrated antennas printed on the same substrate. Apart from enhancing the gain performance of antennas, significant work has been carried out in the field of Frequency Selective Surfaces (FSS). The behaviour of FSS-based reflectors in enhancing the gain while maintaining the operating bandwidth has been demonstrated for UWB applications. A concept of phase coherence over the UWB bandwidth has been proposed in this work and it is demonstrated with some practical examples of antenna design and implementation. These multi-layer FSS reflector surfaces help to achieve a good gain enhancement in terms of flatness and directional radiation properties over the UWB bandwidth. A gain flatness of $\pm 0.5$ dB has been demonstrated over a 110 % impedance bandwidth.

## STATEMENT OF CANDIDATE

I certify that the work in this thesis has not previously been submitted for a degree nor has it been submitted as part of the requirements for a degree to any other university or institution other than Macquarie University.

I also certify that the thesis is an original piece of research and it has been written by me.

In addition, I certify that all information sources and literature used are indicated in the thesis.

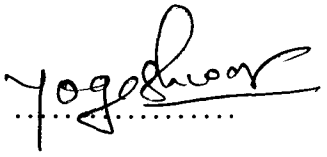

Yogeshwar Ranga

## ACKNOWLEDGMENTS

I would like to express my profound gratitude to my principal supervisor, Professor Karu P. Esselle, for his support, encouragement, supervision and guidance during this research work. His vision, technical knowledge, moral support and continuous guidance helped me to complete my work successfully. He always stood with me whenever I encountered any difficulties during my postgraduate studies.

I also benefitted from assistance from a number of people during my graduate studies. I am highly thankful to my associate supervisors, Dr Andrew R. Weily and Dr Y. Jay Guo from CSIRO ICT Centre, for their research collaboration, guidance and valuable suggestions throughout this study. I should also like to thank Professor A. K. Verma from University of Delhi for his guidance and support during this study and A/Professor Ladislau Matekovits for being a collaborative partner in the last year of my studies and providing significant guidance in that part of my PhD program.

I owe my sincere thanks to Dr Keith Imrie for proofreading this thesis and Mr Ken Yuen from METS of Macquarie University for precise hardware fabrication on time.

I sincerely appreciate the financial support from the International Macquarie University Research Scholarship (iMURS), Macquarie University Postgraduate Research Fund, Division of ICS Postgraduate Research Fund and CSIRO top-up scholarship that made this study and my stay in Australia possible.

I express gratitude to all my friends in the Electronic Engineering research lab that helped make my stay enjoyable. Particularly, I would like to thank Dr Arif Khan and Dr Ozgur Isik and Mr Dushmantha Thalakotuna for being my coffee and lunch mates and listening to all my ideas patiently.

I would like to thank my wife Yogita for reading the thesis and providing valu-

able feedback, being patient and making compromises throughout my studies, and my sweet little baby Master Ayush for giving me lighter moments in hard times. My Mum and Dad who have always been proud of me and were always there for me. I could never ask for more. I should also like to thank my younger brother, Lovekesh and younger sister Deepti, for being the best brother and sister.

Last but never least, I would like to thank *GOD* for giving me strength, opportunity and wisdom to carry out this work.

*To my loving wife and son*

# Contents

# List of Figures

# List of Tables

# Chapter 1

# Introduction

An antenna is a specialised transducer that converts unguided radio-frequency (RF) fields into guided fields or vice versa. They play a key role in most wireless systems from the beginning (transmitter) to the end (receiver). The focus of this thesis is on the design of antennas for ultra-wideband (UWB) systems. These systems are primarily intended for short-range wireless communication and are expected to handle an unprecedented bandwidth, which imposes additional challenges in antenna design because satisfactory input match, gain and radiation patterns need to be maintained over a broad range of frequencies.

The UWB field originated from research in time-domain electromagnetics (EM) that was strong even in the early sixties and was able to fully describe the transient behaviour of a certain class of microwave networks through their characteristic impulse response. During the 1960s and 1970s impulse radars were investigated for military purposes to obtain greater resolution through their larger relative bandwidth. The experiments with radar led to research on impulse radio or broadband radio. In these impulse radios, signals are transmitted in the form of very narrow pulses. This is also called carrier-less transmission because no sinusoidal carrier is used. These extremely short pulses use a large bandwidth and therefore fall in the category of UWB signals. Prior to 1994, much of the work in the UWB field, particularly in the area

of impulse communications, was performed under classified programs. The only commercial non-classified application was Ground Penetrating Radar (GPR). The concept of GPR extended to new applications and is now being applied to new imaging devices which enable law enforcement, fire and rescue personnel to see through walls and debris during emergencies. These devices can also improve safety in construction sites by locating steel bars, electrical wiring, and utility pipes hidden inside walls or underground. UWB offers several unique capabilities that can enable a host of new sensing, positioning, and communication applications. Since ultra-wideband systems use very narrow pulses they can be separated out at the receiver. This has two benefits: firstly, multi-path components from the same transmitter can be well resolved thereby reducing multi-path interference. Secondly, pulses from two different users can be well separated offering lower inter-symbol interference.

With the release of the spectrum of 7.5 GHz from 3.1 GHz to 10.6 GHz by the Federal Communication Commission (FCC) in 2002, the wireless market saw the commercial potential in UWB communication. Apart from the applications explained above their scope extends to collision-avoidance radars that are being developed to reduce auto accidents. For personal-area networking, UWB can provide wireless links among camcorders, personal computers, DVD players, flat-screen television displays, printers, MP3 players and other devices. These UWB devices, which potentially support data rates in excess of 1 Gb/s, pose a range of regulatory concerns. In these realisations, the UWB transmission takes the form of noise-like signals at or below the background noise floor. They work across an unprecedented range of the radio spectrum, which is already licensed to a large number of government and commercial users. A key concern from other spectrum users is the interference that UWB transmissions potentially cause. To prevent such interference, a restricted spectrum mask has been imposed to limit the use of this enormous bandwidth.

Challenges in antenna design for UWB systems can be readily identified:

- Ultra-wideband matching is a prime requirement. GPR systems need the widest possible

matching while FCC-based UWB systems need a good impedance match from 3.1 GHz to 10.6 GHz. This matching is attributed to the connection between the antenna input port and the feed transmission line. In UWB antennas this may be viewed as reflections at certain locations within the antenna, which produce ripples in the time domain and resonant behaviours in the frequency domain.

- Antennas with the maximum possible gain are highly desirable for any wireless system. More gain from the transmitter antenna gives the flexibility to pump less power from the RF transmitter circuitry. This helps in reducing the design complexity of transceivers and reduces the size and weight of overall systems, which is highly desirable for compact, hand-held devices.

- Both pulse-based Direct Spread-spectrum UWB (DS-UWB) and carrier-based Multi-Band Orthogonal Frequency Division Multiplex (MB-OFDM) UWB systems are available and the gain of the antennas play a critical role in pulse shaping as well as carrier enhancements in both types. A flat gain over a broad range of frequency is highly desirable.

- The gain of printed and planar UWB antennas increases with frequency, which is a challenge for both technologies (DS-UWB and MB-OFDM) in maximising the dynamic range of the link while still meeting the very low FCC transmitted power spectral density (PSD) threshold. Due to the wide spectrum of UWB, frequency-dependent tilt severely compromises the dynamic range of the link. Since RF attenuation increases with frequency, the wider the frequency band the more tilted the received spectrum and the more dynamic range is lost to receiver equalisation or transmitter pre-distortion [6].

- The angular and spectral stability of UWB antennas is a key concern over the UWB bandwidth. Printed antennas being counterparts of conventional dipoles and monopoles,

have radiation patterns that are independent of distance but strongly dependent on frequency. This dependency leads different spectral components in a UWB signal to radiate in different directions with varying field strengths. The variation of pattern will cause the degradation of gain in the main beam direction, which in turn creates a problem in pulse transmission and the Line-of-Sight (LOS) scenario.

- The designers of UWB antennas should consider the overall performance of UWB systems. For most of these systems, the improvement of the link budget, even by a few dB, is of great importance. A low-cost lightweight directional antenna is highly desirable for LOS applications, as opposed to a conventional bulky dielectric-loaded horn or a several wavelength-long TEM horn.

- An appropriately designed antenna reflector, which works over a broad range of frequencies, can serve the purpose of enhancing the system performance and redirecting the energy going in an undesirable back-lobe direction towards the main beam.

- Reflectors with in-phase reflection characteristics can be realised using periodic structures. However, the designs available in the literature are mostly narrow band or dual band. Periodic structures capable of providing good reflection and appropriate phase over a UWB bandwidth are required for UWB antennas as reflectors, but their design is quite challenging.

- Near-field interactions lead to several imperfections in antenna performance unless they are accounted for in the design. For example, in GPR/imaging applications the hand-held devices need to be placed over lossy surfaces like the earth or human tissues, and in commercial devices like DVD players, HDTV, laptops and desktop computers, antennas are mounted in or over the metallic chassis. Such scatterers (feed cable, casing, furniture or human body) contribute to the far field radiated and even reflections into the source.

This thesis addresses the design aspect of UWB antennas. The main objective is to develop techniques to achieve the maximum possible flat gain from the existing printed antenna configurations available in the literature. Several new concepts are introduced to achieve this objective without compromising the antenna impedance matching over the UWB band. Low-cost, low-profile antennas with flat gain and a good impedance match over a UWB bandwidth are demonstrated in this work. Various hardware profiles are implemented and tested to prove the concepts employed to enhance the antenna gain and gain flatness.

## 1.1 Organisation of The Thesis

Chapter 2 presents a partial literature review, which is common to all chapters. Other chapters also have a literature review section relevant to individual chapters. Various problems caused by the variation in gain of printed and planar UWB antennas are explained in detail. Chapter 2 also contains a brief history of UWB technology and current trends and application prospects of UWB systems.

Chapter 3 describes the gain stability of printed antennas over a broad range of frequencies. A concept of proximity-coupled metallic patches, incorporated on the surface along the printed UWB radiators, is presented. Two novel MS-fed and CPW-fed printed UWB antennas are designed to prove the concept of proximity coupling. To the best of the author's knowledge, these monopoles are the first of this kind capable of achieving the UWB bandwidth while maintaining the gain over a broad range of frequencies. This work is in contrast to the surface-wave suppression techniques used in the past for patch configurations, where metallic patches and resistive cards are used around the antenna to reduce the propagation of surface waves. In addition to simple metallic patches/cavities coupled to printed monopoles, an array of these patches/cavities is proposed to enhance gain further from 3.1 GHz to 10.6 GHz. This flat gain contributes to an improved system dynamic range while meeting the limits of the FCC spectral

mask.

Chapter 4 describes a new class of short two-plate and short TEM horn antennas and a novel feed mechanism for a short TEM horn with printed monopoles. These antennas possess flat gain characteristics and are capable of reducing near-zone scattering due to the chassis and the lossy materials present in the neighbourhood. A complete study, and an effective field analysis to justify the evolution of these short TEM horns, are presented in this chapter. Three different antennas are introduced in Chapter 4 to prove the concept of printed-monopole feeding of short TEM horns. Complete hardware profiles and validations of predicted results by measurements are presented. The limitation of the restricted bandwidth from the antennas proposed in Chapter 3 are addressed and resolved by the antenna designs presented in Chapter 4.

Chapter 5 starts with a change of topic to periodic structures but ends with antenna design. Based on multi-layer periodic structures, UWB antenna reflectors are designed and demonstrated in this chapter. A novel concept of phase coherence over the UWB bandwidth is presented. Based on the concept, frequency selective surface (FSS) are designed to achieve desirable phase and stop bands over a UWB bandwidth. Two different FSSs are proposed in this chapter. The first surface is a dual-layer FSS while the second is is a four-layer FSS. The optimisation of the dual-layer FSS, its oblique-incidence performance, experimental implementations and measurements are presented in Chapter 5. This FSS has a 133% transmission bandwidth, which seems to be the best available; the previous best has an bandwidth of 52% (explained in more detail in Chapter 5). Based on the concept of the dual-layer FSS a four-layer FSS is also presented in Chapter 5. Both FSSs were tested as a reflector with a UWB slot antenna. The dual-layer FSS needs a shorter gap between the antenna and the reflector. The four-layer FSS offers more control of gain by controlling the periodicity in each layer.

Chapter 6 concentrates on slot antennas and high-gain antennas with directional radiation patterns. Slot antennas are treated as magnetic monopoles, and they are capable of providing good immunity to the near-field interaction. The key challenge in the design of slot antennas is

matching the feed of the slot to a 50Ω or 75Ω transmission line. Several bow-tie configurations show the potential of being used in hand-held GPR applications. Chapter 6 starts with the design of a compact semicircular slot antenna. This antenna is fed with a CPW line which forms a compact step transformer to match the impedance of the semicircular slot aperture to the feed. After optimising the structure, a short two-plate horn, proposed in Chapter 4, was mounted on top of the slot. This hybrid configuration of a slot with a short two-plate horn leads to significant gain enhancement over the UWB band. In addition to the design of this short horn a four-plate short horn is introduced, which is fed by a rectangular slot antenna. The newly designed short horn is capable of giving an average gain of 10 dBi with a compact size of around $\lambda/4$ (at 3 GHz) while maintaining the UWB impedance bandwidth. An initial study and experimental results proves the potential of such a short horn antenna as compared to the conventional dual- and quad-ridge horns.

Chapter 7 provides the overall conclusions of the thesis, followed by a brief summary of all the design and suggestions for future work.

Commercial software packages used in the project are (a) High Frequency Simulation Software (HFSS) from ANSOFT (based on the Finite Element Method), and (b) CST Microwave Studio (based on the Finite Integration Technique).

## 1.2 Thesis Contributions

The key contributions of this thesis are in understanding and developing antennas with enhanced gain over an ultra-wide bandwidth.

Specifically, the contributions include:

### 1.2.1 Main Achievements

1. The effectiveness of proximity coupling to printed monopole antennas is investigated and proven (Chapter 3).

2. A novel concept of a short TEM horn and a feed mechanism for a short horn with printed monopoles are introduced (Chapter 4).

3. The phase-coherence principle is introduced for UWB antenna reflector design and a UWB antenna with periodic reflector has been designed to achieve 133% impedance bandwidth (Chapter 5).

4. A novel short four-plate UWB horn is introduced fed by a slot antenna. It has the performance comparable to dual- and quad-ridge horns (Chapter 6).

### 1.2.2 Other Contributions

1. Proximity-coupled printed circular monopole antenna with good angular stability (Chapter 3).

2. Extending the concept of proximity-coupled monopoles to CPW-fed antennas and designing thin antennas for a MB-OFDM System (Chapter 3).

3. Developing an array of proximity-coupled metallic slot antennas to further control the gain over the UWB band (Chapter 3).

4. Designing and developing unique monopole-fed surface-mounted short two-plate and TEM horn for hand-held UWB applications (Chapter 4).

5. Complete field analysis and optimisation of short TEM horn to understand the evolution of the present structure with TEM horns (Chapter 4)

6. Demonstrating the concept of the short TEM horn with a surface-integrated horn fabricated on the same substrate with a printed monopole (Chapter 4).

7. Two different UWB periodic structures are introduced to design an antenna reflector with controllable gain performance (Chapter 5).

8. The optimisation of the dual-layer FSS, its oblique incidence performance, experimental implementations and measurements are presented (Chapter 5).

9. Designing and developing a compact slot antenna and proving the effectiveness of short horns coupled to a slot antenna in UWB applications (Chapter 6).

## 1.3 Publications

Some of the thesis contributions have been published in journal and conference proceedings. The list of papers is provided below. Several journal papers are under an internal review process and are yet to submitted to the corresponding editorial boards (listed under a separate category). The papers listed under other publication category are not explained in detail in thesis chapters but considered as a part of the process for gaining an understanding of periodic structures which are used in Chapter 5 of this thesis.

### 1.3.1 Invited Papers *(IP)*

1. **[IP1] Y. Ranga**, L. Matekovits, Karu P. Esselle and Andrew R. Weily, "*Enhanced gain UWB slot antenna with multilayer frequency-selective surface reflector*," 2011 IEEE International Workshop on Antenna Technology: Small Antennas, Novel Structures and Innovative Metamaterials, pp 176-179.

2. **[IP2] Y. Ranga**, Karu. P. Esselle, A. Weily and A. K. Verma, "*CPW-Fed Printed Semi-circular Disc Monopole Antenna Enhanced with Surface-Mounted Short Horn*," ISMOT 2009, Delhi, India.

### 1.3.2 Journal Papers *(JP)*

**Accepted Papers**

3. **[JP1] Y. Ranga**, A. K. Verma and Karu. P. Esselle, "*Planar-Monopole-Fed, Surface-Mounted Quasi- TEM Horn Antenna for UWB Systems*," IEEE Transactions on Antennas and Propagation vol 58, no.7 Pages 2436-2439.

4. **[JP2] Y. Ranga**, Karu. P. Esselle and Andrew R. Weily, "*Compact Ultra-Wideband CPW-Fed Printed Semicircular Slot Antenna*," Microwave and Optical Technology Letters, vol. 52, no. 10, October 2010, Pages: 2367-2372.

5. **[JP3]Y. Ranga**, Karu. P. Esselle, Andrew R. Weily and A. K. Verma, "*A Constant Gain Printed Circular Monopole Antenna for UWB Applications*," Microwave and Optical Technology Letters, vol. 52, no. 6, June 2010, Pages 1261-1264.

6. **[JP4] Y. Ranga**, L. Matekovits, Karu P. Esselle and Andrew R. Weily, "*Multioctave Frequency Selective Surface Reflector for Ultra-wideband Antennas*," IEEE Antennas and Wireless Propagation Letters, vol.10, Pages 219-222.

**Papers Under Internal Review**

7. **[JP5] Y. Ranga**, L. Matekovits, Karu P. Esselle and Andrew R. Weily, "*Ultra-Wideband Phase Coherence with a Dual-Layer Frequency Selective Surfaces Reflector*," IEEE Transactions on Antennas and Propagation.

8. **[JP6] Y. Ranga**, L. Matekovits, Karu P. Esselle and Andrew R. Weily, " *Ultra Wide-Band Frequency-Selective-Surfaces with Angle and polarisation Study*," IEEE Antenna and Wireless Propagation Letters.

9. **[JP7] Y. Ranga**, L. Matekovits, Karu P. Esselle and Andrew R. Weily, " *Constant Gain Antenna with Ultra wideband Frequency-Selective-Surface Reflector*," IEEE Transactions on Antennas and Propagation.

10. **[JP8] Y. Ranga**, Karu. P. Esselle, Andrew R. Weily and A. K. Verma, " *Compact Short Horn Antenna for UWB Radars and Communication Systems*," IEEE Antenna and Wireless Propagation Letters.

11. **[JP9] Y. Ranga**, Karu. P. Esselle, Andrew R. Weily and A. K. Verma, " *Compact surface mounted Short Horn TEM Horn for hand-held UWB Applications*," IEEE Antenna and Wireless Propagation Letters.

### 1.3.3 Conference Papers *(CP)*

**Year 2012**

12. **[CP1] Y. Ranga**, A. K. Verma, Karu. P. Esselle and Andrew R. Weily, " *An Ultra Wide-band Antenna with Uniform Gain*," 6th European Conference on Antenna and Propagation (EuCAP 2012), Czech Republic (Under internal review).

**Year 2011**

13. **[CP2] Y. Ranga**, Karu. P. Esselle, Andrew R. Weily and A. K. Verma, "*Compact High-Gain Short-Horn Antenna for UWB Applications*," 5th European Conference on Antenna and Propagation (EuCAP 2011), Rome, Italy.

14. **[CP3] Y. Ranga**, L. Matekovits, Karu P. Esselle and Andrew R. Weily, "*Multi-layer Frequency-Selective Surface Reflector for Constant Gain Over Ultra wideband*," 5th European Conference on Antenna and Propagation (EuCAP 2011), Rome, Italy.

15. **[CP4] Y. Ranga**, L. Matekovits, Karu P. Esselle and Andrew R. Weily, "*Design and Analysis of Frequency-Selective Surfaces for Ultrawideband Applications*," EUROCON 2011 Lisbon, Portugal.

16. **[CP5] Y. Ranga**, L. Matekovits, Karu P. Esselle and Andrew R. Weily, "*Oblique Incidence Performance of UWB Frequency Selective Surfaces for Reflector Applications*," IEEE Antennas and Propagation Society International Symposium, 2011.

17. **[CP6] Y. Ranga**, L. Matekovits, Karu P. Esselle and Andrew R. Weily, "*The Use of A Multi-layer Frequency Selective Surface Reflector to Achieve Antenna Gain Flatness Over a Ultra-wideband*," 12th Australian Symposium on Antennas; Sydney, NSW. CSIRO ICT Centre; 2011: ISBN: 9780643096271.

**Year 2010**

18. **[CP7] Y. Ranga**, A. K. Verma, Karu. P. Esselle and Andrew R. Weily, "*A Gain-Enhanced Semicircular Disc Antenna with A Quasi-Planar Surface-Mounted Short TEM Horn*," European Microwave Week 2010, Paris France.

19. **[CP8] Y. Ranga**, Karu P. Esselle and Andrew R. Weily, "*A Simple Thin Antenna with An Enhanced Gain for MB-OFDM UWB Systems*," Fourth International Conference on Signal Processing and Communication Systems, ICSPCS 2010.

20. **[CP9] Y. Ranga**, Karu. P. Esselle and Andrew R. Weily, "*Gain Enhancement Techniques for UWB Antennas*," WARS 2010, Canberra.

21. **[CP10] Y. Ranga**, A. K. Verma, Karu. P. Esselle and Andrew R. Weily, "*Gain Enhancement of UWB Slot with the Use of Surface Mounted Short Horn*," IEEE APS URSI/UNSC 2010 Canada.

22. **[CP11] Y. Ranga**, Karu. P. Esselle, Andrew R. Weily and A. K. Verma, "*An Ultra-Wideband Printed Monopole Antenna Enhanced Using A Surface-Mounted Short Horn*," EuCap 2010, Spain.

**Year 2009**

23. **[CP12] Y. Ranga** and Karu. P. Esselle, "*CPW-Fed Semicircular Slot Antenna for UWB PCB Applications*," IEEE Antennas and Propagation Society International Symposium, 2009.

24. **[CP13] Y. Ranga**, Karu. P. Esselle, Andrew R. Weily and A. K. Verma, "*A Compact Antenna with High Gain for Ultra Wide Band Systems*," Microwave Conference, 2009. EuMC 2009, Rome, Italy.

25. **[CP14] Y. Ranga**, Karu. P. Esselle and A. K. Verma, "*Wide band High Gain Antenna for UWB Application*," 11th Australian Symposium on Antennas; Sydney, NSW. CSIRO ICT Centre; 2009: 2. ISBN: 9780643096271.

### 1.3.4 Other Publications *(OP)*

26. **[OP1]** L. Matekovits, **Y. Ranga**, Karu P. Esselle and Mario Orefice, "*Scattering of a Width-Modulated Microstrip Line for an Arbitrary Angle of Incidence*," Metamaterials '2011: The Fifth International Congress on Advanced Electromagnetic Materials in Microwaves and Optics, Barcelona, Spain, pp. 823-825, ISBN 978-952-67611-0-7.

27. **[OP2]** L. Matekovits, **Y. Ranga**, Mario Orefice and Karu P. Esselle, "*Width-Modulated Microstrip line Unit-Cell: Quasi Periodic Combinational Sequence for Holographic Array Applications*," Asia Pacific Microwave Conference (APMC) 2011, Melbourne, Australia (Accepted for publications).

# Chapter 2

# Literature Review and Background

## 2.1 Introduction

UWB is one of the oldest radio technologies dating back to the early $20^{th}$ century. In 1918, UWB was banned for interfering with narrow-band frequencies and restricted to military applications. In the early 1980s UWB made a resurgence but was limited to military applications and used the terminology of baseband or impulse radio [7]. Some commercial civilian applications like Ground Penetrating Radars (GPR) exist as UWB applications. More recently this technology re-emerged in 2002 after the approval of an unlicensed band from 3.1 GHz to 10.6 GHz for short-range wireless technology by the Federal Communications Commission (FCC) [8]. A similar document was released by the Office of Communications of the United Kingdom in 2005 to be considered by the European Conference of Postal and Telecommunications Administrations (CEPT) [9].

The current masks approved by different authorities are presented in Figure 2.1. In current developments, Alereon announced in September 2010 that their UWB "*NoWire(TM)*" technology will be used in a Wireless Video/Audio Extender providing an up to 220 Mbps link. Alereon chips will also power the Toshiba Wireless Dynadock W20 system. EZAir is offering a variety

of UWB video/USB extenders powered by Wisair UWB chips. Staccato Communications and Artimi joined forces in a 2008 merger to form a company called VeeBeam, which is working on the development of UWB wireless data systems. More recent developments can be found from [10] and [11].

This chapter contains background information and a literature review. More information and specific literature related to each chapter is also included in each chapter.

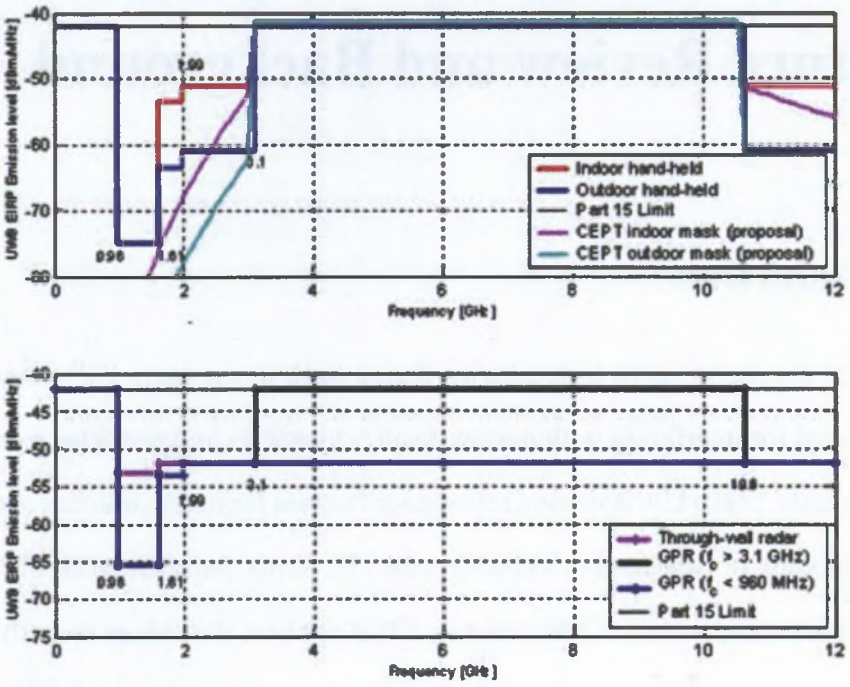


**Figure 2.1:** Power spectral density mask approved by various authorities.

## 2.2 UWB System Characterisation

Since the release of 7.5 GHz of unlicensed spectrum, UWB technology developers started working in two different groups. The first group is the UWB forum headed by Motorola and the second group is the Multi-band Orthogonal Frequency Division Multiplexing (MB-OFDM) alliances headed by Intel, which includes other well known companies like Microsoft, NEC,

Philips and Samsung. These groups are divided on physical-layer standards. The UWB forum adopted the policies of traditional direct spread spectrum (DS)-UWB, which spreads the information over a wide band using a pseudo-random bit sequence. The MB-OFDM alliance favours the division of the entire spectrum of 3.1 GHz to 10.6 GHz into 14 subcarriers, each with 528 MHz bandwidth, which enables the incorporation of well established concepts of narrowband techniques. In the current market the MB-OFDM alliance appears to be progressing more rapidly than the DS-UWB groups.

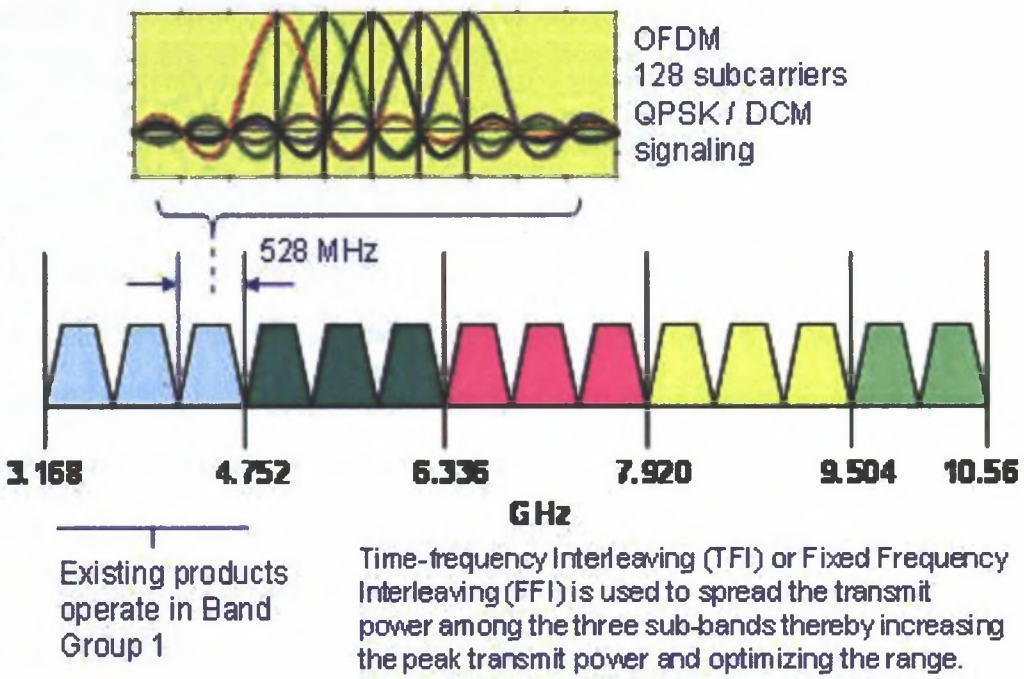


**Figure 2.2:** WiMedia MB-OFDM channel assignment in the 3.1 GHz to 10.6 GHz band. Most existing products support Band Group 1. The 528 MHz OFDM sub-bands in each Band Group can be used to interleave the signal and spread its power [1].

One successful partner alliances of MB-OFDM is Wi-Media. The details of the WiMedia specifications are available online at [12] in a document with the title "Standard ECMA-368: High Rate Ultra Wideband PHY and MAC Standard". The WiMedia specification divides the available UWB spectrum into five Band Groups that are further subdivided into 528 MHz subbands (Figure 2.2). Data transmissions can be frequency hopped among the three sub-bands

to reduce the average transmit power while maximising the instantaneous power of symbol transmissions. For example, the OFDM signal can be pulsed in the time domain over any of the 3 frequency sub-bands with one-third duty cycle, thereby reducing the average transmit power by a factor of 3 or 4.77 dB. The WiMedia techniques for spreading the power include what WiMedia calls Time-Frequency Interleaving (TFI) and Fixed Frequency Interleaving (FFI). TFI is essentially a technique of frequency hopping the 528 MHz wide OFDM pulses over three bands. The FCC relaxed the -41.3 dBm/MHz limit to -36.5 dBm/MHz for peak power in the 528 MHz sub-bands since the 1/3 duty cycle averages to -41.3 dBm/MHz. To avoid the UNII band 5.8 GHz interference from Wi-Fi, the current generation of WiMedia products operate in Band Group 1. WiMedia uses MB-OFDM with data rates of 53.3, 80, 106.7, 160, 200, 320, 400 and 480 Mbps. Quadrature Phase Shift Keying (QPSK) modulation is used for data rates up to 200 Mbps and Dual-carrier Modulation (DCM) is used for data rates of 320 Mbps and higher. On the TX side a single 4- to 6-bit digital-to-analogue converter running at 1 GHz is typically used to generate the 528 MHz TX spectrum and on the RX side two 4-bit, 1 GHz analog to digital converters (one for "I", the other for "Q" component) are typically required to detect and recover the MB-OFDM sub-carriers [6].

## 2.3 Application Prospects

### 2.3.1 High-Data-Rate Applications

UWB technology started with much hype in the consumer market and high-data-rate applications were the main target of this technology. The standard definition of ultra-wideband, a bandwidth exceeding 500 MHz (for carrier frequencies above 2.4 GHz), and an extremely low power spectral density (75 nW/MHz between 3.1 GHz to 10.6 GHz, according to FCC rules).

The problem of designing transceivers with reasonable complexity, also suitable for handheld devices, is one of the main challenges for high-rate applications. Robustness against jam-

ming is also very important, as a large number of electrical devices emitting narrowband noise are usually found in home and office environments, as well as interfering signals from other wireless services operating in sections of the UWB bandwidth.

The main application areas include:

- Internet Access and Multimedia Services: Regardless of the envisioned environment (home, office, hot spot), very high data rates ( $>$ 1 Gbit/s) have to be provided - either due to high peak data rates, high numbers of users, or both.

- Wireless peripheral interfaces: A growing number of devices (laptop, mobile phone, PDA, headset, etc.) are employed by users to organise themselves in their daily life. The required data exchange is expected to happen as conveniently as possible or even automatically. Universal standardised wireless plug and protocols are highly desirable in this field.

- Location-based services: To supply the user with the information he/she currently needs, at any place and any time (e.g. location-aware services in museums or at exhibitions), the user's position has to be accurately measured. UWB techniques may be used to accommodate positioning techniques and data transmission in a single system for indoor and outdoor operation.

- Home Networking and Home Electronics: One of the most promising commercial application areas for UWB technology is wireless connectivity of different home electronic systems. It is thought that many electronics manufacturers are investigating UWB as the wireless means to connect together devices such as televisions, DVD players, camcorders, and audio systems, which would remove some of the wiring clutter in the living room. This is particularly important when we consider the bit rate needed for high-definition television that is in excess of 30 Mbps over a distance of at least a few metre. Some UWB products are already on the market for connecting computers to monitors.

### 2.3.2 Wireless Body-Area Networks (WBAN)

WBANs are another example where our life is potentially dependent on UWB for medical monitoring. Due to the proposed energy-efficient operation of UWB, battery-driven handheld equipment is feasible, making it suitable for medical supervision. Moreover, UWB signals are inherently robust against jamming, offering a high degree of reliability, which will be necessary to provide accurate patient health information and reliable transmission of data in a highly obstructed radio environment. UWB also offers good penetrating properties that could be applied to imaging in medical applications; with the UWB body sensors this application could be easily reconfigured to adapt to specific tasks and would enable high data rate connectivity to external processing networks. Some brief outlines of applications and advantages of UWB systems are listed below:

- **Penetrating through obstacles**: In discussing this capability, we could compare UWB with ultrasound. The major difference is that ultrasound is basically a line-of-sight technology and it is very short range (It is used for medical imaging but it typically works only over a few inches). However, UWB is different because it does not use high frequency sound waves which cannot penetrate obstacles. This makes UWB viable for wide-area applications where obstacles are certain to be encountered, although ultrasound may be inoperable in these circumstances. The feature makes it easy to image organs of the human body for medical applications.

- **High-precision ranging at the centimetre level**: Another feature of UWB is high-precision ranging at the centimetre level based on the ultra-short pulse characteristic. High precision of ranging also means strong multi-path resolving capability. The conventional wireless technique used continuous waves and the standing time is much longer than the multi-path transmission time. The UWB pulse is much shorter, thus it has very strong temporal and space resolving capability (For a 1 nanosecond pulse, the multi-path

resolving power equals 30 cm ), which is suitable for the localization and detection in the medical applications.

- **Low electromagnetic radiation**: The third feature of UWB is the low electromagnetic radiation due to the low-radio-power pulse, less than -41.3 dB in an indoor environment. The low radiation has little influence on the environment, which makes it suitable for hospital applications. Furthermore, the low radiation is safe for the human body, even at a short distance, which makes it possible to apply UWB to the imaging equipment.

- **Low processing energy consumed**: Since UWB uses very short pulses for radio transmission and very careful design of signal and architecture, the transmitter could be designed to be simple, allowing extremely low energy consumption, which also enables the usage of long-life battery-operated devices.

### 2.3.3 Low-Data-Rate Applications

Apart from the previously discussed high-data-rate applications, low-data-rate technology is also a viable UWB candidate. The use of very short pulses in impulse radio transmission, and careful signal and architecture design, facilitate the design of very simple transmitters, permitting extremely low energy consumption and thus long-life battery-operated devices, which are mainly used in low-data-rate networks with low duty cycles. The inherent noise-like behaviour of UWB systems makes robust security systems highly feasible. They are not only difficult to detect, but also excel in jamming resistance. These characteristics are essential, not only for traditional security alarm systems, but also for Wireless Body-Area Networks (WBANs), which are envisaged for medical supervision as discussed above.

## 2.4 Antennas for UWB Applications

Defining an antenna for any application, we need to fulfil certain parameters like impedance bandwidth, gain, directivity, efficiency and radiation stability; based on these parameters we can define the bandwidth for any antenna system. In the case of UWB systems, with an enormous bandwidth of 7.5 GHz, the stabilisation of gain, efficiency or radiation patterns proved to be a tough task. A more standard definition based on impedance bandwidth and approved by the Defense Advanced Research Projects Agency (DARPA) and further modified with some suggestions and adopted by the FCC, is as follows [8]:

*"UWB devices have -10dB radiated power density fractional greater than 0.20 or -10 dB bandwidth greater than 500 MHz. The fractional bandwidth is defined by* $2(F_H - F_L)/(F_H + F_L)$*, where* $F_L$*, the lower end of the band, is the frequency at which power is 10dB down from that of the center frequency and* $F_H$ *is the frequency greater than the center frequency with 10dB less power than that of the center frequency".*

UWB antennas are mostly characterised on the basis of impedance bandwidth, which is the first step for any antenna design. Recent research on UWB antennas has mostly concentrated on commercial compact printed or planar antennas. Several UWB antennas are available in the literature, based on the geometries and orientation of the radiating element with ground; some of them are explained in next section under three different categories.

### 2.4.1 Planar Antenna Configurations

In planar monopole antennas the planar elements are orthogonal to the finite ground plane. These antennas are traditionally fed using coaxial cable and are of different shapes and sizes, which determine their lower cutoff frequency. A detailed analysis of these antennas was carried out as elements comparable to a thick dipole [13]. The antennas demonstrated in [13] have more than 10:1 (VSWR $< 2$) bandwidth ratio. In most of the elliptical and circular antenna examples

the feed has a smooth transition because of the curved geometry, and so wide-band matching was achieved. The gap between the feed and the start transition for planar geometries holds the key for impedance matching. Similar kinds of planar configurations with a different basis were optimised in the past; these shapes are primarily square or rectangular but additional bevels, multiple feeds or shorting posts were incorporated for wideband operations [14–16]. Apart from the impedance bandwidth, gain is important for wideband applications. The performance of several antennas based on gain is listed below.

A multiple (trident feed) square monopole was presented in [16]. For frequencies up to about 6 GHz, it was seen that the antenna gain monotonically increases from about 4.0 to 7.0 dBi for the higher-frequency portion of the impedance bandwidth, however the antenna gain varies by a relatively small amount in the range of 6.5 dBi to 7.0 dBi. In the most popular planar inverted-cone antenna (PICA) [17] the gain gradually increases with frequency. It was about 5 dBi at the lowest operating frequency of 1 GHz and was about 8 dBi at the high end of impedance operating bands, 7 and 10 GHz. In an annular monopole presented in 2002 [18] the antenna exhibited typical omnidirectional monopolar patterns with a maximum gain of 4.8 dBi, which is constant to within $\pm 0.5$ dB over a small range of polar angles from $\theta = 48^0$ to $\theta = 63^0$. It was clearly mentioned in the paper that the gain in the ground plane ($\theta = 90^0$) was 0.3 dBi. The introduction of the hole had no effect on the maximum gain at this frequency. As the frequency was increased, a slight increase in directivity was observed, accompanied by a reduction in the half-power beam-widths in the vertical planes. The gain in the ground plane ($\theta = 90^0$) also fell. In the case of the circular annular configuration [19] the maximum gain at 1.8 GHz was found to be 2.8 dBi while the maximum gain in the ground plane ($\theta = 90^0$) was 0.8 dBi. A monopolar patch antenna with very wide impedance bandwidth was presented in 2005 [20]. This antenna had an average gain of 3.7 dBi with a variation of 2 dB from over 1 GHz to 3 GHz. In [21] a discone with tapered cylindrical wire was presented. The measured gain in the 1 GHz frequency range had an average of 3 dBi or more with a variation of 3.5 dB

over the whole bandwidth.

These variations in gain were attributed to diffraction on the edges and on the corners of the ground plane [22], and the beam tilt due to the finite ground plane [23], [24]. A clearer picture of system gain was presented for a rolled monopole [25]. The monopole pair had a system gain that was almost unchanged for different orientations and higher than that of the monopoles presented in [21], [22], [23], [24], [25]. It was clearly seen that, as compared with the other monopoles, the rolled monopole has the advantage of a perfectly omnidirectional radiation characteristic in the horizontal plane. The other planar monopoles exhibit direction-independent radiation characteristics in the multi-band scheme. Thus constant antenna gain [26] has been highly desirable since the start of the design of UWB antennas.

### 2.4.2 Printed Antenna Configurations

Planar antennas have shown great potential in the past but for UWB portable devices, the protruding nature of the planar monopole and the probe feed is not an attractive option. A low-profile version of the planar monopole antenna has been presented in [27]. This antenna is a folded monopole antenna supported by an edge ground plane, with a shorting pin employed for impedance matching. Printed monopole antennas have an even lower profile than the above antenna. These antennas are either fed with a microstrip line [4], [13] or a Coplanar Waveguide (CPW) [28]. They are supported by a truncated ground plane in contrast to the planar conducting ground of the monopoles described earlier. Various geometries/shapes are available in the literature for these printed configurations; most of them emphasise the optimisation of the impedance bandwidth.

Recently, many techniques have been examined to enhance the antenna bandwidth, including the use of a trident-shaped feeding strip and a tapered impedance transformer [29], and embedding a pair of notches in the two lower corners of the patch and the notch structure in the upper edge of the ground plane [30]. Other techniques such as using two bevel slots on the

upper edge and two semicircular slots on the bottom edge of the ground plane [31], and using a half-bowtie radiation patch with a staircase shape, have also been reported for bandwidth enhancement [32]. The concept behind the large impedance bandwidth of these printed antennas was highlighted in one chapter of [2]. According to the study, at the low-frequency end (the first resonance) when the wavelength is bigger than the antenna dimension, the electromagnetic waves (EM) can easily couple into the antenna structure so it operates in an oscillating mode, i.e. a standing wave. The antenna starts to operate in a hybrid mode of standing and travelling waves with increase in frequency. These antennas also have a significant variation in gain across the whole UWB band. Several examples from the literature are described next.

A microstrip-fed printed circular monopole antenna (PCMA) [4] has a gain of around 0.58 dBi at the lower band cutoff frequency. The gain increases up to 6.7 dBi at higher frequencies, which gives a variation of $\pm 3.06$ dB over the whole impedance bandwidth. A CPW-fed PCMA [5] shows a gain of 0.88 dBi to 5.8 dBi, which leads to a variation of $\pm 2.46$ dB across the band. Another similar configuration of a printed elliptical monopole antenna (PEMA) [33] has larger physical dimensions and covers a 1.10 GHz to 13.61 GHz band, and a similar increasing trend in gain was noted. The gain of the PEMA varies from 1.5 dBi to 8.3 dBi with a variation of $\pm 3.40$ dB. Similar behaviour of the gain is noticed in several other printed monopoles where the antenna gain increases monotonically [34] with frequency. A constant gain and constant pattern is a very desirable feature for a UWB antenna, since it avoids the waveform dispersion and distortion associated with a pattern that varies with frequency. Further discussion on the flat gain is presented in Section 2.5.2. Gain enhancement is possible by narrowing the field of view of these antennas. Leon Brilluoin's coaxial horn is one of the best examples, demonstrating the enhancement in gain by narrowing the field of view [35]. The concept of proximity-coupled slot presented in Chapter 3 and short horns presented in Chapter 4 follow the principle of narrowing the field of view and enhancing the gain.

### 2.4.3 Printed Magnetic/Slot Monopoles

Slot antennas were developed in the late 1940s to early 1950s [36]. In recent years, printed slot antennas are under consideration for use in UWB systems and are getting more and more attention due to their attractive merits of simple structure and low profile. These antenna structures have the advantage of low coupling with nearby metallic objects. Metallic interference is discussed in later sections and more detailed designs of printed monopoles which are capable of avoiding metallic interference are presented in Chapter 4. In the literature several slot configurations have been demonstrated for UWB applications. In order to enhance the bandwidth and match to a 50Ω impedance several modifications in the feed have been demonstrated in [37–40]. In one configuration, by extending a small rectangular slot of proper dimensions along the direction of the microstrip feed line, an impedance matching of about 46% is achieved [37]. This is about three times that of a corresponding conventional printed wide rectangular slot antenna and the gain over this wide operating band is about 3.4 dBi to 5.1 dBi. A printed slot antenna with a fork-like tuning stub and a simple rotated slot has also been studied [38], giving a wide operating bandwidth of about 2.2 GHz (49.4%). However, this bandwidth is not wide enough to cover the entire FCC UWB frequency band. To provide a compact solution with good isolation and low ground inductance for shunt elements, several CPW-fed bow-tie slot antennas (BTSAs) have been developed [41,42] . A BTSA fed by a CPW has been investigated for broadband applications [43], but it does not cover the UWB band because the feed transmission line is not well matched to the high input impedance at the vertex. This mismatch problem has been overcome through the use of tapered metal stubs [41] and inductive coupling [42]. All these methods are complex and involve adjustment of the slot flare angle to enhance bandwidth along with loading the slot with stubs, patches or inductive coupling. A simple and innovative impedance transition in the CPW feed of the BTSA has been investigated, achieving a match over the complete UWB band [44]. A study on the effect of vertex angle has also been conducted, illustrating the variation in bandwidth for different vertex angles when the overall surface area is 2500 $mm^2$

(50 × 50 mm) [44]. Slot antennas have a relatively constant directive gain between 2.0 dBi to 3.0 dBi with only 1 dB variation in gain over the complete bandwidth [45]. However high-gain slot antennas have exhibited a stronger gain variation of between 2.0 dBi to 7.0 dBi. [46]. In Chapter 6 the novel feeding mechanism of a step taper transformer for a semicircular slot antenna is presented. This antenna is compact and suitable for the various printed-circuit-board (PCB) applications and has relatively constant gain, like other slot configurations. Toward the end of Chapter 6 the enhancement of gain is also demonstrated for a slot antenna.

## 2.5 Current Trends and Issues in UWB Antennas

Before describing the current trends in UWB, this section discusses GPR, which is one of the prime applications of UWB, and several other applications that have been developed recently based on the concepts of GPR.

### 2.5.1 Ground-Penetrating Radar Imaging Systems

Ground-Penetrating Radar (GPR) was considered as the prime commercial application for the UWB bandwidth. Apart from mine detection by the military, several civilian applications like imaging, surveying (road inspection, archaeology and forensics) take advantage of GPR technology. In fact some GPR-based applications do not involve the ground. For example through-wall imaging and medical imaging, which arose from the principles followed in GPR, do not involve the ground. GPR antennas are designed to operate with pulse waveforms and need to have the large bandwidth corresponding to the shortest pulse available. GPR systems explore targets within a short range of interest. These diverse GPR applications demand extra care in design of antennas with a wide impedance bandwidth. Most often, systems are installed out of laboratory environments and need to be human- or machine-portable. A system design is heavily influenced by the the size and weight of the antenna installed in the system. Additional

difficulties are imposed by the ground medium or human tissues or high-loss media involved in some applications. Such lossy media heavily attenuate the signals in any case. More details of attenuation in ground and human tissues are available in Chapters 19 and 20 of [2].

In these systems, if the depth of penetration, medium characteristics and scanning are kept constant, an antenna with low gain requires extra RF power from the transmitter, hence high-power RF components needs a heat sink for the components, which contribute to the cost and weight of the system. A 3dB improvement in antenna gain saves half the power consumption in the RF transmitter device. GPR is one of the well-established areas in the field of UWB systems. The requirements for antennas are mostly dependent on the system requirements and may vary from application to application, but the key component is as much bandwidth as possible across the operating frequency region. Traditional configurations of dipoles [47], resistive loaded dipoles [48], V-dipoles [49], [50], bow-tie [51], [52], [53] and horn antennas [54], [55] are the most popular categories in GPR applications proposed in the past. Out of all the demonstrated solutions the Transverse Electromagnetic (TEM) Horn is a popular choice for most GPR applications. These antennas are capable of radiating an impulse with small distortion while their directionality contributes to high gain. A conventional TEM horn structure consists of two conductor plates flared at a certain angle to support TEM waves and accomplish the transition from a uniform feed line to a travelling wave in space [54]. These antennas are typically $\lambda$ to $10\lambda$ long; this normally implies increased weight. These TEM horns also need a feed balun at the input network, which sometimes restricts the bandwidth of the antenna. A printed microstrip balun presented in [55] operates over a broad range of frequencies. The reduction in the size of these antennas is achieved with dielectric loading. Chapter 4 presents the concept of a short TEM horn antenna, which may be useful in these applications. The antennas presented in Chapter 4 are less than $\lambda$ in length and capable of achieving more than 110% impedance bandwidth. The gain flatness of short horns fed by UWB printed monopoles is impressive. This should lead to a less dispersive pulse. The only drawback of these antennas is the bidirectional

nature of their radiation, which can be rectified by using an appropriate reflector, as demonstrated in Chapter 5. Along with conventional horn antennas a new printed class of slot antenna fed using microstrip and CPW transmission lines shows great potential in imaging and GPR applications [56], [37], [38], [39] and [40]. These antennas have stable gain of around 2 to 3 dBi depending on the size of the aperture. Chapter 6 presents a novel design of a semicircular slot antenna based on the concept of bow-tie antennas. The step transformation in the feed network helps to improve the bandwidth in a compact size. A short TEM horn mounted on top of a slot antenna is discussed in Chapter 6. The short TEM horns proposed in Chapter 4 and Chapter 6 are TEM or quasi-TEM horns with bidirectional radiation patterns. At the end of Chapter 6 we introduce another four-plate horn, which is equivalent to a dual- and quad-ridge horn and is capable of giving a directional pattern. This demonstrated concept of the four-plate horn avoids the complexity of designing a feed transition from coaxial to ridge structures.

### 2.5.2 Flat-Gain UWB Antennas

In UWB antennas, apart from the impedance bandwidth, gain is a critical parameter for efficient system performance. Most antenna research and design has been carried out with impedance as the prime focus. Only a few publications observe the gain variation of the proposed antennas. In the case of planar antennas a few articles from [16–24, 26] mention the gain and significance of gain. In particular [4] shows the clear trend and variation of gain of printed monopole antennas. This trend in gain variation is similar for similar printed antennas with different shapes. A significant increase of gain with frequency and relatively stable gain at higher frequencies were observed in most of the printed antennas. This tendency of gain was quantified in the UWB band in relation to Friis's transmission equation [57] as follows.

According to Friis's law [58], the power received by an antenna is given by

$$P_R = P_T \frac{G_T G_R \lambda^2}{4\pi r^2} = P_T \frac{G_T G_R c^2}{4\pi r^2 f^2}, \tag{2.1}$$

where $P_R$ is the received power, $P_T$ is the transmitted power, $G_T$ and $G_R$ are transmitting and receiving antenna gains respectively, $\lambda$ is the wavelength, $f$ is the frequency, $c$ is the speed of light and $r$ is the distance between two antennas. For UWB transmission, the equation can be rewritten as:

$$dP_R(f) = \frac{c^2}{4\pi r^2} P_T(f) \frac{G_T(f) G_R(f)}{f^2} \tag{2.2}$$

We need to integrate over frequency band to find the total received power

$$P_T = \int dP_R(f) df \tag{2.3}$$

and the effective isotropic radiated power is defined as :

$$EIRP(f) = P_T(f) G_T(f) \tag{2.4}$$

where $G_T(f)$ is the peak gain of the antenna. In order to follow the regulatory limits imposed by the FCC and other regulatory bodies (shown in Figure 2.1) this $EIRP$ should be constant. This means that the product $P_T(f)G_T(f)$ should be constant. In most of the printed antennas the gain increases significantly with frequency. As a result the transmitter consumes more power from the source than a system with a frequency-flat antenna system for the same received power.

This increasing gain causes another challenge for both UWB technologies (DS-UWB and MB-OFDM) in maximising the dynamic range of the link while still meeting the very low FCC transmit power threshold. Due to the wide spectrum of UWB, a frequency-dependent tilt severely compromises the dynamic range of the link. Since the RF attenuation increases with frequency, the wider the frequency band the more tilted the received spectrum and the

more dynamic range is lost to receive equalisation or transmit pre-distortion. In this scenario an antenna with a flat gain response at the transmitter and an antenna with a flat aperture at the receiver will be ideal. In this work the possibility of transforming a printed monopole antenna into a flat-gain antenna is explored. Various configurations are presented in Chapters 3, 4 and 5 of this thesis to aim for a flat antenna gain. Chapter 3 explains the novel techniques used to enhance the gain over a broad range of frequencies. In most UWB communication scenarios, a high-gain antenna with a reasonable field of view is highly desirable.

The regulatory EIRP constraints require power to be decreased when using high-gain directional antennas in transmitters but there is no such restriction at the receive side. Directional high-gain antennas are always desirable for UWB communication [57]. These antennas are capable of reducing emission in undesirable directions and potentially reduce clutter and enhance the system performance. The low gain of UWB printed antennas is a severe limitation in the lowest three mandatory modes of MB-OFDM systems (3.1 GHz to 4.674 GHz). The gain of typical UWB printed antennas is 0 dB to 1 dB at these frequencies. To get a good signal-to-noise ratio (SNR) in such a system we can either reduce the noise or increase the transmitted power. Reducing noise means additional hardware complexity, and designing a low-noise amplifier (LNA) with UWB bandwidth is not an easy task. Increased transmitted power is regulated by EIRP limits; an other way is to enhance the carrier by enhancing the gain of the antenna.

In Chapter 3 the concept of proximity coupling is introduced for printed antennas. This concept is based on the surface-wave suppression techniques used in microstrip patch antennas in [59] and [60]. A significant gain enhancement over the UWB band is achieved with proximity-coupled slot radiators. A complete design guideline, hardware verification and comparison with conventional PCMA is presented. Chapter 4 presents surface-mounted short TEM horns with relatively high and flat gain. Chapter 5 targets the design of reflectors for UWB printed antennas while Chapter 6 presents the work on slot antenna integration with high-gain short horns.

### 2.5.3 Angular Stability of UWB Antennas

The UWB printed or planar antennas are considered as the equivalent of slim linear monopoles. The traditional Hertzian Dipole [61] is shown in Figure 2.3.

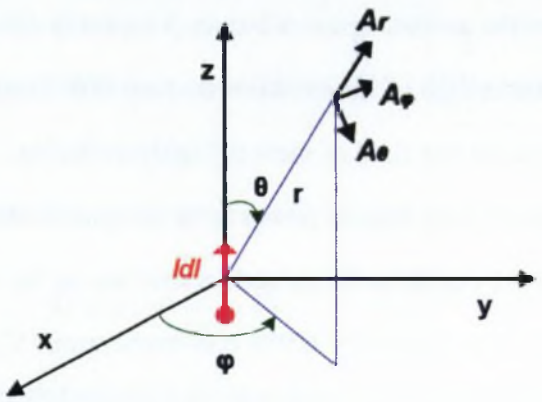


**Figure 2.3:** Hertzian Dipole.

The Hertzian Dipole is a dipole whose length $dl$ is much smaller than the wavelength (i.e. $dl < 50$). Besides, it has zero thickness. As shown in Figure 2.3, the dipole is positioned symmetrically at the origin of the coordinate system and oriented along the z -axis. The infinitesimal dipole is equivalent to a current element $I_0 dl$. Since it is very short, the current is assumed to be constant. Although infinitesimal dipoles are not practical, they are utilised as building blocks of more complex geometries.

The current in the dipole element is given as $I(t) = I_m e^{jwt}$ where $I_m$ is the maximum current and $w$ is the angular frequency. This current radiates an electromagnetic wave of the form $E(r,t) = E(r).e^{jwt}$ and $H(r,t) = H(r).e^{jwt}$. In a spherical coordinate system the field components are represented as $E(r) = (E_\phi, E_\theta, E_r)$ and $H(r) = (H_\phi, H_\theta, H_r)$. With a traditional solution of Maxwell's equation given in [62] and [2] one can get the non-zero field solutions.

**Radiation Intensity**

The radiation intensity $U$ is defined as the power $P$ per solid angle $\Omega$.

$$U = \frac{dP}{d\Omega} . \tag{2.5}$$

In the case of Hertzian dipole it turns out to be

$$U = \frac{\eta I^2 sin^2(\theta)}{8} \left(\frac{\delta l}{\lambda}\right)^2 . \tag{2.6}$$

The radiation patterns are independent and strongly dependent on frequency. This dependency leads different spectral components in a UWB signal to radiate in different directions with varying field strength. This situation is explained in more detail in [63] for dipole and discone antennas. Detailed frequency-dependent field patterns for various antenna configurations at different frequencies are plotted in Figure 2.4. This collection of radiation patterns is taken out from Chapter 9 of [2].

The variation of pattern causes a degradation of gain in the main beam direction. This in turn creates a problem in pulse transmission and the line-of-sight (LOS) scenario. In order to have a good temporal response of pulses a flat-gain transmitter antenna is highly desirable. A complete statistical analysis of antenna gain and group delay was carried out in [64]; these parameters play a critical role in the pulse-preserving capabilities of ultra-wideband antennas. Two parameters, the fidelity factor and the pulse-width stretch ratio (SR), were considered in those studies. Analytical results shows that Fidelity drops from 0.9867 and SR results increase from 1.202, with larger variations of the gain and the group delay for UWB antennas operating in the band 3.1 GHz to 10.6 GHz. Communication scenarios require radiated waveforms of constant shape in every direction from the transmitting antenna. The directions not only include directions in the azimuth plane but also directions off the azimuth plane as well. The techniques

presented in Chapter 3 help to solve the problem of variable gain encountered in most of the printed antennas available in the literature. The concept enhances the gain in the UWB region and make gain nearly constant over the UWB band.

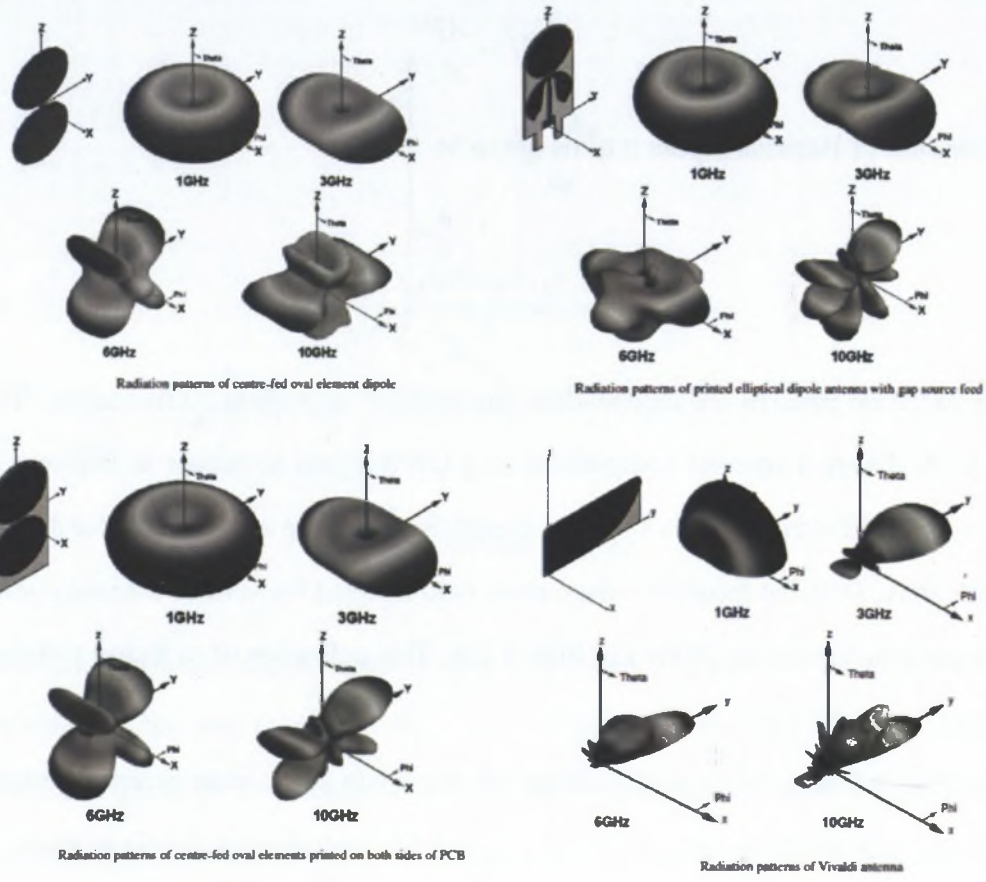


**Figure 2.4:** Radiation Patterns of various printed and planar configurations at different frequencies [2].

### 2.5.4 Developments in Ultra-wideband Horn Antennas

A horn is widely used as a feed element for large-reflector radio astronomy antennas used in satellite tracking and communication [62]. When broadband or ultra-wideband (UWB) horn antennas are required, ridges have been added to the waveguide transition region and the flare region [65], [66], [67]. In [3], an E-sectoral double-ridged horn antenna was demonstrated

for wideband operation. A detailed investigation on a 1 to 18 GHz broadband double-ridged horn antenna was reported in [68]. An improved design of the double-ridged horn antenna was presented by Rodriguez [69], showing that a good single radiation beam is maintained for the frequency range from 1 to 18 GHz. Some commercial designs of horn-based UWB antennas are shown in Figure 2.5. Figure 2.5(a) is a wideband commercial horn available from *Q-par Angus Ltd.* This horn has a physical aperture of $119 \times 86$ mm and a physical length of around 119 mm. It is capable of operating from 2 to 18 GHz with a minimum gain of 7 dBi, which rises up to 14 dBi at 18 GHz. Its VSWR is less than 2.5:1. Another miniaturised version of horn from the same company is shown in Figure 2.5(b). This version has a $96 \times 90$ mm physical aperture and the physical length is 148 mm. The gain variation of this horn is greater. It varies from 1.3 dBi to 13 dBi within 1 GHz to 18 GHz bandwidth. Its VSWR is also less than 2.5:1. More details of the horns from *Q-par Angus Ltd.* are available from [70]. Most of the ridge-based broadband horns needs a coaxial-to-waveguide transition at the feed point. A typical example of a transition is shown in Figure 2.5(c). As a recent development, printed UWB horn is presented by *Next-RF*. Their model 310C horn antenna meets the following specifications: usable frequency range 2 GHz to 10 GHz, optimised for 3 GHz to 10 GHz, matching: VSWR better than 2:1 ($f > 2.2$ GHz), gain: +6 dBi at 3 GHz; +9 dBi at 6 GHz; approximately constant aperture and linear phase.

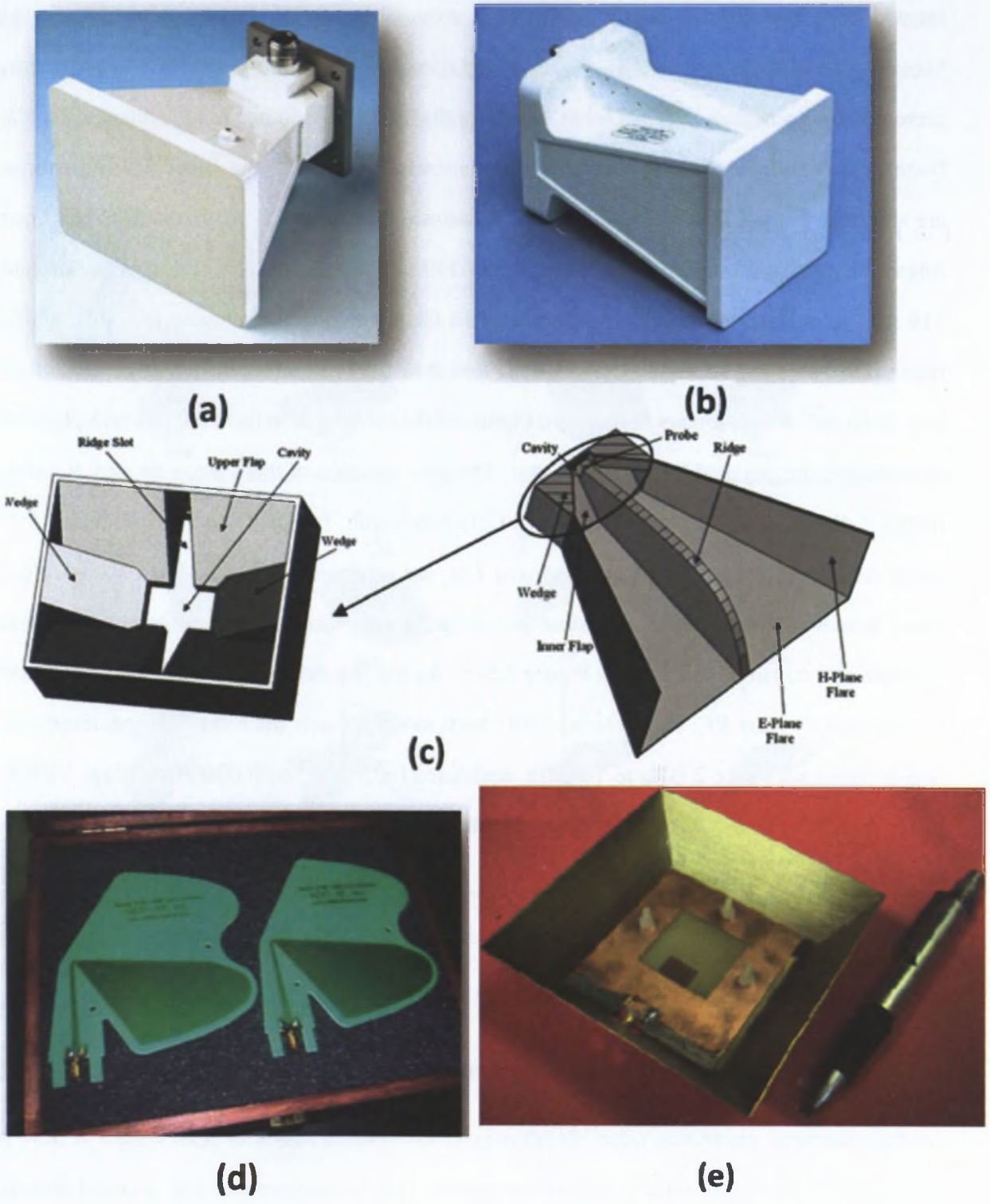


**Figure 2.5:** (a) Model WBH2-18: 2 to 18 GHz Wideband Horn from Q-par Angus Ltd. (b) Model WBH1-18S: 1 to 18 GHz Miniaturized Single Polarization Horn from Q-par Angus Ltd. (c) Typical feed transition for quad- and dual-ridge horn [3] (d) Next-RF's 310C UWB Horn Antennas (e) Surface-mounted short horn (SMSH).

Chapter 6 of this thesis presents a surface-mounted short horn (SMSH), fed using a slot antenna as shown in Figure 2.5(e). The concept of the short horn (SH) was first introduced in [71], [72] for achieving high gain from microstrip antennas. Furthermore, the performance and effectiveness of the short horn was evaluated for linear and circular polarisation in case of dielectric resonators and dielectric resonators over patch antennas [73], [74], [75], [76]. This research work is an extension of the short horn concept over the UWB band. Work is in an initial stage and more research needs to be done in future to stabilise the radiation patterns, and to assess pulse and phase responses. The SMSH is optimised from 2.9 GHz to 18.39 GHz for a VSWR of less than 2:1. The minimum gain of around 9.15 dBi at 4 GHz. It rises to 14.53 dBi at higher frequencies. The aperture dimensions are $93 \times 93$ mm while the physical length is 35 mm. The feed arrangement is quite simple compared to the transitions needed in the feeding of dual- and quad-ridge horns. The proposed horn does not have high power-handling capabilities because of the microstrip feed arrangement, and the radiation pattern is not stable at higher frequencies.

## 2.6 UWB Periodic Structures: A Possibility of Reflector Design

After the approval of the UWB band by the FCC in 2002, there has been a surge in research addressing UWB printed and planar antennas as outlined in the previous sections. These antennas have small gain at the lower frequencies and that is not desirable for some systems as noted in previous sections. Apart from these issues another critical aspect is the integration of printed antennas with real-world commercial devices. The near-field interactions between the antenna and the device can degrade the impedance performance of printed antennas and they will no longer be omni-directional after integration. These near-field interactions are due to the metallic conducting parts in the close vicinity of antennas [77] or lossy materials like

the earth's surface or human tissues. According to the theory an antennas works properly only when the radiation generated by the antenna and that reflected back by other parts are in phase. This happens when the distance between the antenna and the conductor plane is a multiple of one fourth of the working wavelength. In compact devices like GPR hand-held instruments, DVD players, HDTV, laptops or portable hard disks the flexibility of having a space of one fourth of the working wavelength is limited. In UWB antennas, it is impossible to maintain a $\lambda/4$ gap over a wide band. A suitable reflector structure capable of giving in-phase radiation without such a large gap is highly desirable. This will not only avoid the destructive reflection but also increases the gain by reflecting power otherwise going in the backward direction. This increase in gain is highly desirable in many UWB communication systems. In the design of reflectors or surfaces capable of giving in-phase radiation, periodic structures emerge as the prime candidate. In the recent past these structures have demonstrated the potential of creating a perfect magnetic conductor (PMC) with in-phase reflection enabling efficient radiation from antennas placed close to an electromagnetic bandgap (EBG) ground [78]. In addition, by forbidding the propagation of electromagnetic (EM) waves in certain frequency bands, these configurations can be used to block the propagation of waves and/or guide them in a desired direction [79], [78]. These structures exist in 1D, 2D and 3D periodic arrangements and are capable of producing a bandgap, which is suitable for in-phase reflections. However, mostly periodic structures available in the literature have small bandwidths. In the recent past rapid growth of research in this area led to improved designs suitable for dual-band and broadband applications. The structures with metallic vias or 3D complex geometries are not suitable for low-profile applications because they add design complexity and bulkiness to the systems. Frequency Selective Surface (FSS) have proven to be a useful periodic arrangement for printed implementations with no vias through to the ground, and they are more favourable for current applications.

### 2.6.1 Frequency Selective Surfaces

Historically, the idea of a FSS may be first found in a patent issued by G. Marconi and C. S. Franklin in 1919. In that patent they noted that for certain frequencies the reflection from a reflector made of wire grids was much higher if the elements composing the grid are resonant. Moreover, they also noted that it is possible to vary the response from the grid by modifying some geometric parameters of the wires. According to [80] the principle of FSSs re-emerged at the end of the Fifties and at the beginning of the Sixties, thanks to W. F. Bahret and E. M. Kennaugh who first imagined some new applications. They were followed by B. A. Munk who issued a classified patent in 1968, re-issued in 1974 for public release, concerning a new type of FSS based on a shape which was called four-legged.

Development of FSSs started with the design of radomes for antennas. A radome should provide protection to the antenna without interfering with the normal functioning of the antenna. Therefore radomes need to allow signals in the operating frequency range of the antenna to pass through while keeping out other signals. Thus a radome is a frequency selective surface (FSS). In reflecting back out-of-band signals a FSS can produce a weak reflected signal in the backscatter direction while producing a strong reflection in other directions. This reduces the Radar Cross Section (RCS) of antennas and is particularly useful for antennas mounted on military aircraft. Various examples of FSSs available in the literature include arrays of dipoles, slots, loops and other geometries. These FSSs are categorised into four sub-groups. The first group shown in Figure 2.6a consists of N-poles or centre connected such as dipoles, tripoles, square spirals. Figure 2.6b shows the second group, which primarily consists of looped types, such as circular, square and hexagonal loops. Figure 2.6c represents the third group known as patch type while Figure 2.6d shows the mixed FSS, which usually have a combination of two different elements.

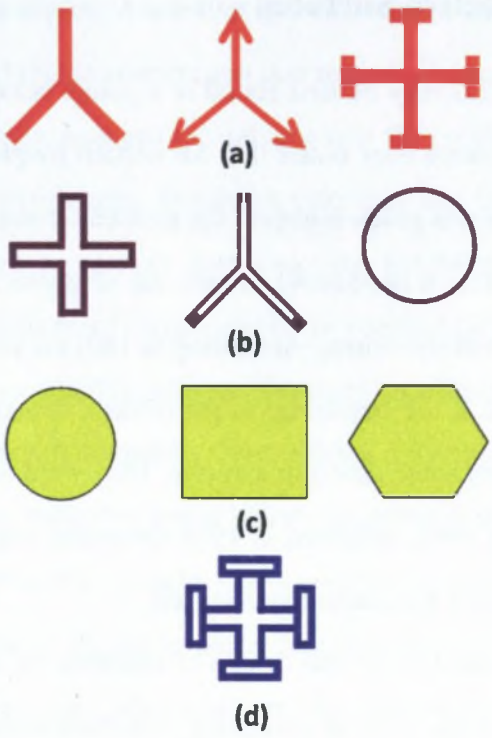


**Figure 2.6:** Various available subgroup unit cells (a) N-pole (b) Loop type (c) Patch type (d) Mixed .

Each of these designs has some advantages and disadvantages. A combination of any such single element over a substrate acts more or less as a spatial filter. Figure 2.7 shows different periodic arrangements of unit cells capable of providing low-pass, high-pass, band-stop and band-pass reflections. Repeated patterns of unit cells have frequency-dependent behaviour exploiting the resonance effects of a planar periodic layout along the surface. In particular, stop-band FSSs are usually composed of several metallic patches of arbitrary shape printed on a dielectric substrate. Pass-band FSSs are generally fabricated by creating apertures in a metallic plate. In this thesis, the focus is primarily on stop-band and pass-band reflectors. In order to design a reflector, stop-band behaviour is more appropriate, while the multi-layer design demonstrated in Chapter 5 shows the use of pass-band behaviour for the first layer and stop bands on the subsequent layers of the FSS screen. Apart from the magnitude response of the FSS the phase

of the reflecting signal plays a critical role in maximising the gain of the antenna in the main beam direction. Antennas on periodic ground surfaces like a mushroom-like EBG surface and Uni-planar compact photonic band-gap (UC-PBG) surfaces [78] were demonstrated in the past for narrowband designs.

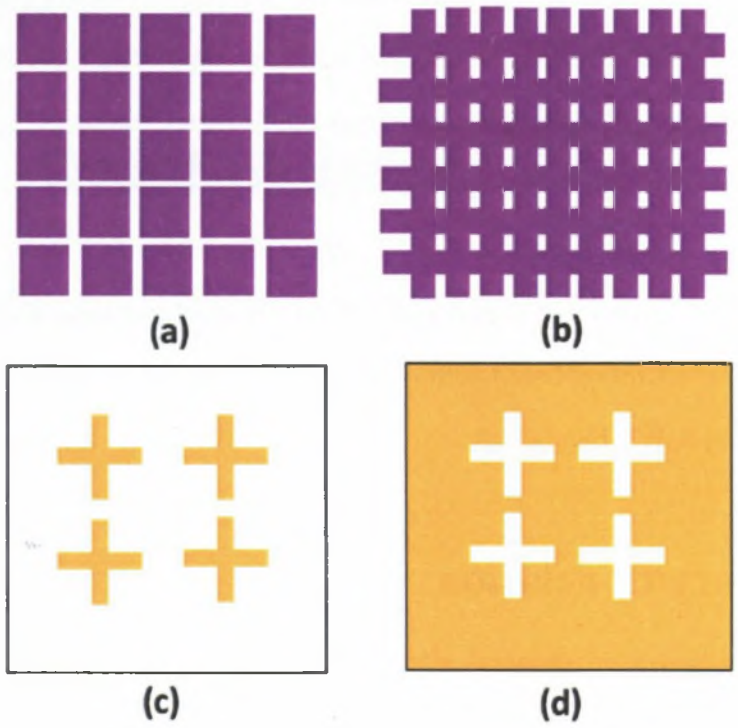


**Figure 2.7:** Different FSS configurations acting in different filter configurations.

FSS configurations have been extensively studied in the past as replacements for narrowband EBG and UC-PBG surfaces. These FSSs also have narrowband or multi-band [78] behaviour but, due to the printed nature of the structure, stacking different surfaces gives the possibility of achieving broadband behaviour. In [81], a reconfigurable printed dipole array is examined in the presence of a multi-layer FSS. The FSS is positioned in the ground plane of a reflector array, aiming to achieve broadband operation by controlling the phase of the reflected wave. In some recent articles a FSS is used as a backing reflector and for extending the frequency range

of usability. In another wideband application, reported in [82], a FSS has been sandwiched between the antenna and the ground plane, providing an additional reflecting plane for the most critical higher-frequency band. Most of the designs published have impedance bandwidths of less than 40%, and design of such a FSS with a desirable phase over a 110% impedance bandwidth is really a challenging task. The maximum impedance bandwidth published so far to the best of my knowledge is 52%; that is achieved with the combination two different patch elements over a single unit cell, namely a square loop and a crossed dipole [83]. The configuration presented in [83] gives no phase information and antenna testing scenarios. Nevertheless, this design motivated the research presented in Chapter 5 where two different FSS configurations are presented and tested with UWB antennas. The dual-layer and multi-layer FSSs presented in Chapter 5 have an operating bandwidth of over 130% with the desirable linearly decreasing phase over the whole UWB bandwidth.

## 2.7 Summary/Conclusion

Various systems available for UWB applications were discussed and different applications targetting the UWB bandwidth were highlighted in previous sections. Several printed and planar monopole antennas and slot antennas were explained in detail. The problems associated with a flat gain for UWB antenna were discussed and several complications in term of MB-OFDM systems, LOS, gain equalisation, multimedia scenarios and GPR communications were highlighted as the theme of the work presented in coming chapters.

# Chapter 3

# Surface-Wave-Enhanced, Proximity-Coupled Printed Monopole Antennas

## 3.1 Introduction

This chapter examines the angular and spectral behaviour of printed monopole antennas. The variation of gain with the look-angle of an antenna was studied in Chapter 2 and techniques to enhance the gain stability over a wide bandwidth are proposed in this chapter. At first the patterns of conventional dipoles are considered in this study and then more emphasis is given to printed ultra-wideband antenna (UWB) configurations. A detailed study and the problems associated with angular and spectral behaviour are presented in Chapter 2. This Chapter focuses on a solution to the problem with gain instability. From previous studies of the UWB bandwidth and look angle, the effective available bandwidth of a system is found to be highly sensitive to the angular behaviour of the antenna at each end of the link. It was demonstrated in the past that the bandwidth was severely limited in some directions, and careful orientation of the an-

tennas is required to achieve full UWB operation for a range of antenna designs [84]. This is particularly important for indoor communications systems such as wireless personal-area networks and indoor UWB connectivity where dense multi-path propagation gives rise to a wide range of angles of arrival [85–87]. In the absence of an ideal isotropic radiator, a transmitter using an omnidirectional antenna is expected to radiate the signal in all directions within the azimuthal plane with constant gain and group delay such that the wavefronts have near uniform intensity and planar shapes. In practice, however, this condition is sometimes violated by UWB antennas, causing look-angle dispersion [84]. Instead of analysing the frequency and look-angle distortion separately to solve the problem, novel configurations of angular and spectral stable UWB antennas are proposed in this chapter. Conventional printed circular monopole antennas (PCMA) were considered by the candidate as a reference and various configurations with microstrip and CPW feeds were explored. Ultra-wideband (UWB) systems are widely categorised into two types: (a) pulse-based systems transmitting pulses that occupy the UWB bandwidth and (b) carrier-based systems that rely on multiband orthogonal frequency-division multiplexing (MB-OFDM) [88, 89]. A more detailed explanation of these systems is given in Chapter 2. Several UWB planar monopole antennas have been investigated during this PhD project and by other authors [4, 5, 28, 33, 90–96] for FCC-based UWB systems operating from 3.1 GHz to 10.6 GHz. Most of these antennas have very wide impedance bandwidths and nearly omnidirectional radiation patterns in the azimuth plane. All antennas exhibit a significant directivity variation with frequency, typically a seven-fold increase from the lowest frequency to the highest in the FCC UWB frequency range (3.1 GHz - 10.6 GHz). To get a better understanding of the trends, a simple example of a printed circular monopole antenna (PCMA) [4] is studied. Its gain variation mentioned in the reference was evaluated theoretically, and stability in gain is then evaluated experimentally. With the concept of surface waves and proximity-coupled metallic cavities and patches the enhancement in gain is demonstrated in this chapter. The results of this chapter illustrate the phenomenon of proximity coupling and highlight its consequences

without loss of generality.

### 3.1.1 Chapter Contributions

The main contributions of this chapter are:

- The possibility of proximity coupling is identified and the use of surface waves demonstrated in the literature for patch antennas is extended to monopoles for enhancing the gain.
- A wide angular and spectral stable printed microstrip-fed PCMA is presented.
- The performance of the proposed printed proximity-coupled monopole antenna is compared with conventional printed monopoles.
- A simple CPW-fed thin antenna suitable for most MB-OFDM systems with significant enhancement in gain in the lower UWB region is presented.
- The proposed proximity coupling enhances the gain while maintaining the UWB characteristics of printed antennas.
- Based on the concept of proximity coupling, an array of metallic cavities for controlling the gain in the whole UWB bandwidth is demonstrated.

This chapter is organised as follows. Section 3.2 presents a brief overview of work related to the highlighted problems in term of directivity, look angle or angular disposition. In Section 3.2, conventional dipole and printed UWB antennas are discussed. Section 3.3 shows the implementation of proximity coupling on printed circular monopole antennas and the simulation results to demonstrate the resulting enhancement in gain stability. Section 3.3.2 validates the theoretical results of the previous section with experimental results for a microstrip-fed PCMA. Section 3.4 proposes a thin configuration of a UWB antenna, following the concept introduced in previous

sections. Optimisation of thin UWB antennas and a complete parametric analysis is carried out in Section 3.4.2, which is followed by experimental verifications in Section 3.4.4. Sections 3.4.4 and 3.4.5 discuss frequency-domain and transfer-function characterisation. Section 3.4.6 is devoted the performance of antennas with FCC-approved UWB regulations. Further, based on the concept of proximity coupling demonstrated in Sections 3.3 and 3.4, an array of cavity slots is presented in Section 3.5, which shows more control on gain over the UWB bandwidth. It is followed by conclusions in Section 3.6.

## 3.2 Related Work

### 3.2.1 Conventional Dipole Antenna

Traditional antenna characterisation is focused on fundamental antenna parameters related to the input characteristics and radiation patterns [63]. While this is usually sufficient for narrow-band antennas, several issues arise in the case of UWB antennas that merit deeper analysis. A detailed analysis of the UWB characteristics of dipole and discone antennas are presented in [63]. According to the authors the dipole is inherently a narrowband antenna but is representative of many other more complex antenna shapes. Also, its fields are analytically tractable and well understood. On the basis of its compact, simple and economical design, the dipole has been suggested for use in short-range UWB transmission. For a vertically oriented dipole, the elevation-plane far-field radiation pattern can be expressed in terms of the angle of elevation $\theta$ and frequency f as:

$$F(\theta, f) = \frac{\cos\left(\frac{kl}{2}\right) - \cos\left(\frac{klsin\theta}{2}\right)}{\cos\theta}, \tag{3.1}$$

where $l$ is its length, $k = 2\pi/\lambda$ where $k$ is the wavenumber and $\lambda$ is the wavelength.

(Details of the field of a Hertzian Dipole and other few printed configurations are given in Chapter 2.) For a 0.1 m long dipole, the power radiation pattern varies significantly within the FCC-allocated UWB band (3.1 GHz-10.6 GHz). This is shown in Figure 3.1, where the normalised elevation-plane radiation patterns at four equally spaced frequencies within that band are plotted. An increase in operating frequency leads to higher directivity and increases the number of lobes. The directions of the lobes also change with frequency. This will cause variations of gain and in turn creates the serious problem of frequency-dependent antenna radiation in UWB communications.

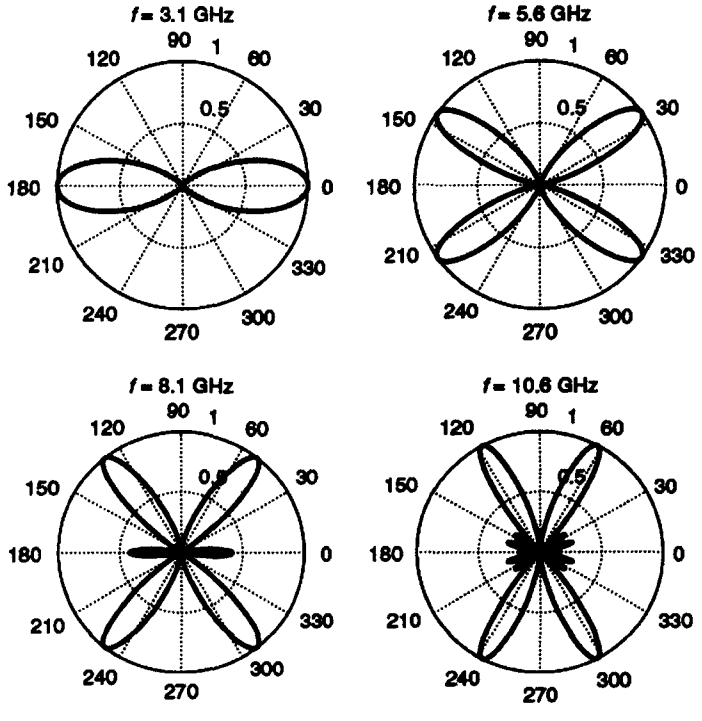


**Figure 3.1:** Normalised radiation patterns on the elevation plane at various frequencies (a) Vertical polarised dipole (b) Discone Antenna.

A concept of surface waves, controlled using parasitic patches or a resistive card around the microstrip patch antenna, was demonstrated by Rojas in [59, 60]. The only concern is that, in a microstrip patch, because of the full ground plane in the back, the surface-wave phenomenon is

more dominant but, in the case of printed monopole antennas where the ground plane is of limited size (restricted to just underneath the feed network), surface waves are not as strong as those in printed patches. Any parasitic structures can be excited using proximity coupling instead of surface waves. In this chapter, a proximity-coupled mechanism is presented for enhancing the performance of antennas in a single direction ($\pm 90^0$) over a large angular bandwidth. This concept is tested for the popular UWB printed circular monopole antennas (PCMA) [4]. Theoretical and experimental validation of the proposed structures is included in this chapter. This work studies these effects on printed antennas. A detailed outlined of the proposed study is presented in the next section. The variation of gain as a function of angle is considered. An effort is made to stabilise the gain and provide angular stability to antennas used for UWB communication.

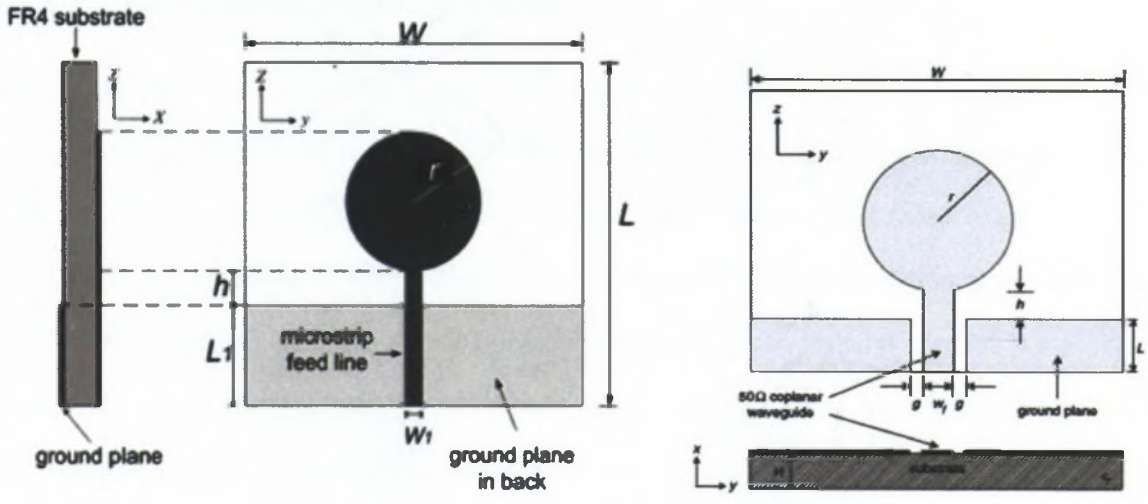


**Figure 3.2:** (a) Microstrip-fed [4] and (b) CPW-fed [5] printed circular antennas .

### 3.2.2 Printed Circular Monopole Antennas (PCMA)

Printed antennas are usually fed using microstrip or co-planar transmission lines. The most popular configurations of printed antennas are circular monopoles because of the ease of impedance

matching over a wide range of frequency. These kinds of printed antennas have been well explored. Both microstrip and CPW-fed configurations are easily available in the literature. One of the most popular is printed circular monopole antenna (PCMA). The configurations of microstrip-fed [4] and CPW-fed PCMA [5] are shown in Figure 3.2.

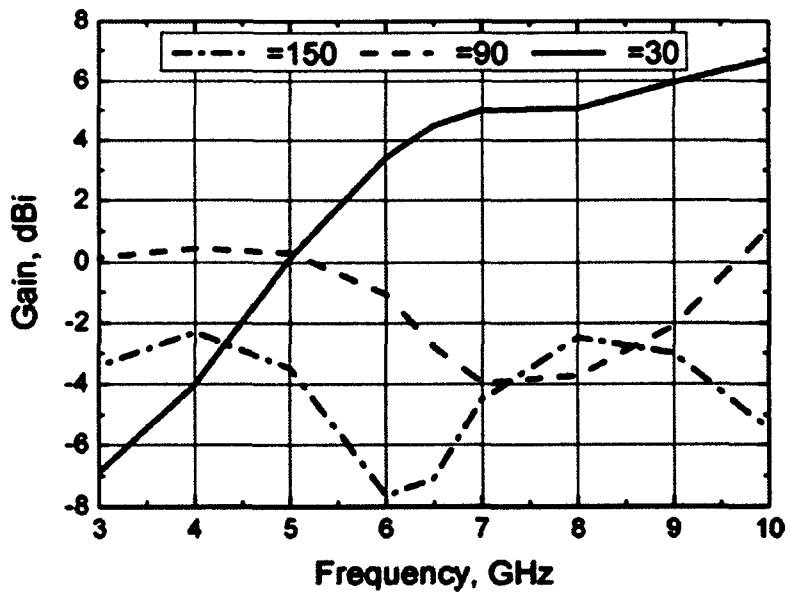


**Figure 3.3:** Gain of Microstrip-fed printed circular antennas for various theta directions.

As an example the demonstrated 10 dB return-loss (RL) bandwidth of a microstrip-fed antenna ranges from 2.78 GHz to 9.78 GHz while a CPW-fed counterpart yields return-loss bandwidth from 2.64 GHz to more than 12 GHz. A study of gain presented for a microstrip-fed PCMA shows an almost linear increase of gain with frequency. The maximum gain is in the direction where theta equals 90 degree for lower frequencies and it shifts to a 30-degree direction after 5 GHz. Figure 3.3 shows a picture of the gain variation presented in [4]. CPW-fed PCMA and other conventional printed monopole antennas have a similar trend of peak gain variation with frequency.

This chapter presents the technique of using proximity coupling to enhance and maximise the gain. To demonstrate the concept a constant-gain PCMA with a surface-wave-excited,

proximity-coupled, conductor-backed metallised, twin-slot radiator is described. The proposed antenna has an impedance bandwidth of more than 8.14 GHz, from 3.86 GHz - 12 GHz. It has an average gain of 5.5 dBi $\pm$ 1.5 dB over the complete bandwidth with broad radiation patterns in the XY plane.

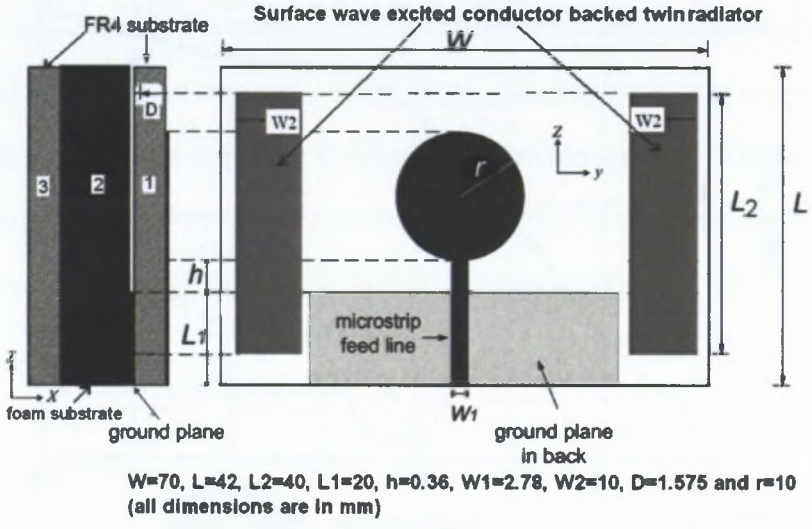


**Figure 3.4:** Constant-gain printed circular monopole antenna with surface-wave-excited, proximity-coupled (SW-PC), conductor-backed, twin-slot radiator.

## 3.3 Constant-Gain Proximity-Coupled Printed Antenna

An ultra-wideband antenna with uniform gain is presented in this section. The antenna operating bandwidth is from 4 to 12 GHz. The novel concept of multiple cavities with proximity coupling is used to enhanced the gain performance of the antenna. A complete parametric analysis and design guideline define the gain enhancement achieved over a broad range of frequency.

### 3.3.1 Antenna Design

The configuration and dimensions of the antenna are shown in Figure 3.4. The PCMA is designed on an FR-4 ( $\varepsilon_r$=4.4, D=1.575 mm) substrate that is supported by a 3 mm layer of foam followed by another 1.575 mm thick FR-4 substrate (no copper on either side). The dielectric substrates can support guided waves (surface waves) and the surface-wave power tends to increase for thicker substrates. The metallised twin-slots (W2=10 mm, L2=40 mm) in the top FR-4 substrate are created to enhance the gain of the PCMA at the lower end of the frequency band such that the gain of the proposed antenna over the complete bandwidth remains nearly constant. The slots are excited by the combination of surface-wave as well as proximity coupling by the near field of the PCMA and they radiate perpendicular to the monopole axis (z-axis) in a controlled fashion.

### 3.3.2 Theoretical Study of Gain and Comparison of Proposed Antenna with Conventional UWB PCMA

Variations in gain at lower frequencies of 3 to 8 GHz are compared with those for the PCMA in Figure 3.5 and Table 3.1. In case of PCMA [5], [4] the gain varies linearly with frequency and the maximum occurs at $90^0$ for lower frequencies up to 5 GHz and after that it shifts towards $30^0$.

In the case of a PCMA-SW-PC-conductor-backed, twin-slot radiator the maximum remains in the direction of $270^0$. This data also shows a significant increase of 4 to 5 dB in gain at the lower frequencies (3 to 8 GHz). To compare the gain flatness between a standard PCMA and the new SW-PC PCMA the average and the theoretical peak gain variation bandwidths with 2 dB and 3 dB are listed in Table 3.1. It indicates a significant improvement in 2 dB and 3 dB peak gain bandwidth in the XY plane ($\theta = 90^0$). Figure 3.5 demonstrates the theoretical gain equalisation of the PCMA achieved by the conductor-backed metallised twin slots.The use of

twin slots increases the gain between 3 GHz - 6 GHz and decreases it between 8 GHz - 10 GHz and above.

The experimental gain variation of the proposed antenna is compared in Figure 3.6 with both a standard PCMA on a FR-4 substrate and a PCMA on a composite substrate. The gain of the standard printed monopoles increases almost linearly with frequency. There is an improvement of approximately 0.5 dB in the measured gain of the PCMA when the standard FR4 substrate is replaced by a composite substrate. However, the gain still increases almost linearly from 0.5 dBi to 4.8 dBi as the frequency changes from 3 GHz to 6 GHz. The gain further increases from 4.8 dBi to 6.7 dBi with a lower gradient as the frequency changes from 6 GHz to 10 GHz. The proposed antenna has a nearly constant gain of 5.5 dBi $\pm$1.5 dB over a large bandwidth from 3 GHz to 10 GHz and above.

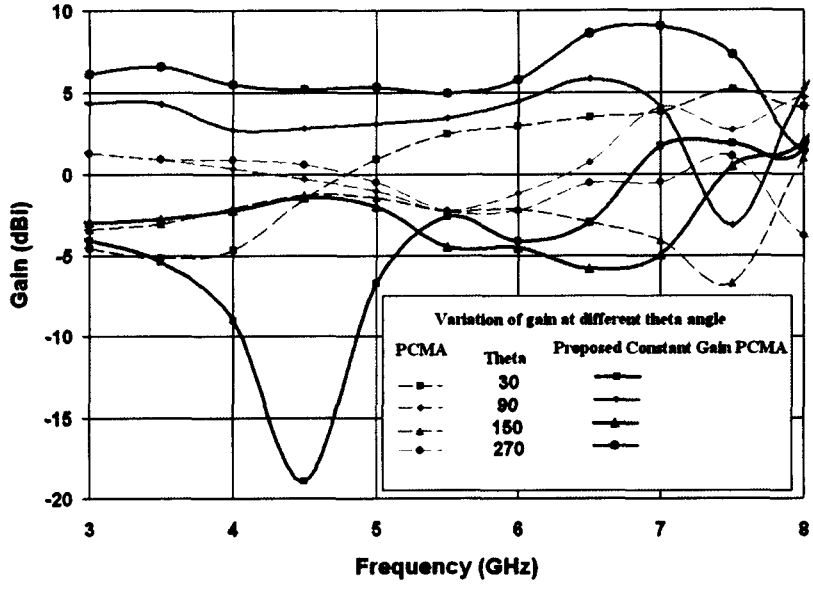


**Figure 3.5:** Constant-gain printed circular monopole antenna with surface-wave-excited, proximity-coupled (SW-PC), conductor-backed, twin-slot radiator.

**Table 3.1:** Theoretical Variation of Gain for Different Theta Directions for PCMA and Constant-gain PCMA with Surface-Wave Excited/Proximity-Coupled Conductor-backed Twin-slot Radiator.

| PCMA | Theta | $\pm 1dB$ | | BW | Avg. Gain (dBi) | $\pm 1.5dB$ | | BW | Peak Gain (dBi) |
|---|---|---|---|---|---|---|---|---|---|
| | | $f_L$ GHz | $f_H$ GHz | | | $f_L$ GHz | $f_H$ GHz | | |
| | $90^0$ | 3.0 | 4.2 GHz | 1.2 | 1.4 | 3.0 | 5.0 | 2.0 | 4.2 |
| | $270^0$ | 3.0 | 4.2 GHz | 1.2 | 1.4 | 3.0 | 5.0 | 2.0 | 4.2 |
| Proposed | Theta | $\pm 1dB$ | | BW | Avg. Gain | $\pm 1.5dB$ | | BW | Peak Gain |
| | | $f_L$ GHz | $f_H$ GHz | | | $f_L$ GHz | $f_H$ GHz | | |
| | $90^0$ | 3.0 | 4.2 GHz | 1.2 | 1.4 | 3.0 | 5.0 | 2.0 | 4.2 |
| | $270^0$ | 3.0 | 4.2 GHz | 1.2 | 1.4 | 3.0 | 5.0 | 2.0 | 4.2 |

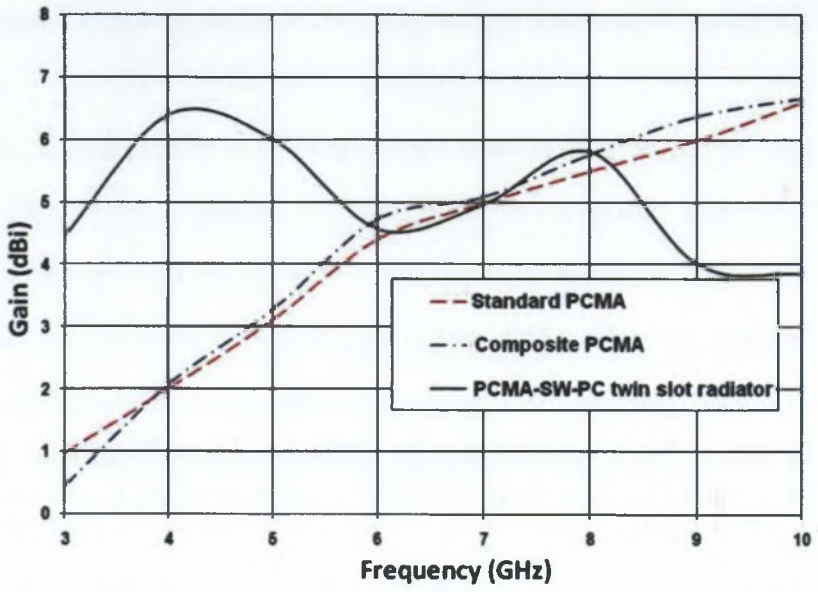


**Figure 3.6:** Constant-gain printed circular monopole antenna with surface-wave-excited, proximity-coupled (SW-PC), conductor-backed, twin-slot radiator.

### 3.3.3 Experimental Results

A photograph of the fabricated antenna is shown in Figure 3.7. After narrowing the pattern and field of view, a significant increase in the gain of the antenna and the minimum beam squint was achieved. The thickness of each substrate and the foam spacing are optimised to achieve a maximum impedance bandwidth. The performance of the surface-wave-excited, proximity-coupled (SW-PC), conductor-backed, twin-slot radiator is predicted using commercially available software (CST Microwave Studio). The theoretical impedance bandwidth for different PCMA configurations, shown in Table 3.2, indicates that the proposed antenna covers a wide band from 4 GHz to 10 GHz. Figure 3.8 shows the theoretical and measured reflection coefficients of the antenna.

**Table 3.2:** Theoretical impedance bandwidth comparison of different configurations of PCMAs

| **Configurations** | $f_L$ (GHz) | $f_H$ (GHz) | **Bandwidth** (GHz) |
|---|---|---|---|
| **PCMA** | 2.76 | 9.78 | 7.02 |
| **Composite PCMA** | 2.65 | 8.45 | 5.80 |
| **Constant-gain PCMA** | 4.00 | 10.0 | 6.00 |

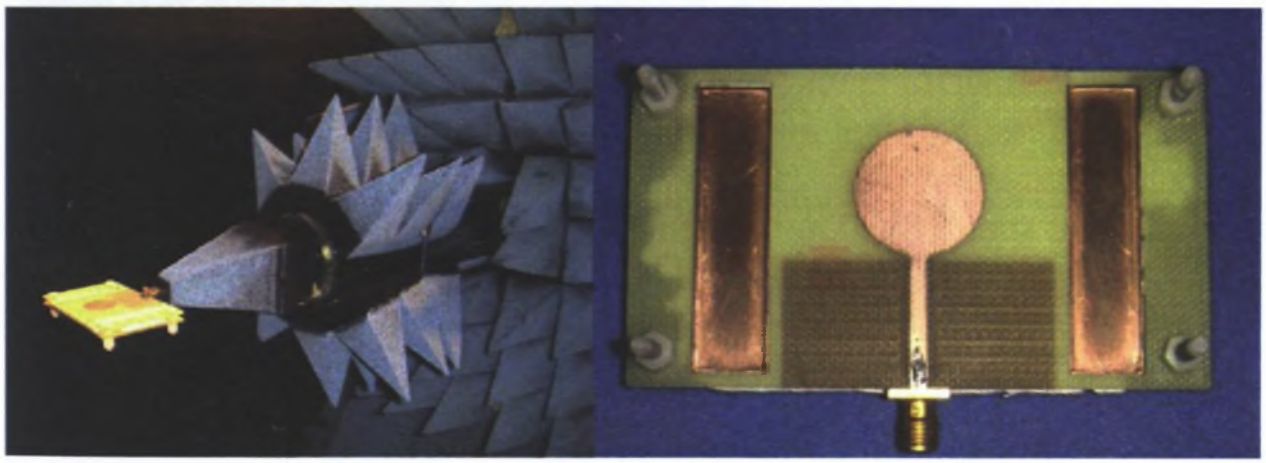

**Figure 3.7:** Photograph of printed circular monopole antenna with surface-wave-excited, proximity-coupled (SW-PC), conductor-backed, twin-slot radiator.

The theoretical 10 dB return loss bandwidth of the PCMA on the composite substrate is 7.25 GHz, from 2.72 GHz - 9.97 GHz. The presence of the twin slots shifts the lower limits of the return loss bandwidth to 4.0 GHz and the upper limit of the frequency band to 10 GHz, giving a 6 GHz theoretical bandwidth. However, the measured bandwidth is 8.14 GHz, from 3.86 GHz to 12 GHz. The slot dimensions can be further optimised to lower the minimum operating frequency. Figure 3.9(a) shows the measured azimuth radiation patterns of the new antenna at 4.0 GHz, 6.5 GHz and 9.0 GHz. Figure 3.9(b) shows that the twin-slot radiator narrows the figure-eight-pattern beam widths in the elevation plane at 3.0 GHz and 6.5 GHz, while the beam width increases at 9.0 GHz. Thus the directivity increases in the lower frequency range and decreases in the upper frequency range. Even in the elevation plane, the impact of the

printed monopole is evident through the appearance of a null along the axis of the monopole. The figure-eight radiation pattern of the twin-slot radiator remains relatively constant in the elevation-plane over a large bandwidth. The elevation pattern rotation is relatively insensitive to the operating frequency over a large bandwidth.

The next section describes a simple proximity-coupling concept, a printed, low-profile thin antenna consisting of a CPW-fed printed circular-disc monopole antenna (PCMA) and two metallic patches co-planar to the disc. This structure again improves the gain in lower frequencies of the 3.1 GHz-10.6 GHz UWB bands (where the gain is otherwise low) while maintaining a small gain variation and good impedance characteristics over the whole band.

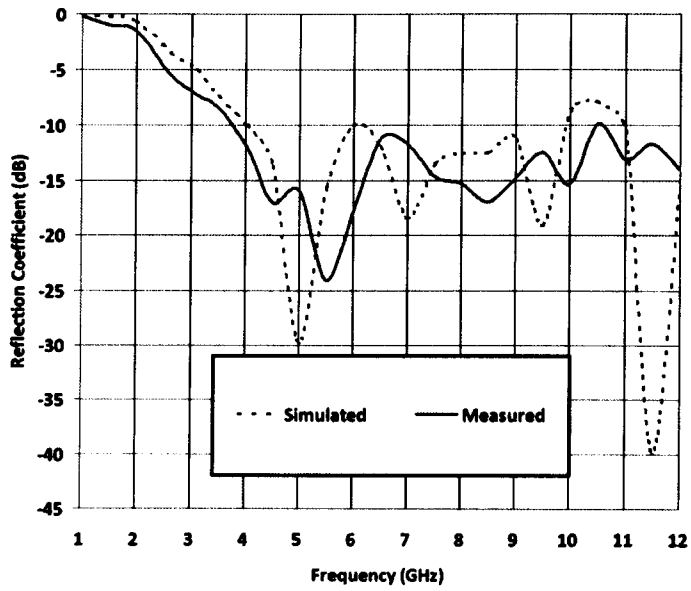


**Figure 3.8:** Simulated and measured reflection coefficients for high-gain PCMA with SW-PC conductor-backed, twin-slot radiator antenna.

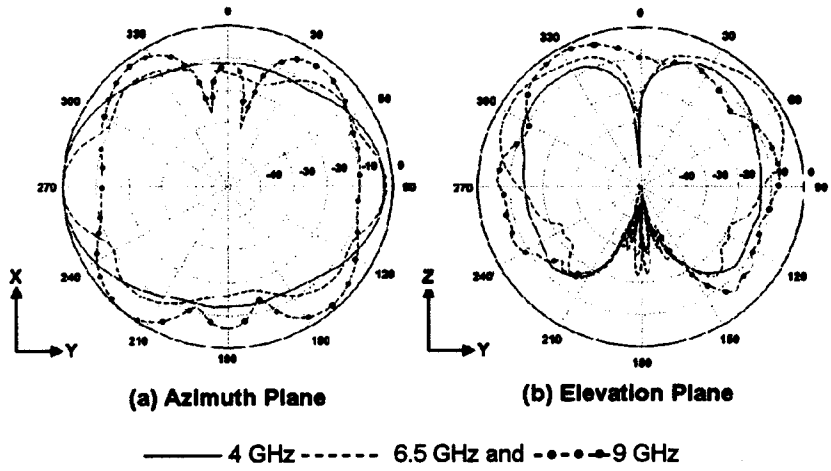


**Figure 3.9:** Measured radiation patterns at 4 GHz, 6.5 GHz and 9 GHz.

## 3.4 A CPW-Fed Printed Antenna with Constant-Gain Over a Large Bandwidth

This section discusses the complete design and parametric study of a gain-enhanced low-profile antenna (GE-LPA). From the initial design process to complete UWB characterisation of antenna is presented in this section.

### 3.4.1 Antenna Design

The geometry of the gain-enhanced low-profile antenna (GE-LPA) is shown in Figure 3.10. The optimum design parameters are: $L = 42$ mm and $W = 96$ mm. The antenna is printed on a 1.524 mm thick substrate with a dielectric constant ($\varepsilon_r$) of 2.33.

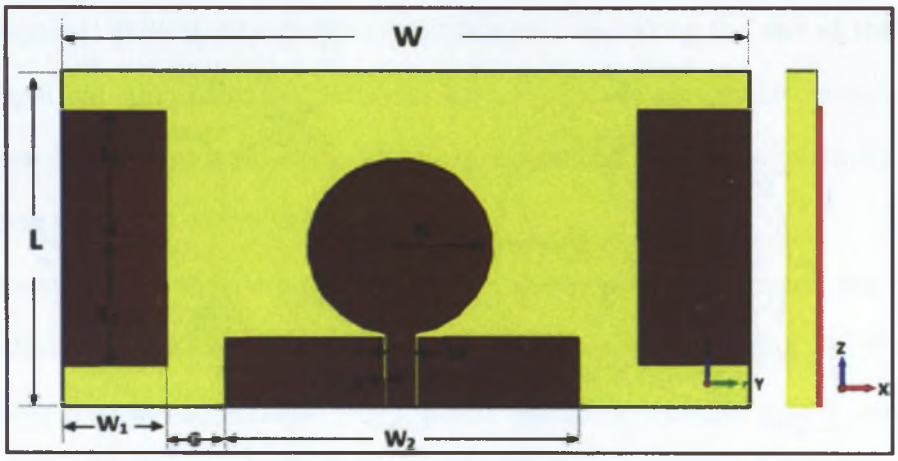


**Figure 3.10:** CPW-fed gain-enhanced low-profile antenna (GE-LPA).

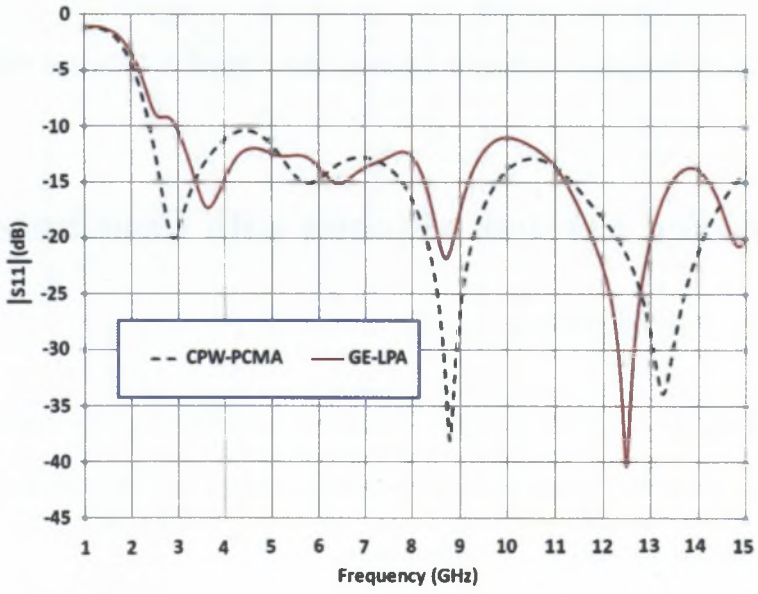


**Figure 3.11:** Theoretical reflection coefficient of the proposed GE-LPA and a conventional CPW-fed PCMA.

The antenna top surface is on the ZY plane. Two optimised rectangular metallic patches of equal dimensions are placed parallel to the monopole and on the same plane. The gap $G$ between the ground planes of the CPW-fed line and the rectangular patches is optimised for minimum reflection and maximum gain with minimum variation across the impedance bandwidth. A

complete list of design parameters is listed in Table 3.3. These parameters have been optimised for impedance bandwidth and gain. This study is explained in the next section. Figure 3.11 compares the theoretical reflection coefficients for the proposed antenna and a conventional CPW fed monopole. It is seen that, with unconventional optimised metallic patches on the top of the surface along with a conventional antenna structure, the lower cutoff frequency is shifted from 2.42 GHz to 3 GHz while the proposed antenna maintains a 10 dB return loss bandwidth from 3 GHz to 15 GHz.

**Table 3.3:** Optimised values of the designed GE-LPA

| **Parameters** | Values (All dimensions are in mm) |
|---|---|
| **W** | 96 |
| **L** | 42 |
| **R** | 12 |
| **L1** | 18 |
| **W** | 3 |
| **W1** | 20 |
| **W2** | 40 |
| **s** | 0.33 |
| **G** | 4 |
| **Substrate thickness** | 1.524 |

### 3.4.2 Parametric Analysis

A parametric study was carried out for all parameters of the antenna using the CST Microwave Studio [97] software package to maximise the bandwidth and enhance the gain. The metallic patches hold the key for gain enhancement as explained in the previous text. Parameters like

gap $G$, patch length $L1$, and patch width $W1$ have been considered for the study. A complete analysis of impedance bandwidth and gain has been carried out.

### Variation of The Gap-G

The gap $G$ between the CPW ground and metallic patches is one of the critical parameters in optimising the impedance bandwidth. These metallic patches have a strong effect on antenna matching.

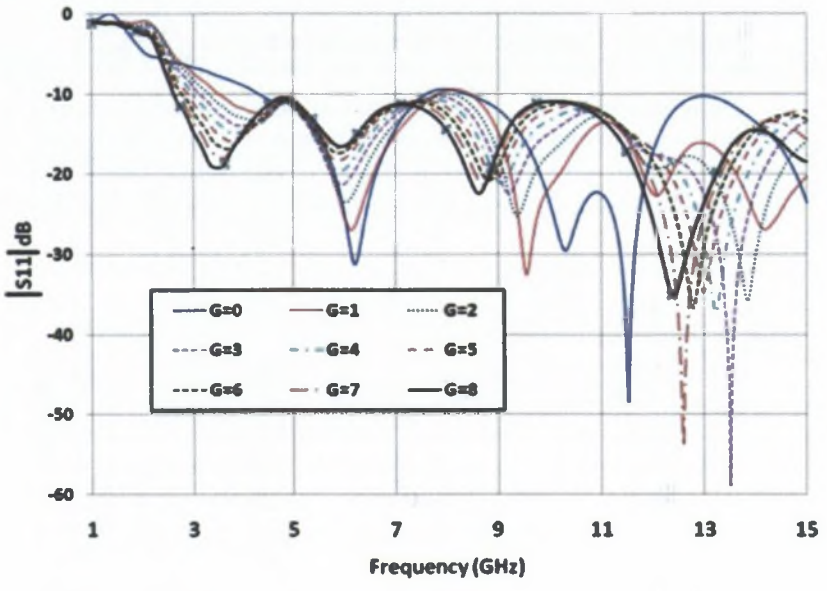


**Figure 3.12:** Input matching for different gaps $G$.

Figure 3.12 shows the variations of impedance match with gap $G$ when length $L1$ is fixed at 48 mm, which is equal to the length of the substrate, and $W1$ is fixed at 10 mm. The impedance bandwidth is improved by increasing $G$. For values of $G$ greater than 4 mm, the antenna impedance bandwidth meets or exceeds the FCC-approved band for UWB. It also shows that, with the addition of metallic patches, the lower limit of the antenna bandwidth shifts from 4.38 GHz to 2.61 GHz. Figure 3.13 shows the variation in bandwidth and lower cut-off with Gap $G$. It's clearly visible from Figure 3.13 that there is a slight variation in the impedance bandwidth

after $G = 2$ mm and the lower cut-off of 2.68 GHz is achieved at $G = 4$ mm. To minimise the size the value of $G$ is set to 4 mm. Next the length and width of metallic patches were optimised for gain, while maintaining the antenna bandwidth.

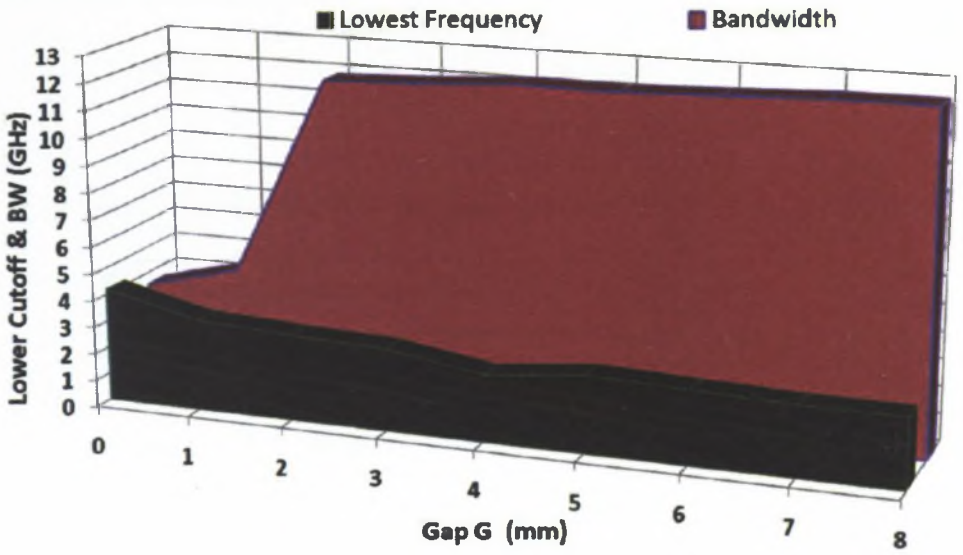


**Figure 3.13:** Antenna lower cut-off frequency and bandwidth for different gaps $G$.

### Variation of The Patch Length-L1

After changing the length of the metallic patches, a change in antenna gain is noticed. Figure 3.14 illustrates that the gain is enhanced as the patch length increases from 12 mm to 48 mm, for the considered frequencies (i.e. 3 GHz, 7 GHz and 10 GHz). For lengths above 36 mm, the gain decreases. This confirms that $L1 = 36$ mm is a good choice since the design aims to obtain gain enhancement. The impedance bandwidth variation with these heights is also examined. With changing height of the metallic patches, a change in antenna impedance bandwidth can be seen, especially across the lower UWB frequencies. Figure 3.15 shows that, when the parameter $L1$ of the patches is varied between 12 and 48 mm, the impedance bandwidth changes significantly. When $L1 = 36$ mm the bandwidth extends from 3.5 GHz to 15 GHz, while $L1 = 48$ mm yields

the maximum bandwidth from 2.78 GHz to 15 GHz.

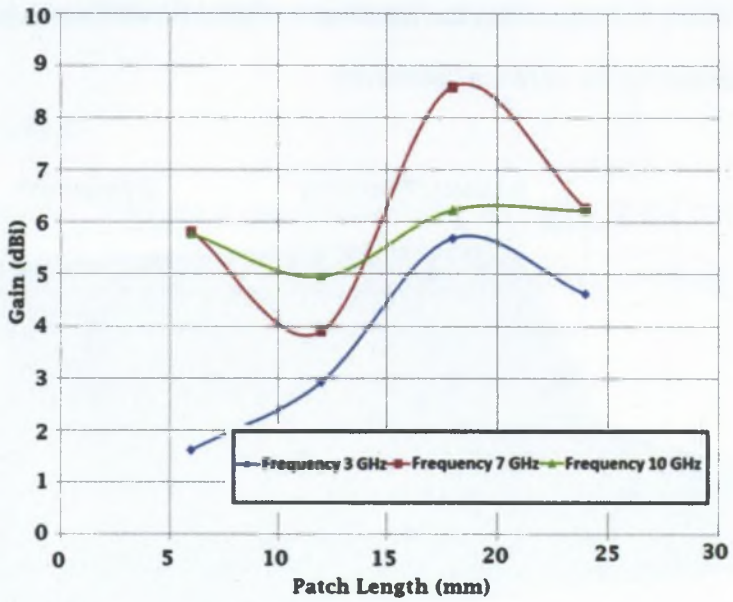


**Figure 3.14:** Antenna gain for different patch lengths $L1$.

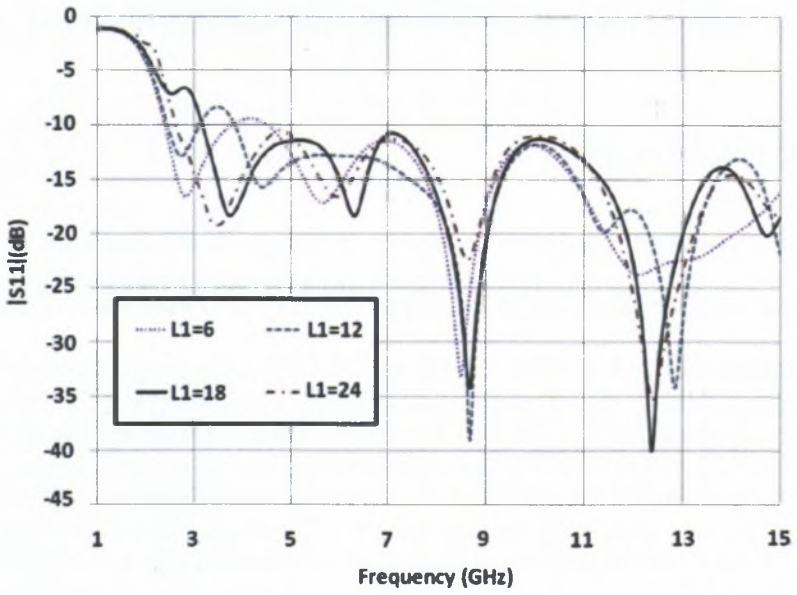


**Figure 3.15:** Input matching for different patch lengths $L1$.

**Variation of The Patch Width-W1**

The lower limit of the antenna impedance bandwidth is now 3.5 GHz and does not meet the FCC limit of 3.1 GHz. To meet this specification the lower frequency limit of the impedance bandwidth is reduced by optimising the patch width $W1$.

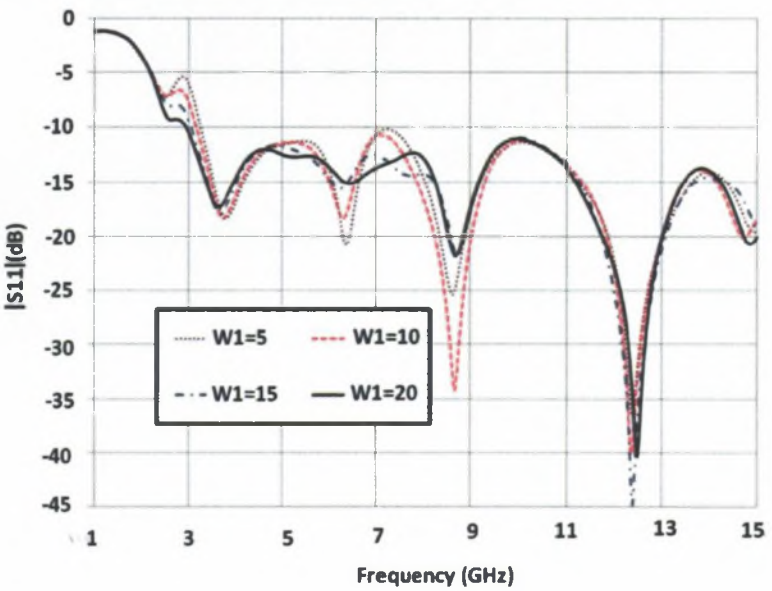


**Figure 3.16:** Variation in impedance matching with patch width W1.

It is clearly seen from Figure 3.16 that the lower frequency limit can be moved downward to 3 GHz, as required, without significantly disturbing the matching over the whole band. For W1=20 mm the value of 3 GHz is obtained. A further reduction in the lower frequency limit can be achieved at the cost of additional substrate area. Figure 3.16 shows the variation with width $W1$.

### 3.4.3 Surface Currents and Field Analysis for Proximity coupling

Figures 3.17 and 3.18 show the average current distribution of the proposed antenna as well as the CPW-PCMA antenna at 3 GHz.

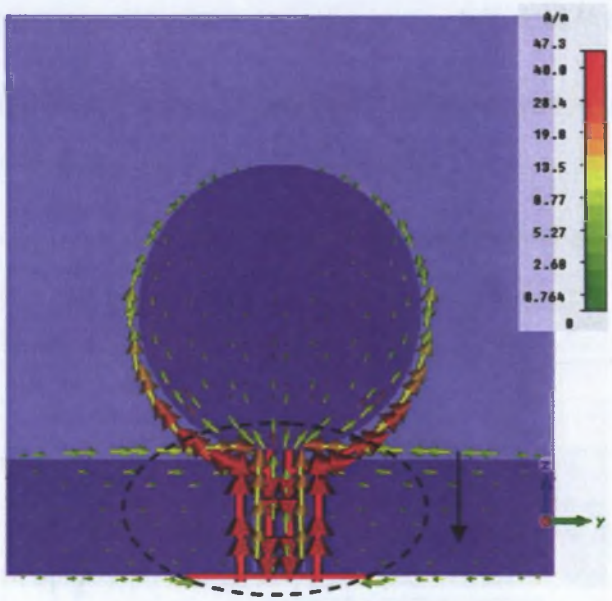

**Figure 3.17:** Average current distribution of CPW-fed PCMA [4].

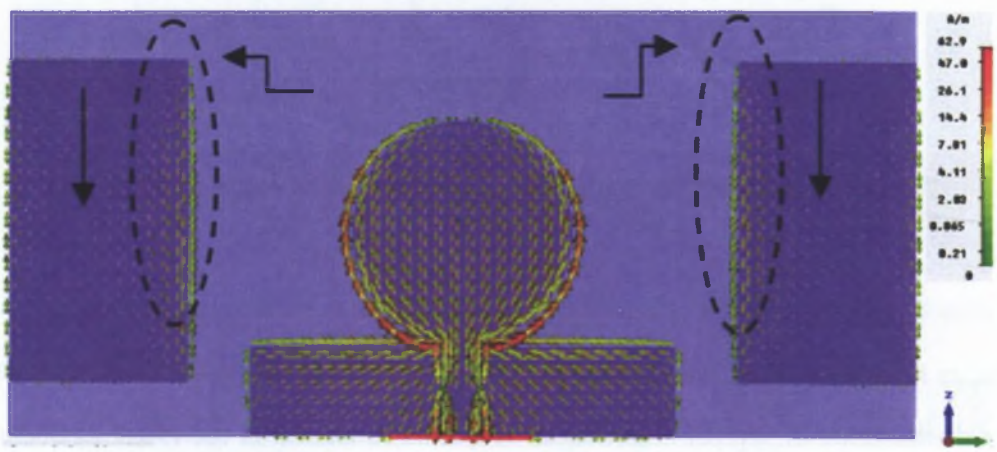

**Figure 3.18:** Proposed GE-LPA (Frequency 3 GHz).

It is evident from Figure 3.17 that the horizontal component of current along the CPW feed of the antenna is strongly in the opposite direction (as shown in the dotted region). This results in cancellation of some radiated energy and thus limits the overall gain of the antenna. In the case of the GE-LPA there is a reduction of current density near the CPW feed line; current is directed

toward the proximity-coupled metallic patches and returns toward ground along a different path shown by arrows in Figure 3.18. This reduction in density results in less cancelation of fields and thus increases the maximum gain of the antenna. To further analyse the effect of proximity coupling between unconventional metallic patches and a conventional CPW-PCMA, the same electric field distributions are plotted in Figure 3.19 at various frequencies.

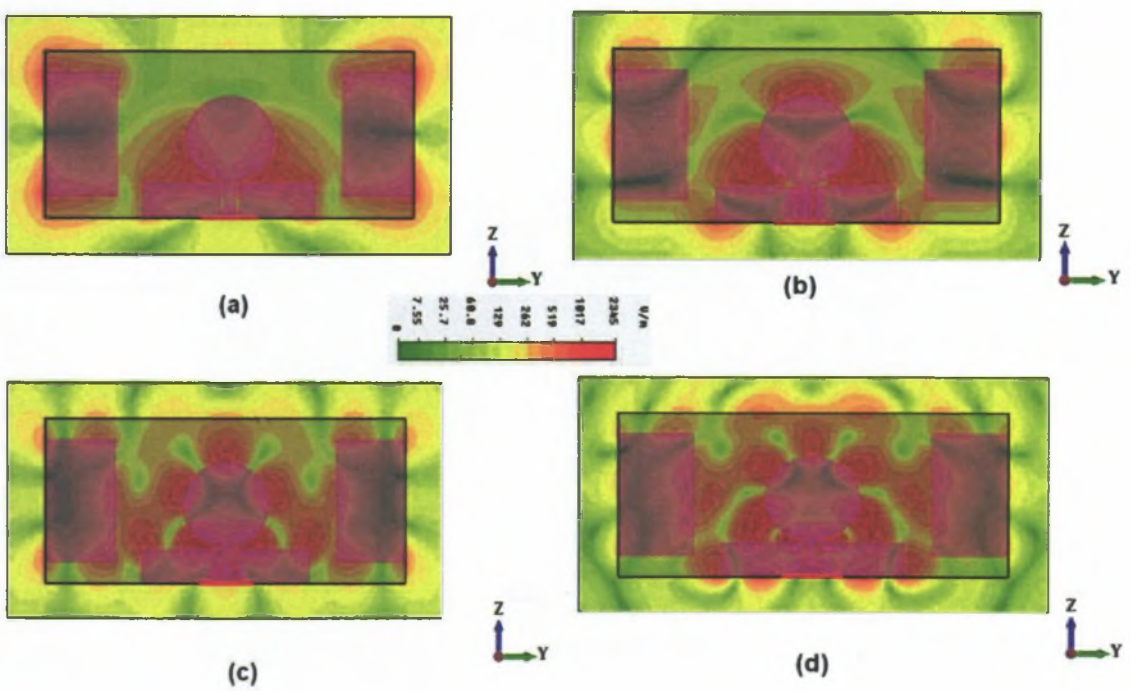


**Figure 3.19:** Electric field distribution of GE-LPA (a) 3 GHz (b) 6 GHz (c) 8 GHz and (d) 10 GHz.

At lower frequencies around 3 GHz the antenna behaves as an ideal $\lambda/2$ dipole. It has a null in the Z direction so that most of the fields are guided toward the theta $\pm 90$ degree ($\pm$y) direction, and metallic patches shows a strong coupling with the main antenna as shown in Figure 3.19(a). At higher frequencies, the conventional dipole is no longer $\lambda/2$. Therefore the fields are more scattered and distorted as visible from Figure 3.19 (c) and (d). Also, in terms

of wavelength the sizes of the patches start reducing. This phenomenon result in less proximity coupling between the antenna and the coplanar patches on top of the substrate, which limits gain enhancement at higher frequencies.

### 3.4.4 Experimental Results and Discussion

The parametric study discussed in Section 3.4.2 completes the antenna design, with the final parameters as follows: $G = 4$ mm, $L1 = 36$ mm, and $W1 = 20$ mm. Figure 3.20 shows the hardware prototype of the antenna fabricated on a 1.524 mm thick substrate with a dielectric constant ($\varepsilon_r$) of 3.0.

**Figure 3.20:** Hardware prototype of proposed antenna.

#### Frequency-Domain Analysis

The performance of the proposed antenna was evaluated with a HP 8720D network analyzer and the NSI 2000 Spherical Near field test range.

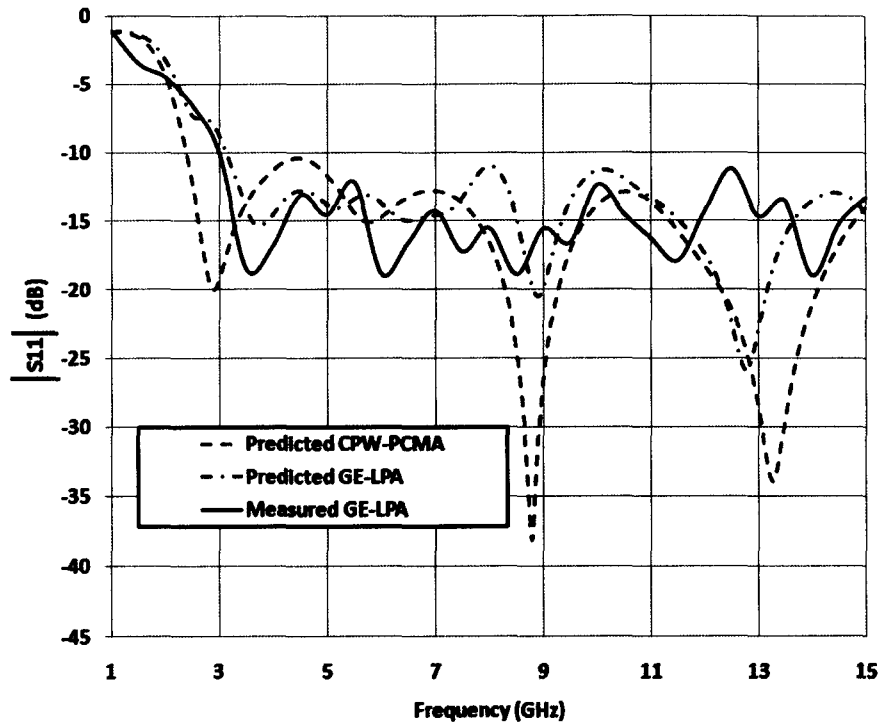


**Figure 3.21:** Theoretical and measured reflection coefficients of the proposed GE-LPA and a conventional CPW-fed PCMA.

Figure 3.21 compares the theoretical and experimental input reflection coefficients of the proposed antenna and a conventional CPW-fed printed circular monopole. It is seen that, with the addition of metallic patches on the sides of the monopole, the lower limit of the impedance bandwidth changes from 2.45 to 3 GHz. However, a return loss greater than 10 dB is maintained over the whole UWB band approved by the FCC. Predicted results show an 10 dB return loss bandwidth from 3 to 15 GHz or 133% . The measured results are in good agreement with the simulated data and show an impedance bandwidth of 3.15 GHz to 15 GHz or 130.5%. The predicted and measured antenna gain is shown in Figure 3.22. The gain is measured at various frequency points from 3 to 15 GHz. Good agreement between predicted and measured data is found. Results show a significant increase in antenna gain in the lower frequency region. A maximum gain enhancement of 2.5 dB is achieved around 7 GHz. The gain across the whole band is 6 dBi $\pm$ 2 dB while the conventional antenna shows a gain of 4 dBi $\pm$ 2 dB.

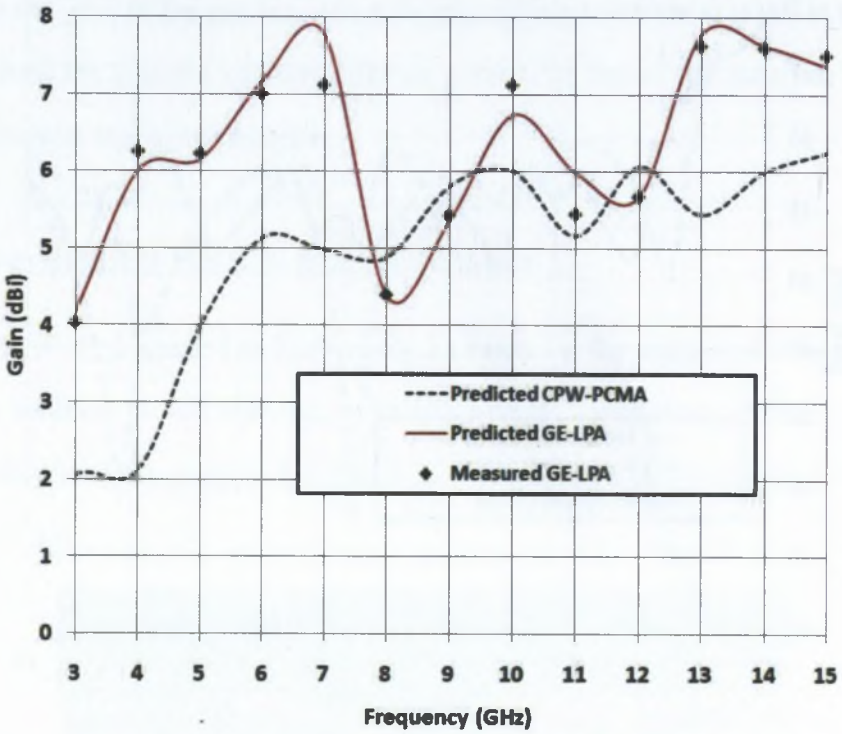


**Figure 3.22:** Theoretical and measured gain of the proposed antenna and a conventional CPW-fed PCMA.

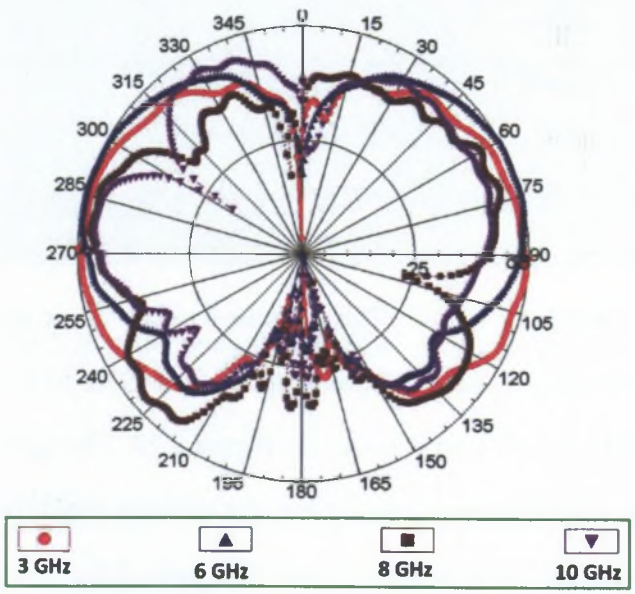


**Figure 3.23:** Measured radiation patterns on the xz plane at 3, 6, 8 and 10 GHz.

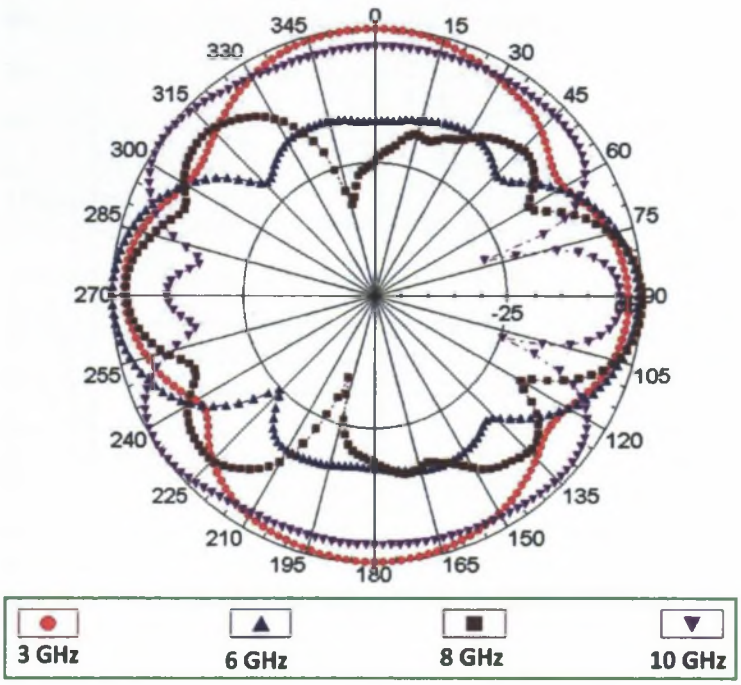


**Figure 3.24:** Measured radiation patterns on the xy plane at 3, 6, 8 and 10 GHz.

Figure 3.23 shows the measured radiation patterns at four different frequencies: 3 GHz, 6 GHz, 8 GHz and 10 GHz. These radiation patterns have been measured for the xy (azimuth) and the zx (elevation) planes (co-ordinate axes are defined in Figure 3.10). Due to the metallic patches the antenna is no longer omnidirectional in the azimuth plane (xy plane). The new antenna provides broad beam coverage in the azimuth plane and a figure-of-eight-type beam in the elevation plane, with only a small change of beam direction over its ultra-wide operating bandwidth. The beam in the azimuth plane is much more directional in the direction of $\pm 90$ degrees.

### 3.4.5 Transfer Characteristic of Proposed Antenna

To compare the transmission performance of the CPW-PCMA and proposed GE-LPA (AUT), measurements have been conducted.

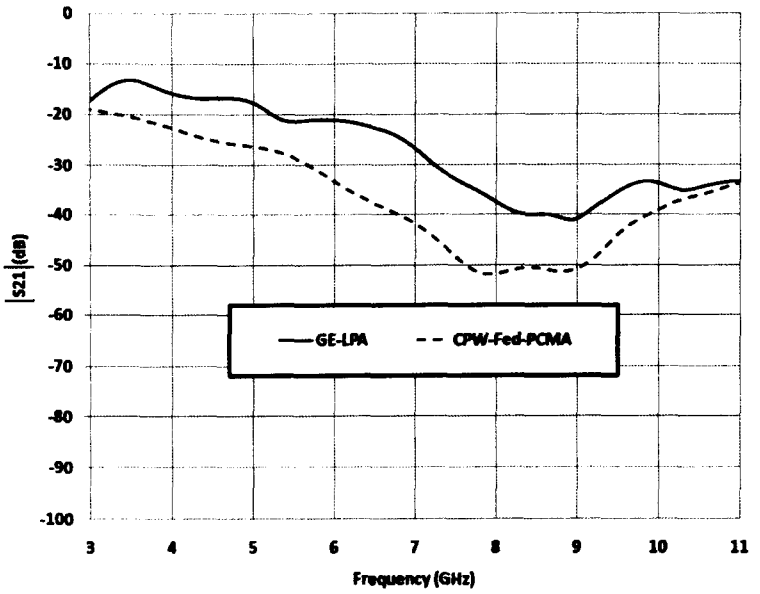


**Figure 3.25:** Transfer function magnitude.

During the measurements the transmitting antenna was fixed while the AUT or the standard antenna was mounted as the receiving antenna. The transmitting and receiving antenna pair was placed in an on-axis orientation with a separation distance of 2.561 m, and a BAE Systems dual-ridge horn H-1498 was chosen as the transmitting antenna.

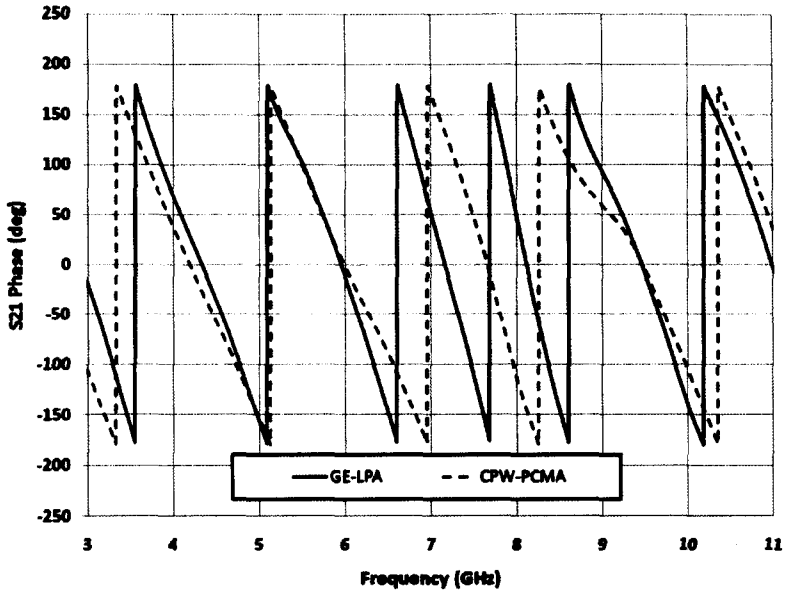


**Figure 3.26:** Transfer function phase.

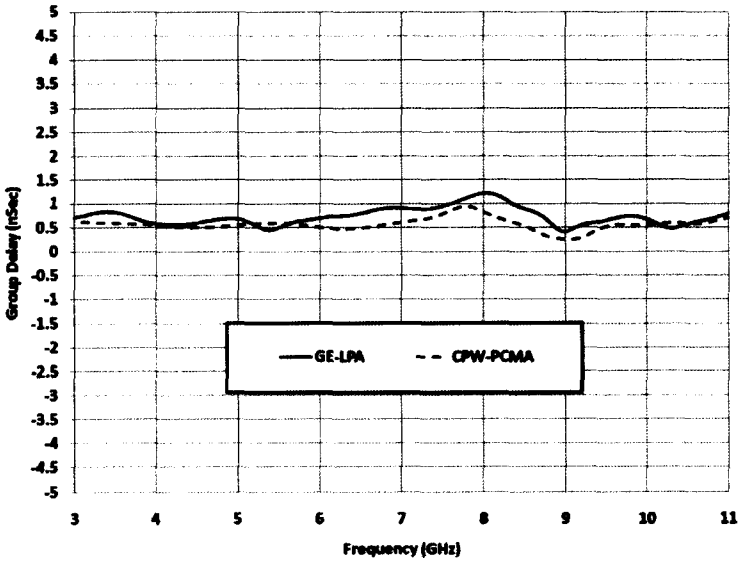


**Figure 3.27:** Group delay of GE-LPA.

This antenna has proved to be well matched by the measurement system from 2 to 20 GHz. The transmission scattering parameters were then measured by the HP 8720D network analyzer.

Figure 3.25 shows measured magnitude, phase and group delay comparisons of CPW-PCMA and the proposed GE-LPA.

This data shows that the CPW-PCMA and proposed the GE-LPA antennas have very similar characteristics. The magnitudes shown in Figure 3.25 of the transmission scattering parameters are relatively constant. Figure 3.26 also shows that the transmission transfer function of the new antenna has an almost linear phase response, and the group delays are relatively constant over the whole UWB frequency range. These characteristics should help to maintain the integrity of a transmitted short pulse transmitted in a pulse-based UWB system. As a consequence, the GE-LPA has proved to be very suitable for UWB radios.

### 3.4.6 UWB FCC Compliance Performance

In order to fully match with the UWB FCC compliances, the power spectral density (PSD) has been plotted for various source pulses as shown in Figure 3.28. The PCMA and proposed antenna PSDs are plotted in Figure 3.29 for comparison. Some classical UWB antenna designs use Rayleigh pulses [98], which are the first derivative of Gaussian pulses. Some authors also used fourth and fifth derivatives of Gaussian pulses.

$$s_i(t) = A\left(3 - 6\left(\frac{4\pi}{T_{au}^2}\right)t^2 + \left(\frac{4\pi}{T_{au}^2}\right)t^4\right)e^{-2\pi(\frac{t}{T_{au}})^2}\ (V/m)\ . \tag{3.2}$$

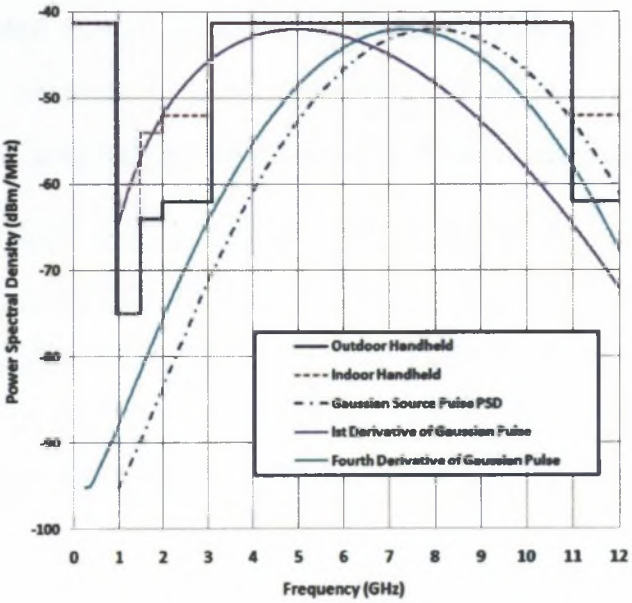


**Figure 3.28:** FCC Indoor and outdoor mask with various pulses.

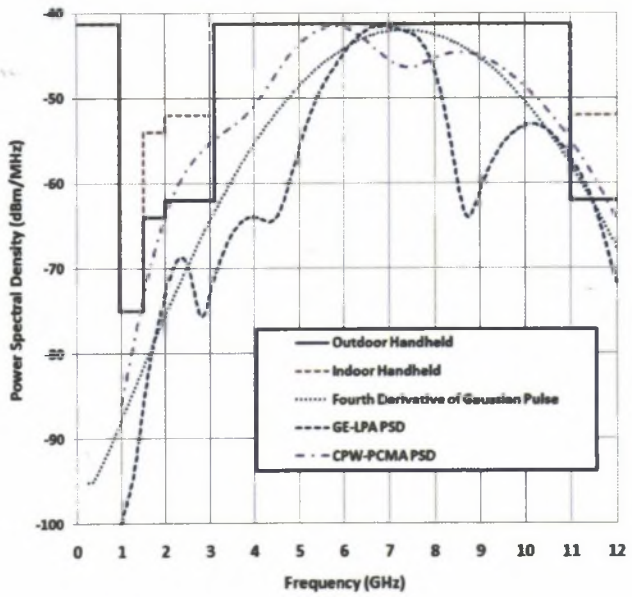


**Figure 3.29:** Performance of GE-LPA and comparison with CPW-fed PCMA.

Figure 3.28 shows the power spectral density of various pulses considered in this study. It is clearly evident from Figure 3.28 that the first derivative of a Gaussian pulse (also known as a

Rayleigh pulse) exceeds the FCC mask at lower frequency for both indoor and outdoor power spectral densities approved by the FCC. However the fourth derivative of a Gaussian pulse is well under the FCC mask and is well suited for UWB applications. Figure 3.29 shows the performance of proposed GE-LPA and a comparison of an antenna with conventional CPW-PCMA. The Gaussian function pulse described in [98], Equation 6.1 with the parameters of $A$ =0.1 and $Tau$ =175 ps, is considered. It is clear from Figure 3.29 that their power spectral densities (PSD) comply with the required FCC indoor emission mask and closely to the outdoor mask. The fidelity of these pulses is better than 0.95 and only minor ringing is observed during simulations.

## 3.5 Array of Proximity Coupled Metallic Slots

In Section 3.2.2 printed monopole antennas were discussed; the antennas usually have low gain at the lower end of the band, at 3.1 GHz, and it increases with frequency. Generally the gain varies from 1 to 5 dB across the UWB band. However a more constant gain over the complete bandwidth was discussed as a desirable feature in printed monopoles. A constant-gain printed circular monopole antenna (PCMA) with twin-slot radiator for microstrip-fed and CPW-fed configurations was presented in Section 3.3 and Section 3.4 respectively. The conductor-backed metallised twin-slot radiators were excited by the proximity coupling and also by the surface wave generated by the monopole. However these antennas proved to be quite useful in enhancing gain in the lower region of UWB bandwidth. The gain falls at the high frequency range, particularly from 8 GHz - 10 GHz. This reduced gain leads to a larger gain variation over the whole 3.1 GHz - 10.6 GHz band. In the coming sections the improved gain performance of the UWB antenna is presented. Gain is increased in the higher frequency range by increasing the number of proximity-coupled metallic-slot radiators. This arrangement also improves the average gain of the UWB antenna by 2 dB with a variation of 1.17 dB over whole of the UWB

bandwidth.

### 3.5.1 Proximity-Coupled Array of Cavity Slot Radiators

The schematic design of an antenna structure with an array of cavity slot radiators is shown in Figure 3.30. Complete dimensions of the antenna are given in caption of Figure 3.30. The PCMA is again designed on an FR-4 ( $\varepsilon_r = 4.4$, $h1 = 1.575$ mm) substrate that is supported by a 3mm layer of foam followed by another 1.575mm thick FR-4 substrate without any copper cladding. The dielectric substrate supports the surface wave that excites the array of eight conductor-backed slot radiators. The slot radiators are also excited by the proximity coupling.

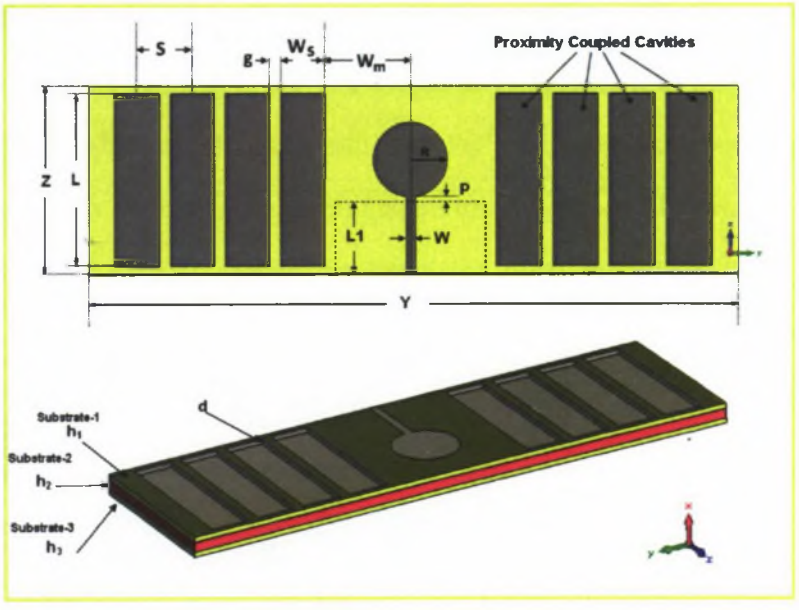


**Figure 3.30:** Proximity Coupled cavity arrays antenna with uniform gain printed circular monopole, Dimensions: $Y = 174, Z = 50, L = 45, W = 2.6, R = 10, g = 11, W_s = 6, W_m = 23, L1 = 20, h1 = h3 = 1.575$ and $h2 = 3$. (All dimensions are in mm)

The size and separation of the slots must be optimised for flatter gain and higher gain at the higher-frequency end. For this purpose a parametric study of the proposed structure is needed.

### 3.5.2 Parametric Analysis of Array of Cavity Slots

A parametric study of the proposed antenna structure is carried out in CST Microwave Studio [97]. The metallic cavities hold the key for gain enhancement. The separation gap $g$ between the metallic slots, and the length $L$ and width $W_s$ of the slot cavity are optimised for better gain performance of the antenna. In the process of gain optimisation over the complete bandwidth, the impedance bandwidth has also been maintained.

#### Optimization of Gap g Between Slot Cavities

The two-slot cavity structure from the investigation carried out in Section 3.3 is taken and the number of slot cavities is increased to eight. The design process started with the optimisation of the gap $g$ between the slot cavities. The distance of the first cavity from the antenna, $W_m$, is fixed from the monopole and the gap g between the subsequent cavities is varied over a large range of values. Figure 3.31 shows the simulated impedance matching for the antenna.

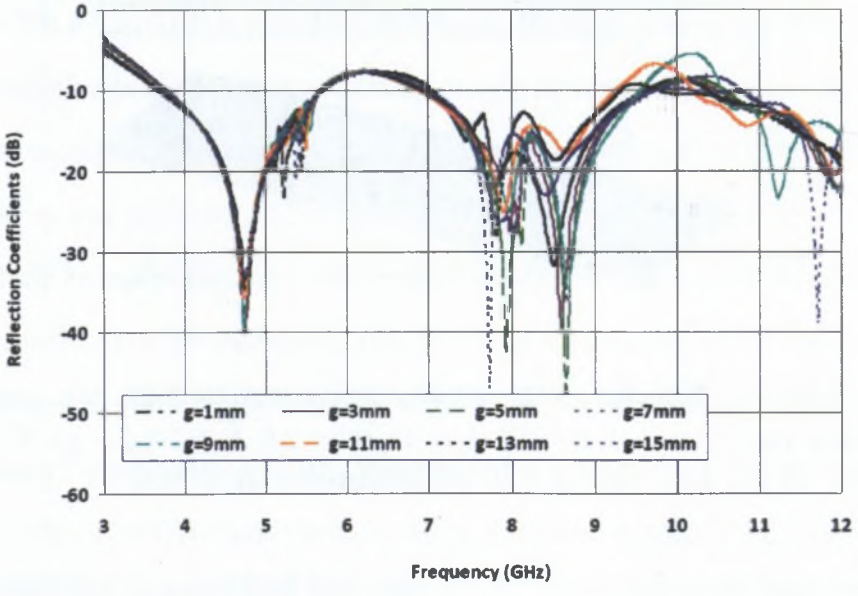


**Figure 3.31:** Variation in reflection coefficients with frequency; slot gap $g$ as parameter.

The return loss bandwidth is not significantly influenced by the parameter $g$. The return loss is 7.5 dB at around 6.2 GHz. The gap parameter $g$ has a significant influence on the gain of the antenna, as shown in Figure 3.32. The narrow gap $g$ =1 mm provides above 10 dBi gain at 12 GHz and 4.8 dBi gain at 3.1 GHz. A flatter gain is achieved for gaps 9 mm and 11 mm. The average gain of the 11 mm gap is greater. Therefore $g$ =11 mm chosen for further investigation on the optimisation of the length and width of the slot radiators.

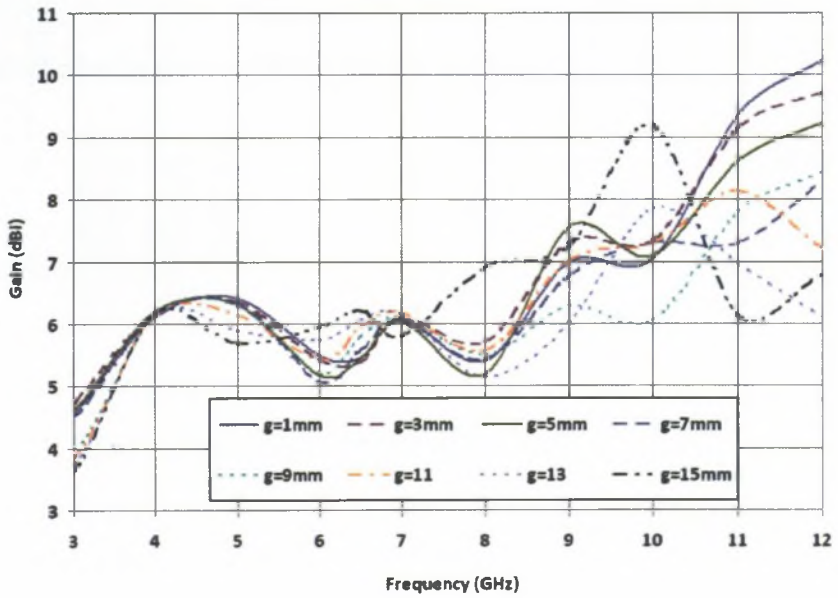


**Figure 3.32:** Variation in gain with frequency; slot gap $g$ as parameter.

### Optimization of Length L and Width Ws

The cavity slot length $L$ and width $Ws$ are the critical dimensions for improving the gain performance of the antenna. The effect of these parameters are studied on the impedance bandwidth and gain of the proposed antenna. Figure 3.33 shows the impedance bandwidth of the antenna for several sizes of the slot radiators. The lengths of the slots are varied from 3 mm to 46 mm, while their widths are varied from 2 mm to 6 mm. The size of the slot has an insignificant influence on the impedance bandwidth.

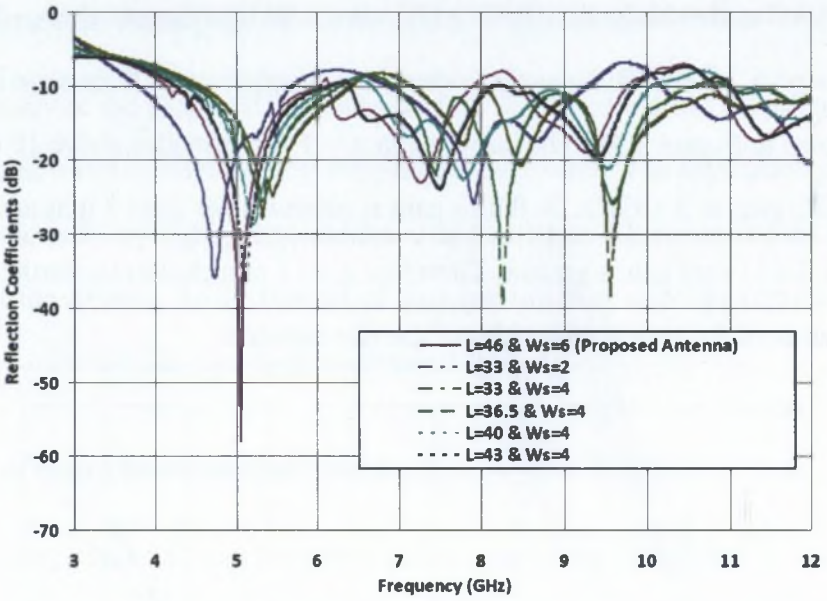


**Figure 3.33:** Variation in reflection coefficients with frequency for few combination of $L$ and $W_s$.

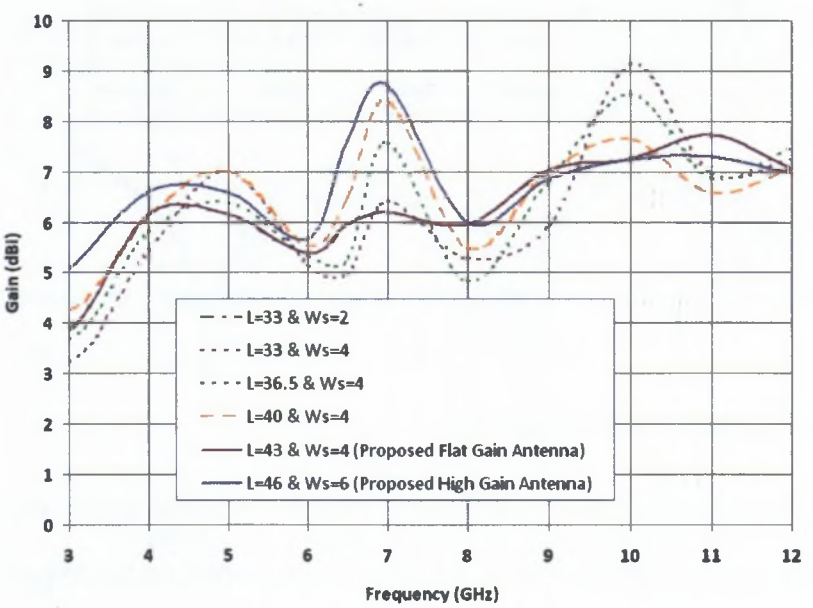


**Figure 3.34:** Variation in gain with frequency for few combination of $L$ and $W_s$.

The slot dimensions have a significant influence on the gain performance, as shown in Figure 3.34. In this study the emphasis is on three frequencies: 3.1 GHz, 7 GHz and 10 GHz; these

correspond to the lower, middle and upper frequency bands. The large slot size $46 \times 6$ mm$^2$ provides high gain at 3.1 GHz and 7 GHz i.e. 5 dBi and 8.7 dBi respectively. However, at 10 GHz the gain is 7.2 i.e. the minimum. The dimension $33 \times 4$ mm$^2$ provides a large gain of 9 dBi at 10 GHz. However its gain at 3.1 GHz is only 3.2 dBi, which is minimum over the band. Both these cases have a large variation in the gain over the band. These structures could be used to get enhanced the gain either at the lower frequency or at the higher frequency depending on the need. The dimension $43 \times 4$mm$^2$ provides flatter gain with average gain 6.24 dBi and 1.17 dB gain variation over the complete band.

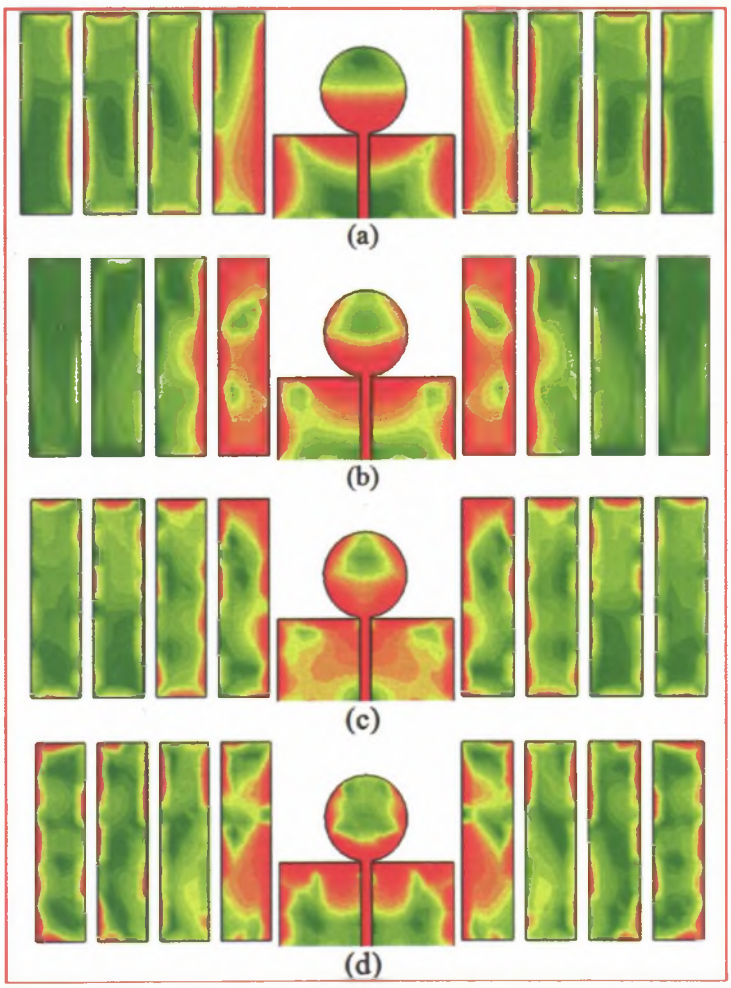


**Figure 3.35:** Electric field distributions at (a) 3 GHz (b) 6.5 GHz (c) 8 GHz (d) 12 GHz.

### 3.5.3 Theoretical Results and Discussions

In order to understand the functionality of the slot cavities the field distributions at 4, 6.5, 8 and 12 GHz are plotted in Figure 3.35. Figures 3.35a and 3.35b demonstrate that at lower frequencies the cavities closer to the antenna radiates, and as the frequency goes higher more fields are visible in the cavities (Figure 3.35c and 3.35d) located far away from the printed circular monopole antenna. The radiation increases from the more distant cavities and result in enhancement of the gain at higher frequencies. Figure 3.36 shows the return loss of the final design. The results with our previous two-slot design [99] are compared. The bandwidth is matched to 10 dB up to 8 GHz; it deteriorates slightly at 8.3 GHz and 10.6 GHz. The significant variation in gain is noticed in Figure 3.37 for the 2-slot case. The present design shows enhanced gain from 8 GHz-10 GHz. It gives flatter gain and higher average gain. Figure 3.38 shows the predicted radiation patterns of a high gain antenna at four different frequencies. The main beam is concentrated in the 0 or 180 degree direction and the gain does not drop significantly at higher frequencies compared to the maximum values

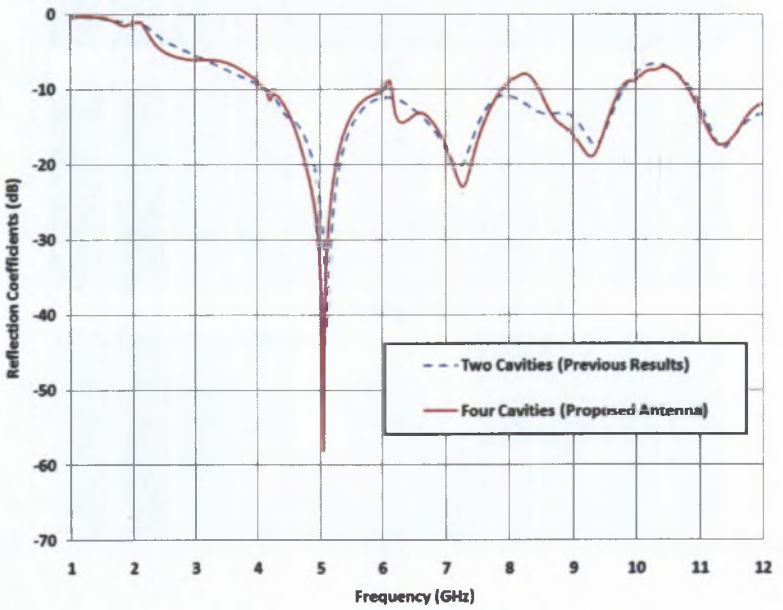


**Figure 3.36:** Predicted comparison of proposed antenna with the previous results.

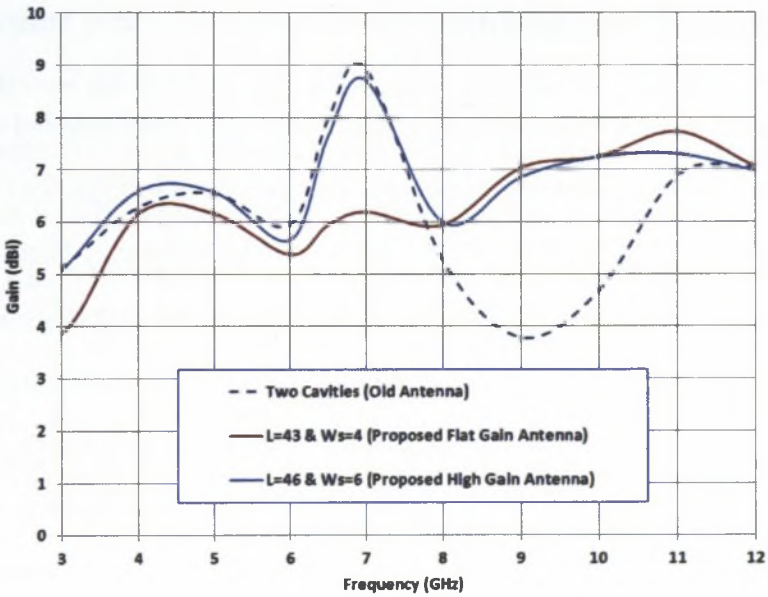


**Figure 3.37:** Predicted Gain of proposed antenna compared with 2-slot old antenna structure. $L = 46$ and $Ws = 6$ mm gives high-gain region at 7 GHz while $L = 43$ and $Ws = 4$ mm help in achieving flatness in gain.

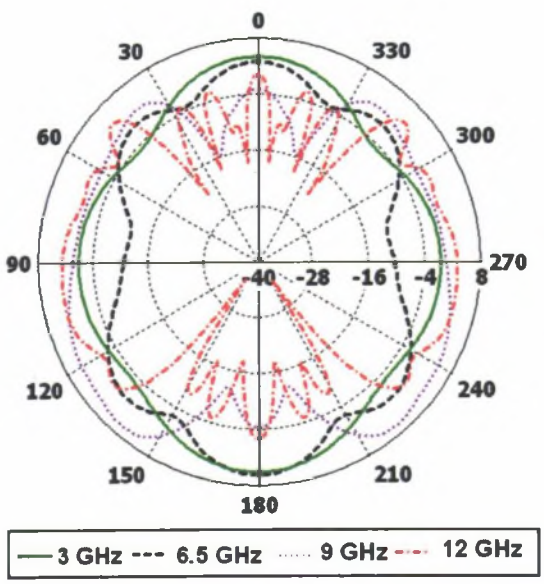


**Figure 3.38:** Predicted Radiation Patterns at different frequencies for the high-gain antenna.

## 3.6 Summary/Conclusions

A new microstrip-fed PCMA with a surface-wave-excited, proximity-coupled conductor-backed, metallised twin-slot radiator has been presented. The antenna is suitable for UWB systems operating from 4 GHz to 12 GHz. Over the 3 GHz to 10 GHz frequency band, the gain remains nearly constant at 5.5 dBi $\pm$ 1.5 dB. The radiation pattern in the azimuth plane is very broad, and in the elevation plane it has a figure-of-eight shape over the entire operating bandwidth. Based on that, a simple new antenna configuration with an enhanced gain, suitable for MB-OFDM UWB systems, is presented. With the use of proximity coupling, a maximum gain enhancement of 2.5 dB is achieved around 7 GHz while maintaining an impedance bandwidth of 12 GHz to cover the entire UWB band approved by the FCC. The average gain across the band is 6 dBi while a conventional PCMA antenna has an average gain of 4 dBi. A low gain variation of $\pm$ 2dB is maintained across the band. An antenna design has been presented with relevant theoretical results.

The second antenna presented here is a CPW-fed simple configuration with an enhanced gain, suitable for MB-OFDM UWB systems. With the use of proximity coupling, a maximum gain enhancement of 2.5 dB is achieved around 7 GHz while maintaining an impedance bandwidth of 12 GHz to cover the entire UWB band approved by the FCC. The average gain across the band is 6 dBi while a conventional PCMA antenna has an average gain of 4 dBi. A low gain variation of $\pm$2 dB is maintained across the band. An antenna design has been presented with relevant theoretical and measured results.

In the third design the concept of proximity coupling is extended to an array of cavity slots in a microstrip-fed PCMA. With appropriate design of an array of metallic cavities the control of gain is theoretically demonstrated. A flat or high gain can be achieved over a certain range of frequencies with appropriate dimensions of the metallic cavities. The antenna operating bandwidth is from 4 to 12 GHz. A complete parametric analysis and design guidelines highlighting

the gain enhancement over a broad range of frequency are presented. A significant improvement of 2 to 3 dB over the whole range of frequency is achieved with the concept of proximity coupling. The antenna shows a theoretical gain of 6.24 dBi with a maximum variation of 1.17 dB over a band of 8 GHz. The theoretical 10 dB return loss bandwidths are 6 GHz (4 GHz to 10 GHz) and 8 GHz (4 GHz to 12 GHz) for return loss less than 7.5 dB.

# Chapter 4

# Compact Surface-Mounted Short TEM Horn Antennas

## 4.1 Introduction

In Chapter 3 the angular gain stability of antennas was discussed. The technique of proximity coupling was shown to enhance the gain and make it nearly constant over a broad range of frequencies. The unstable angular spectral coverage of antennas leads to gain drop in the main beam directions which also raises a question of link stability in Line of Sight scenarios for ultra wideband systems.In case of ultra wide band (UWB) systems the role of antennas on the quality of the radio is more difficult to assess compared to narrow-band or wideband communication systems. In UWB systems extra complexity implied by the time (impulse response) or frequency (transfer function) dependence of the antenna characteristic. For instances to what extent is a fall in the antenna gain at some specific frequency detrimental, or to what extent is a late ripple in the temporal response really unfavourable, are questions which have no immediate and intuitive answers. This situation is worsened in the case of the near-field interaction of an antenna with a metallic object or in close proximity to reflecting or absorbing objects. Ad-

ditional problems arise when integrating these antennas in commercial products or hand-held devices. This chapter targets the design of a suitable antenna addressing the issues previously raised by several authors, which are outlined in the Related Work Section 4.2. Development of a new class of short TEM horn antennas suitable for various UWB systems like communications, Ground Penetrating Radar (GPR) and medical/imaging systems, is described in the subsequent sections.

### 4.1.1 Chapter Contributions

Prime contributions of this chapter are listed below

- Various ultra-wideband antennas have been categorised based on their size, bandwidth, radiation pattern and gain.
- A novel feed mechanism is proposed for a TEM horn with monopoles.
- A novel quasi-TEM short horn is proposed for various hand-held applications.
- The field distribution in various horn configurations is analysed to justify the claims.
- A surface-integrated compact horn based on studies is presented for integrated circuits.
- Complete time-domain and frequency-domain analyses of the proposed the horn antennas are presented.

This chapter starts with related work which includes the discussion of bandwidth limitation carried out in Chapter 3. Section 4.2 presents the background and related work. Section 4.3 starts with the design concept of a novel short TEM horn. Section 4.3.5 describes the field analysis of a short two-plate horn and some short TEM horn antennas followed by experimental verification in section 4.3.6. Based on the concepts discussed in the previous section, Section 4.4 introduces the concept of a surface integrated TEM horn with the flexibility of a folded horn

mounted on top of an ultra-wideband antenna. These sections are followed by a summary and conclusions in section 4.5.

## 4.2 Related Work

The Federal Communications Commission (FCC) [8] allocated the licence-free spectrum for 3.1 GHz to 10.6 GHz in 2002 as the UWB band. This technology offers an enormous bandwidth of 7.5 GHz at a centre frequency of 6.85 GHz. Work in UWB technology was started in early 50s and getting pace in 60s. GPR was the front candidate using this technology in the past for land-mine detection in the military sector [100], [101] and this became interesting for civilian applications like detection of trapped people [102] or non-destructive evaluation of concrete, pavements, and walls [103], [104]. Other industrial uses of UWB can be found in tank-level gauging in order to separate different liquid layers [105]. Some products are already commercially available, e.g. a wall scanner for the analysis of building material [106].

In the biomedical area, UWB emerged as a promising candidate for breast-cancer detection [107], [108] and vital-signs monitoring [109], [110] as well as for tracking of inner organs for improved magnetic-resonance tomography [111]. In addition to radar/sensing applications, enormous bandwidth of ultra-wideband (UWB) provides a promising solution for indoor communication systems. Digital data from high-speed signals carrying multiple HDTV programs to low-speed signals used for timing purposes will be shared over a digital wireless network. Such indoor and home networking is unique, in that it simultaneously requires high data rates (for multiple streams of digital video), very low cost (for broad consumer adoption), and very low power consumption (for embedding into battery-powered hand-held appliances). For most of the applications the devices are either hand-held or small portable terminals, and the antenna is the prime candidate to improve the performance of the systems. The performance of several system has been evaluated for various communication [112], [113], [114] and multimedia-terminal

scenarios [77, 115–117]. These studies highlight the limitation incurred due to antenna imperfection in various systems. The next sections describe a more detailed study and will outline the motivation behind the work presented in this chapter.

### 4.2.1 GPR and Other Medical/Imaging purposes

TEM horn antennas developed for ground-penetrating radar (GPR) and other such applications [118–121] have ultra-wide bandwidth and high, nearly constant gain over the operating bandwidth. However, these antennas are $\lambda$ to $10\lambda$ long and in addition a UWB balun is usually required to feed the balanced TEM horn from a coaxial cable. Dielectric loading may be applied to reduce the size of the antenna, however, this carries a penalty in terms of weight. For example the University of Liverpool have developed a dielectric-loaded TEM horn with 180% fractional bandwidth (bandwidth ratio of 30:1) and length of half-a-wavelength, but it weighs 8 kg. These antennas are too bulky for compact UWB wireless communication systems. On other fronts, novel feeding methods have been reported for metallic horn antennas, including a Yagi antenna feeding a long metallic horn and a microstrip patch feeding a compact, surface-mounted , short horn [71, 122]. However, the metallic horn itself is not an UWB radiator. Also the Yagi and the microstrip patch are not ideal UWB feed elements because of their dispersion and relatively narrow impedance bandwidth respectively. An adaptation of the horn antenna for biomedical imaging has been presented in [123]. This pyramidal horn is compact in size and coaxially fed via a subminiature version-A (SMA) connector and hence needs no balun. The directional behaviour of these antennas is well suited for GPR/sensing and biomedical applications, mentioned in the start of section 4.2. In this Chapter a novel concept of monopole feed short TEM horn is demonstrated, which shows the significantly flat gain over the UWB band with a compact light weight structure makes it more suitable for various hand-held devices.

### 4.2.2 LOS Communication Scenario

Lets us start with the UWB research conducted in two major projects, named PULSER 1 and PULSER 2, at the Adaptative Antennas and high data rate Radio communications (AAR) lab at ENSTA, France. According to several studies and published articles by the group [124], [125] and [126]. The design of UWB antennas should consider the overall performances of UWB system. For most of these, the improvement of the link-budget, even by a few dB, is of practical importance, because of the constraints imposed by regulation authorities, e.g. FCC, as regards the transmitted power. Since regulatory limits are defined in terms of the effective isotropic radiated power (EIRP) at transmitter side, one way to enhance system performance is to introduce antenna gain at the receiver side. Moreover using a directional transmit antenna helps reduce emissions in undesired directions. This could be desirable where a narrower field of view can be tolerated. Many scenarios in UWB short range communications indeed are in line of sight (LOS) or quasi-LOS conditions. However, when the terminal is mobile, high antenna directionality is not adequate. Furthermore directional antennas are larger in size than omni-directional ones, whereas several UWB systems require small-sized, easy to integrate and particularly low complexity/cost antennas.

### 4.2.3 Integration issues and Origin of Physical Imperfections

A group at the Institute of Electrical and Information Engineering, University of Kiel, Germany conducted research on integration issues of UWB antennas with commercial devices [77, 115–117]. During the studies carried out on integration of antennas in various commercial products, several antenna imperfections were noted. They are broadly classified as follows:

**Internal imperfections**

Internal imperfections arise from the inner structure of the antenna, due to the unfavourable behaviour experienced by waves, fed from the antenna input port, termed as a mismatch between the feed and antenna systems. In UWB antennas this may be viewed as reflections at certain locations within the antenna, which produce ripples in the time domain and resonant behaviours in the frequency domain.

**Near-zone imperfections**

An antenna is seldom isolated in space; it is influenced in its near-field zone by all sorts of scatterers (feed cable, casing, furniture or human body). This contributes to the far-field radiated signal and even reflections into the source. The difference from the previous imperfection is the greater distance between the antenna feed port and the scatterer. This larger distance increases the time delay of the reflected signals, and thus enhances the antenna temporal dispersion. As a result, more variation in the return loss and far-field gain of the antenna in the frequency domain can be expected.

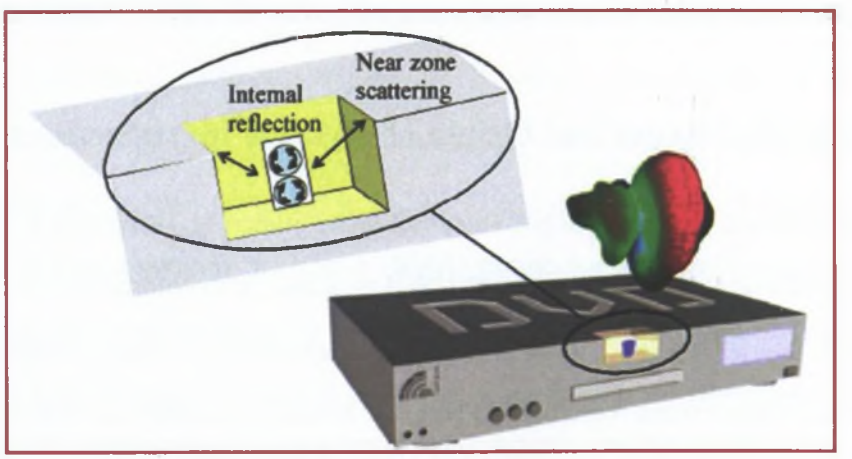


**Figure 4.1:** Antenna Mounted on a DVD player [2].

These imperfections will in general affect both the amplitude and the phase of the radiated

signals in the frequency domain. The phase in particular has a strong effect on the antenna impulse response, which is broadened or dispersed. Figure 4.1 shows an antenna mounted on a DVD player where there is strong scattering from the casing of the device. A concluding statement on the performance of antennas integrated on commercial products, based on various studies conducted by researchers at University of Kiel in chapter 10 of [2], is:

*"In general we can conclude that even if the assumption of a metal chassis with only a small integration volume for the antenna may be quite pessimistic, it is clear that we cannot reach a quasi-omnidirectional radiation which is stable over the frequency range when the antenna is integrated in (or even mounted on) a realistic device."*

### 4.2.4 Proposed Solution for Antenna Design

A directional transmit antenna helps to reduce emissions in undesired directions. This could be desirable where a narrower field of view can be tolerated. Many scenarios in UWB short-range communications are indeed line-of-sight (LOS) or quasi-LOS conditions. However when the terminal is mobile, high antenna directionality is not adequate. Furthermore, directional antennas are larger in size than omni-directional ones, whereas several UWB systems require small-sized, easy to integrate and particularly low complexity/cost antennas. Another proposed solution for the problem described above is a semi-directional antenna which should be a good trade-off in order to improve the link-budget margin while preserving the robustness of the link and the small size of the antenna. Some UWB semi-directional antennas have been presented in [95,96] and a statistical analysis, to compare their performance, was conducted in [127]. They demonstrated a dual-fed microstrip monopole (DFMM) combined with a quasi omni-directional radiator with a dielectric lens, which focuses the radiation and produces a larger variation in gain over the UWB. In order to overcome several imperfections arising due to integration of antennas on the various metallic chassis and mounting, the proposed antenna provides a semi-directional radiation pattern. Short TEM horn structures were optimised in close proximity to antennas to

handle the near-field interaction and to avoid the bulkiness of a conventional TEM horn. Such a short, UWB, quasi-TEM horn antenna has not been reported previously.

### 4.2.5 Study and Characterisation of Printed UWB Antennas

Several planar monopole UWB antennas have been investigated [4,5,28,92–95] for FCC-based UWB systems operating from 3.1 GHz to 10.6 GHz. Most of these antennas have very large impedance bandwidths and nearly omni-directional radiation patterns in the azimuth plane. These antennas have low gains and their gain increases with frequency at lower frequencies in the UWB band as discussed in Chapters 2 and 3. On the other hand, the transmission transfer function of an ideal UWB antenna should have a flat gain response and a linear phase response for faithful radiation of short UWB pulses [128, 129]. Various configurations of UWB antennas were studied initially. The performance of few printed monopole configurations are evaluated in Table 4.1 detailed study discussion is presented in Chapter 2. Most of the antenna configurations for UWB systems cover bandwidths in excess of 10:1. However, the gain of most compact antennas (e.g. PCMA) is frequency dependent. For example, a maximum gain of 6.8 dBi is possible at higher frequencies, but it is usually much less at lower frequencies, especially from 1 GHz to 6 GHz. Most of these printed antennas have a linear gain variation (e.g increasing about 0.3 dBi to 5 dBi) at lower frequencies (e.g. 1 GHz to 6 GHz) and then the gain becomes nearly constant. In contrast, slot antennas have a relatively constant gain between 2 dBi and 3 dBi and only a 1 dB variation in gain over the complete bandwidth [37–40, 43, 56]. However high-gain slot antennas have exhibited a stronger gain variation between 2 dBi to 7 dBi [46] (they are not considered in the current chapter and are discussed in detail in chapter 6). Indeed, gain enhancement is a challenging task for UWB systems where gain flatness from 3 GHz to 10 GHz is preferred.

**Table 4.1:** Comparisons of various printed monopole antennas

| Antenna Config. | Bandwidth | Bandwidth Ratio | Gain (dBi) | Variation (dB) | Size (mm) |
|---|---|---|---|---|---|
| **Printed Circular Monopole Antenna (PCMA) [4]** | 2.78-9.78 GHz | 3.51:1 | 0.58-6.7 | ±3.06 | 42 × 50 |
| **CPW-fed PCMA [5]** | 2.88-12.0 GHz | 4.16:1 | 0.88-5.8 | ±2.46 | 47 × 47 |
| **Printed Elliptical Monopole Antenna [33]** | 1.10-13.61 GHz | 12.40:1 | 1.5-8.3 | ±3.40 | 90 × 90 |
| **Trapezoidal Metal-Plate Monopole [34]** | 1.07-12.2 GHz | 11.4:1 | 0.5-4.5 | ±2.50 | 89 × 89 |
| **Printed Inverted Cone [17]** | 1.00-10.0 GHz | 10.0:1 | 0.3-8.6 | ±4.15 | 89 × 89 |
| **Circular Monopole with Trapezoidal Ground [130]** | 1.76-8.17 GHz | 4.64:1 | 0.65-4.2 | ±1.776 | 35 × 35 |
| **Square Monopole with Semicircular Base [90]** | 1.05-12.2 GHz | 11.31:1 | 0.8-7.3 | ±3.25 | 90 × 90 |

## 4.3 Surface-Mounted Short TEM Horn Design

Various configurations of short TEM horn are studied theoretically before starting the design of the final configurations presented in this chapter. The best possible solution for orientation of the monopole feed and the mounting of a short horn is explained and discussed in the following sections depending on the bandwidth and gain flatness. In design process the PCMA [4] is considered as the base antenna and the geometries of two different surface mounted short horn named as two plate surface mounted short horn (TP-SMSH) and surface mounted short TEM (SMS-TEM)horn is presented in this work. The design process of two configurations is followed by the parametric study of both configurations, effective nature of TEM inside the horn and reason for investigating different configurations is explained.

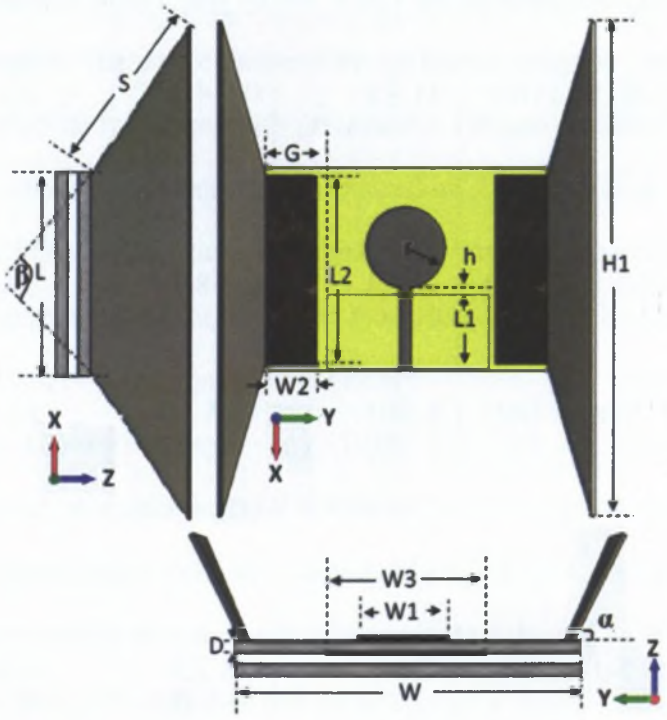


**Figure 4.2:** Two-Plate Surface-Mount Short Horn (SMSH): W=70, L=42, L2=40, L1=20, h=0.36, D=1.575, W1=2.78, W2=10, W3=40, S=45, H1=100, G=15, r=10, $\alpha = 50^0$ and $\beta = 65^0$ (All dimensions are in mm). The brown (or dark) region shows the two holes in the upper FR4-substrate .

### 4.3.1 Structure-1: Two-Plate Surface-Mount Short Horn (TP-SMSH)

The configuration of the proposed structure-1 is shown in Figure 4.2. The PCMA, which was discussed earlier in Chapter 3, is incorporated with the surface-mounted short horn and optimised using the CST Microwave Studio simulator. The PCMA is made on a FR-4 ($\varepsilon_r$=4.4 , $D$ = 1.575 mm) substrate, which is separated from a second FR-4 substrate by a uniform air gap, maintained using Teflon spacers. Unlike in standard PCMAs, two rectangular holes ($W2$ = 10 mm, $L2$ = 40 mm) have been cut in the top FR-4 sheet on either side of the monopole. The second FR-4 sheet is just a plain dielectric layer with no copper on either side. The air gap between the FR-4 sheets and the holes cut in the upper FR-4 sheet produce a good impedance bandwidth for the PCMA. During the design of the short horn, it was noted that the mounting location of the horn on the monopole and the slant angle of the horn side walls were critical to the performance.

### 4.3.2 Structure-2: Surface-Mounted Short TEM Horn (SMS-TEM)

Another important orientation of the short horn is discussed in this section. A more detailed analysis and a reason for discussing two different horns is explained in the next section, which also justifies calling it a short TEM horn instead of a two-plate horn. To avoid interference between the microstrip feed line and the horn plate an aperture of dimension $a \times a$ mm is cut in the horn plate of structure 2 (Figure 4.3) and, for more accurate analysis of simulation results, a SMA feed is also modelled in the software design process. Initial values for the design were: apex angle $\alpha = 50^0$, conducting horn-plate slant length = $\lambda$/2.5 at 2.75 GHz; flare angle fixed at $\beta = 90^0$; mount gap $G$ = 5 mm ($G$ is the distance to the bottom of the horn from the end of the microstrip ground plane) , while the final optimisation is explained in the next section.

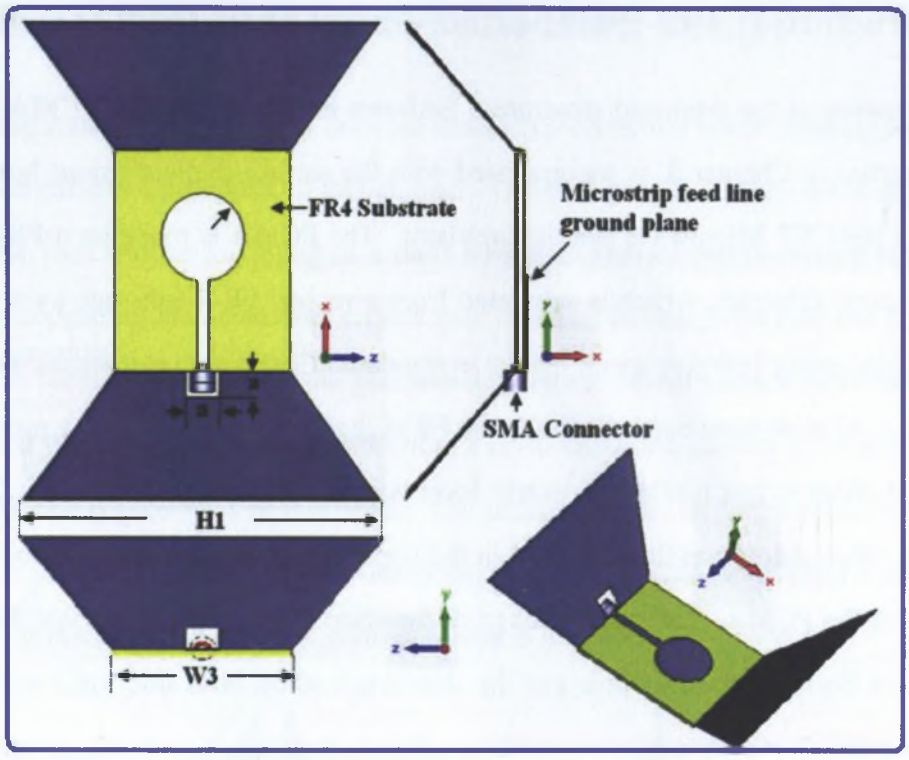


**Figure 4.3:** Surface-mounted short TEM horn (All dimensions except the slant angle are the same as the horn shown in Figure 4.2).

The short horns shown in Figures 4.2 and 4.3 have a slant length of only $s/\lambda$, so the gain is expected to be moderate. If it is approximated as a TEM horn antenna, its estimated gain by extrapolating results would be 2.1 dBi as shown in Figure 6 of [120]. The simulation results from CST Microwave Studio indicate that this short horn integrated with the PCMA has a more constant gain over a wide bandwidth. The properties of the new antenna are a combination of those of the short two-plate horn and the PCMA. The new antenna considered as structure-1 (Figure 4.2) has a moderate but nearly constant gain over a large bandwidth while the antenna shown as structure-2 (Figure 4.3) has a higher gain with more variations over the whole UWB bandwidth.

### 4.3.3 Optimisation of Two Structures of Surface-Mount Short Horn

**Structure-1: Two-Plate Surface-Mount Short Horn (TP-SMSH)**

Initial values for the design were: apex angle $\beta = 50^0$, conducting horn plate slant length=$\lambda/2.5$ at 2.75 GHz; flare angle fixed at $\alpha$=$90^0$; mount gap $G = 5$ mm ($G$ is the distance to the bottom of horn from the end of the microstrip ground plane).

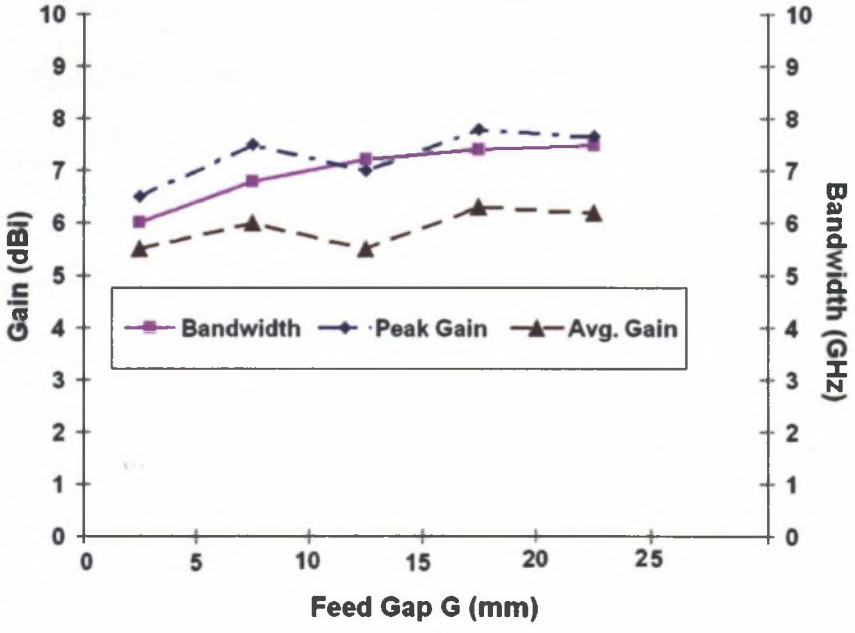


**Figure 4.4:** Variation of bandwidth and gain for different horn locations (Structure-1).

The mount gap $G$ is optimised for maximum bandwidth and gain performance. Figure 4.4 shows the variation of average gain, maximum gain and bandwidth with $G$. A mount gap of 15 mm gives good average and maximum gain and a bandwidth of 7.5 GHz, which is good enough to cover the FCC approved UWB band. In the next design stage, $G$ is fixed at 15 mm and the slant angle ($\alpha$) is optimized with the objective of achieving maximally flat gain. Figure 4.6. shows the gain variation as a function of slant angle for different frequencies for structure-1.

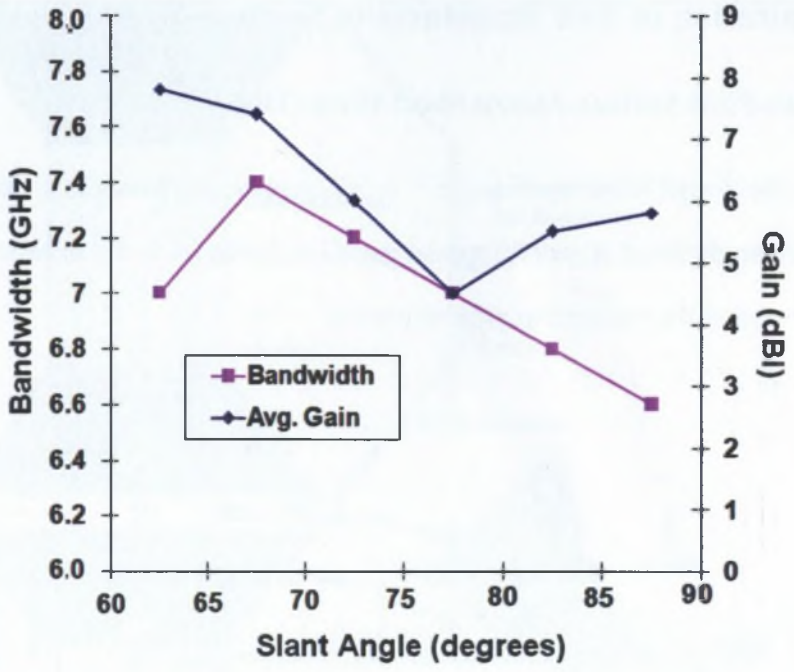


**Figure 4.5:** Variation of average gain and bandwidth with slant angle locations (Structure-1).

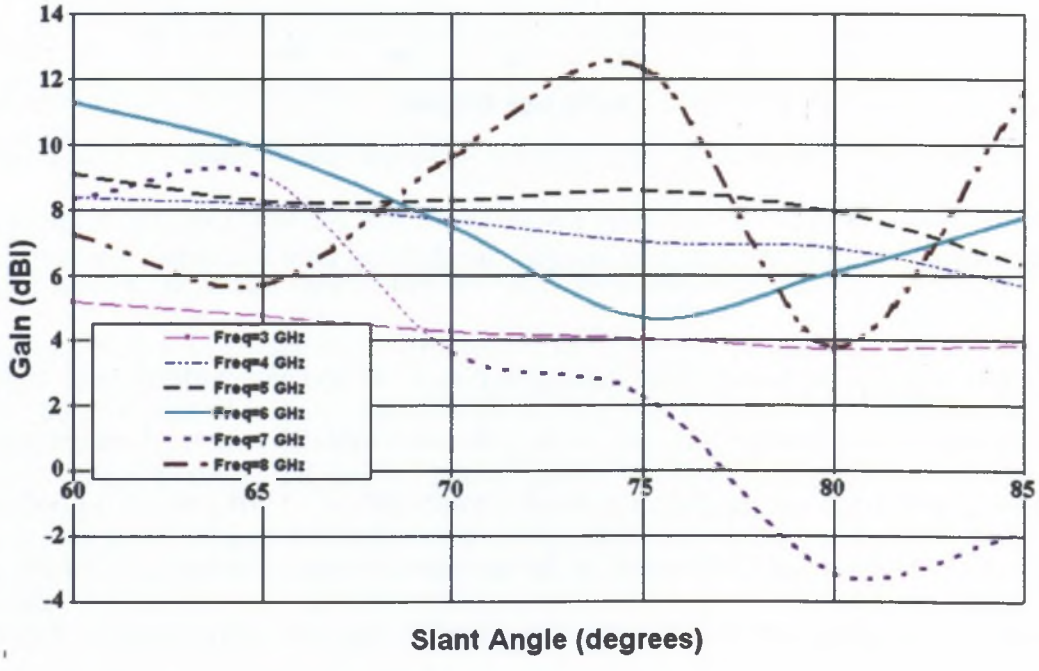


**Figure 4.6:** Gain vs. slant angle ($\alpha$) for Structure-1 Two-plate horn.

It can be noted that slant angles in the range of $60^0$ to $70^0$ leads to small gain variations for the short TEM horn. A Slant angle of $68^0$ gives maximum flat gain of around 6.5 dBi average gain. Furthermore, with the flatness the bandwidth at various slant angles are also considered in studies. The study of gain and bandwidth is shown in Figure 4.5. With a slant angle $\alpha = 65^0$ a maximum 10 dB return-loss bandwidth of around 7.4 GHz, with an average gain of 7.5 dBi, is attainable.

**Structure-2: Surface-Mounted Short TEM Horn (SMS-TEM)**

In both the proposed short horns (structure 1 and 2) due to extreme shorting of V plates, its hard to evaluate apex angle beta ($\beta$), so for ease of optimisation parameter aperture ratio ($H1/W3$) is taken for short horns which is optimised for maximum flat gain. The mounting location of the horn on the monopole (at the microstrip feed end)and the slant angle are critical parameters. One wall of the short horn could potentially short the feed-line in structure-2 or interfere with the field in the feed-line. To avoid this interference and shorting of the feed line an aperture is cut at the base of feeding structure. The design process for the short horn to get optimised values of slant length and aperture ratio (which corresponds to the conducting plate angle $\beta$) is given below.

Values for the design are: aperture ratio = 2, conducting horn plate slant length=$\lambda/2.5$ at 2.75 GHz; flare $\beta$ is optimised for flat and gain response. This slant angle is different for structure-2. Figure 4.7 shows the variation in gain over various frequencies. A Slant angle of $45^0$ gives the maximum flatness for structure-2.

In the next stage of design, $\alpha$ is fixed at 45 degrees for structure-2 and the aperture ratio is optimised with the objective of further gain enhancement and compact size. From Figure 4.8 it can be noted that an aperture ratio of 2 leads to small gain variations between the considered frequency ranges and an average gain of around 5 dBi.

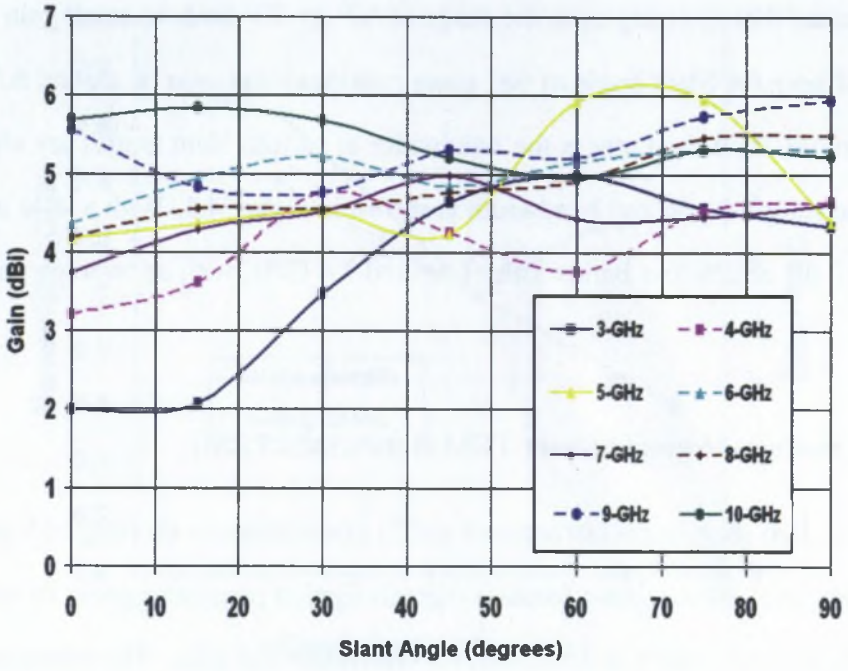


**Figure 4.7:** Gain vs slant angle ($\alpha$) for Structure-2 surface-mounted short TEM horn.

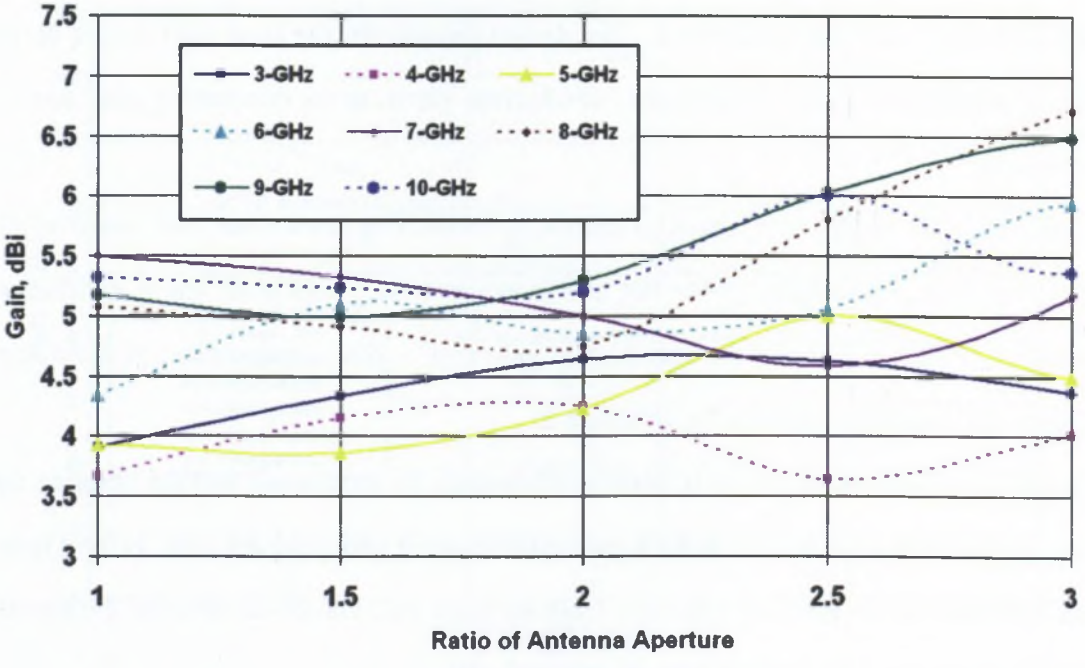


**Figure 4.8:** Gain vs aperture ratio for Structure-2, surface-mounted short TEM Horn.

### 4.3.4 Hardware Prototypes and Other Validations

For fabrication, to reduce mechanical complexity, $\alpha = 65^0$ is chosen for the design of structure-1 and $\alpha = 45^0$ is chosen for structure-2. Predicted results in Figure 4.9 show that, for $\alpha = 45^0$, a maximum 9-dB return-loss bandwidth of around 7.4 GHz with an average gain of 7.5 dBi is attainable in the case of structure-2. For the sake of comparison the return loss of an optimised surface-mounted four-plate horn proposed earlier [71] is also plotted in Figure 4.9.

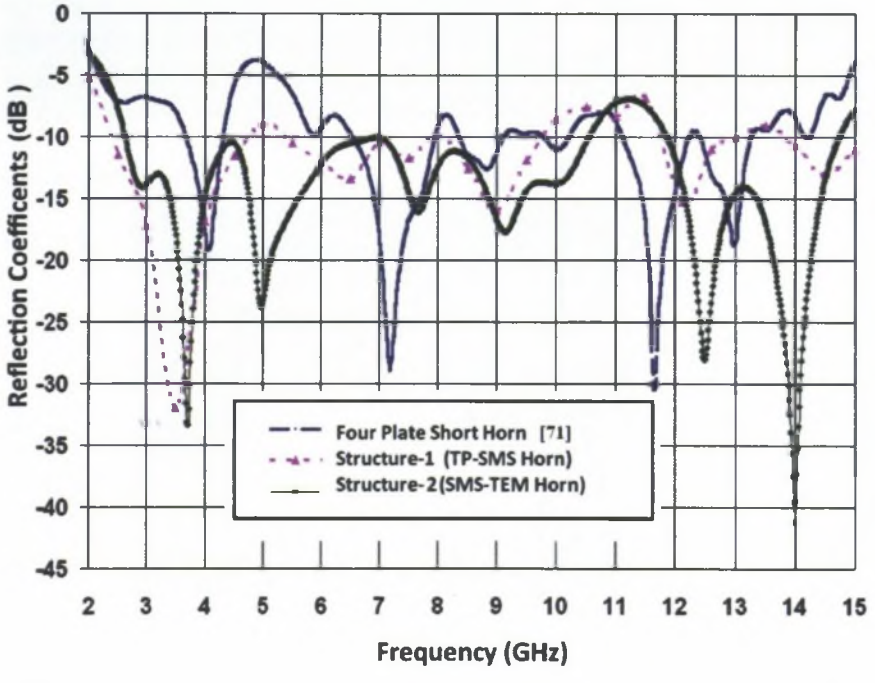


**Figure 4.9:** Predicted $|S11|$ magnitude for different configurations of short horns.

The impedance bandwidth of the four-plate horn is quite poor compared to the short two-plate configurations. The advantage of using two-plate horns instead of a four-plate horn for an UWB printed monopole can easily be seen from Figure 4.9. The two-plate short horn has a slant length of only $\lambda/2.5$, so the gain is expected to be moderate. If it is approximated as a TEM horn antenna, its estimated gain (by extrapolating results) would be 2.1 dBi as shown in Figure 6 of [120]. The simulation results from CST Microwave Studio indicate that this short

horn integrated to the PCMA provides an improved constant gain over a large bandwidth. The properties of the new antennas are a combination of those of the short two-plate horn and the PCMA. Hardware prototypes of both antennas are shown in Figure 4.10.

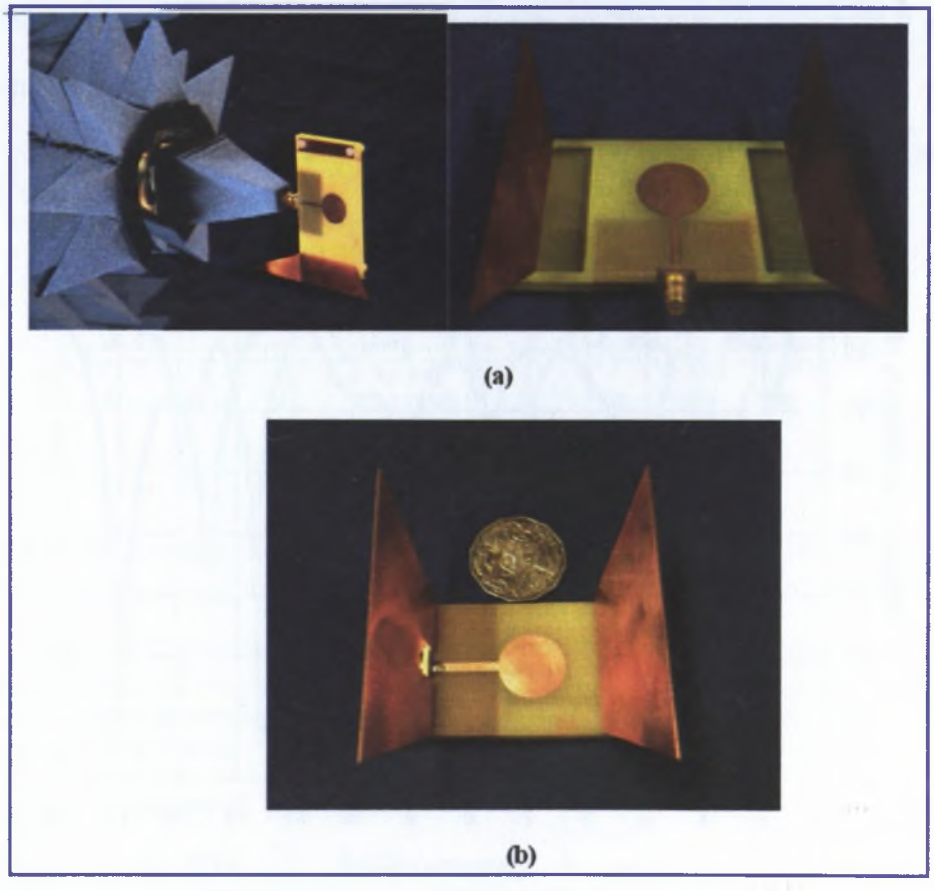


**Figure 4.10:** Hardware profile of (a) Two-plate surface-mounted short (TP-SMS) horn (Structure-1) (b) Surface-mounted short TEM (SMS-TEM) horn (Structure-2).

### 4.3.5 Field Analysis and Suitability of Various Feed Structures and Orientation

The field distribution of the short horn antennas were analysed to show the evolution along the horn and also to understand the differences between TP-SMS horn and SMS-TEM horn. Inside the short-horn region, the field distribution in the transverse (X-Y) plane depends on z. This

field distribution also changes with frequency. Figures 4.11(a) and 4.11(b) show the transverse electric fields (i.e. Ex and Ey) at heights (z) of 10 mm and 45 mm, respectively, at 3 GHz. It may immediately be noted that the aperture field at the mouth of the horn shown in Figure 4.11(b) is polarised in a direction orthogonal to the direction expected in a conventional TEM horn antenna. This aspect is further discussed in the following paragraph. Figure 4.12 shows that inside the horn all three field components could exist and could be significant depending on the location but, for large values of z, Ex becomes the dominant field component.

In addition to being extremely short (quarter-wavelength slant length) the main difference is that the polarisation of our two-plate horn is orthogonal to that of a TEM horn. From Figure 4.11(b), it is evident that the E-field polarisation of the proposed antenna is parallel to the x axis (i.e. the E-plane of the antenna is in the X-Z plane) which is set by the orientation of the PCMA. For a TEM horn the E-field polarisation would be parallel to the y-axis (i.e. the E-plane of a TEM horn would be in the Y-Z plane) since the TEM horn is similar to a twin-wire TEM transmission line with the opposing wires flattened and tapered to form a horn antenna. In a TEM horn antenna, the electric field lines are between the two plates, as in a two-wire transmission line. Such a field can exist with zero longitudinal electric field (i.e. Ez = 0) but the field in structure-1 (short two-plate horn) cannot.

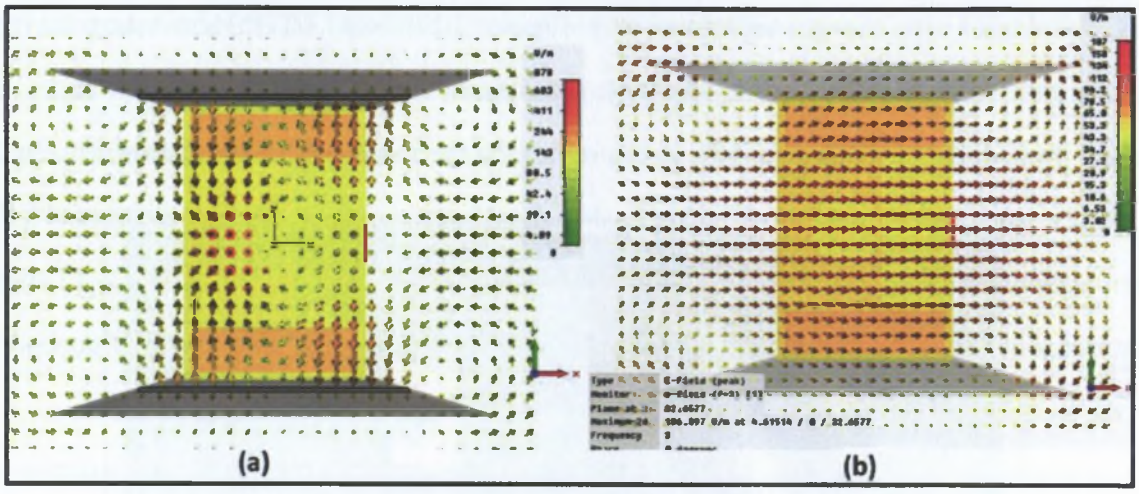


**Figure 4.11:** Transverse electric-field for Structure-1 (TP-SMS) on the x-y plane inside the horn at (a) z = 10 mm and (b) z = 45 mm.

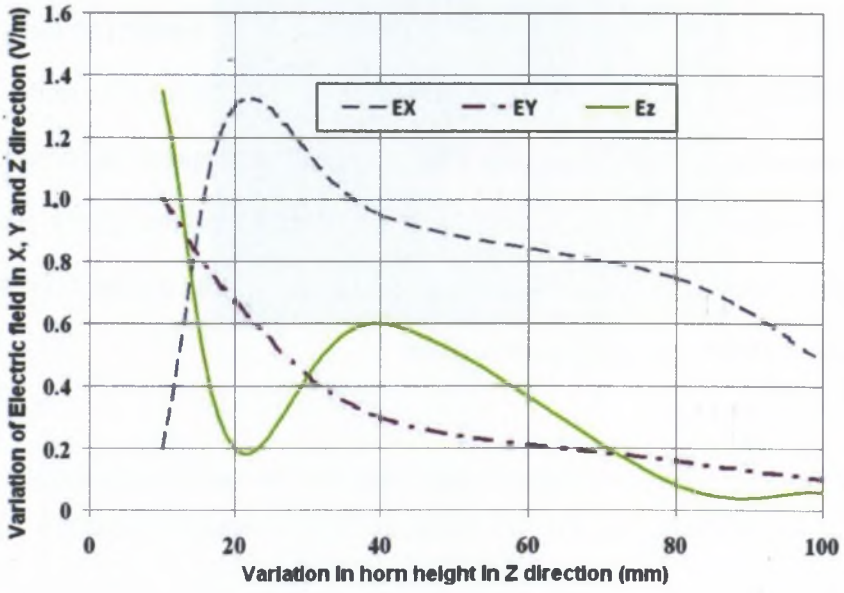


**Figure 4.12:** Variation of Electric-field components with z at 3 GHz for Structure-1 (TP-SMS) horn.

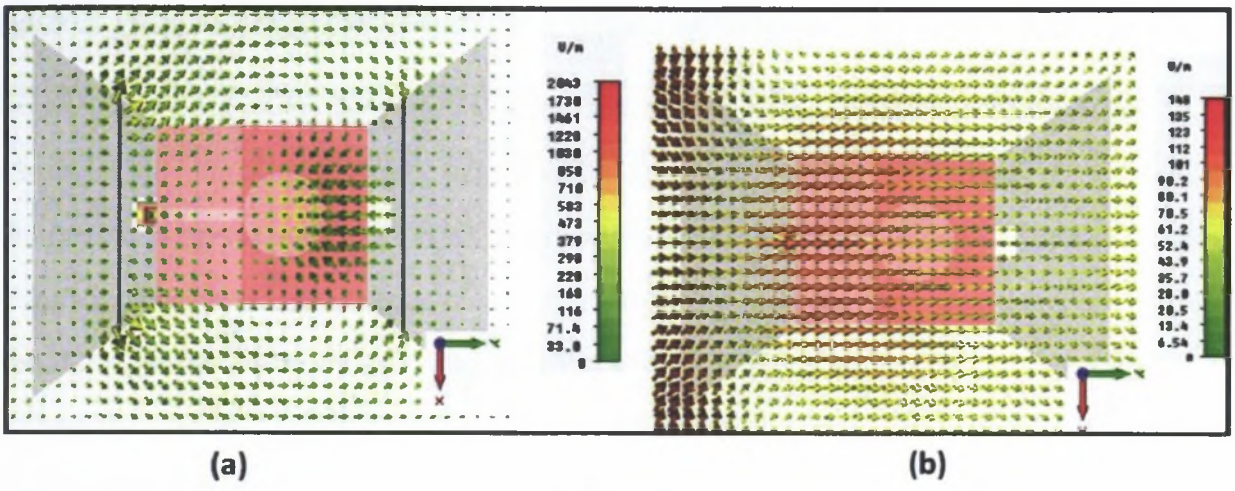


**Figure 4.13:** Transverse electric field for Structure-2 (SMS-TEM) horn on the x-y plane inside the horn at (a) z = 10 mm and (b) z = 45 mm.

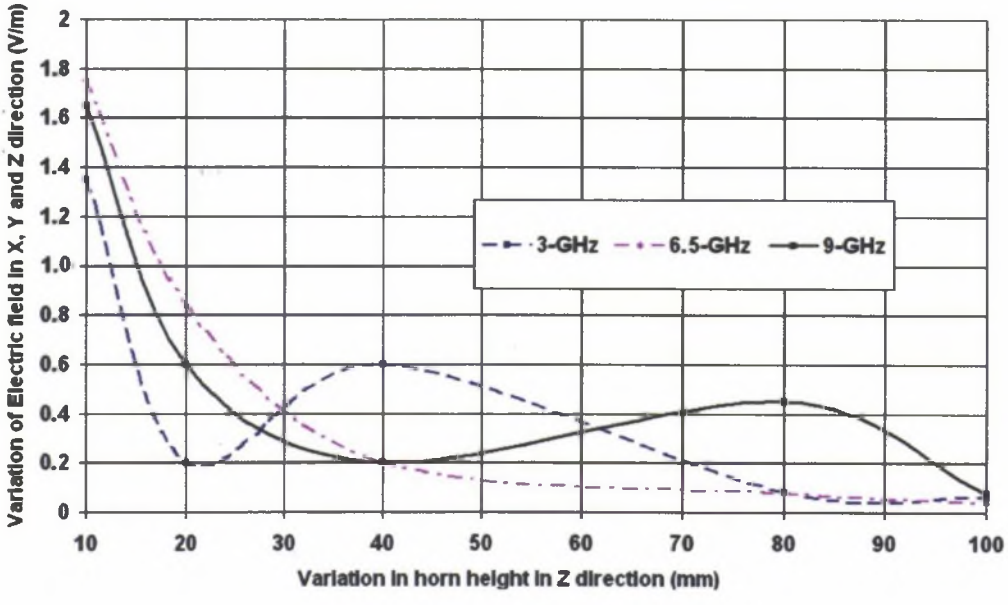


**Figure 4.14:** Variation of Electric-field components with z, at 3 GHz for Structure-2.

In the previous study of the field we tried to mount the short horn to form a true short TEM configuration as shown in Figure 4.3. Figure 4.13(b) shows that, for a short TEM horn, the E-field polarisation is parallel to the y-axis (i.e. the E-plane of a TEM horn would be in the Y-Z

plane), which follows the analogy of the traditional TEM horn. In a short TEM horn antenna, the electric field lines are between the two plates, as in a two-wire transmission line. Such a field can exist with zero longitudinal electric field (i.e. Ez = 0) as shown in Figure 4.14.

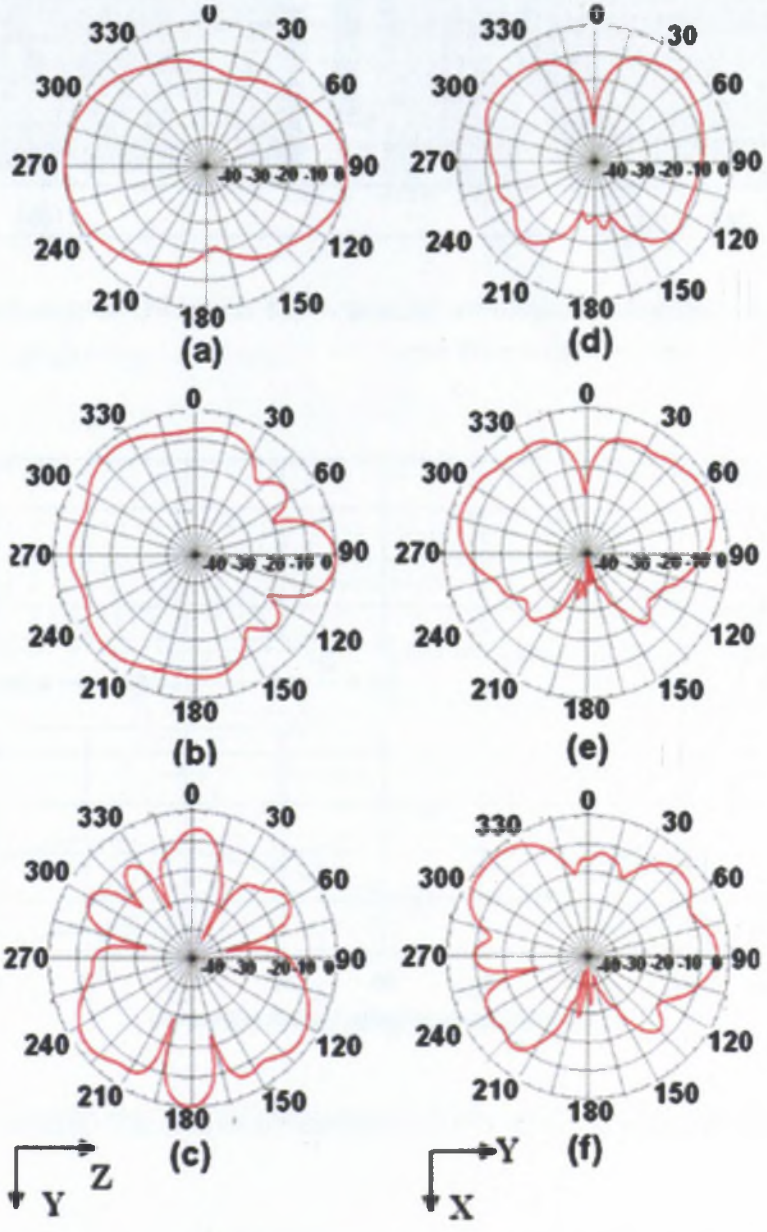


**Figure 4.15:** Radiation patterns at 3 GHz(a,d), 6.5 GHz(b,e), 9.0 GHz(c,f).

### 4.3.6 Theoretical Results and Practical Validation

Further simulation studies show that the performance of the structure is satisfactory with the air spacing. Using the air spacing, the field distribution is more like the TEM mode. As the field distribution is altered for the TP-SMS horn mounted on the FR-4 substrate, its performance degrades. To approximate an air medium at the base of the TEM horn, the two slots ($W2 = 10$ mm, $L2 = 40$ mm) were created in the top FR-4 sheet and an air gap was established between the two FR-4 sheets using Teflon spacers. It was noted that even the PCMA (without horn) made on this composite substrate has 1 dB higher gain between 8 GHz and 11 GHz as shown in Figure 4.17.

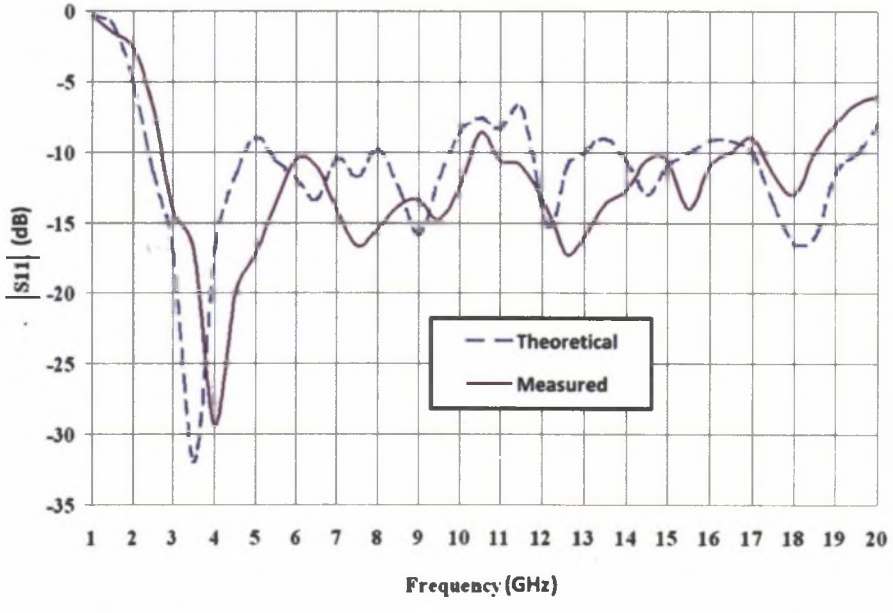


**Figure 4.16:** Predicted and measured input reflection coefficient magnitude of the structure-1 surface-mounted short horn.

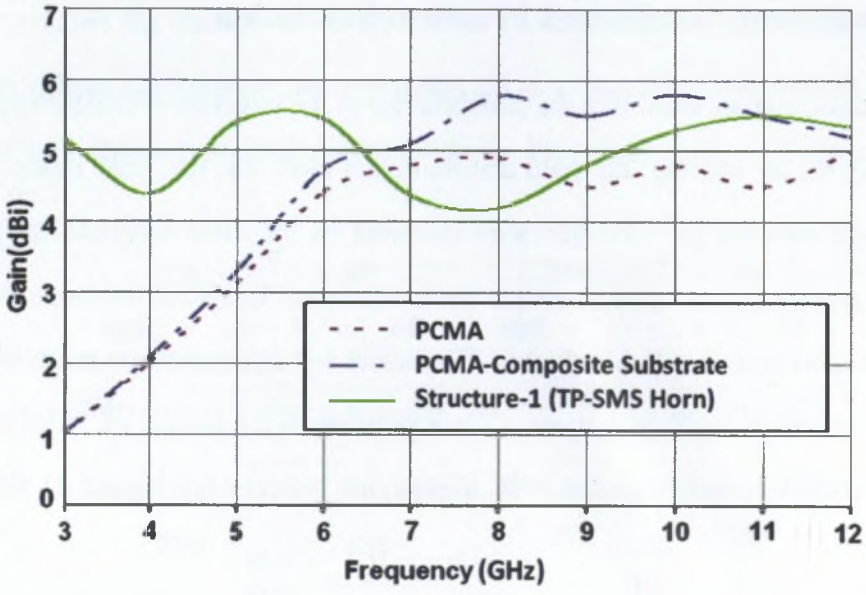


**Figure 4.17:** Measured gain of a standard PCMA, a PCMA on a composite substrate and structure-1.

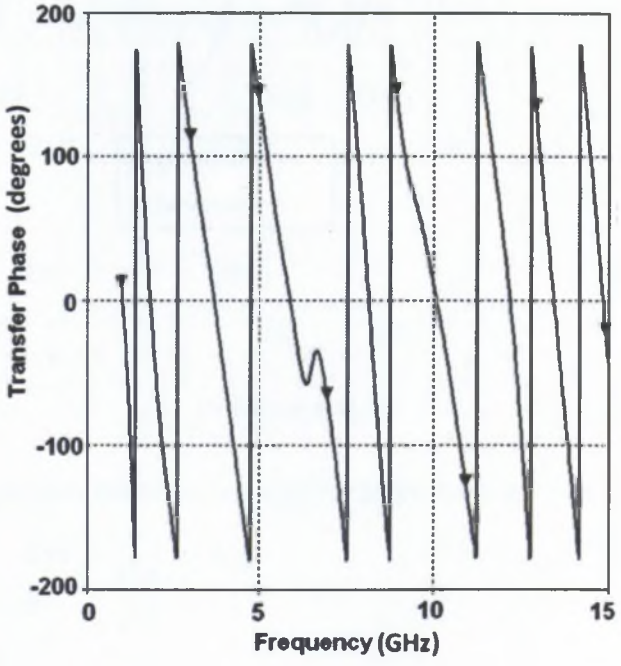


**Figure 4.18:** Phase response of structure-1.

Simulation results from CST Microwave Studio indicate that the integrated PCMA feed with

the short two-plate horn (structure-1) has improved the gain and provides flatness over a wide band. Structure-1 provides broad beam coverage in the azimuth plane and a relatively narrow pattern in the elevation plane, with only a small change of beam direction over its ultra-wide operating bandwidth as shown in Figure 4.15. The slant length chosen for the example design is 4.5 cm, which is equal to $\lambda/2.5$ at 2.7 GHz. Figure 4.16 indicates that at 1.7 GHz the predicted and measured $|S11|$ of the antenna is about -3 dB. The predicted $|S11|$ becomes -10 dB at 2.42 GHz; in measurements, -10 dB $|S11|$ occurs at 2.75 GHz.

The measured $|S11|$ is below -10 dB from 2.75 GHz to 10.14 GHz (covering most of the FCC-approved UWB bandwidth). Figure 4.17 shows the measured gain of a comparable printed circular monopole antenna (PCMA) on a standard FR-4 substrate and also on the same composite substrate. The PCMA on the composite substrate shows about 1 dB gain improvement for a range of frequencies. Otherwise the gain variation is similar in both cases a linear increase with frequency up to 6 GHz and then nearly constant gain up to 12 GHz.

The incorporation of the short horn improves the gain at the lower frequencies up to 6 GHz. Structure-1 has nearly constant gain within 5.0 dBi $\pm$ 0.5 dBi up to 12 GHz. Figure 4.18 shows that the transmitting transfer function of the new antenna has an almost linear phase response. This phase response should help to maintain the integrity of a transmitted short pulse in a pulse-based UWB system [128, 129].

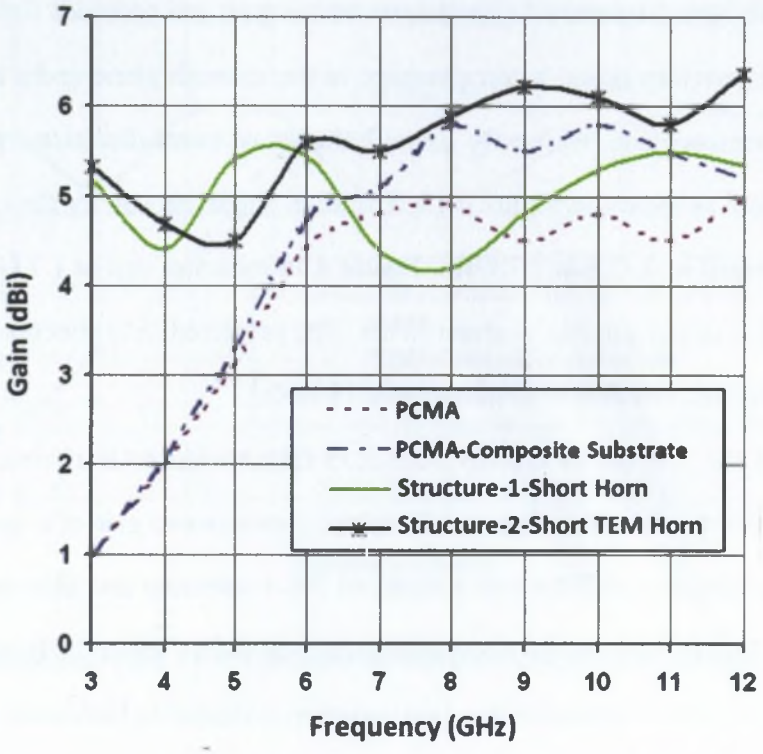


**Figure 4.19:** Experimental comparisons of gain of two different configurations of short TEM horns.

Figure 4.15(a-c) shows measured radiation patterns of structure-1 (TP-SMS horn) on the azimuth (Y-Z) plane at 3.0 GHz, 6.5 GHz and 9.0 GHz respectively. These extremely wide radiation patterns highlight the dominance of the printed monopole radiation in this plane. The presence of nulls in some directions at 9 GHz would distort the radiated pulse in those directions. Structure-1 (TP-SMS horn) narrows the beam in the elevation (X-Y) plane, as shown in Figure 4.15(d-f) for 3.0 GHz, 6.5 GHz and 9.0 GHz, respectively. The narrowing of the beam results in an increase in the directivity and gain. Even in the elevation plane, the impact of the printed monopole is evident from the null along the axis of the monopole at lower frequencies. At 9 GHz this null disappears and the beam has a small asymmetry. The beam changes its direction slightly as frequency changes over the ultra-wide bandwidth.

After evaluating the performance of structure-1 (TP-SMS horn), the gain and radiation pat-

terns of structure-2 (also called a short TEM horn) were evaluated theoretically and experimentally.

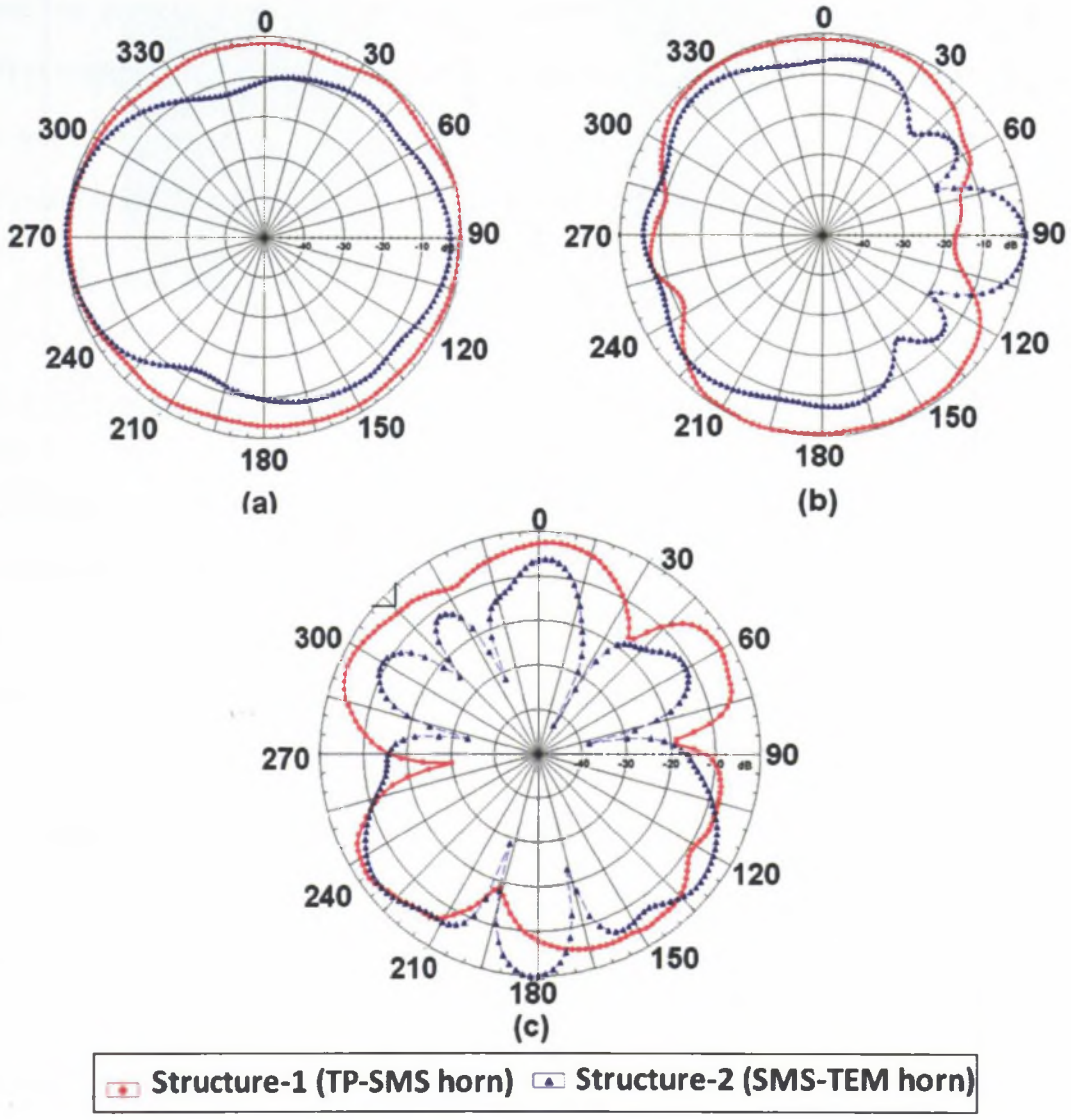


**Figure 4.20:** Comparison of measured radiation patterns of stucture-1 (TP-SMS horn) and structure-2 (SMS-TEM horn) shown in Figure 4.10.

As shown in Figure 4.19, the gain increases significantly at higher frequencies for the structure-2 horn. There are more variations in gain at the cost of higher average gain over the whole bandwidth. Further, the comparison of the radiation patterns in the elevation plane

and the azimuth plane is shown in Figure 4.20(a-c) for structure-1 and structure- 2. At lower frequencies structure-2 has a broader beam than structure-1.

In structure-2 the effect of PCMA is more dominated at the lower frequency and antenna leads to a broad beam coverage. In previous studies of the field component highlighted in Figure 4.12 and 4.14 the $E_x$ and $E_y$ component are significantly low in structure-2 compare to the structure-1 which possibly results in less cross polarisation and more gain in the main beam direction at higher frequencies.

## 4.4 Substrate Integrated Short TEM Horn Antenna (SIS-TEM)

In the previous designs of structure-1 and structure-2, the horn mounted on the substrate does not have great flexibility in design and fabrication. The horn structure was fabricated separately and mounted on top of the printed monopole substrate using teflon/nylon screws. This increases the fabrication complexity. To overcome the shortcomings of structure-1 and structure-2, a printed surface integrated short TEM (SIS-TEM) horn fed by a printed semicircular disc monopole antenna is presented in this section. It has ultra-wideband impedance matching and broad beam coverage with a small gain variation across the band which helps in non-dispersive pulse transmission and enhances the performance of UWB systems using the MB-OFDM techniques discussed in chapter 2. The semicircular-disc monopole design is well matched and provides an impedance bandwidth of over 20 GHz. The integrated horn is fabricated on the same substrate as the monopole, and bent at a suitable slant angle, which provides a complete integrated structure compared to structure-1 and structure-2.

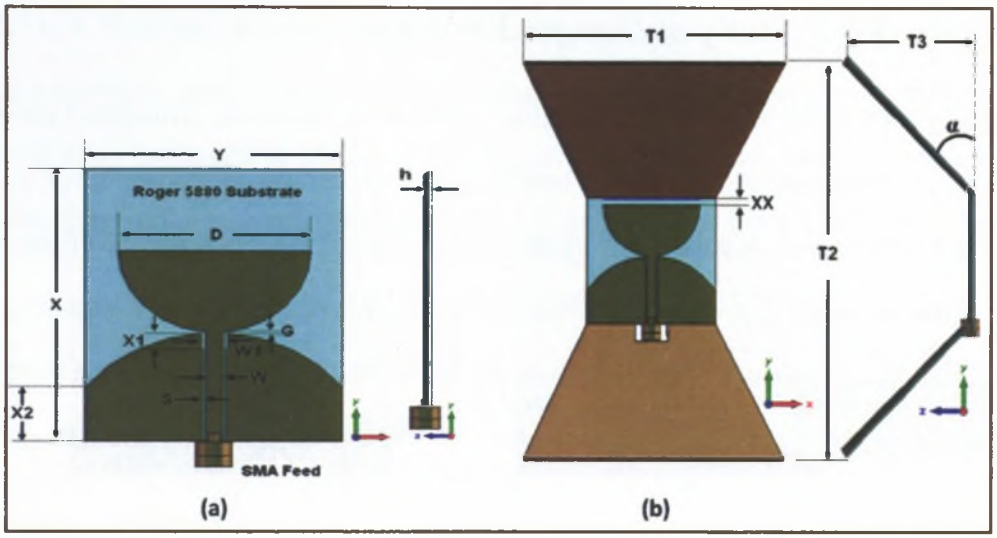


**Figure 4.21:** (a) CPW-fed semicircular disc monopole antenna (b) Surface integrated short TEM horn.

### 4.4.1 Antenna Design

The proposed antenna is shown in Figure 4.21. It consists of a two-plate short horn mounted on the surface of a CPW-fed semicircular-disc monopole. Figure 4.21(a) shows the semicircular-disc monopole with a rectangular slit etched out from the ground plane of the CPW-fed line to improve impedance bandwidth. The antenna is made on a Rogers 5880 substrate with dielectric constant of $\varepsilon_r$ = 2.2, thickness $h$ = 0.787 mm. The overall dimensions of the semicircular disc are $X = Y = 40$ mm. The 50$\Omega$ CPW feed line has a 3mm-wide $(W)$ metal strip and a 0.3 mm gap $(S)$. The feed gap G and the rectangular slit dimensions are optimised as described in the next section. After optimising the semicircular-disc dimensions, the short horn is mounted on the top surface of the substrate. Figure 4.21(b) shows the geometric arrangement of the integrated antenna. Some of the optimised parameters, as described in the next section, are: mount gap $XX = 2$ mm, aperture lengths $T1 = 80$ mm and $T2 = 114$ mm, physical height $T3 = 40$ mm and slant angle $\alpha = 45^0$.

### 4.4.2 Parametric Study of Designed Antenna

The integrated SIS-TEM horn presented in this section is similar to the structure-2 presented in section 4.3.3. The values of slant angle, height and aperture ratio are chosen same as the one optimised for structure-2. A parametric study was carried out to investigate the effects of other important parameters on impedance matching and gain. This will be helpful for antenna designers during the design process. The effects of the slit etched in the ground plane of monopole and the mount gap $XX$, are critical parameters for impedance matching when designing the antenna.

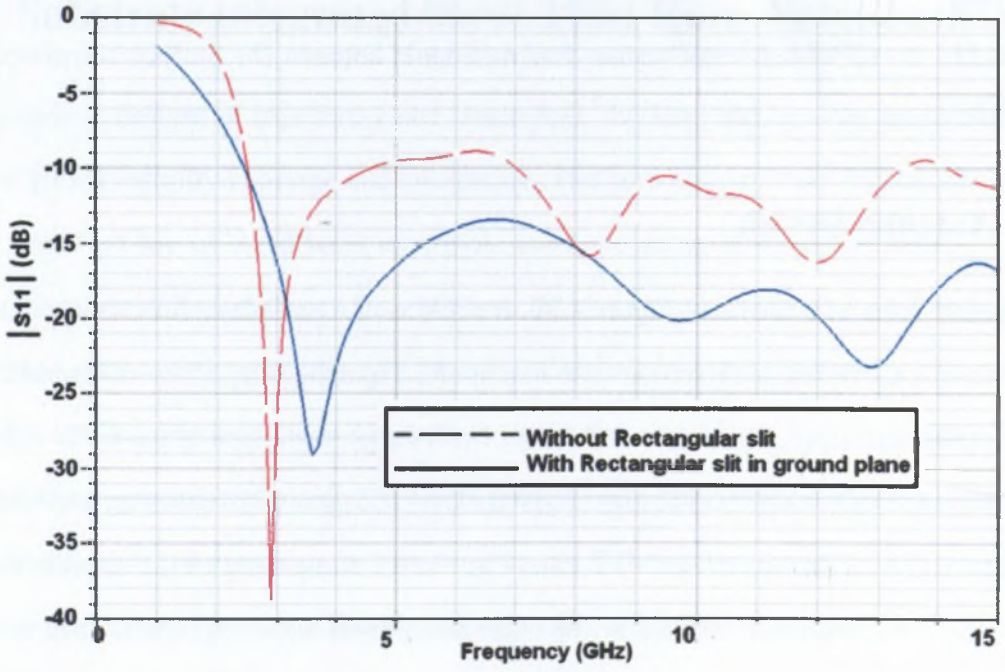


**Figure 4.22:** The $|S11|$ of the CPW-fed disc monopole antenna with and without the rectangular slit.

As shown in Figure 4.22, the predicted reflection coefficient of the semicircular-disc monopole antenna is significantly improved due to the introduction of the slit. With the slit, the return loss is greater than 13.4 dB from 2.5 GHz to 15 GHz. The mount gap $XX$ near the top of the monopole is critical in maintaining the impedance match across a wide band as illustrated in

Figure 4.23. A 2mm gap provides good impedance matching across the band and hence it was chosen in the present design. The slant angle $\alpha$ can be used to control the gain variation across the bandwidth as explained in section 4.3.3. Figure 4.7 shows that, with a slant angle of 45 degrees, the gain variation is minimal across the frequency range from 2 GHz to 10 GHz.

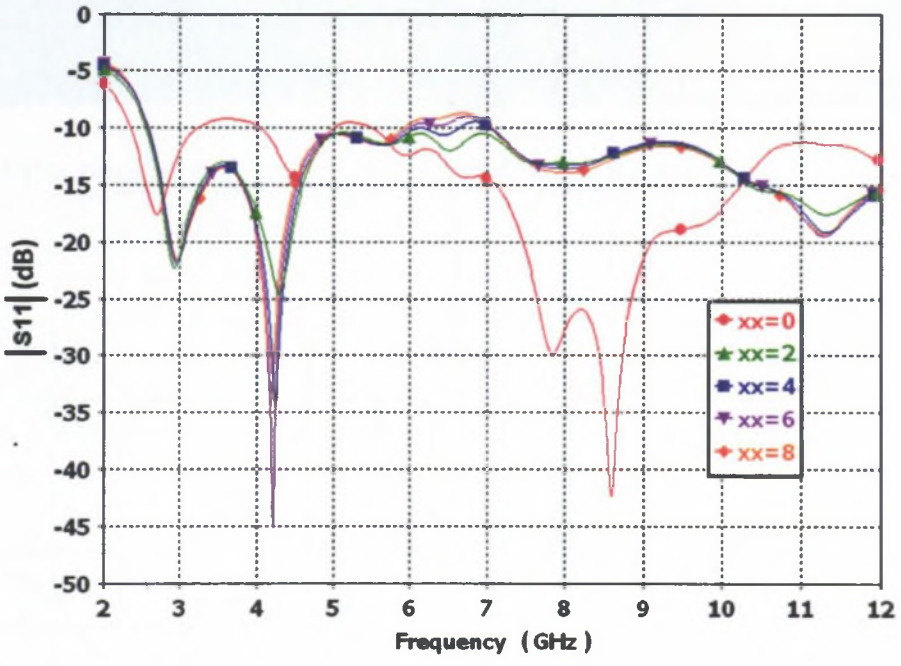


**Figure 4.23:** $|S11|$ for different mount gaps $(XX)$ between the short horn and the top of the monopole.

### 4.4.3 Results and Discussions

A prototype of the surface integrated short TEM horn is shown in Figure 4.24. An optimised physical height $(T3)$ of 40 mm is chosen for the design example, and is approximately equal to $\lambda/4$ at 3 GHz. Note that the walls of the horn and the monopole are fabricated from the same substrate.

**Figure 4.24:** Hardware prototype of CPW-fed semicircular-disc monopole antenna with the surface integrated short TEM horn.

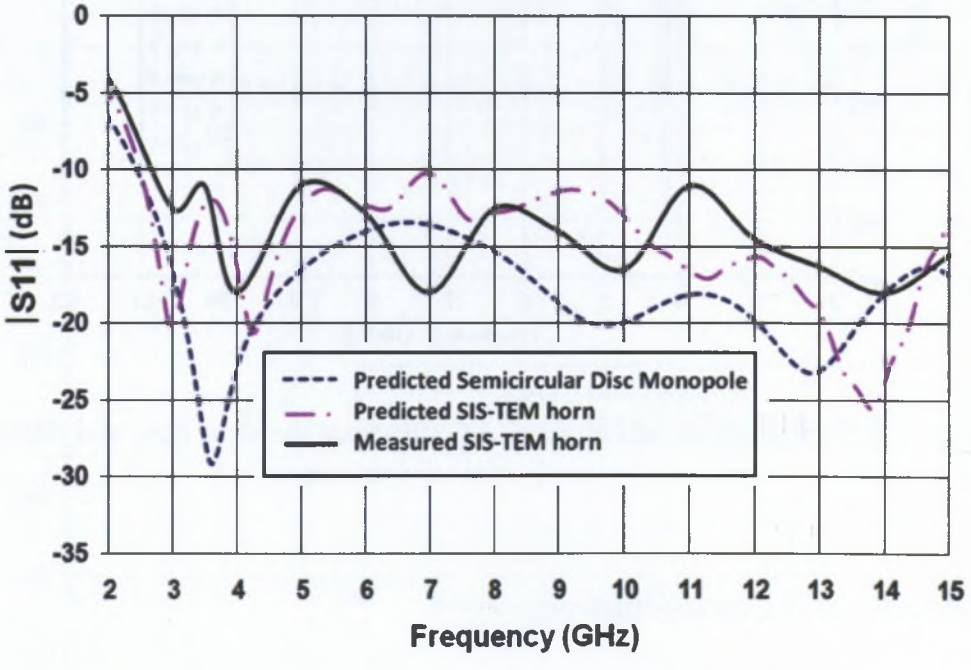


**Figure 4.25:** Comparison of measured $|S11|$ of the CPW-fed disc monopole antenna, with and without the short horn.

The predicted and measured return loss of the integrated antenna is shown in Figure 4.25. It reaches 10 dB at 2.52 GHz and it continues to be greater than 10 dB up to 15 GHz, covering the entire FCC-approved UWB band. Figure 4.26 compares the gain of the proposed antenna with that of a similar semi-circular disc monopole antenna without the horn on the same Rogers

5880 substrate.

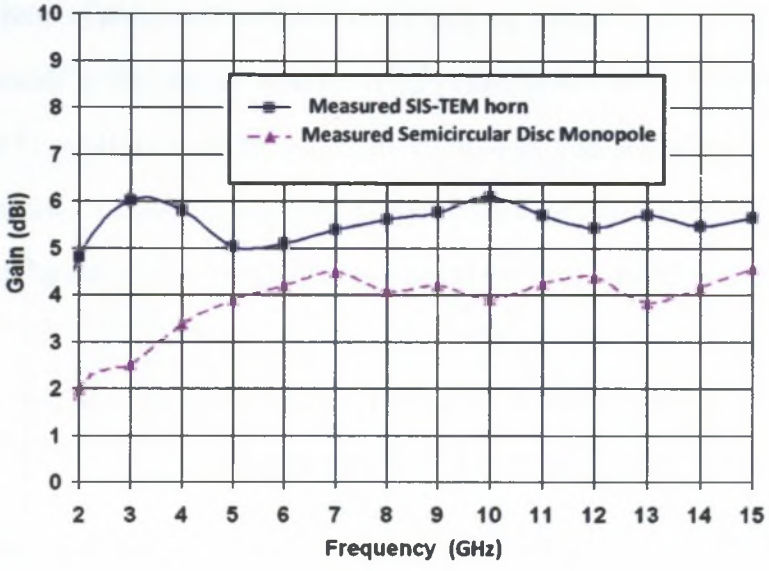


**Figure 4.26:** Comparison of measured gain of the CPW-fed disc monopole antenna with and without the short horn.

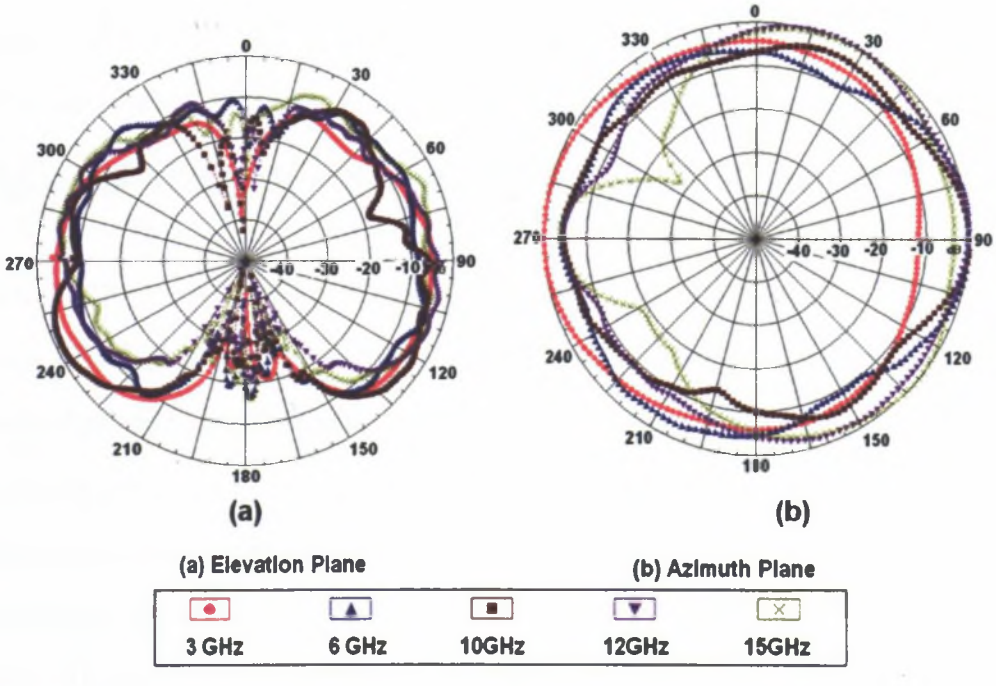


**Figure 4.27:** Measured radiation patterns of surface integrated short TEM horn (a) E-Plane (b) H-Plane.

The gain of the antenna without the horn exhibits an almost linear increase with frequency up to 6 GHz and then a nearly constant gain up to 15 GHz. The incorporation of the short horn improves the gain at the lower frequencies up to 6 GHz. As a result of this enhancement, the new antenna has a nearly constant gain of 5.5 dBi $\pm$ 1.1 dB from 3 GHz to 15 GHz. Figure 4.27 shows the radiation pattern at five representative frequencies: 3, 6, 10, 12 and 15 GHz. The azimuth plane shows a broad beam coverage and as frequency is increased the beam becomes more directional due to the horn aperture.

### 4.4.4 Reflector Design for the UWB Antennas

The antennas presented in the above sections have bidirectional radiation, and power is lost in the wanted direction. In order to further improve the gain, which is an essential feature for the LOS scenario (Discussed in section 4.1), a reflector must be optimised suitable for the short horn, which makes the antennas more directional and improved gain in the main beam direction. A semicircular reflector is presented in this section. This reflector increases the average gain of the antenna by 1 dB over the UWB band while maintaining the gain variation in the same band. It was found that a planar reflector does not provide these advantages. The result of this investigation is shown in Figure 4.28, where $'ref'$ is the radius of the reflector. A reflector radius in the range of 30 mm to 35 mm gives minimum mismatch from 2.5 GHz to 15 GHz. For a compact structure, a 30 mm reflector height is adopted in the design. All simulations were carried out with CST Microwave Studio. The final antenna structure has a physical height (T3) of 40 mm for the short horn and a reflector radius (ref) of 30 mm. The predicted return losses of the integrated antenna with and without reflector are compared with those for the semi circular-disc monopole in Figure 4.29. The lowest frequency with a 10 dB return loss is 2.52 GHz and 2.86 GHz for the short horn with and without reflector respectively. The upper limit is above 15 GHz and the return loss is greater than 10 dB over the entire FCC-approved UWB band.

Figure 4.30 and Table 4.2 compare the predicted gain and its variation in the proposed antenna against those of the semi circular-disc monopole. The gain of the monopole shows an almost linear increase with frequency up to 6 GHz and then a nearly constant gain up to 15 GHz.

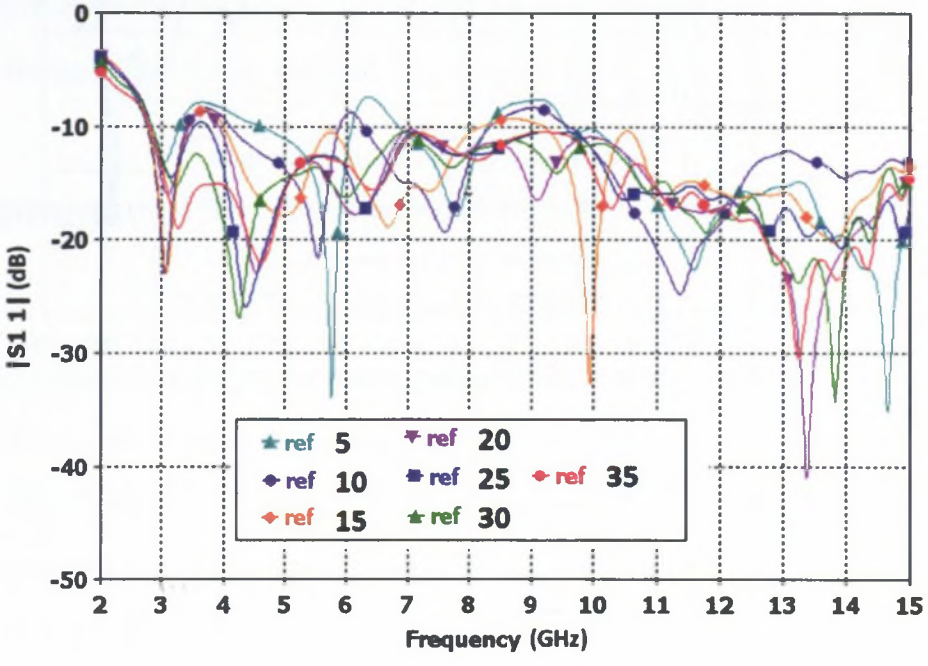


**Figure 4.28:** Predicted $|S11|$ for different reflector heights (ref) for the short horn.

**Table 4.2:** Predicted gain and its variation for three antenna designs

| **Configurations** | $f_L$ (GHz) | $f_H$ (GHz) | Bandwidth (GHz) | Avg. Gain and Variations |
|---|---|---|---|---|
| **Semicircular Disc** | 2.50 | 15 | 12.50 | 3.8 dBi $\pm$ 1.6 dB |
| **SIS-without reflector** | 2.52 | 15 | 12.48 | 5.5 dBi $\pm$ 1.1 dB |
| **SIS-with reflector** | 2.86 | 15 | 12.14 | 6.5 dBi $\pm$ 1.1 dB |

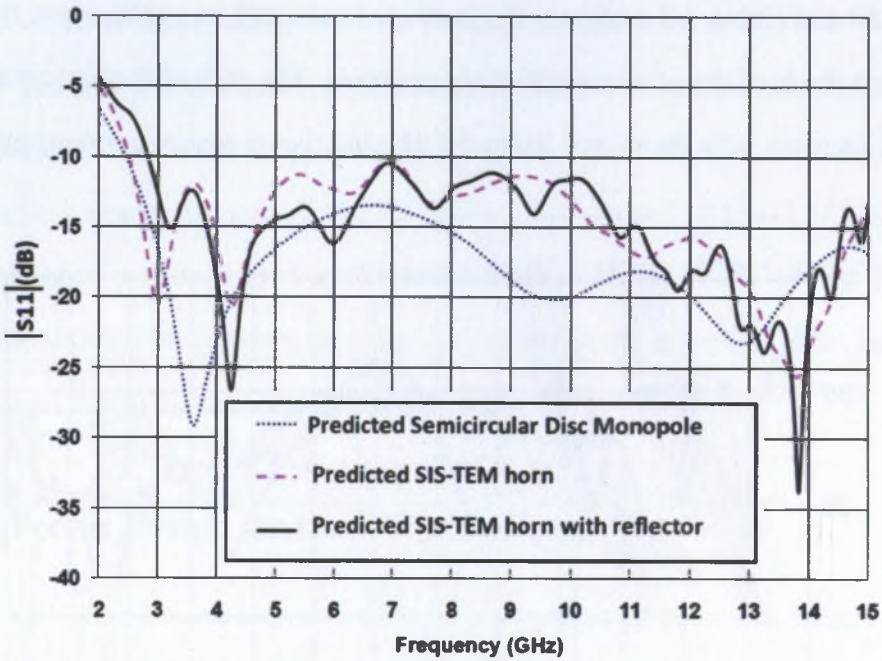


**Figure 4.29:** Comparison of predicted $|S11|$ of monopole, with short horn and with reflector.

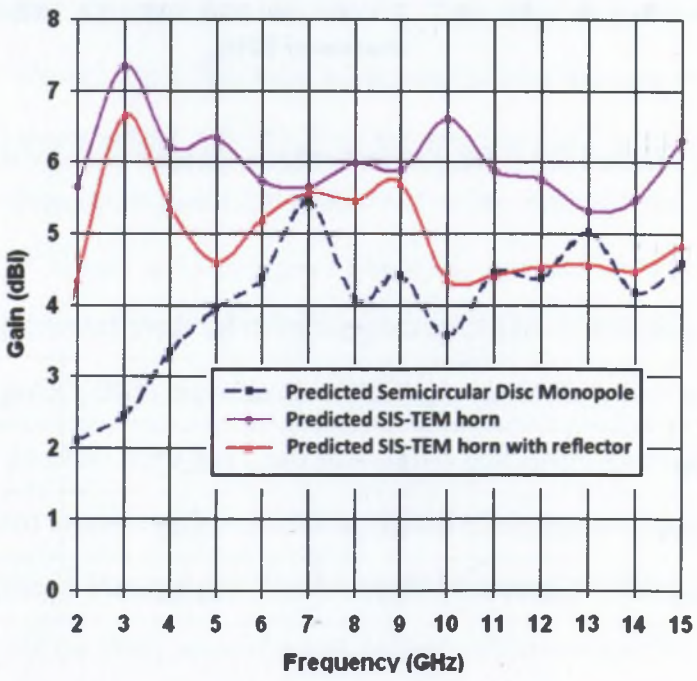


**Figure 4.30:** Comparison of gain of monopole with short horn and with reflector.

The incorporation of the short horn improves the gain at the lower frequencies up to 6 GHz. As a result of this enhancement, the new antenna has a very flat gain of 5.5 dBi ± 1.1 dB from 2 GHz to 15 GHz. The peak variation of 1.7 dB is noticed at 3 GHz. The antenna with a short horn and a reflector has a nearly constant gain of 6.5 dBi ±1.1 dB from 2 GHz to 15 GHz. The peak variation at 3 GHz is 1.1 dB. Thus the reflector further improves the average gain by 1 dB and limits the gain variation to ± 1.1 dB.

## 4.5 Summary/Conclusions

In this chapter the new concept of a surface-mounted short TEM horn fed by a printed monopole has been discussed. In many practical situations, identified in section 4.2, these antennas can be used for a better system performance. Four different configurations of antennas, with hardware testing of three antennas, is carried out in this work to prove the concept. A complete field analysis is presented, justify the claims presented for various short TEM horn configurations. A complete study of the effect of various parameters like slant angle, slant height and mounting location of the short horn is presented in this work.

The various feed arrangements for a short horn are demonstrated successfully with two different monopoles, namely PCMA and semi-PCMA. The PCMA-fed structure-1 (TP-SMS horn) and structure-2 (SMS-TEM horn) have been presented in section 4.3. The TP-SMS horn has nearly constant gain within 5.0 dBi ± 0.5 dB up to 12 GHz. Compared to the antenna presented in Chapter 3 based on proximity-coupling, these antennas have improved bandwidth at the cost of additional size of the short horns, while the advantage of gain flatness makes these antennas useful for various systems. Structure-2 (SMS-TEM horn) proved to be a closer match to a conventional TEM configuration in term of field components inside the aperture of the horn. The effect of a printed-feed antenna is more dominant at a lower frequency, and as frequency goes higher the gain increases with the frequency. A broad beam coverage is noticed

with structure-2 compared to the structure-1. Structure-2 shows an increase in the gain at higher frequency; the gain is approximately 1.2 dB higher than for structure-1 from 6 to 10 GHz while maintaining the gain in the lower region of UWB, 3.1 GHz to 6 GHz.

Motivated by the design of a short horn presented in section 4.3, a more promising surface integrated horn is presented in section 4.4. In this antenna the horn structure is fabricated on the same substrate as the printed semi-circular PCMA. This antenna yields a better impedance bandwidth (operates from 2.5 GHz to 15 GHz) compared to the previously introduced short horn structure-1 and 2, while gain shows similar trends with 5.5 dBi $\pm$ 1.1 dB from 2 GHz to 15 GHz. Furthermore, to improve the gain, which is more desirable in LOS and GPR applications a semi-circular reflector is introduced. The design reflector enhances the average gain by 1 dB over the whole operating bandwidth while maintaining the gain variation. The proposed curved reflector is hard to fabricate and new means to design a suitable reflector need to be explored for the UWB antenna. An effort to design a reflector using the UWB periodic structure is presented in the next chapter, and is more suitable to the printed nature of UWB antennas.

# Chapter 5

# Phase Coherence with Frequency Selective Surface Reflector

## 5.1 Introduction

Several printed configurations of monopole and slot antennas that have been demonstrated for use in UWB systems were discussed in Chapter 3 and 4. These printed UWB antenna configurations have an impedance bandwidth more than 110% (3.1 GHz to 10.6 GHz) with a nearly omni-directional (OD) radiation pattern from 3 GHz to 6 GHz. Beyond 6 GHz these printed antennas lose their OD behaviour and become more directional as previously discussed in this thesis. The previously presented designs have bidirectional radiation patterns as discussed in Chapters 3 and 4, which means that for line-of-sight (LOS) applications half of the power radiates in the wrong direction. An appropriately designed UWB reflector will limit the back radiation and increase the gain in the direction of the forward beam. Designing such a reflector for a bandwidth of 110% is a challenging task indeed. Usually the metallic screen reflectors are placed at a distance of $\lambda/4$ to provide in-phase reflection. At the end of Chapter 4 an attempt is made to design a curved metallic reflector suitable for a TEM horn. Nevertheless, the design

presents interesting results, proposed solution needs special care in making curve geometry of reflector, which increases the design complexity. A new method to design the reflector needs to be explored for eliminating this drawback and filling the gap between present UWB antennas. Research in periodic structures can help in solving this key problem of reflector design. Up to now research on this structure was limited to broadband or multiband operations. This chapter is focused toward the design of a reflector with over 110% bandwidth using periodic structures. Properly designed reflectors are capable of manifesting huge bandwidth and phase coherence over the ultra-wide-bandwidth. A complete reflector design analysis and validation are presented in this chapter.

### 5.1.1 Chapter Contributions

This chapter presents the following contributions:

- The need of a suitable reflector for UWB applications is highlighted.
- The concept of phase coherence over an ultra-wide bandwidth is presented.
- The design mechanism of dual-layer frequency selective surfaces (FSS) shows a potential for a good reflector with over 110% bandwidth.
- A complete parametric and field analysis of a dual-layer surface is presented to explain its operating mechanism.
- A complete normal and oblique incidence study of an ultra-wideband FSS is presented.
- The experimental verification and validation of the surface in the presence of an ultra-wideband antennas is presented.
- A design of a multi-layer(Four-layer) FSS surface with constant gain using UWB antenna is proposed.

- The complete experimental validation and hardware verification of dual-layer and four-layer FSS reflector is demonstrated.

This chapter is primarily organised in six different sections. Section 5.2 one explains the background and related work. In section 5.3 the concept of phase coherence and the understanding of UWB FSS surfaces is highlighted. Section 5.4 covers the complete study of dual layer FSS with oblique studies under subsections. This section also covers the optimisation, parametric analysis and field studies. Section 5.5 covers the design and testing of the designed FSS surfaces with UWB antennas. Section 5.6 covering a multilayer FSS with more stability in gain over UWB bandwidth. The work is concluded in Section 5.7

## 5.2 Background and Related Work

Frequency selective surfaces (FSSs) are spatial electromagnetic (EM) filters that exhibit total reflection or transmission over a given frequency band to an incident electromagnetic wave [78–80]. In recent years, development of periodic structures has helped to solve some of the crucial antenna problems. With the possibility of creating a perfect magnetic conductor (PMC) and its in-phase reflection, efficient radiation for antennas placed close to an electromagnetic-bandgap (EBG) ground plane [78] has been achieved. In addition, by forbidding the propagation of EM waves in certain frequency bands, these configurations can be used to block the propagation of waves and/or guide them in a desired direction [79], [78]. In the case of narrowband applications, controlling the in-phase radiation of incident plane wave over mushroom-like EBG [78] and Uni-planar compact photonic band-gap (UC-PBG) structures were demonstrated in the past [78]. In these categories of periodic structures FSSs or partial reflecting Surfaces (PRSs) are good candidates to be employed in conjunction with printed antennas [80], [131], [132]. Such configurations have been extensively studied in the past for enhancing the performance of antennas for both narrowband and broadband operations [133], [134].

In [81], a reconfigurable printed dipole array is examined in the presence of a multilayer FSS. The FSS is positioned in the ground plane of a reflector array, aiming to achieve broad band operation by controlling the phase of the reflected wave. In some recent articles a FSS is used as a backing reflector to extend the frequency range of usability. In another wideband application, reported in [82], the FSS has been sandwiched between the antenna and the ground plane, providing an additional reflecting plane for the most critical higher-frequency band. In most of these designs the FSS is limited to narrowband operation. Dual- and wide-band operations are targeted in some current publications [83], exploiting the potential offered by the association of two different patch elements over a single unit cell, namely a square loop and a crossed dipole. The demonstrated structures show a -10 dB transmission bandwidth of 52%. In this work a dual layer and a four-layer FSS with a theoretical bandwidth greater than 133% are presented to cover the FCC sectioned 110% UWB bandwidth. Performance of the designed FSSs has been tested in a laboratory environment. These FSSs have the potential to be employed as a reflector for an arbitrary UWB antenna. Such surfaces allow the antenna to be mounted close to the reflector surfaces, with reduced effect on the antenna impedance, and are good candidates for applications where the thickness of the antenna needs to be reduced. Further, to extend the concept and achieve less variation in gain, a four-layer compact design with a UWB slot antenna is proposed with a variation of 0.5 dB in gain over a 110% impedance bandwidth.

## 5.3 Principle and Operation

This section highlights the principles behind the design of a reflector and is further extended to the operation of Frequency Selective Surfaces used for designing UWB reflectors.

### 5.3.1 Reflector Design

It is well known that reflectors behind antennas only work properly when the radiation generated by the antenna and reflected back by the backing plane is in phase with the radiation directly generated by the antenna itself.

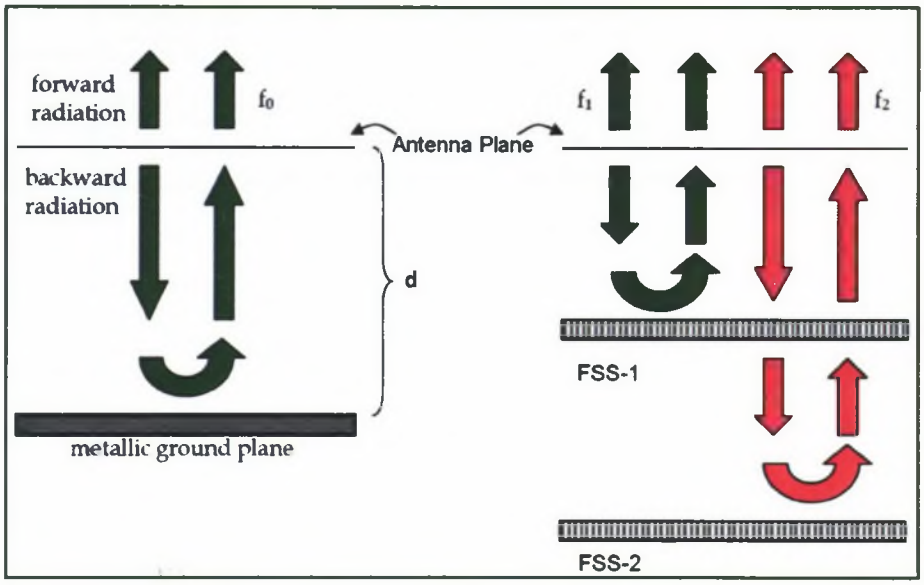


**Figure 5.1:** (a) Standard metallic reflector (b) Multiple FSS reflectors.

This happens when the distance between the antenna and the backing plane is a multiple of one quarter of the working wavelength, as shown by the following equations:

$$2\frac{2\pi}{\lambda}d - \pi = 2\pi N \ , \tag{5.1}$$

while

$$d = \frac{\lambda}{4(1+2N)} \ , \tag{5.2}$$

where d is the distance between the antenna plane and the backing plane, $\lambda$ is the wavelength, $\pi$ is the reflection phase given by an infinite perfect metallic ground plane and **N** is an

integer greater than or equal to zero (The first integer corresponding to **N** equal to zero typically is chosen). Figure 5.1 shows the reflector placement under the antenna and a proposal for a new FSS-based multilayered reflector.

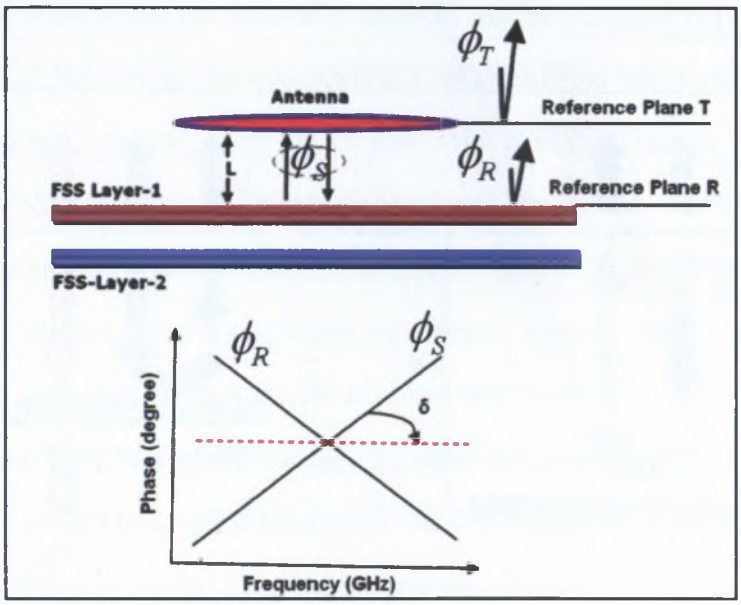


**Figure 5.2:** FSS application for gain enhancement: Reflection at different frequencies occurs at different layers (top). Frequency response of the two phases, $\phi_R$ and $\phi_S$ (bottom).

### 5.3.2 Phase Coherence Over an Ultra-Wideband

FSSs can be efficiently employed in reflector designs for broadband applications. The basic idea is to design a multilayer FSS structure where each layer provides reflectivity for a specific frequency band. This means that each reflective plane may be placed at an appropriate distance from the antenna, generating reflections from different layers and therefore broadening the usable range of the entire backing plane. In order to work properly, the uppermost reflective planes must be transparent to frequencies to be reflected by the lowermost planes. For this type of application it is natural to consider FSSs working in the passband, i.e. away from the stopband for the layer close to the antenna, when signals are reflected from the lower layers. As mentioned earlier, phase plays a critical role, which as explained below for a dual-layer structure.

In order to understand the functionality of the dual-layer FSS, its layout and the components of the reflected wave at the reference plane $T$ are illustrated in Figure 5.2. An antenna placed above the FSS radiates toward the FSS (downwards) as well as away from the FSS (upwards). The downward wave is expected to be reflected almost completely by the FSS layers at all concerned frequencies. To generate a reflected wave with a nearly constant reflection phase over an ultra-wideband the two layers of the FSS must be optimised. FSS Layer-1 is composed of a set of cross dipoles and slots. This layer exhibits a reflection phase of $\phi_1$ (at Reference Plane R) and is responsible for providing reflection at higher frequencies.

Layer-2 of the FSS, placed below Layer-1, consists of similar cross dipole and slots with a rectangular slit cut in the slot. FSS Layer-2 is designed to work for lower frequencies and is characterised by a reflection phase delay of $\phi_2$ ( at the reference plane R). The phase delay of the combined reflected wave from the multilayer FSS is $\phi_R$ at Plane R. At Plane T, the phase $\phi_T$ =$\phi_R$ + $\phi_S$ where $\phi_S$ is the two-way free-space propagation delay over the distance L given by:

$$\phi_S = 2 \times 2\frac{\pi}{c} f \times L \,, \tag{5.3}$$

The objective is to achieve a constant $\phi_T$ over an ultra-wideband as shown in Figure 5.2(b) (dotted line). $\phi_S$ is obviously frequency dependent and its positive slope depends on the spacing between the antenna and the reflector ($L$). Hence, ideally, $\phi_R$ must have a negative constant slope to compensate for the positive slope of $\phi_S$.

$$Phase = 2 \times 2\frac{\pi}{c} f \times L + \phi_R \,, \tag{5.4}$$

while

$$\phi_R \cong f(\phi_1, \phi_2)(at\ reference\ plane\ R) \,, \tag{5.5}$$

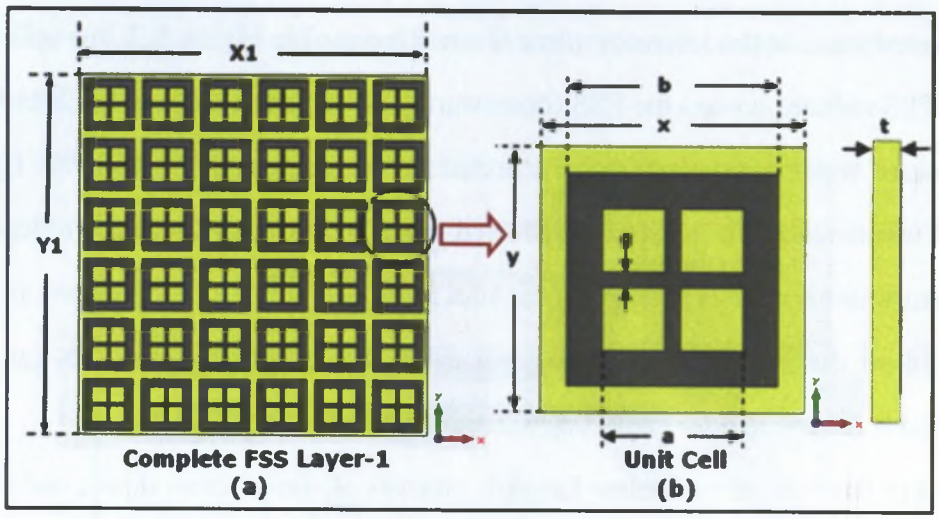


**Figure 5.3:** (a) Frequency selective surface Layer-1, for higher frequency range (b) Unit Cell for Layer -1.

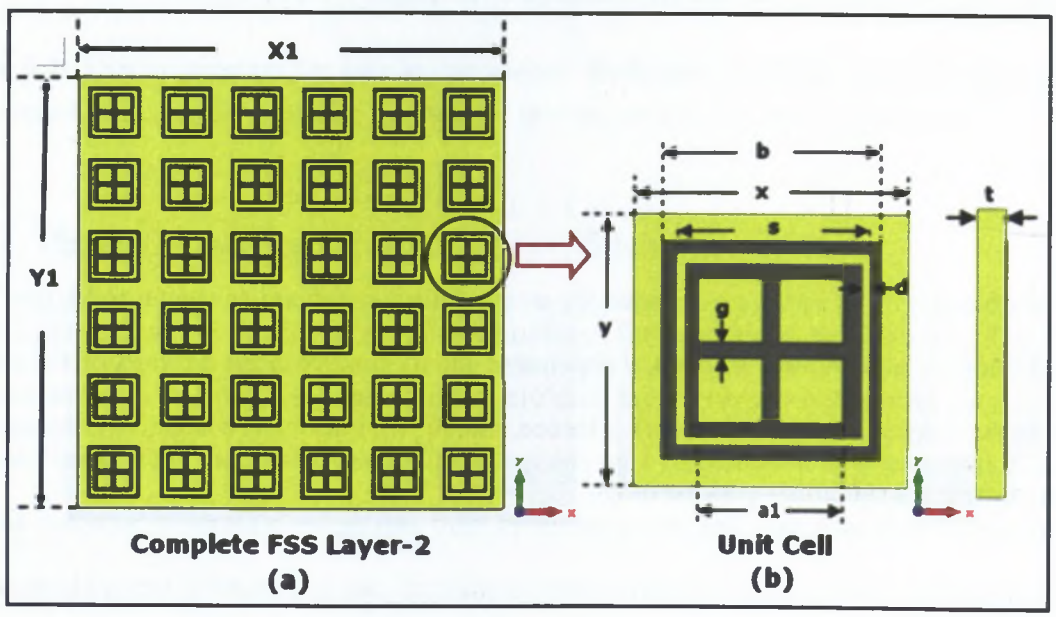


**Figure 5.4:** (a) Frequency selective surface Layer-2, for lower frequency range (b) Unit Cell for Layer-2.

## 5.4 Dual-Layer FSS Design

Initially the design of a dual-layer FSS is considered. The first layer of the FSS unit cell discussed in [83] consists of a cross dipole and a slot.

**Table 5.1:** Dimensions of optimised dual-layer FSS Unit cell

| **Parameter** | X | Y | a | al | b | g | d | s | L |
|---|---|---|---|---|---|---|---|---|---|
| Value (mm) | 15 | 15 | 10 | 8 | 12 | 0.9 | 1 | 11 | 9.5 |

The effect of the slot window width $a$ was numerically studied with the help of CST Microwave Studio [97] using the technique based on the waveguide model. Figure 5.5 shows the waveguide model of the dual-layer unit cell: perfect-magnetic-conductor (PMC) boundaries have been assigned to the two closing walls orthogonal to the x axes while perfect-electric-conductor (PEC) boundaries have been employed on the two surfaces having their normal unit vector parallel to $\pm$y.

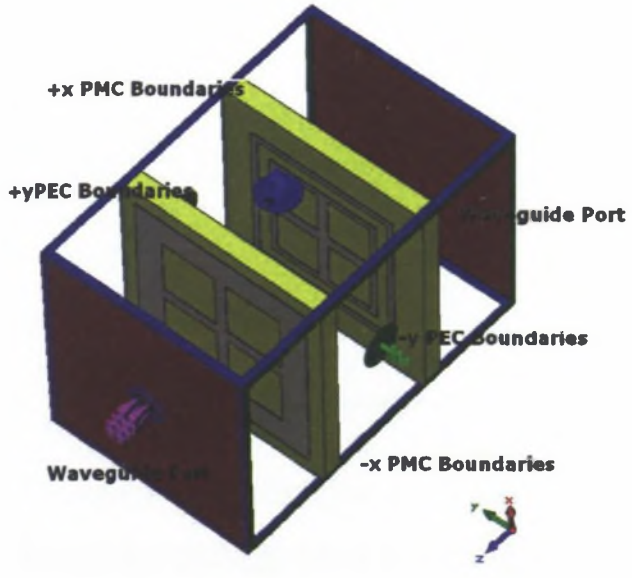


**Figure 5.5:** Waveguide model for multilayer UWB unit cell.

The design parameter $a$ affects the resonance frequency and primarily controls the upper part of the UWB band from 8 GHz onwards, giving a stop bandwidth of around 50%. The complete geometry and unit cell of Layer-1 is shown in Figure 5.3.

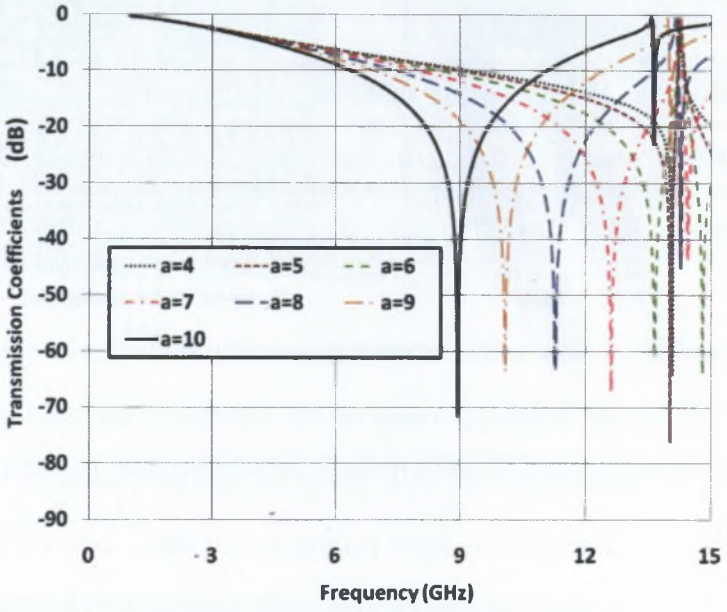


**Figure 5.6:** Parametric sweep of parameter $a$ for the unit cell in Figure 5.3.

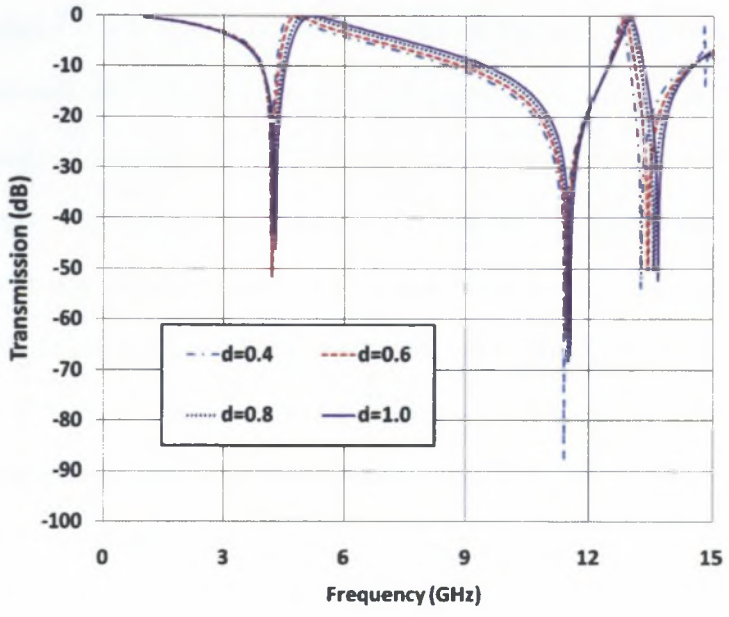


**Figure 5.7:** Parametric sweep of parameter $d$ for the unit cell in Figure 5.4 ($a = 10$ mm).

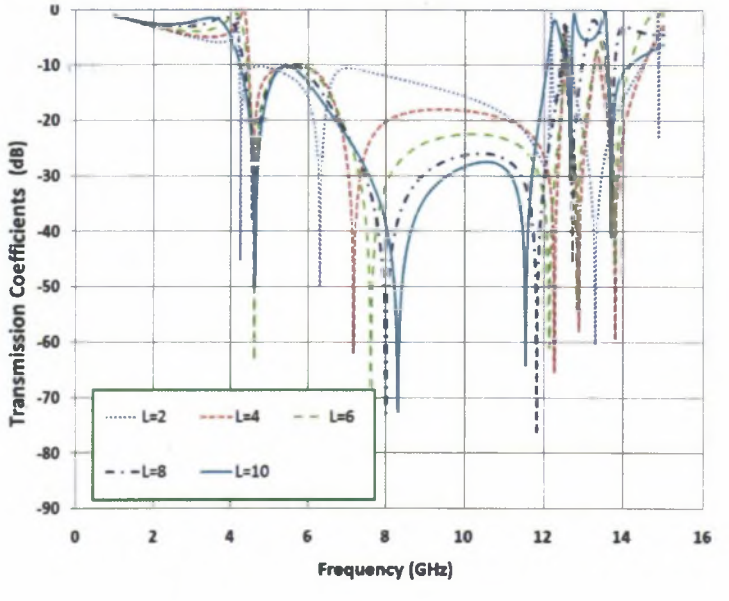


**Figure 5.8:** Parametric sweep for separation length $L$ between layers of the dual-layer unit cell.

The Layer-1 unit cell resonates at frequencies between 8.9 GHz and 13.6 GHz as shown in Figure 5.6 and the widest stop bandwidth is achieved for $a = 10$ mm. Layer-2 is optimized to

reflect the frequencies that are passed by Layer-1. Unit cell in [83] is considered in Layer-1 an additional slit is inserted in the metal frame as shown in Figure 5.4,The thickness $d$ is optimised and set to 1.0 mm to get maximum possible bandwidth for the additional frequencies. These two layers are then stacked together. The gap ($L$) between the two stacked layers plays a critical role and has been optimised. Figure5.9 shows the reflection magnitude and the phase of the dual-layer unit cell. The magnitude of the transmission coefficient is below -10 dB over a 133% bandwidth (3.5 GHz to 11.45 GHz). Note that wave is incident at port 2; Port 1 is the port on the back side of the unit cell. The dimensions of the dual-layer unit cell are given in Table 5.1. Figure 5.10 shows the predicted reflection phase and the transmission coefficient of FSS designed to produce such a coherent reflected wave at the plane of the antenna over an ultra-wide band. More significantly, the variation in phase is almost linear across the whole band (refer S22 curve in Figure 5.10).

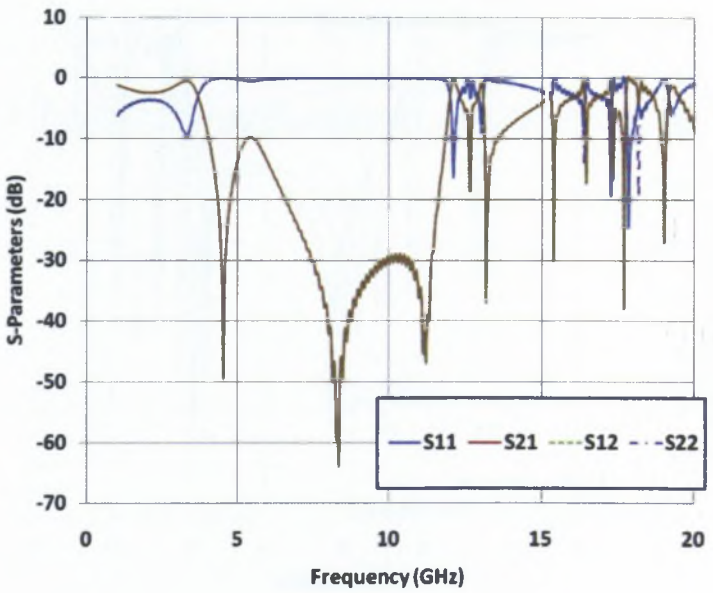


**Figure 5.9:** Theoretical reflection and transmission magnitude .

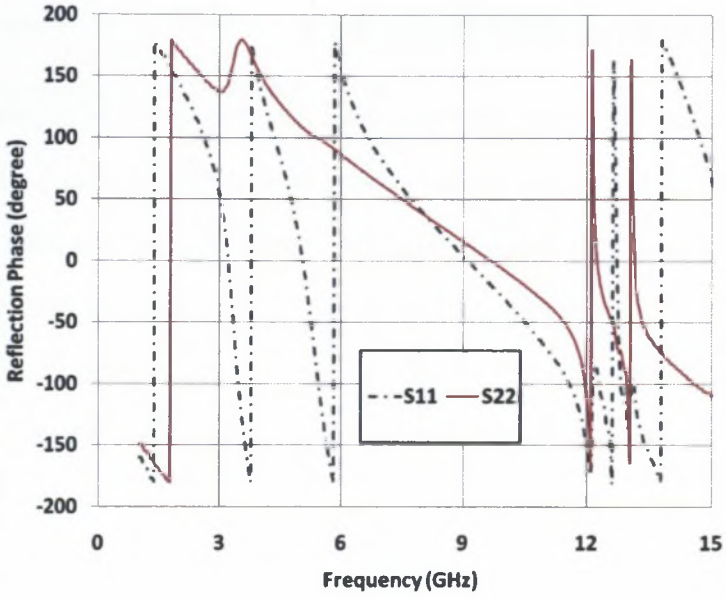


**Figure 5.10:** Theoretical reflection and transmission phase.

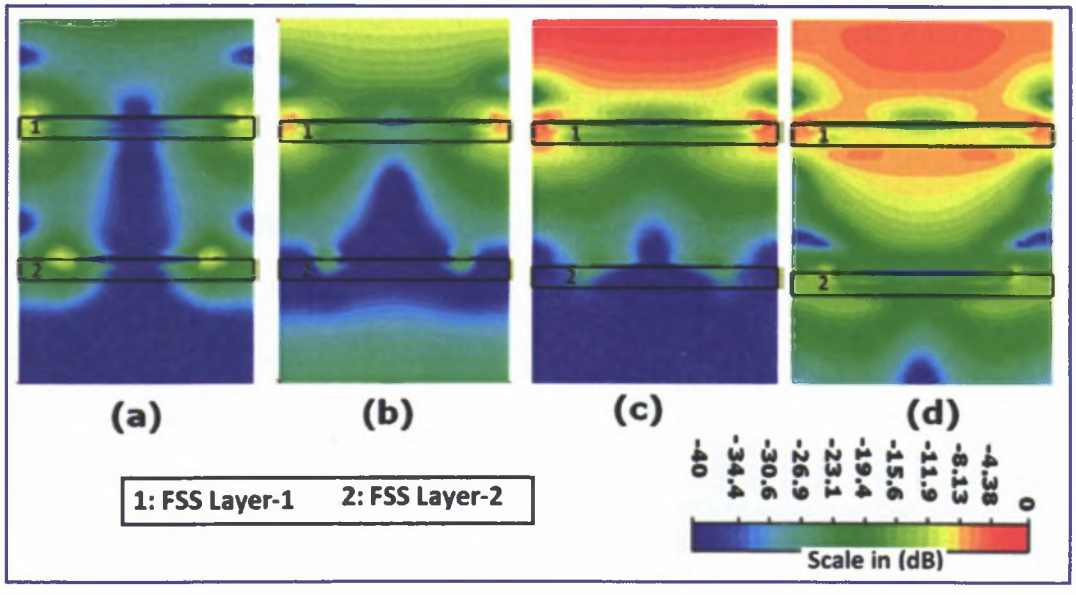


**Figure 5.11:** Electric field distributions orthogonal to the FSS reflector at (a) 3 GHz, (b) 6 GHz, (c) 8 GHz and (d) 12 GHz.

### 5.4.1 Field Analysis of Dual-Layer FSS

The waveguide simulator approach has been used for analysis of the electric fields in the unit cell. Figure 5.11 shows the electric-field distribution in the unit cell at 3 GHz, 6 GHz, 8 GHz and 10 GHz, respectively. It is clearly visible that at lower frequencies fields are reflected from the lower FSS region. As frequency increases more reflection occurs from the top layer of the FSS screen. In particular, Figure 5.11(c) displays the significant reflection above the top layer of the FSS. It corresponds to a transmission coefficient of -50 dB at 8 GHz (see Figure 5.9).

### 5.4.2 Oblique Incidence Performance of Dual-Layer FSS

Before proceeding to hardware fabrication, performance of the dual-layer FSS reflector to obliquely incident electromagnetic waves was investigated in different polarisation. Polarisation is defined as the orientation of electric field in a propagating electromagnetic wave. When the electric field is perpendicular to the plane of incidence, the polarisation is called Transverse Electric (TE) polarisation, and when it is parallel to the plane of incidence, then it is called parallel Transverse Magnetic(TM) polarisation. For normal incidence, the bandwidth is around 100% and it reduces to 70% in the case of TM polarisation at an angle of $50^0$. The widest bandwidth previously described in the literature for normal incidence is 50% [83]. To investigate the oblique-incidence performance, a Floquet port analysis has been carried out for different incidence angles where $\theta$ is defined with respect to the normal to the surface of the reflector.

Figure 5.12 shows the TE polarised behaviour of the FSS up to an angle of $\theta = 50^0$. It is evident from Figure 5.12 that, apart from slight peaks of around -7 dB between 7 GHz and 8 GHz, the FSS transmission is stable over a 90% bandwidth. The performance for TM incidence is evaluated for the same range and the results are presented in Figure 5.13. For this polarisation, with the increase of angle of incidence the lower frequency limit shifts from 4 GHz to 4.41 GHz. It is noted that this limit was stable for TE polarisation for all angles considered. Also

the transmission bandwidth of the FSS reduces from 99% to 70% when the incidence angle changes from the normal to $\theta = 50^0$ respectively.

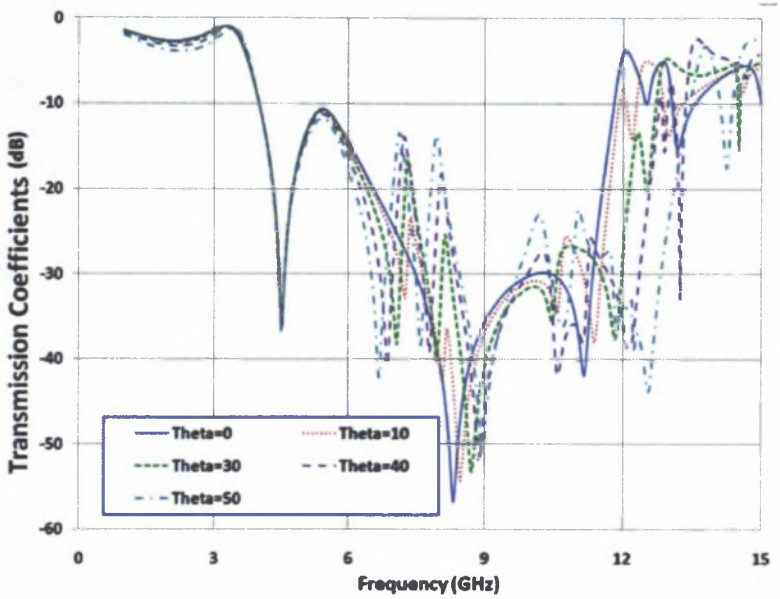


**Figure 5.12:** TE-polarisation predicted transmission coefficients for different angles of incidence.

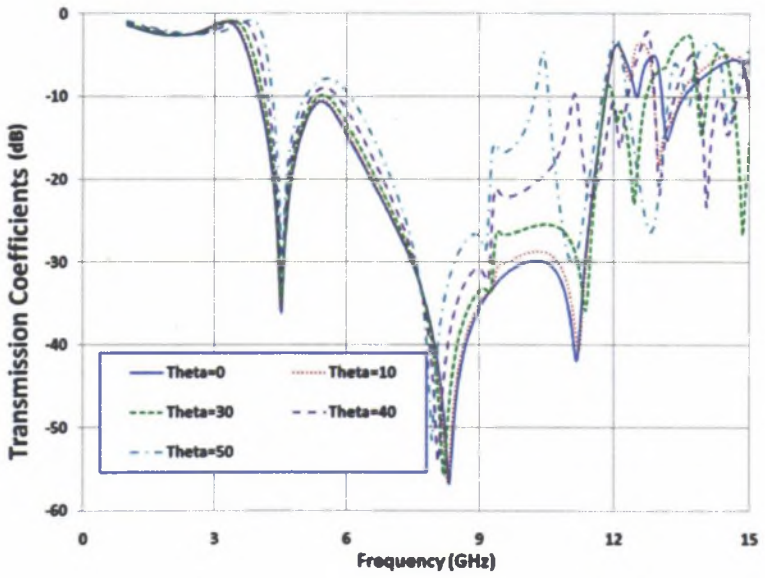


**Figure 5.13:** TM-polarisation predicted transmission coefficients for different angles of incidence.

For further analysis of the field behaviour, several probes have been placed in the unit cell during simulation with the CST software. These probes have been placed below the lower FSS layer, in the middle of the two layers of the FSS, and above the upper FSS layer at a distance of 9.5 mm. Probes have been placed for monitoring both co- and cross-polarisation components at all three locations. Phase results of the co-polarised probes for various probe locations are shown in Figure 5.14. The critical information is conveyed by the upper probe, which is placed on the top of the FSS screen. This corresponds to the location where a planar UWB antenna would typically be placed when the FSS is used in UWB reflector applications. The phase at 9.5 mm above the FSS screen decreases linearly from 4 GHz till 11.5 GHz and the variation over the band of 99% is $\pm$ $70^0$. The magnitudes of the field received by the same probes are reported in Figure 5.15. As can be noted, the electric field magnitude is very low below the two FSS layers (see curve for *Lower probe* in Figure 5.15). In order to quantify the performance of the reflector screens an array of $32 \times 22$ unit cells has been fabricated and measured.

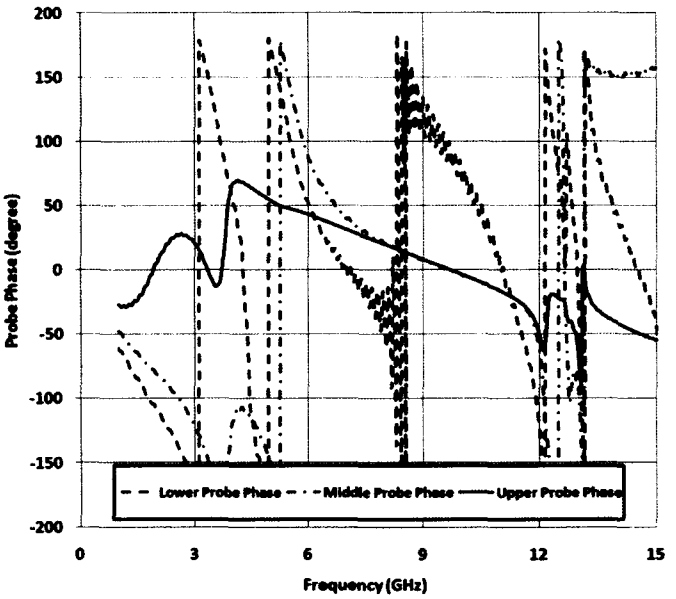


**Figure 5.14:** Phase of the total electric field component parallel to the incident polarisation (Co-Pol) at different levels of FSS.

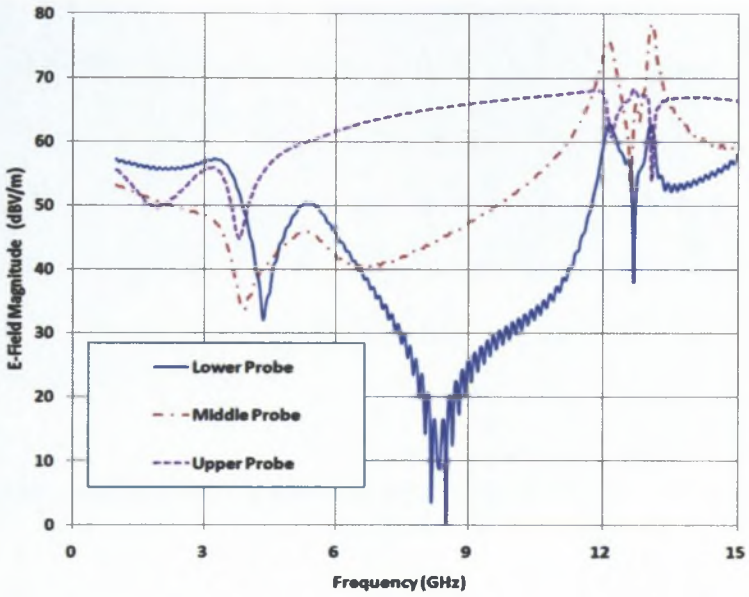


**Figure 5.15:** Magnitude of the total electric field component parallel to the incident polarisation (Co-Pol) at different levels of FSS.

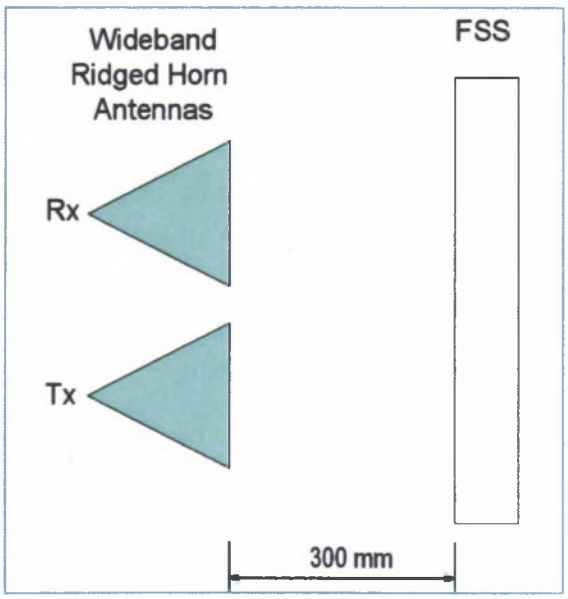


**Figure 5.16:** Schematic of the setup for reflection phase measurement.

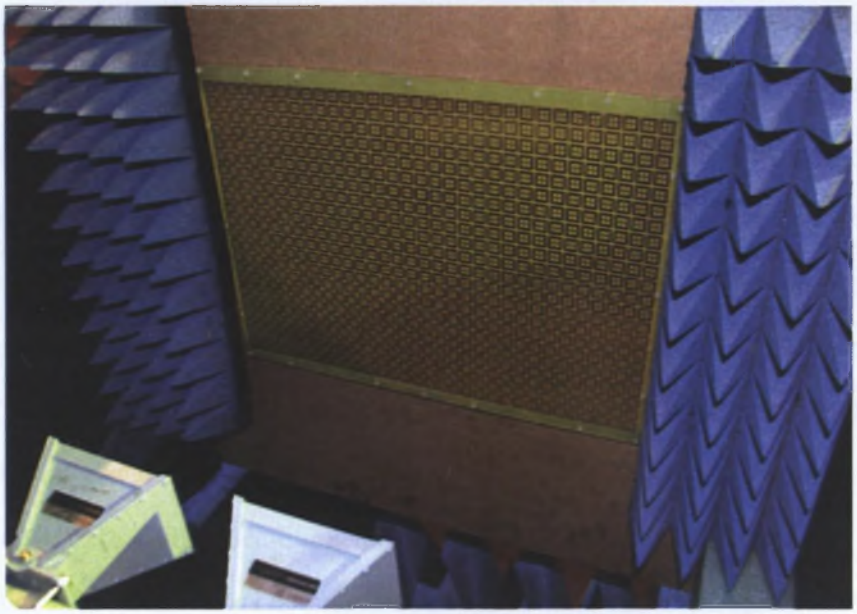

**Figure 5.17:** Actual measurement setup of reflection phase measurement.

### 5.4.3 Measured Results for Larger $32 \times 22$ Array of FSSs

To evaluate the reflection phase and transmission magnitude of the $32 \times 22$ array of FSSs, two dual-ridge H-1498 horns from BAE Systems, with an operating bandwidth from 2 GHz to 18 GHz, were used in the measurement set-up. Figure 5.16 shows a schematic of the measurement set-up. A wooden frame was used to avoid reflections in the anechoic chamber. Additional grooves for mounting provided good support for making the dual-layer structure. To analyse the reflection coefficient 9.5 mm in front of the FSS, the electrical delay for the FSS measurement was set to -19 mm (i.e. $2 \times 9.5$ mm). Phase has been unwrapped from the measured data for comparison with the simulation. The FSS screen is 300 mm away from the horn antennas. Figure 5.17 shows a photograph of the actual measurement set-up used. Teflon spacers of fixed thickness were specially manufactured to ensure the exact spacing between the two layers. A comparison of predicted and measured reflection phase is shown in Figure 5.18.

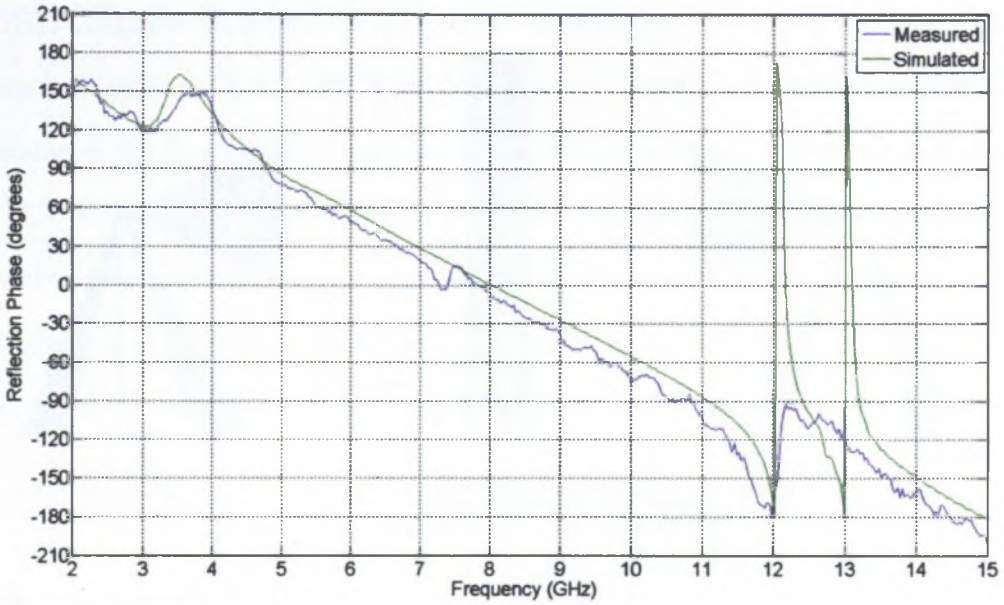


**Figure 5.18:** Comparison of measured and simulated reflection phase.

Transmission magnitude measurements were carried out with a setup similar to that used for reflection phase measurements. The difference in the placement of horns is shown in Figure 5.19 and a photograph of the measurement setup in Figure 5.20. This setup was also used for measurement of different angles of incidence. The FSSs screens placed on the wooden board is manually rotated to appropriate angles.

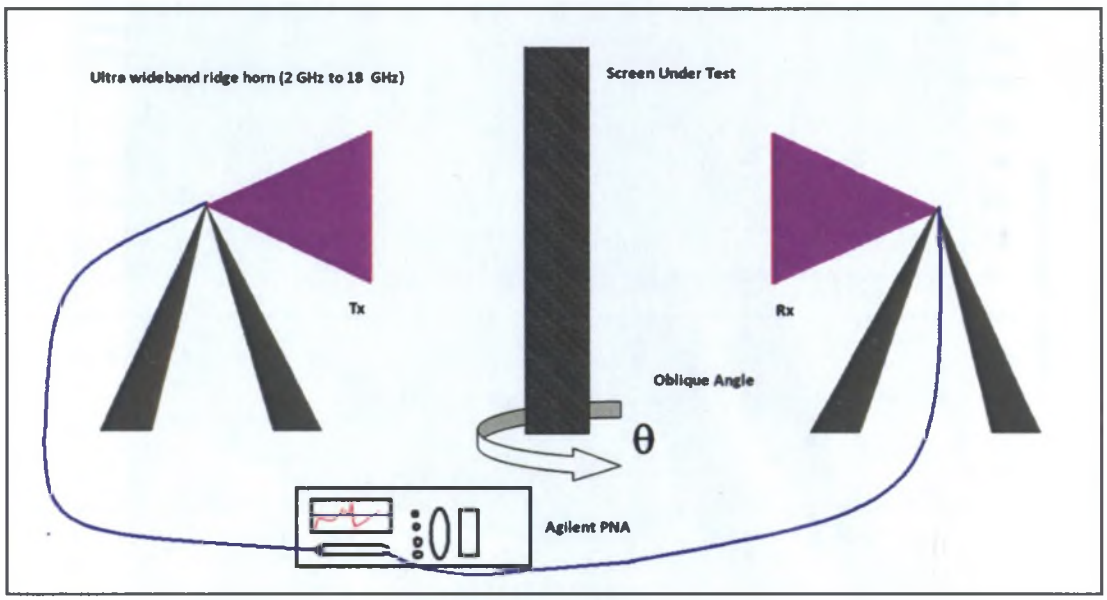


**Figure 5.19:** Schematic of setup used for measuring transmission coefficients.

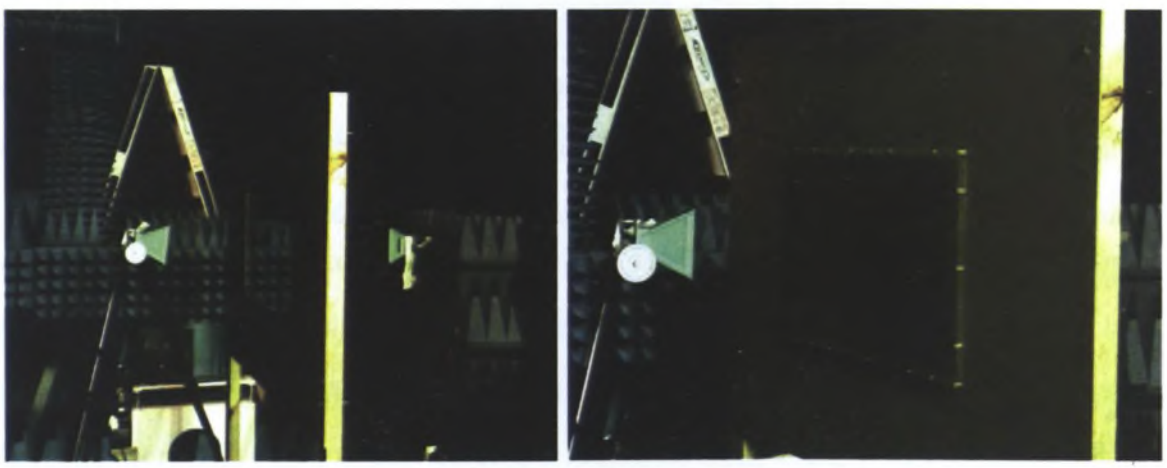

**Figure 5.20:** Actual setup for measurements of normal and oblique incidence study and rotational board with FSSs screens.

The study of the different polarisation of the incident fields at three different angles, namely 15, 30 and 45 degrees, was carried out with the aforementioned setup. Figure 5.21 shows the zero-degree incidence case. Measurement is carried out with the setup and matches well with the simulated results. The measured -10dB transmission bandwidth of 121.8% (3.85 GHz to

11.23 GHz) compares well with the predicted bandwidth of 133% (3.5 GHz to 11.45 GHz). As shown in Figures 5.22, 5.23 and 5.24 in the case of TE polarisation the performance of the FSS is stable as predicted by the theoretical results with the bandwidth maintained over 100%. Figure 5.25, 5.26 and 5.27 shows the performance of screens in the case of TM polarisation at 15, 30 and 45 degrees respectively. A good match in the lower band of frequencies was found. At the higher band of frequencies a slight mismatch was observed. A complete study of the measured bandwidth for different polarisations is given in Tables 5.2 and 5.3.

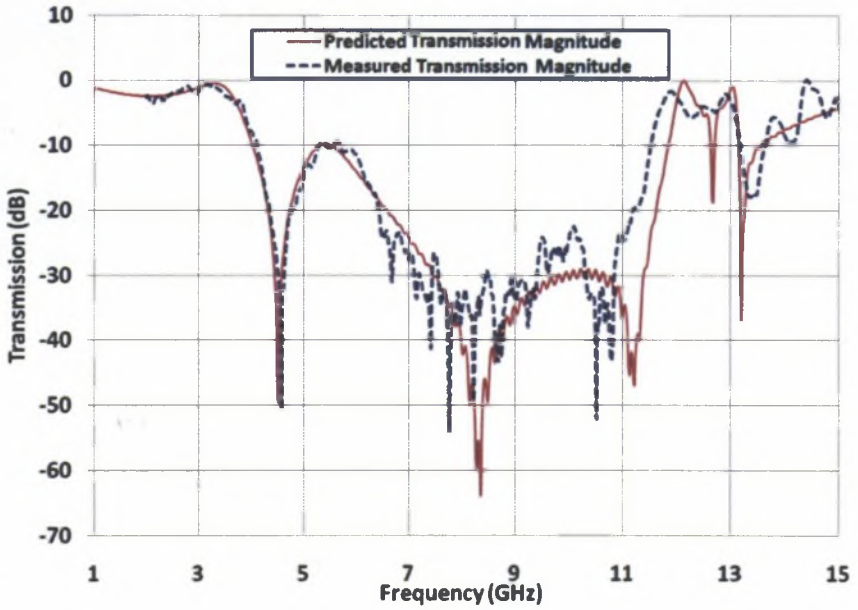


**Figure 5.21:** Theoretical and measured transmission magnitude for normal incidence for $32 \times 22$ array of unit cells.

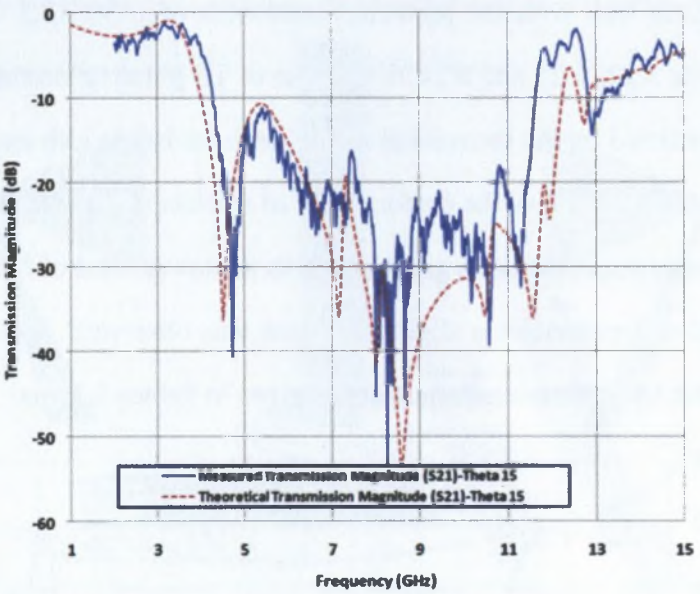


**Figure 5.22:** Theoretical and measured transmission magnitude for TE polarisation with incidence at 15 degrees.

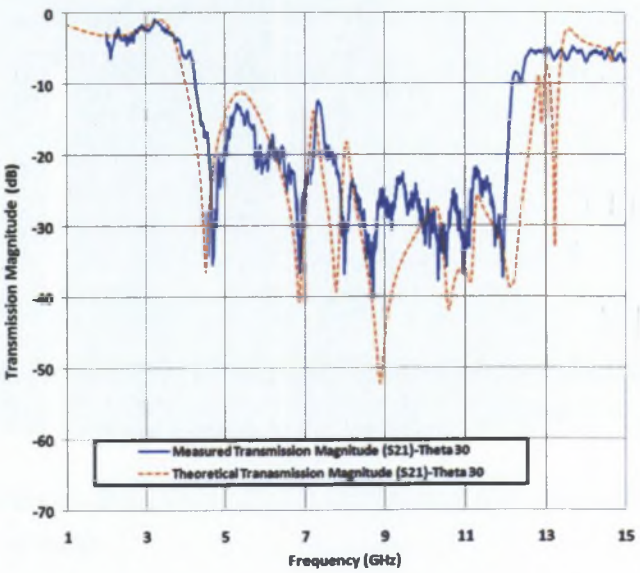


**Figure 5.23:** Theoretical and measured transmission magnitude for TE polarisation with incidence at 30 degrees.

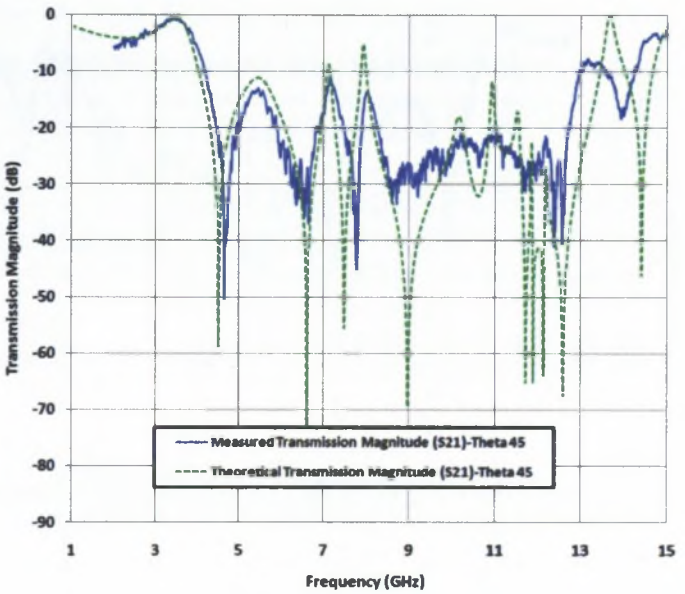


**Figure 5.24:** Theoretical and measured transmission magnitude for TE polarisation with incidence at 45 degrees.

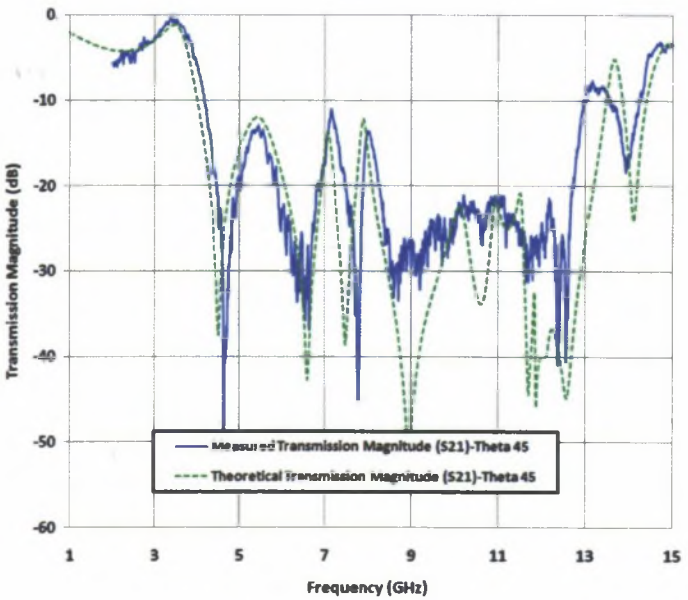


**Figure 5.25:** Theoretical and measured transmission magnitude for TM polarisation with incidence at 15 degrees.

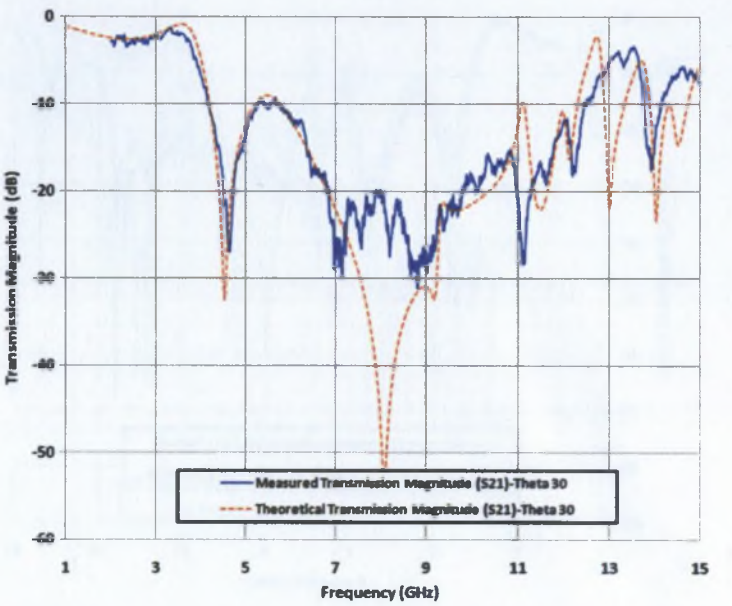


**Figure 5.26:** Theoretical and measured transmission magnitude for TM polarisation with incidence at 30 degrees.

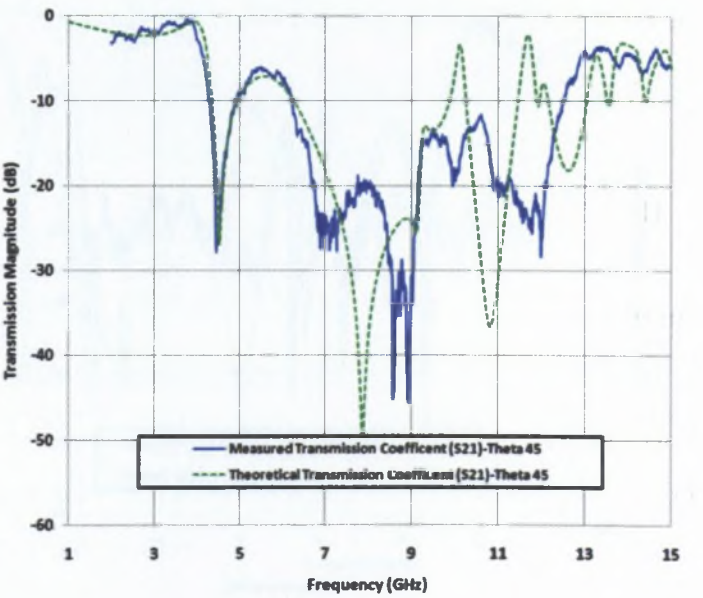


**Figure 5.27:** Theoretical and measured transmission magnitude for TM polarisation with incidence at 45 degrees.

**Table 5.2:** Oblique incidence measured bandwidth of dual-layer FSS for TE polarisation

| | Angle (deg) | 15 | 30 | 45 |
|---|---|---|---|---|
| TE Polarisation | Lower Freq. (GHz) | 4.26 | 4.24 | 4.18 |
| | Upper Freq. (GHz) | 11.63 | 12.18 | 12.97 |
| | Bandwidth (%) | 89.30 | 96.70 | 102.50 |

**Table 5.3:** Oblique incidence measured bandwidth of dual-layer FSS for TM polarisation

| | Angle (deg) | 15 | 30 | 45 |
|---|---|---|---|---|
| TM Polarisation | Lower Freq. (GHz) | 4.16 | 4.15 | 4.25 |
| | Upper Freq. (GHz) | 11.44 | 12.46 | 12.49 |
| | Bandwidth (%) | 93.3 | 100 | 98.4 |

## 5.5 Antenna Performance over Dual-Layer FSS Reflectors

After optimising the FSS screen, a UWB slot antenna excited by a microstrip-fed patch [135] is mounted above the reflector. This concept is not limited to the particular slot antenna described here; designers can use various other UWB antennas available in the literature. The slot antenna and all the FSS reflectors have been designed for fabrication using FR-4 substrates with a relative permittivity of 4.4 and thickness $t = 0.8$ mm and 1.6 mm respectively. A graphical overview of the proposed design with reflectors is shown in Figure 5.28. The complete hardware integration of the antenna with the FSS reflectors is shown in Figure 5.29.

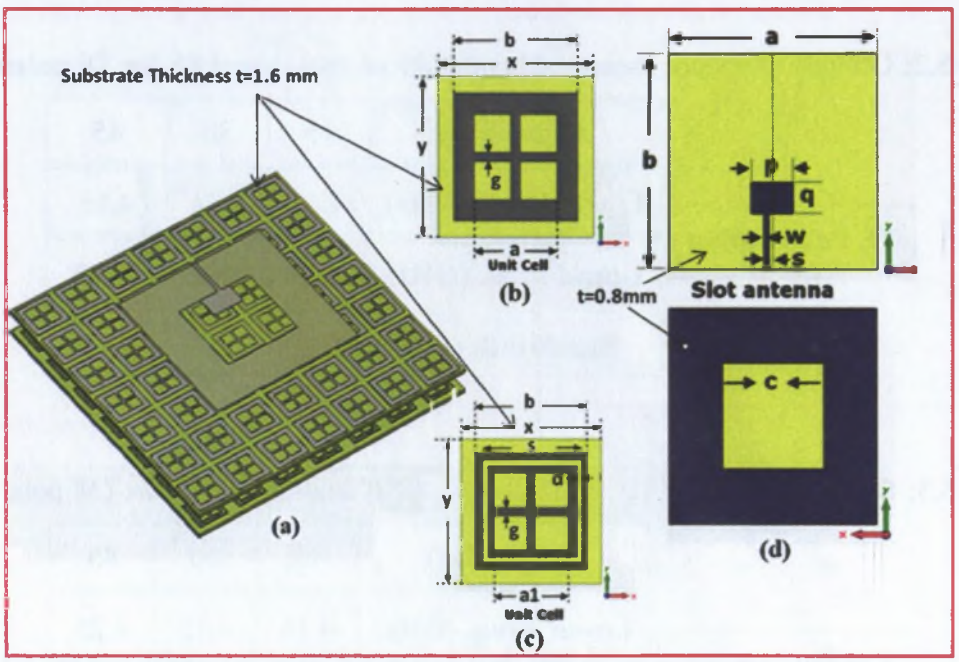


**Figure 5.28:** (a) Complete FSS reflector with a slot antenna (b) Schematic of unit cells of the FSS Layer-1 (c) Schematic of unit cells of the FSS Layer-2 (d) UWB slot antenna [4] $x = y = 15, b = 12, g = 0.9, t = 1.6, d = 1.0, a = 10, a1 = 8, s = 11, L = 8.5$ (All dimensions are in mm).

The radiation patterns and the gain of the antenna were measured using an NSI-700S-50 spherical near-field measurement system while an Anritsu Vector Star Network Analyzer MS4647A (70 MHz to 70 GHz) was used for S-parameter measurements. Figure 5.30 shows the theoretical and measured reflection coefficients of the slot antenna with and without the dual-layer FSS reflector. The measured impedance bandwidth with the FSS reflector is 122% which compares well with the predicted bandwidth of 132%. Some small variations between the theoretical and measured data are probably due to fabrication imperfections.

A maximum gain enhancement of 3.8 dB is achieved at 8 GHz where the FSS has the lowest transmission coefficient magnitude of -50 dB (see Figure 5.21). The measured gain of the antenna with FSS reflector is shown in Figure 5.32 where the theoretical gain of the antenna with and without reflector is also plotted for comparison. The designed FSS reflects efficiently

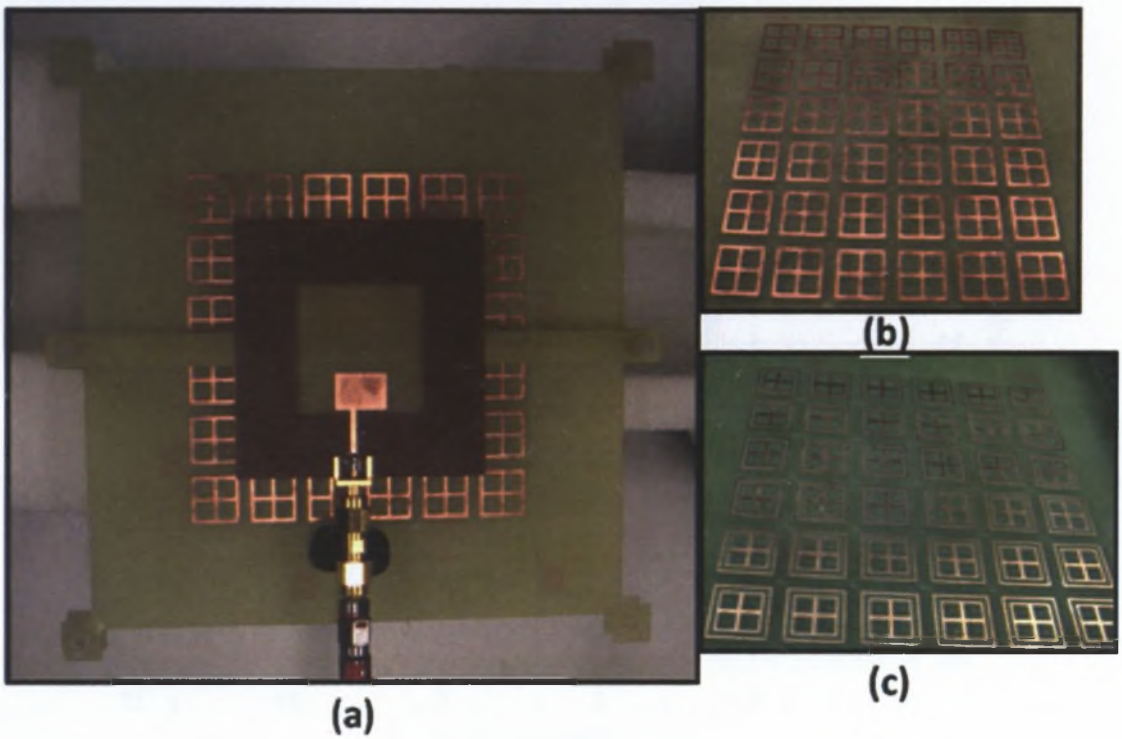


**Figure 5.29:** Hardware profile of antenna integration.

and enhances the gain of the antenna. A measured gain of around 7.5 dBi up to 7 GHz has been obtained for the proposed solution while the gain increases up to 9.8 dBi at 8 GHz. Gain variations within the 3 GHz to 12 GHz band is about 1.8 dB. The measured radiation patterns at 3 GHz, 5 GHz, 8 GHz and 10 GHz on the $\theta = 0^0$ and $\theta = 90^0$ planes are shown in Figure 5.31. Due to the offset feed of the slot antenna, the radiation patterns are not symmetrical in these two principal planes. A similar observation holds for the other planes, but this was not experimentally verified. The dual-layer FSS described should prove valuable for many other applications requiring a low-profile reflector with wideband performance.

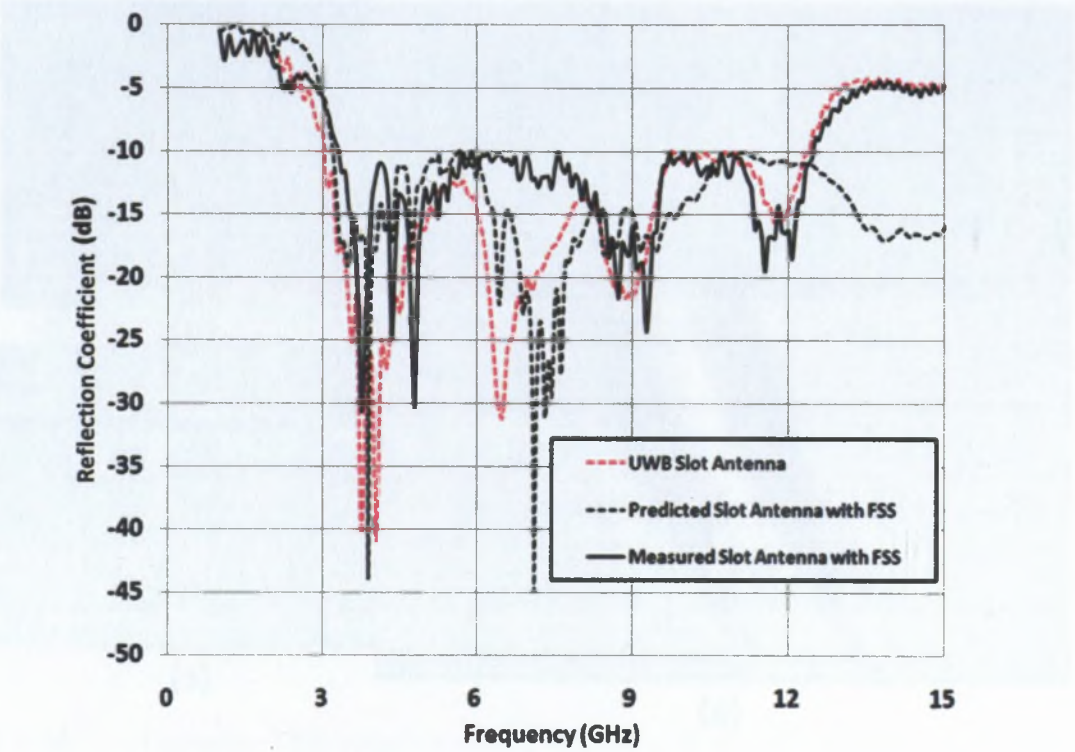


**Figure 5.30:** Input reflection coefficient of the antenna with and without the FSS reflector.

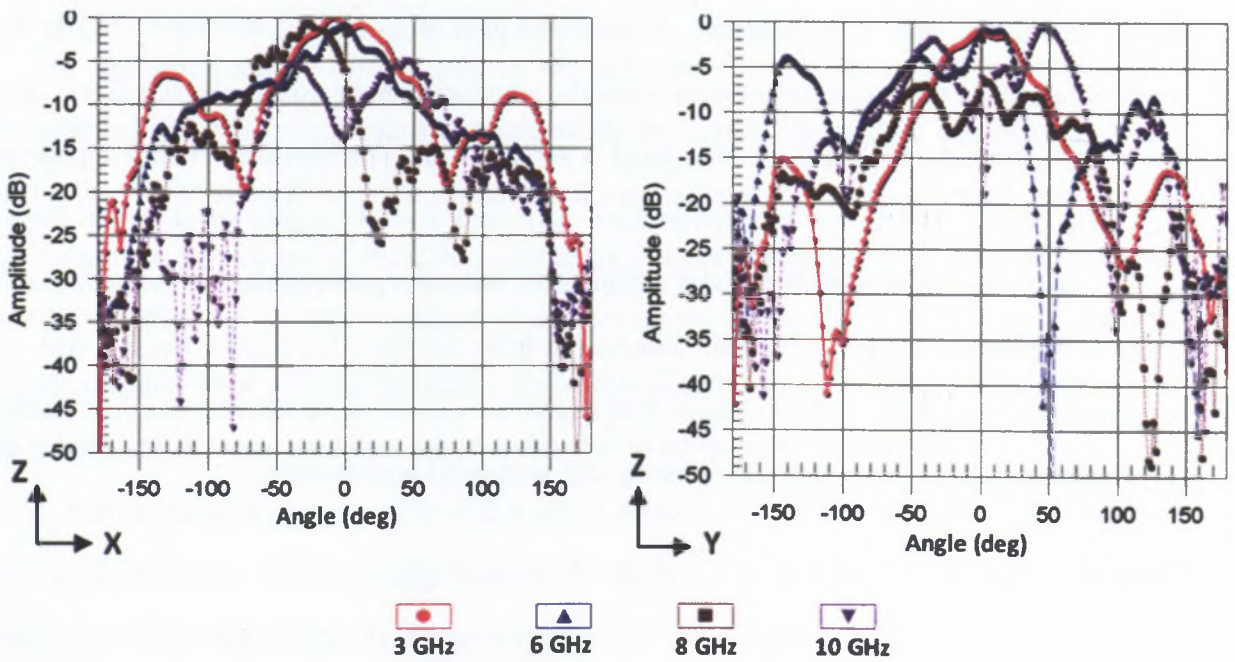


**Figure 5.31:** Measured gain of the antenna with and without the FSS reflector.

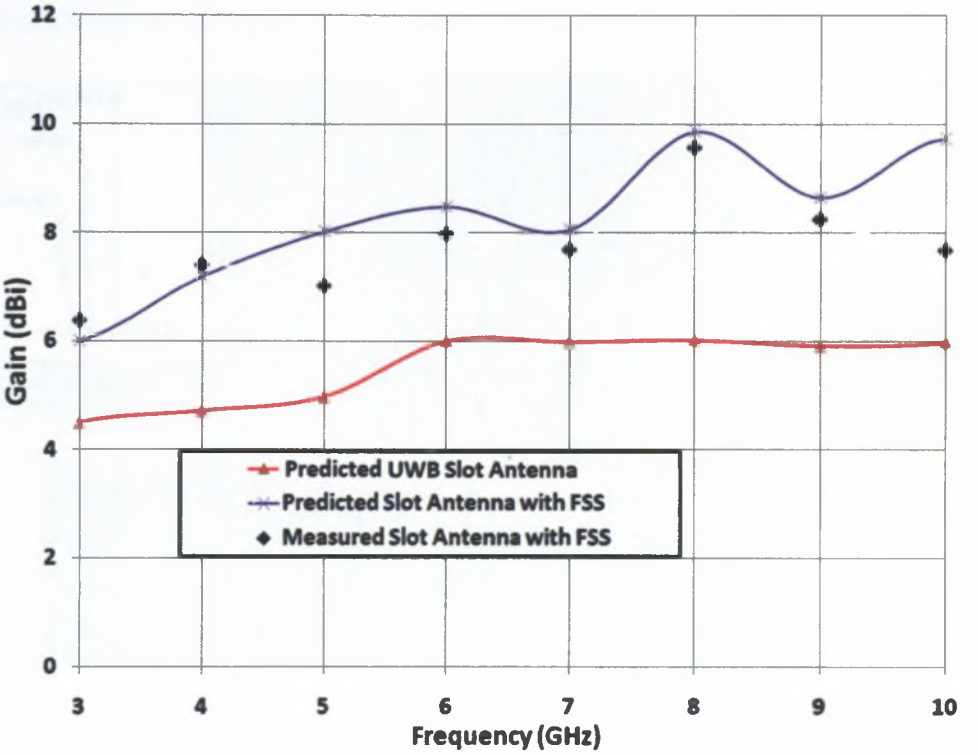


**Figure 5.32:** Measured radiation patterns.

## 5.6 Constant-Gain Antenna with Four-Layer Frequency Selective Surface Reflector

Designed FSS in previous sections, proved to be an efficient is designing the reflectors. After gaining an understanding of the FSS and its usefulness in reflector applications, further improvement in gain flatness and compactness is sought in the design of FSS. To achieve the target the FSS design methodology of previous dual-layer FSS is followed. The first layer of FSS acts on the higher frequency region and the bottom layer on the lower frequency region providing in-phase reflection characteristics. This FSS is not backed by a perfect metal reflector in order to provide some back radiation and lower the gain in the main beam direction, and

provide good gain stability.

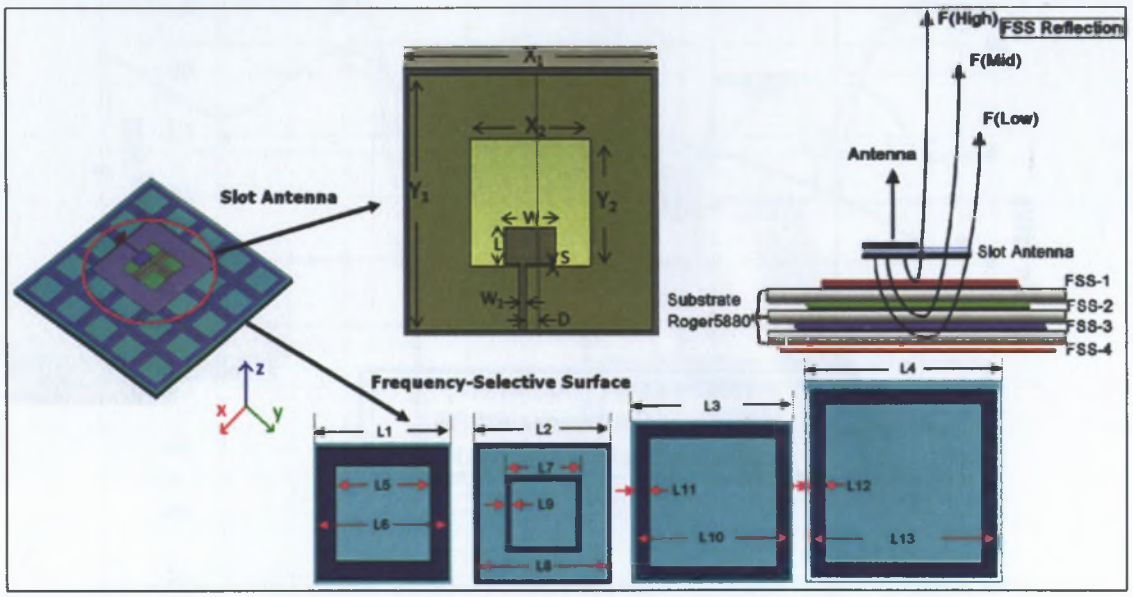


**Figure 5.33:** Passive Frequency-Selective Surface Reflector with UWB Slot antenna.

To demonstrate the concept the same slot antenna is chosen, which was used in previous sections (yields an ultra-wide bandwidth of 140% (2.9 GHz - 18.38 GHz)) [135] and gives a simulated directive gain of 4 dBi at 3 GHz and a gain variation of 2 dB over the impedance bandwidth. In the initial design process the considered FSS screens 1 and 2 are available in the literature [131], [134] for broadband operations. Two further additional layers of FSS-3 and -4 have been added and optimised carefully to provide an ultra-wideband characteristic. FSS-1, FSS-3 and FSS-4 are each a kind of bandpass filters and FSS-2 acts as a bandstop for the low frequencies passed on by FSS-1. In the design process FSS-1 and FSS-2 have the same periodicity but, in order to support lower frequencies, FSS-3 and FSS-4 are large and the periodicity of layers 3 and 4 are different from layers 1 and 2. The shape and dimensions of the geometries are reported in Figure 5.33. A complete optimisation was done for the different layers to improve the gain flatness when combined with a UWB slot antenna. Figure 5.34 shows the hardware profile of the antenna with various FSS layers and Figure 5.35 shows the hardware

profile of each layer individually.

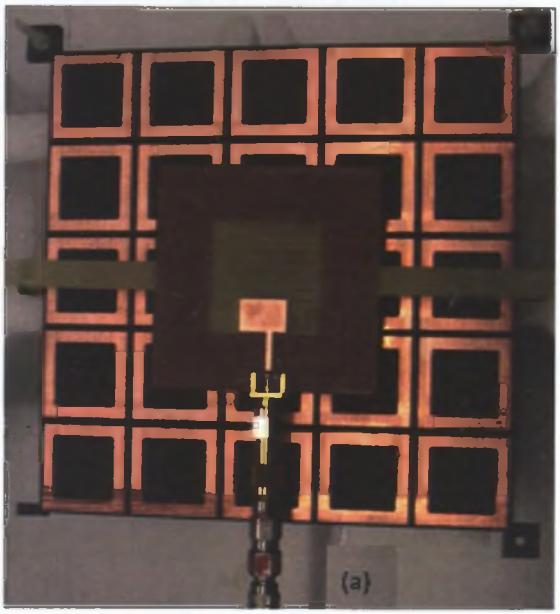


**Figure 5.34:** Hardware profile of antenna with FSS reflector .

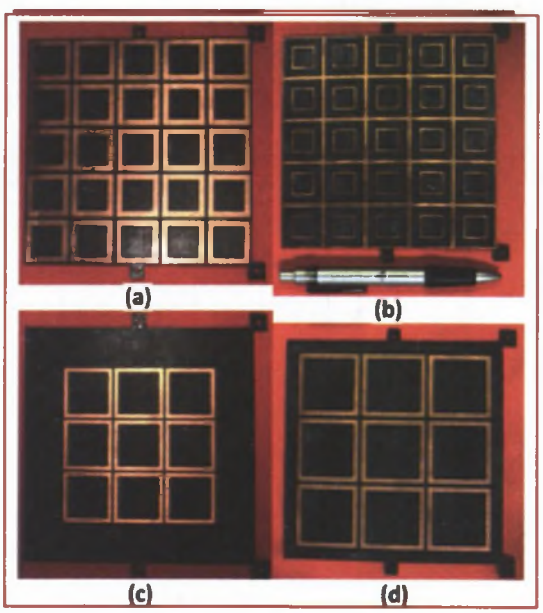


**Figure 5.35:** Hardware profile of FSS screens (a) FSS-Layer-1 (b) FSS-Layer-2 (c) FSS-Layer-3 (d) FSS-Layer-4.

### 5.6.1 Hardware Validation and Measurements

The predicted input reflection coefficient and the gain are shown in Figure 5.36 and Figure 5.37 respectively. It can be observed that the optimised FSS reflector has only a very small effect on the impedance bandwidth (145% bandwidth with FSS and 149% without FSS). However, the gain tends to increase significantly with the FSS reflector. A peak gain of around 9.3 dBi is achieved with the FSS, but the most significant feature of introducing the FSS reflector is the improvement in gain flatness. The variation in the gain is $\pm$ 0.5 dB across the whole impedance band.

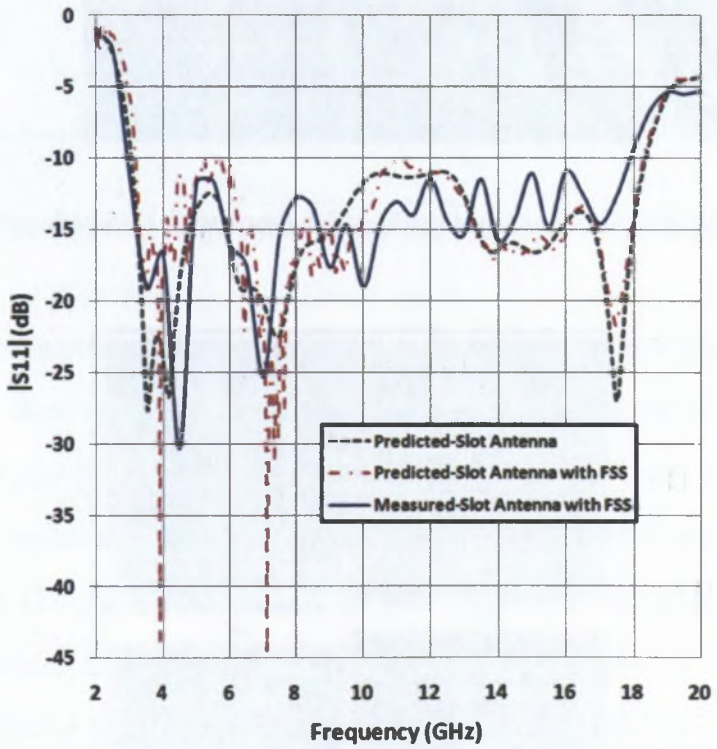


**Figure 5.36:** Measured antenna input reflection coefficient with 4-layer FSS reflector.

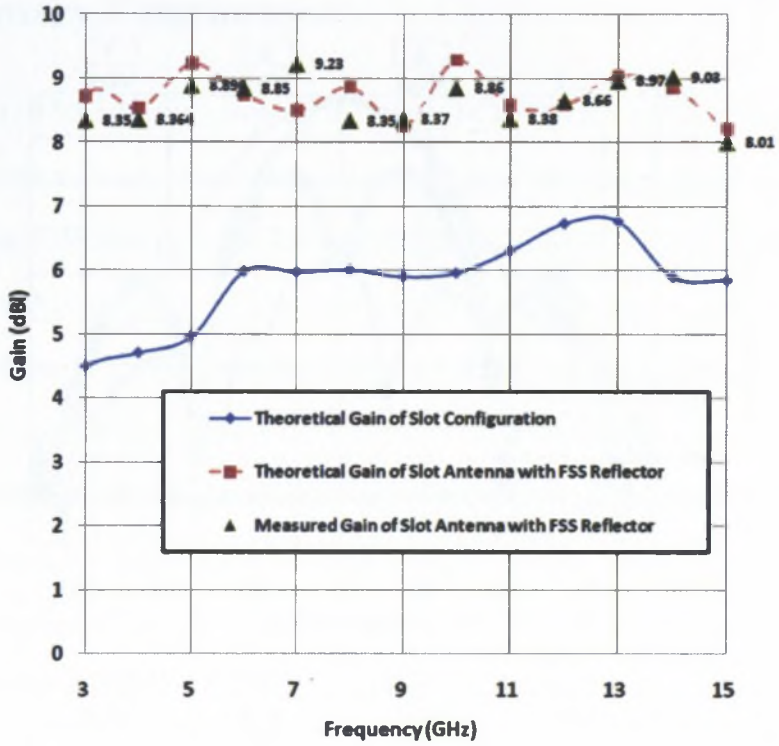


**Figure 5.37:** Measured gain comparison of slot antenna with and without FSS reflector.

Measured and computed results are presented to confirm the performance of the antenna. Figure 5.38 shows the measured radiation patterns in the ZY (H-Cut) and the ZX (V-Cut) planes. A maximum gain of 9.3 dBi and the variation of $\pm$ 0.5 dB have been achieved for the designed structure.

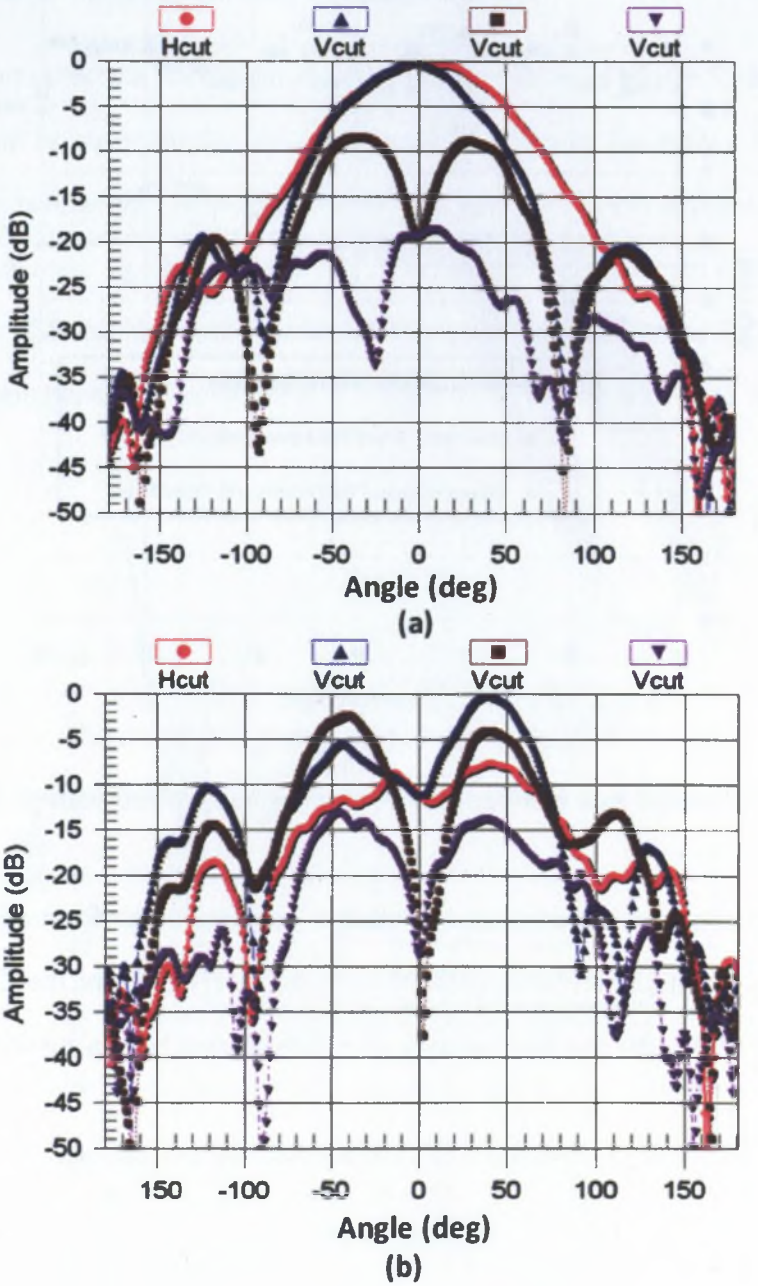


**Figure 5.38:** Measured Radiation Patterns at (a) 3 GHz and (b) 6 GHz.

## 5.7 Summary/Conclusions

A new dual-layer FSS reflector covering the entire FCC UWB band and beyond has been introduced, designed and experimentally verified. It has a low transmission coefficient and sufficiently constant reflection phase to use as a reflector for nearly all types of low-cost (planar and/or printed) UWB antennas. The oblique incidence performance of the dual-layer FSS has also been investigated. Through careful design, the FSS transmission frequency response has been made stable against variations in the incidence angle and polarisation. A significant phase coherent bandwidth of 100% has been reached for reflector applications and a stable frequency response for oblique incidence has been demonstrated. Further, phase analysis and field analysis at various locations of the FSS have been conducted by placing different probes in the FSS structure. The reflector combined with a UWB slot antenna has been demonstrated successfully. The low-profile configuration achieves an impedance bandwidth of 122% and an average gain of around 7.5 dBi over the whole UWB frequency band. The described dual-layer FSS also proves valuable for many other applications requiring a low-profile reflector with wideband performance. Based on the concept of the dual-layer FSS, a multi-layer FSS is demonstrated with measured and computed results. A maximum gain of 9.3 dBi and a variation of $\pm 0.5$ dB have been achieved for the designed multi-layer FSS with antenna structure. When the proposed FSS is used as the separator/shield, the considered UWB antennas can be fitted close to the conducting surfaces (such as metal cases, screens) which are commonly found in modern microwave and wireless devices. It has been verified that its use prevents deterioration of the antenna impedance match and increases antenna gain.

# Chapter 6

# High-Gain Ultra-Wideband Slot Antennas with Short Horns

## 6.1 Introduction

The design aspect of the novel short TEM horns was demonstrated successfully in Chapter 4. These horns were tested with various UWB monopole antennas. The design of antennas in this chapter is inspired by the antennas proposed for the various hand-held devices used in various GPR/through wall-imaging applications. This application demands the greatest possible bandwidth for transmission of extremely short pulses (more details are mentioned in Chapter 2). This chapter explores the possibility of implementing the short horns with slot configurations and studying their effect on the slot antennas. A novel configuration of a compact printed semi-circular slot antenna (PSSA) is first presented. The antenna design shows remarkable behaviour in terms of bandwidth and size as compared to the slot antennas available in the literature. Based on the experience gained with the short TEM/two-plate horn structure in Chapter 4, the short two plate horn of different physical length is mounted on the design PSSA. In addition, a compact four-plate horn excited with a rectangular slot antenna is studied, which shows the

advantages of compactness and performance over the dual- and quad-ridge horns. This antenna is based on the short horns (SH) excited with the microstrip patch antennas and dielectric resonator antennas and demonstrates improved bandwidth and gain performance for narrowband applications [71]. Typically these antennas have bandwidths of around 30%, which is not sufficient for the UWB applications.

### 6.1.1 Chapter Contributions

The chapter presents the following contributions:

- The design of compact printed semicircular slot antenna (PSSA) for various PCB applications is proposed.
- Frequency domain and time domain study of PSSA is presented.
- The concept of short two plate horn is used and the gain enhancement with different physical length of horns for slot antennas is demonstrated.
- A simple compact short UWB four-plate horn excited using slot antennas is proposed, which is comparable to complex bulkier dual and quad-ridge horns.
- Complete theoretical analysis for the validation of design is presented in this studies.

The rest of the chapter is organized as follows. In order to gain the understanding of slot configurations work is begins with the design of a slot antenna configuration. The designed slot antenna is similar to the CPW-fed bow-tie slot configuration and with the novel feeding arrangement of step transformer, a new semicircular slot antenna (SSA) configuration is presented in Section 6.2. With the designed SSA, the short horn proposed in chapter 4 is implemented and the enhancement in the gain with various horn heights is presented in Section 6.3. With the complete design and understanding of slot configuration, a new configuration of four-plated short horn is presented in Section 6.4.

## 6.2 Ultra Wideband Slot Antenna

In this section work relevant to slot antennas is presented. Studies are begin with the design of a simple slot antenna to obtain experience with slot geometries. In the literature, several slot configurations have been investigated to enhance impedance bandwidth while maintaining the gain characteristics of the design [37, 37–40, 43, 56]. In one configuration, by protruding a small rectangular slot of proper dimensions along the direction of the microstrip feed line, good impedance matching of about 46%, which is about three times that of a corresponding conventional printed wide rectangular slot antenna, can be obtained [37]. The gain over this wide operating bandwidth is about 3.4- 5.1 dBi. A printed slot antenna with a fork-like tuning stub and a simple rotated slot has also been studied [37, 38]. As a result, a wide operating bandwidth of about 2.2 GHz (49.4%) has been obtained. However, this bandwidth is not wide enough to cover the entire FCC UWB frequency band. To provide a compact solution with good isolation and low ground inductance for shunt elements, several CPW-fed bow-tie slot antennas (BTSAs) have been developed [41–43] . A BTSA fed by a CPW has been investigated in [43] for broadband applications, but it does not cover the UWB band because the feed transmission line is not well matched to the high input impedance at the vertex. This mismatch problem has been overcome through the use of tapered metal stubs [41] and inductive coupling [42]. All these methods are complex and involve adjustment of the slot flare angle to enhance bandwidth along with the loading slot with stub, patches or inductive coupling. A simple and innovative impedance transition in the CPW feed of the BTSA has been investigated which achieves a match over the complete UWB band [44]. A study of vertex angle has also been conducted, illustrating the variation in bandwidth for different vertex angles when the overall surface area is 2500 $mm^2$ ($50 \times 50mm$) [44]. In this section, the proposed novel design of a compact CPW-fed printed semicircular slot antenna (PSSA) with a simple CPW-to-CPW transition is investigated. With the help of a combined step and taper transition in the CPW feed line, better

matching to the resonant modes of the semicircular slot is obtained. The impedance bandwidth of the designed antenna, defined by the 10 dB return loss, extends from 3.0 GHz to 11.6 GHz (i.e. a percentage bandwidth of 118%). A study of the radiation patterns shows the broad beam coverage in the azimuth plane over a wide range of frequencies while a time-domain analysis shows low pulse dispersion along different directions, making the antenna suitable for pulse-based UWB systems. The small size of the antenna with an overall surface area of 1800 $mm^2$ ($60 \times 30$ $mm^2$) also allows easy integration into a transceiver PCB.

### 6.2.1 Compact Printed Semicircular-Slot Antenna Design

In the design process, a CPW-fed PSSA with no transitions (i.e. no taper and no step transition in the feed), shown in Figure 6.1, has been designed first.

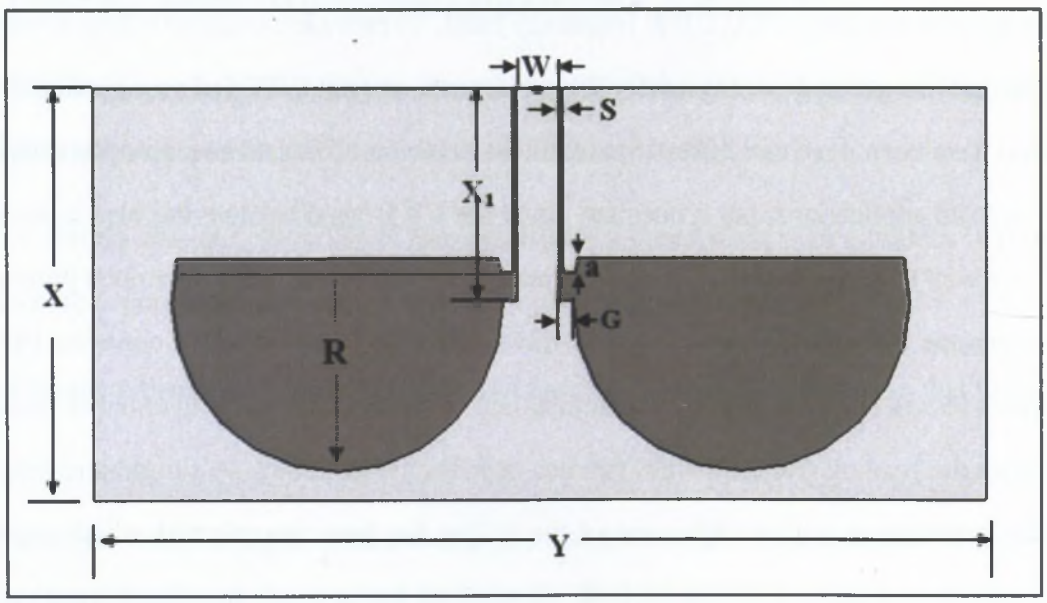


**Figure 6.1:** CPW-fed PSSA with no taper or step transitions, $X = 30, Y = 60, R = 12, X1 = 15, W = 3, S = 0.33, G = 1$ and $a = 1$ (All dimensions are in mm).

With the aim of operating from the lowest frequency of the FCC UWB band (i.e. 3.1 GHz), a radius of 12 mm has been chosen and the feed gap $G$ (shown in Figure 6.1) is optimised

with CST Microwave Studio [97] yielding a value of 1 mm. Also, the flat base of semicircular disk is extended to make $a$=1 mm to ensure a smooth transition from the feed to the slot. The characteristic impedance of the CPW feed line is 50 Ω. Though the feed gap $G$ has been optimised, no design solution was found that could cover the entire FCC-approved UWB band; because of the high input impedance of the semicircular slots near the vertex this cannot be matched to the CPW over this bandwidth. Hence, a tapered CPW-to-CPW transition [44] is implemented to form an impedance transformer along the feed line, as shown in Figure 6.2, with the hope of achieving the desired impedance bandwidth.

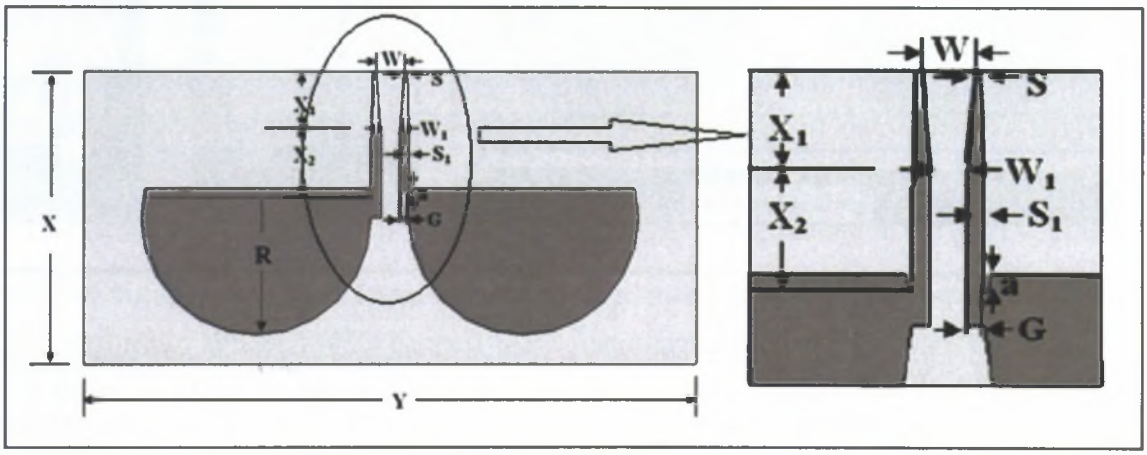


**Figure 6.2:** CPW-fed PSSA with linear-taper CPW-to-CPW transition, $X = 30, Y = 60, R = 12, W = 3, W1 = 2, S = 0.33, S1 = 1, X1 = 7, X2 = 6, G = 1.5$ and $a = 1$ (All dimensions are in mm).

This taper is expected to provide improved matching between the CPW feed line and the high impedance at the vertex of the PSSA. Further optimisation gave a value of $G$ =1.5 mm and the matching indeed improved for the dimensions of the PSSA shown in Figure 6.2. The use of the tapered-transition feed network shown in Figure 6.2 yields a 10dB return loss bandwidth of 2.8 GHz (i.e. 3.4 GHz to 6.2 GHz) as shown in Figure 6.4. The return loss is certainly improved compared to the case without any transitions but the antenna still does not operate satisfactorily over the entire FCC UWB band. To further improve the impedance bandwidth of the antenna, the CPW-to-CPW transition is modified to include steps in addition to the linear taper. The

resulting configuration of the PSSA on a FR-4 substrate is shown in Figure 6.3. An impedance match over the complete FCC UWB band is achieved with the use of a taper $L1$ (implemented in [44]) and a stepped impedance transformer formed by the $L2$, $L3$ and $L4$ segments (with $L5$ and $L6$ steps), with the matching finally controlled by the feed gap $G$.

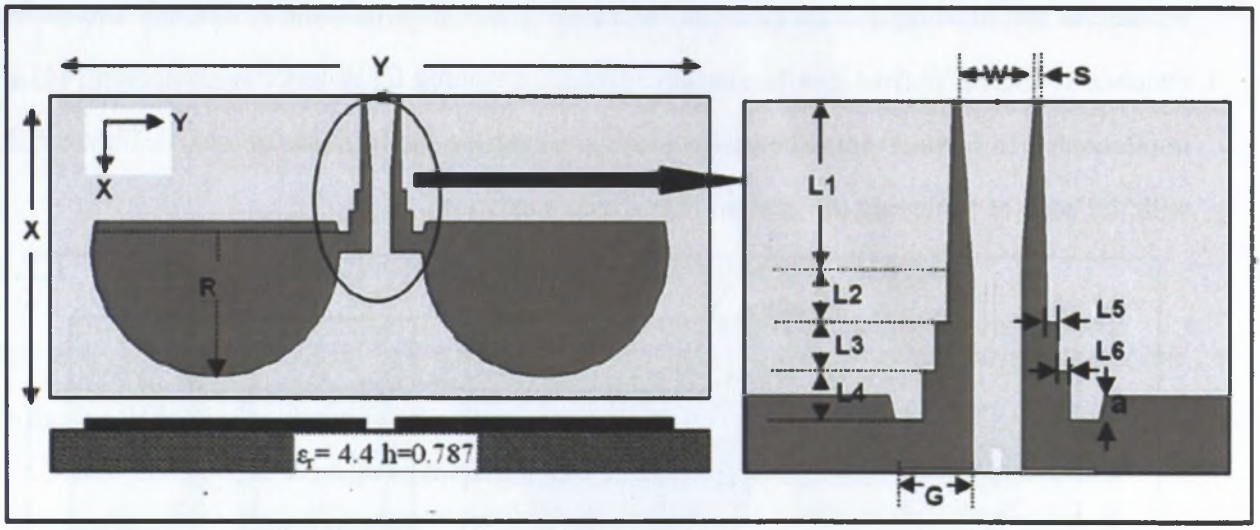


**Figure 6.3:** CPW-fed PSSA with linear-tapered and stepped CPW-to-CPW transitions, $X = 30, Y = 60, L1 = 7, L2 = L3 = L4 = 2, L5 = L6 = 0.5, W = 3S = 0.3, G = 2.5, R = 12$ and $a = 1$ (All dimensions are in mm).

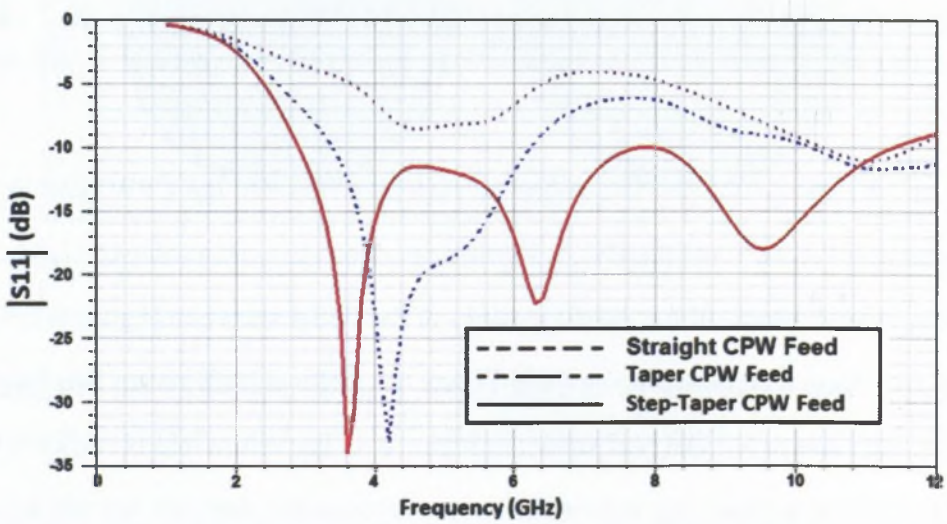


**Figure 6.4:** Predicted reflection coefficients of three configurations shown in Figures 6.1, 6.2 and 6.3 (with radius R=12 mm).

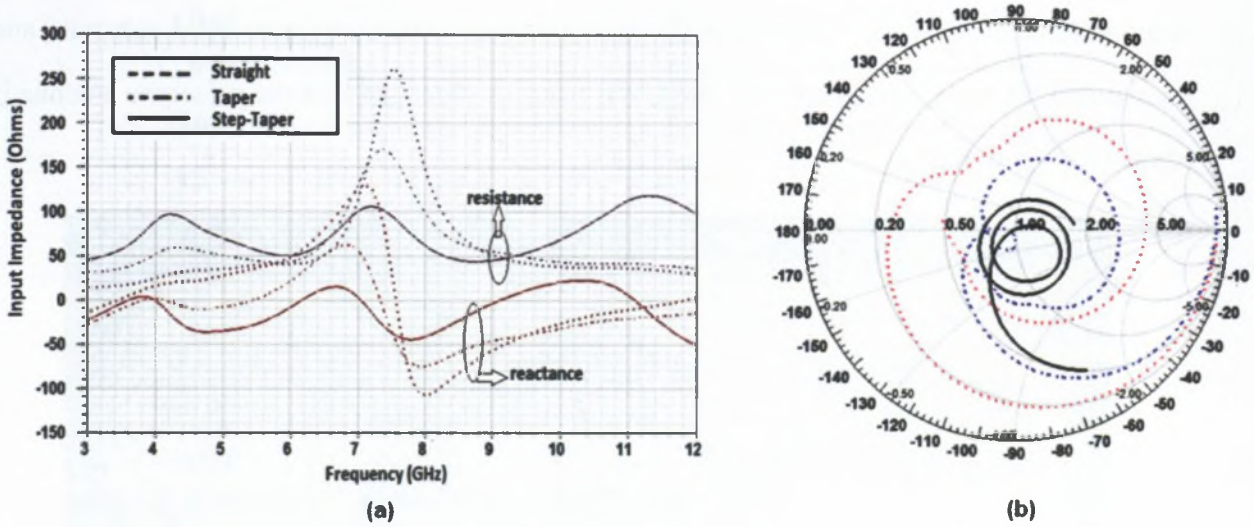


**Figure 6.5:** (a) Input impedance for various PSSA feed schemes (b) Input impedance on Smith chart. Both plots show (i) straight feed (ii) tapered feed (iii) tapered and stepped feed.

This configuration with a step transformer and a taper implemented in the ground plane was optimised through simulation to maximise the impedance bandwidth. The taper/step combination contains four different impedance transitions: At the start of the taper, the CPW characteristic impedance is 50Ω and at the taper end it is 80Ω. The next two steps have the characteristic impedances of 94Ω and 108Ω, respectively. The input impedance values of the three configurations are shown in Figure 6.5(a) for comparison. For the straight feed it shows a high resistance peak that corresponds to a strong resonance while for the tapered feed a flattening is observed for the input resistance curve. With the taper/step combination the input impedance curves improve further and show increased flattening of resistance and reactance across the band. Figure 6.5(b) presents the impedance plotted on a Smith chart to show the variation in matching for the three transitions in an alternative format. The use of the taper/step feed combination provides wideband impedance matching from 3.5 GHz to 12 GHz with a $VSWR < 2$. The theoretical reflection coefficient is plotted versus frequency in Figure 6.4 for the above three configurations for the sake of comparison. It is clear that the step and taper transitions provide good matching between the feed line and the vertices of the slots over a broad frequency range leading to an

ultra-wideband response. This PSSA configuration was fabricated on an FR-4 substrate and measurements were carried out over the UWB band. A photograph of the prototype antenna is shown in Figure 6.6.

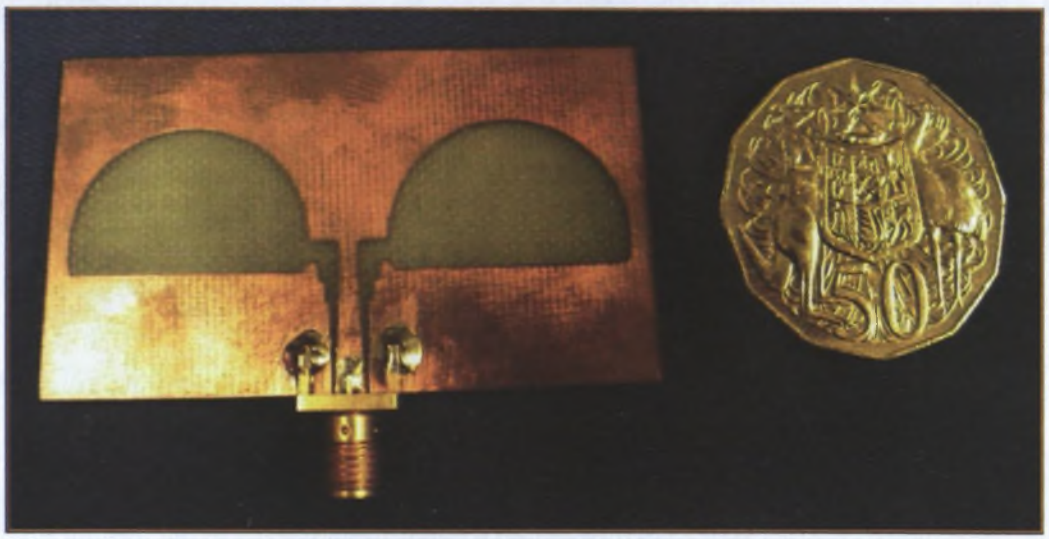


**Figure 6.6:** Photograph of the antenna prototype.

### 6.2.2 Experimental Results and Hardware Validation of SSA

The experimental results for impedance, radiation patterns and gain are presented in this section. A HP 8720D vector network analyser is used for impedance measurements. A NSI 700S-50 spherical near-field antenna range has been used for measurement of the radiation patterns and gain.

#### Impedance Characteristics and Current Distribution

The predicted and measured input reflection coefficient of the final PSSA design is shown in Figure 6.7. With the implementation of the stepped and tapered CPW-to-CPW transitions, the optimised structure yields a predicted impedance bandwidth of 3.0 GHz - 11.6 GHz (118%), which compares reasonably well with the measured bandwidth of 3.1 GHz - 13.8 GHz (126%).

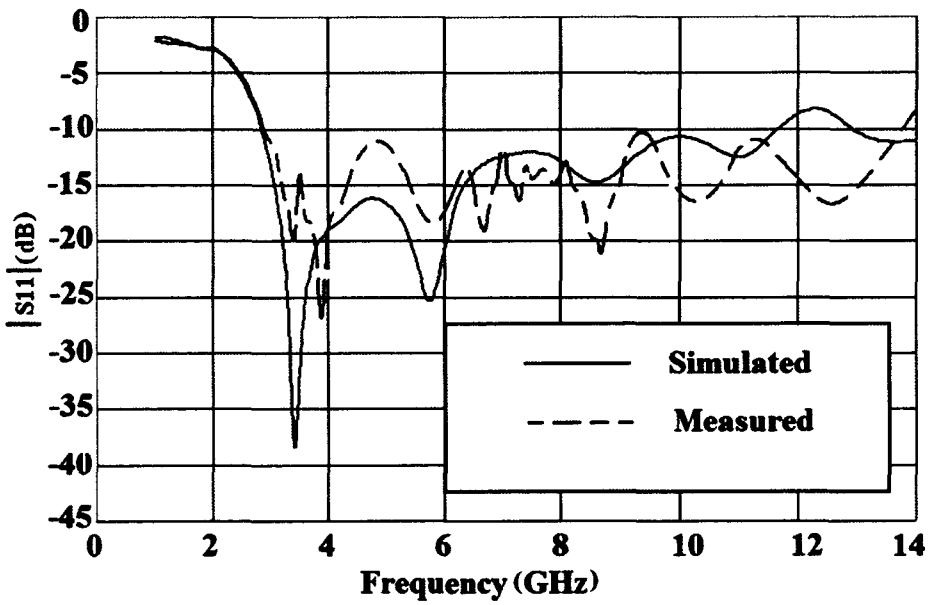


**Figure 6.7:** Predicted and measured reflection coefficient of the final PSSA.

Figure 6.8(a) shows the current distribution near the first resonance at 4 GHz. The current distribution at 7 GHz is illustrated in Figure 6.8(b) and suggests a higher-order mode. Figure 6.8(c) illustrates a more complicated current distribution at 11 GHz indicating even higher-order modes.

### Radiation Patterns and Gain

Figure 6.9 shows the measured radiation patterns at 3, 6, 9 and 12 GHz in the elevation and azimuth planes respectively. The azimuth plane shows broad beam coverage across the band while the elevation plane shows figure-of-eight style patterns. The measured peak gain is plotted for the entire impedance bandwidth in Figure 6.10. The maximum gain of 4.5 dBi occurs at 4 GHz while at the higher frequencies (5 to 10 GHz) a gain of 3.5 dBi $\pm 1$ dB is achieved. This nearly constant gain together with good phase characteristics is expected to create less pulse dispersion. To verify this aspect, a theoretical time-domain study is presented in the next section.

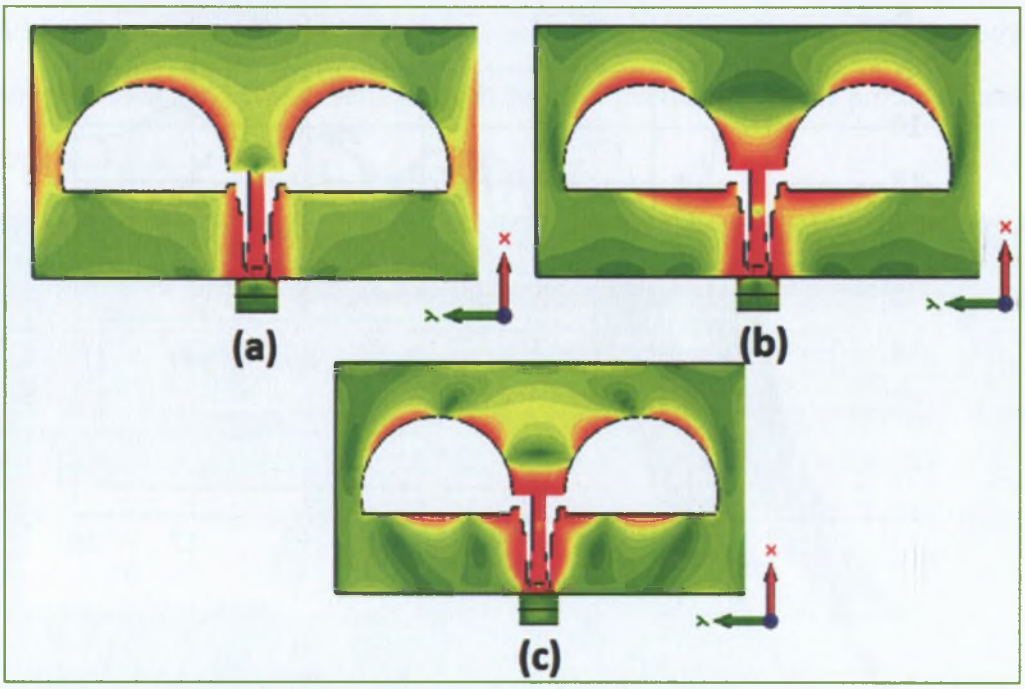


**Figure 6.8:** Simulated current distribution of the PSSA at: (a) 4 GHz; (b) 7 GHz; (c) 11 GHz.

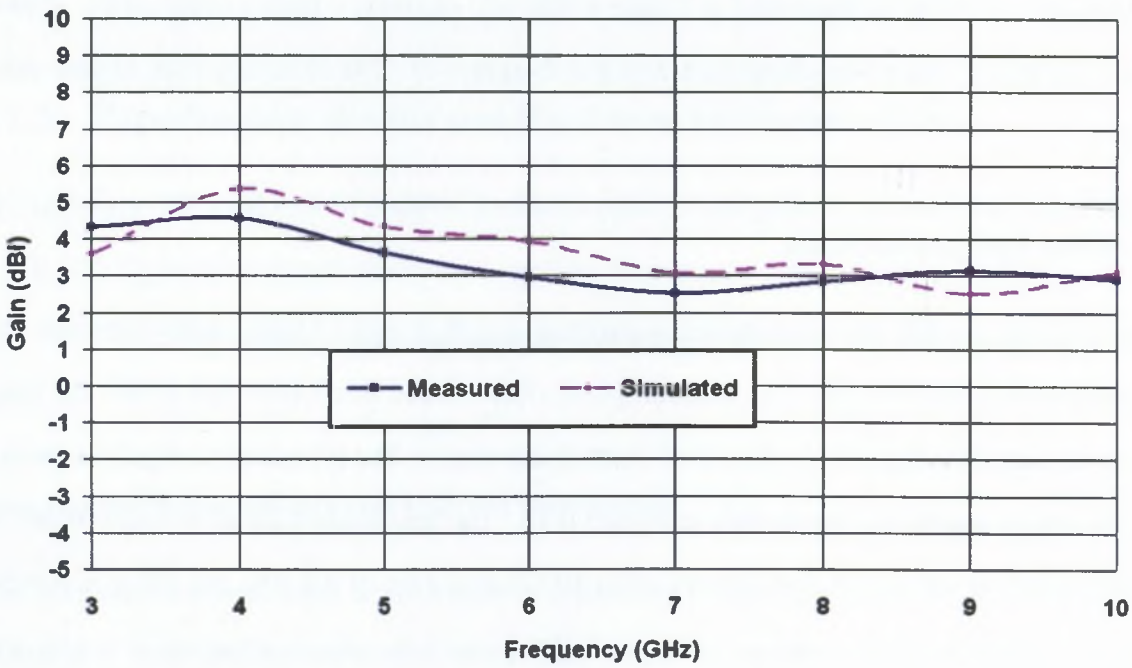


**Figure 6.10:** Measured and theoretical peak gains of the PSSA.

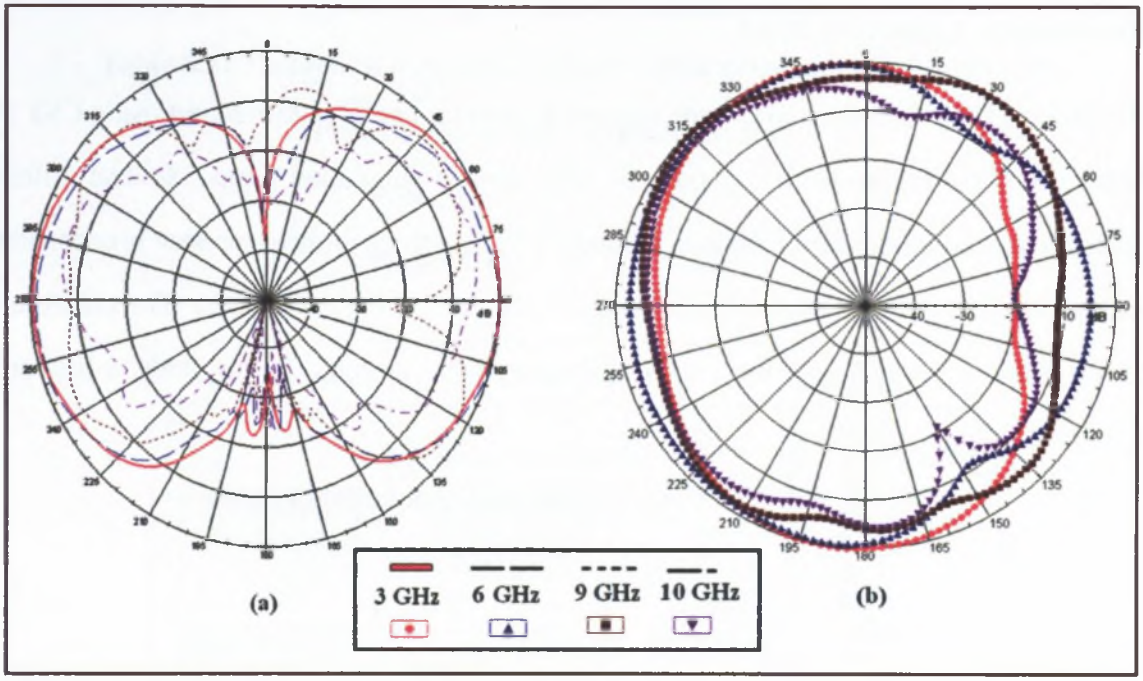


**Figure 6.9:** (a) Elevation plane and (b) azimuth plane radiation patterns at 3, 6, 9 and 10 GHz.

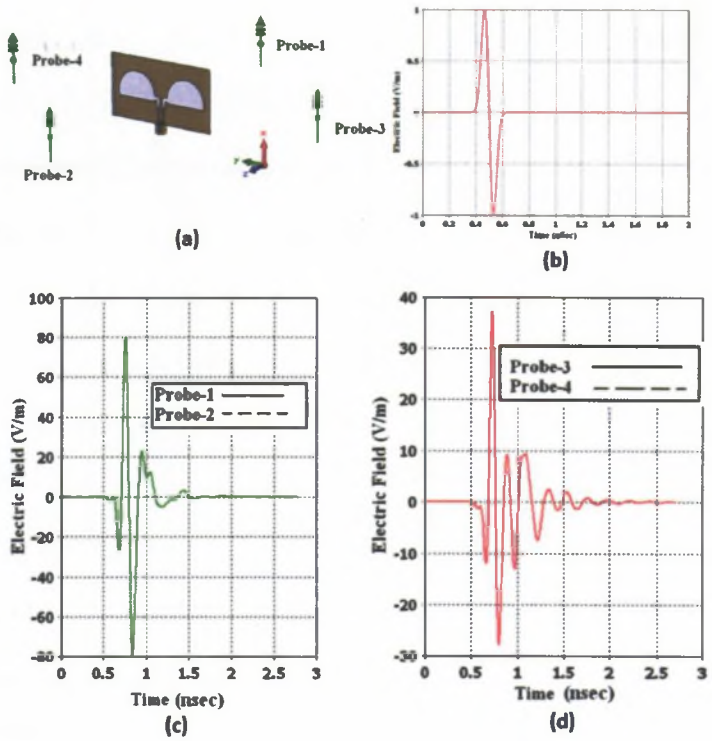


**Figure 6.11:** (a) Time-domain analysis setup (b) Input Rayleigh pulse with a=45 ps (c) Pulse received by Probe-1 and Probe-2 (face-to-face orientation) (d) Pulse received by Probe-3 and Probe-4 (side-by-side orientation).

**Time-Domain Analysis of PSSA**

A theoretical time-domain study of the proposed structure has been carried out using CST Microwave Studio. Figure 6.11(a) shows the time-domain simulation setup. Several different probes are placed at different locations around the PSSA (these probes represent broadband receiving antennas with constant effective length/aperture over the bandwidth). The polarisation of each probe is aligned with the x-axis of the coordinate system. In this study, a first-order Rayleigh pulse [98] given by:

$$f(t) = \frac{-2(t-1)}{a^2} exp\left(-\left(\frac{(t-1)}{a^2}\right)\right) (V/m) . \tag{6.1}$$

is chosen as the input voltage signal, where the pulse parameter $a$ stands for characteristic time. Large $a$ corresponds to a long waveform in the time domain but a small bandwidth in the frequency domain. A pulse with $a = 45$ ps is the closest match to the UWB band, so it is selected as the input pulse for simulation. Figure 6.11(b) shows this first order Rayleigh pulse. In Figure 6.11(a) Probe-1 is placed 100 mm behind the PSSA (the -z direction) while Probe-2 is placed 100 mm in front of the slot antenna (the +z direction). Probes-3 and -4 are placed at a distance of 100 mm to the right and left (in the -y and +y directions) of the antenna, respectively. The pulses received by the probes are shown in Figure 6.11(c) and (d). Due to symmetry, the pulses received by Probe-1 and Probe-2 are identical. The same applies for Probe-3 and Probe-4. As can be seen from Figures 6.11(c) and (d), the pulses received by Probe-1 and Probe-2 show limited ringing, while those in Probe-3 and -4 show a small amount of distortion. To quantify these effects the fidelity of the received pulses is examined by calculating the correlation between the time-domain input signal $f(t)$ and the pulse received by ideal probes $s(t)$. The normalised correlation factors of the received pulses are listed in Table 6.1. Due to the symmetrical location of the probes, only results for Probe-1 and Probe-3 are listed. The high correlation values lead to the lower distortion in the pulse.

**Table 6.1:** Theoretical correlation between transmitted and received pulses

| **Probe Orientation** | Correlation Factor |
|---|---|
| **Probe 1, 2** | 0.912 |
| **Probe 3, 4** | 0.829 |

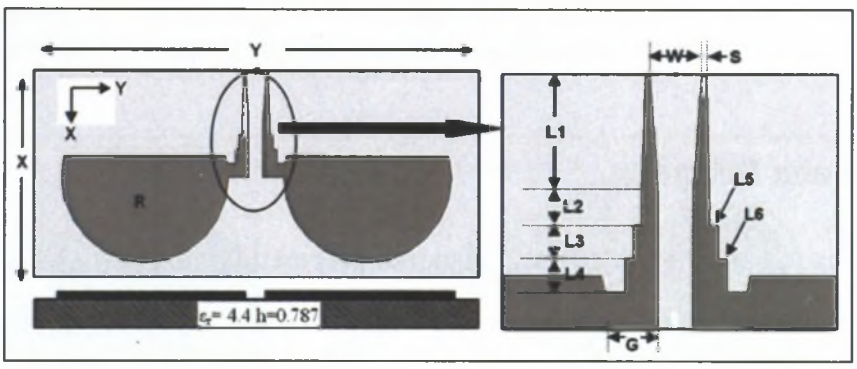


(a)

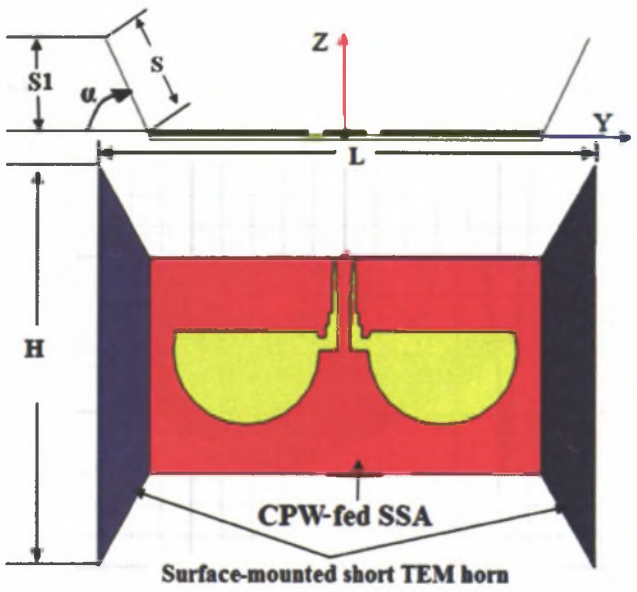


(b)

**Figure 6.12:** (a) A CPW-fed semicircular slot antenna: $X = 30, Y = 60, L1 = 7, L2 = L3 = L4 = 2, L5 = L6 = 0.5, W = 3, S = 0.3, G = 2.5, R = 12$; (b) Semicircular slot antenna with a surface-mounted, short, two-plate horn: $H = 65, L = 80, S1 = 18.13, S = 20$ and $\alpha = 65^0$ (All lengths are in mm).

## 6.3 Slot Antenna with Short Two-Plate Horn

The TEM horn is a popular antenna design in GPR applications, consisting simply of a flared pair of conductors, that supports a TEM wave and gradually accomplishes the transition from the feed line to a travelling wave in space. The antenna is capable of radiating an impulse with little distortion and their directionality results in useful gain. This motivation provokes the mounting of the short two-plate horn on top of the slot antenna proposed in the previous section.

### 6.3.1 Antenna Design

The main aim is to enhance the gain of the earlier proposed semicircular slot antenna, which is shown in Figure 6.12(a). For this purpose, the concept of a surface-mounted short horn described in Chapter 4 is used with the slot antenna as shown in Figure 6.12(b).

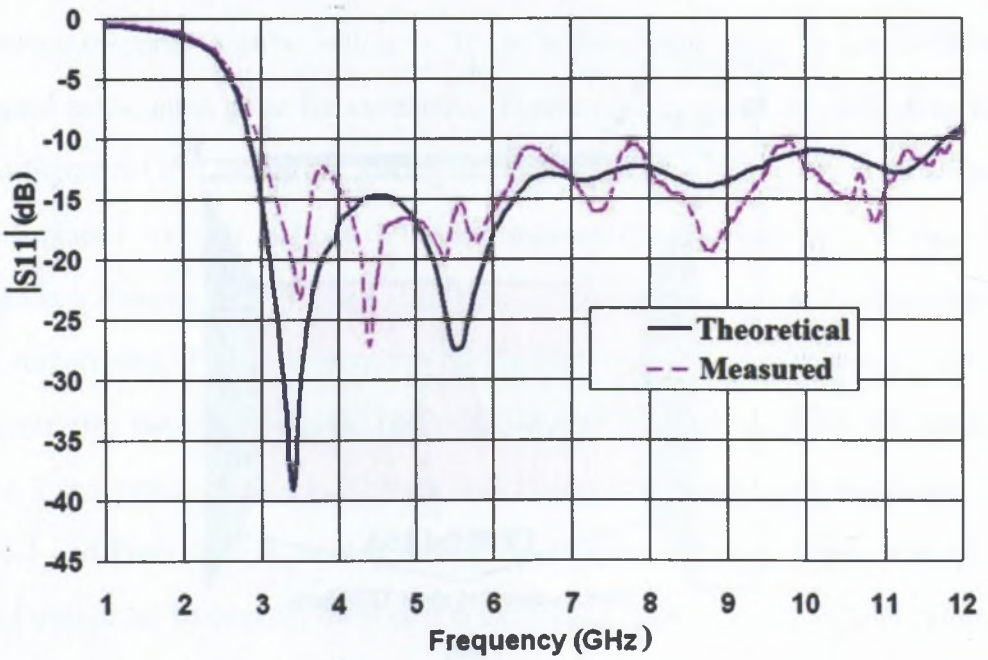


**Figure 6.13:** Theoretical and measured reflection coefficients of the new antenna consisting of the CPW-fed slot antenna and the surface-mounted short two-plate horn.

The overall size of the PSSA structure (including feed and semicircular aperture) is half a

wavelength at the lower cutoff frequency (3 GHz) with a 10 dB return loss bandwidth of 8.61 GHz (2.99 GHz to 11.6 GHz). Standard TEM horns are usually very bulky as they are several wavelengths long [54]. Lee and Smith [120] have presented TEM horn design charts for $S/\lambda$ from 1 to 7. The key parameters in design of a TEM horn are slant length ($S$), conducting plate apex angle ($\beta$) and horn internal apex angle ($\alpha$) between the two conducting planes. The angle $\alpha = 65^0$ is chosen for optimizing the short TEM horn (a complete study was carried out in Chapter 4).

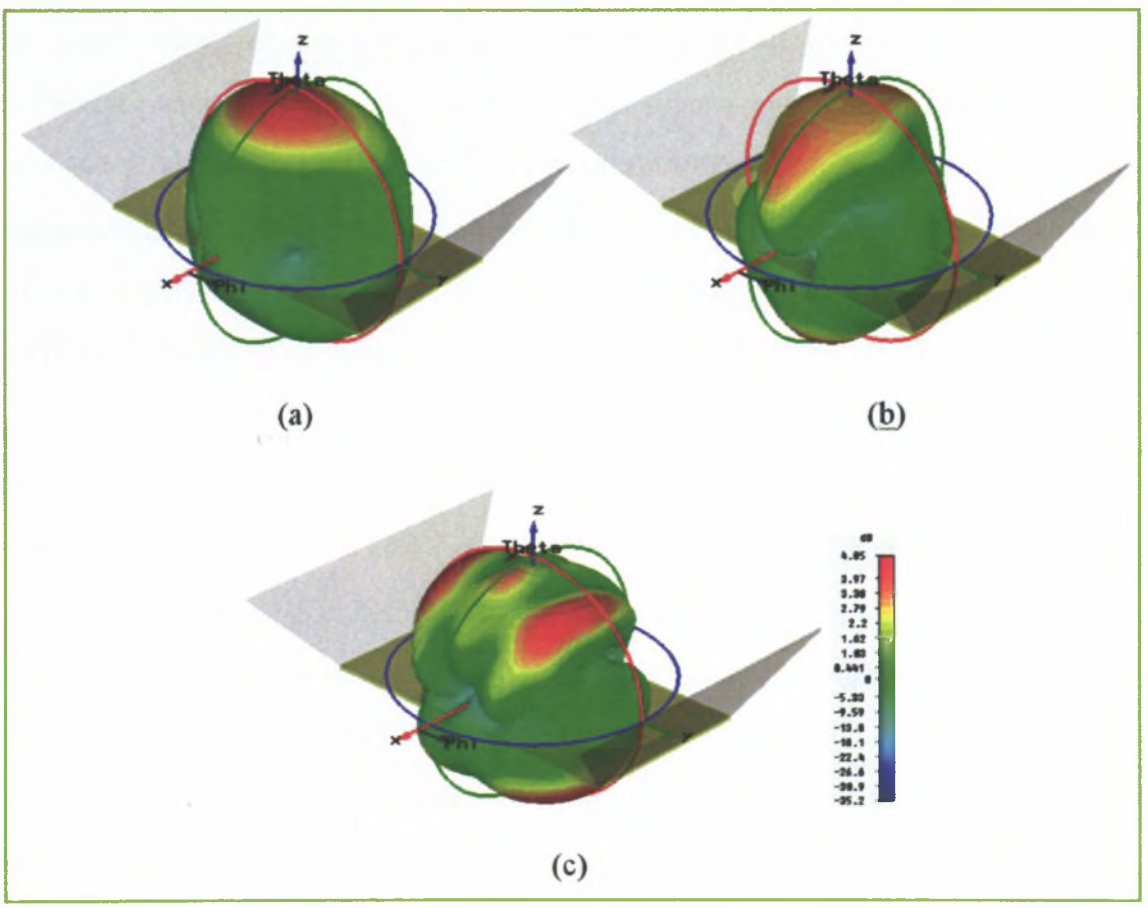


**Figure 6.14:** Theoretical radiation patterns with horn, at (a) 3 GHz (b) 6 GHz and (c) 10 GHz.

### 6.3.2 Theoretical Results and Discussions

Truncated two-plate horns with the slant lengths (shown as S in Figure 6.12(b)) of $\lambda/10$ , $\lambda/2.5$ and $\lambda$ are theoretically analysed. The parameters $W, L$ and slant angle $\alpha$ are optimised to achieve a nearly constant gain and a return loss greater than 10 dB from 2.88 GHz to 10.66 GHz. The final dimensions of the design are shown in Figure 6.12(b).

Simulations are conducted using Ansoft HFSS software. This compact antenna is indeed a combination of a two-plate horn antenna and a semicircular slot antenna. Simulation indicates the new antenna has a moderate and nearly constant gain over a wide bandwidth. It also has a nearly omni-directional radiation pattern in the Z-Y plane with a figure-of-eight patterns in the X-Y plane, with only a slight change in the beam direction over the large operating bandwidth. The predicted and the measured reflection coefficient of a prototype PSSA was shown previously in section 6.2.2. This optimised design yields a 10 dB return loss bandwidth of 8.61 GHz (2.99 GHz to 11.6 GHz) which compares well with the measured bandwidth of 10.7 GHz (3.1 GHz to 13.8GHz).

Next the two-plate horn is mounted on top of the substrate containing PSSA. The theoretical and measured reflection coefficient curves of the new antenna (i.e. with the surface-mounted short horn) shown in Figure 6.13 are not significantly different from those of the PSSA in Figure 6.7. This optimised design with a slant height of $\lambda/5$ (at the lowest frequency) has a theoretical 10dB return loss bandwidth of 8.74 GHz (2.86 GHz to 11.6 GHz). It compares well with the measured bandwidth of 8.82 GHz (2.98 GHz to 11.88 GHz). Figure 6.14 shows the effect of the horn on the radiation patterns at three representative frequencies: 3, 6 and 10 GHz. It confirms that at lower frequencies the maximum radiation is in the direction of the horn but as frequency increases the beam splits. The PSSA without horn shows a gain of 3.5 dBi with a variation of 1 dB across the band from 3 to 10 GHz. In the theoretical studies of a 20 mm horn, the gain is around 6 dBi with a variation of 1 dB across the band from 3.5 GHz to 10 GHz. As the length of the horn is increased from 10 mm to 100 mm, the peak gain increases significantly.

For the testing, a 20 mm horn is chosen due to its compact size and relatively flat gain curve. A theoretical time-domain study of the new antenna is also carried out with the help of CST Microwave Studio.

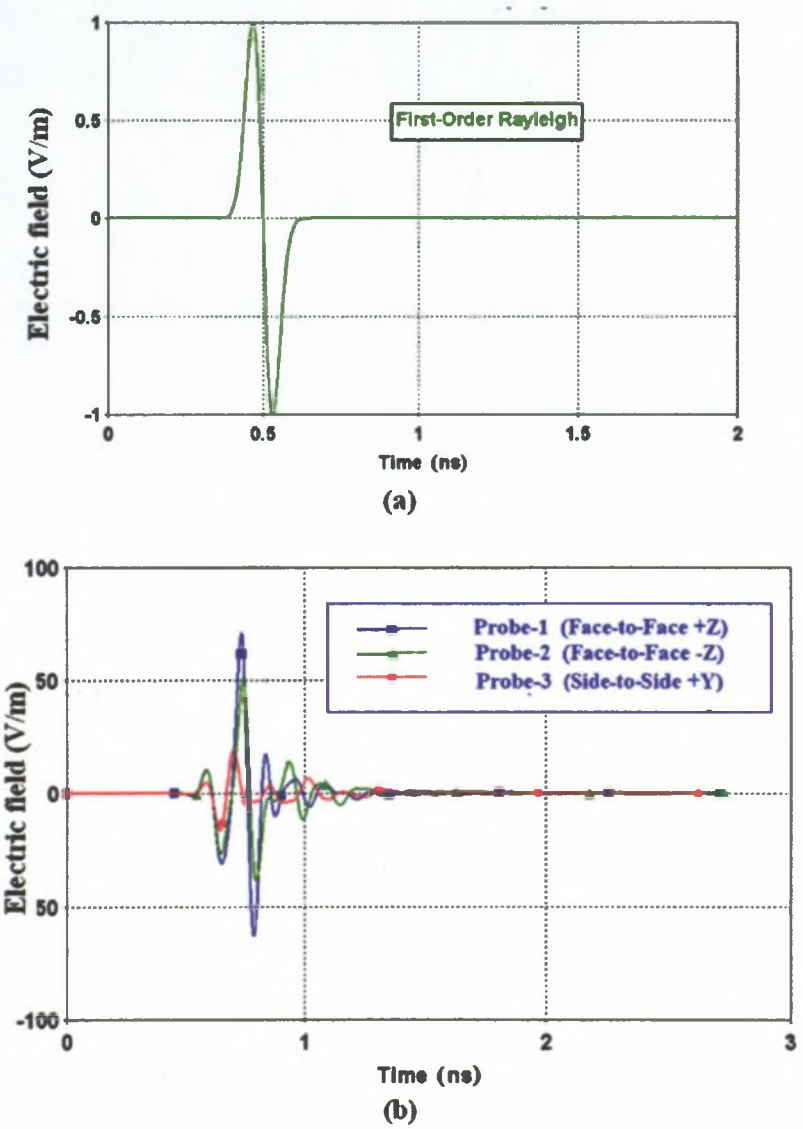


**Figure 6.15:** (a) Input Rayleigh pulse (b) Electric-field waveforms detected at a distance of 100 mm in three different directions.

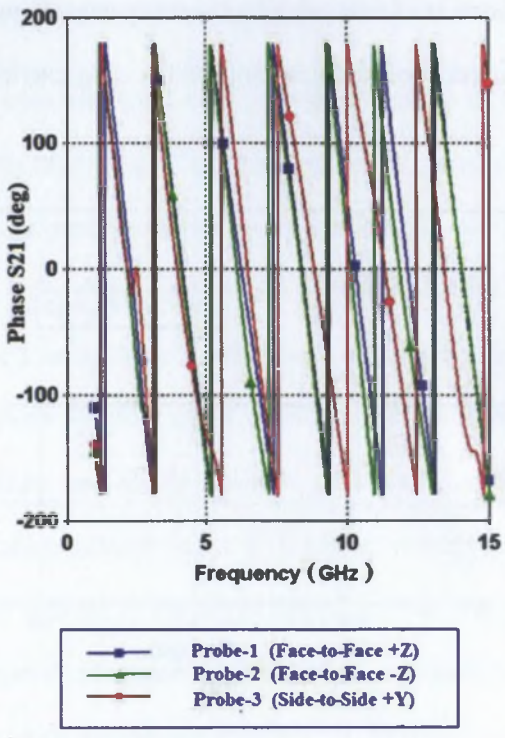


**Figure 6.16:** Transfer function phase for different orientation of TEM horn.

Three different X-polarised probes are placed in different directions. Probe-1 is placed in front of the horn aperture (i.e. in the +Z direction) and it is aligned with the centre of the antenna. Probe-2 is placed in the same way but behind the antenna (i.e. in the -Z direction underneath the slot antenna) and Probe-3 is placed along the side of the antenna (+Y). These probes detect the received pulses in three different directions at a distance of 100 mm from the antenna. A typical first-order Rayleigh pulse [98] is used as the source signal. Pulses received at the three locations are plotted in Figure 6.15. The phase of the antenna transmitting transfer function at these three probes is plotted in Figure 6.16, which shows a nearly linear variation of phase across the bandwidth.

### 6.3.3 Measurement and Hardware Validation

Figure 6.17 shows the complete hardware prototypes of antennas with various short horns.

**Figure 6.17:** Hardware prototype of PSSA with integrated horn and various other short horns of different length.

The gain of the slot antenna as measured with and without horn of physical length 20 mm is compared in Figure 6.18. The integration of the 20 mm compact horn is considered to be the most suitable because it enhances the gain of the antenna across the entire frequency range. The proposed antenna exhibits a gain in the range of 6.5 dBi $\pm$ 1.5 dB over the entire bandwidth. This is a significant enhancement over the gain of the slot antenna in the range of 3.5 dBi $\pm$ 1 dB. Figure 6.19 shows the measured radiation patterns at 3 GHz, 5 GHz and 8 GHz. In the elevation plane the design antenna has figure-of-eight type patterns similar to the PSSA, while in the azimuthal plane the effect of short horn comes into the picture and the beam is narrower, which results in high peak gain for the configuration.

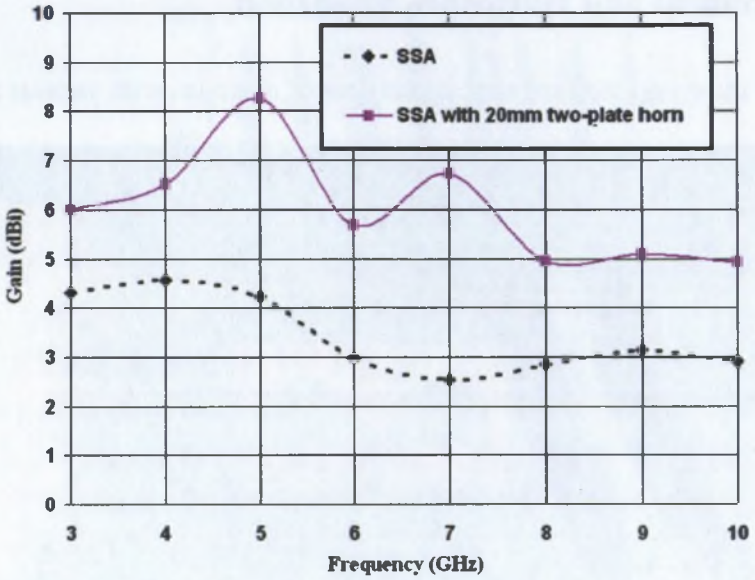


**Figure 6.18:** Measured antenna gain versus frequency, for the PSSA with a 20mm two-plate horn.

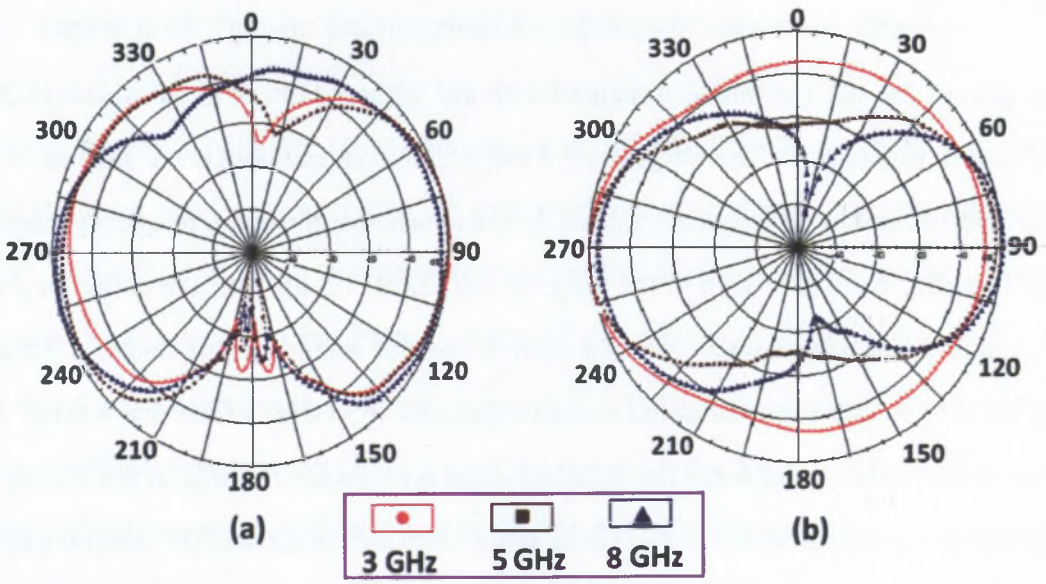


**Figure 6.19:** Measured antenna radiation patterns of PSSA with 20mm short two-plate horn (a) Elevation Plane (b) Azimuth Plane.

## 6.4 Bidirectional Surface-Mounted Short Horn (SMSH) Antenna

The dual- and quad-ridge horns are traditional wideband horns [136], [68], [137] as described in the literature. These horns achieve the desire UWB characteristics and increase the power handling capacity, but this in turn increases the design complexity and the bulk. A typical coaxial line to a ridged-waveguide transition is also needed to improve the impedance matching over the whole UWB band. In this section novel surface-mounted short horns are presented, which can be used as replacements for bulkier ridged horns in UWB applications where the power handled is low.

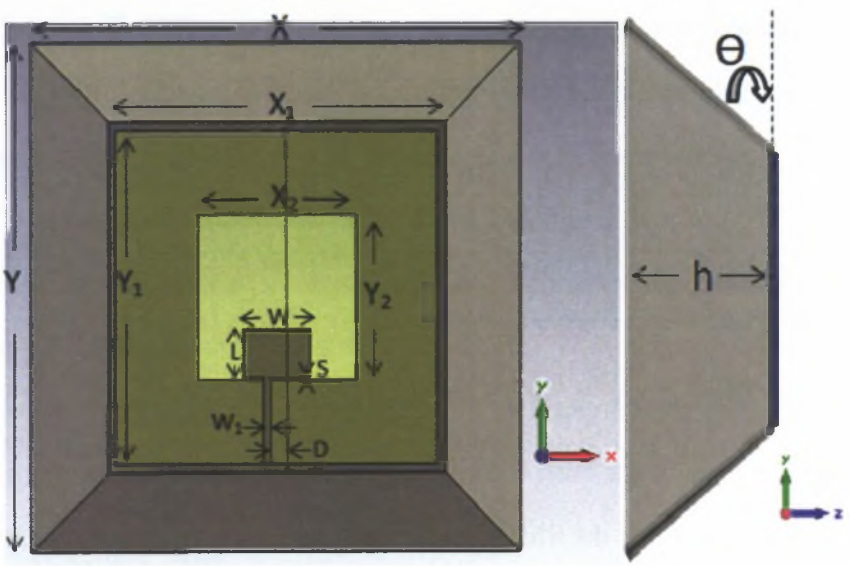


**Figure 6.20:** Surface-mounted short horn (SMSH) with Slot antenna at the base.

These horns take their inspirations inspiration from the short horn (SH) first introduced in [71], [72] for achieving high gain from microstrip antennas. The performance and effectiveness of short horn was further extended to linear and circular polarised dielectric resonators, and dielectric resonators over patch antennas [73], [74], [75], [76]. These antennas have bandwidths

of around 30%. A short horn excited by a slot is presented in this section. This horn is capable of producing high gain and is optimised over the UWB bandwidth.

### 6.4.1 Bi-directional Surface-Mounted Short Horn (SMSH) Design

The design begins by mounting a slot antenna [135] at the base of a short horn. Drawing on our previous experience in the design of horns presented in Chapter 4, the initial slant height and slant angle is chosen. The antenna has a bidirectional radiation pattern because of backward radiation. The proposed UWB high-gain compact antenna structure with short horn mounted on top of a slot antenna is shown in Figure 6.20. A square slot antenna is selected on a FR-4 substrate with $\varepsilon_r = 4.4$ and thickness $h1$ = 0.8 mm. This is the same slot antenna described in Chapter 5. It is excited by an asymmetrically located monopole [135]. The slot dimensions are: $X_2 = Y_2 =$ 31 mm, dimensions of the rectangular patch monopole: $W =$ 13 mm and $L =$ 9 mm, the gap between the patch and slot edges is $S =$ 2 mm. The 50Ω microstrip feed line has width $W1 =$ 1.5 mm and feed offset 2 mm from the centre of the patch. The impedance bandwidth of the slot radiator extends from 2.9 GHz to 18.38 GHz and the simulated average gain is 4 dBi. The gain variation is 2 dB over the impedance bandwidth. A surface-mounted short horn (SMSH) with slant angle $\theta = 60^0$ is mounted on the slot to enhance the directivity and gain. The square base of the horn is fixed at $X_1 = Y_1 =$ 63 mm. Its height $h$ is varied from 5 mm to 50 mm. It is noted that the SMSH has a very small effect on the impedance bandwidth, which is 145% with the horn and 149% without the horn. The gain tends to increase with the horn height and saturates for heights around 50 mm. The peak gain of around 11 dBi is achieved with the short horn. Figure 6.21 shows the theoretical reflection coefficients of the slot antenna with and without the SMSH.

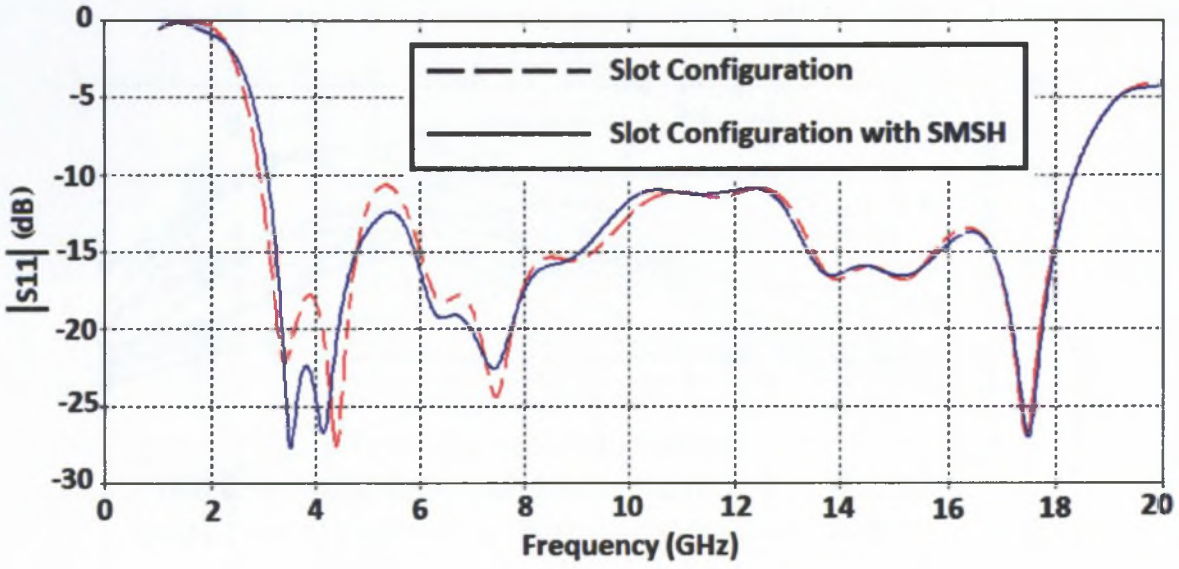


**Figure 6.21:** Predicted reflection coefficients of the slot antenna with and without SMSH.

### 6.4.2 Bi-directional SMSH Study, Results and Discussion

To further investigate the effect of the slant angle on the gain of the antenna, the antenna height is fixed at 35 mm. This choice is a compromise between compactness and gain. The slant angle is varied between $10^0$ to $90^0$. The antenna is simulated over the frequency band 2 GHz to 15 GHz and the results are shown in Figure 6.22. The maximum gain occurs at a slant angle of $60^0$. However, the variation in gain over this frequency band (2 GHz to 15 GHz) is also high, i.e. 2.28 dB. At $30^0$ slant angle, the gain is limited to 7 dBi. However, the gain variation over the band is only 1.07 dB. Figure 6.23 further explores the nature of the gain variation with frequency for the selected slant angles of $30^0, 60^0$ and $90^0$. Results are also presented for the slot radiator without the short horn. Short horns with $30^0$ and $90^0$ slant angles provides more uniform gain over the complete frequency band whereas those with $60^0$ slant angles provide a higher gain at the expense of strong gain variation with frequency. The SMSH with $30^0$ slant angle has higher gain between 2 GHz and 8 GHz. The SMSH with $90^0$ slant angle has higher

gain between 8 GHz and 13 GHz.

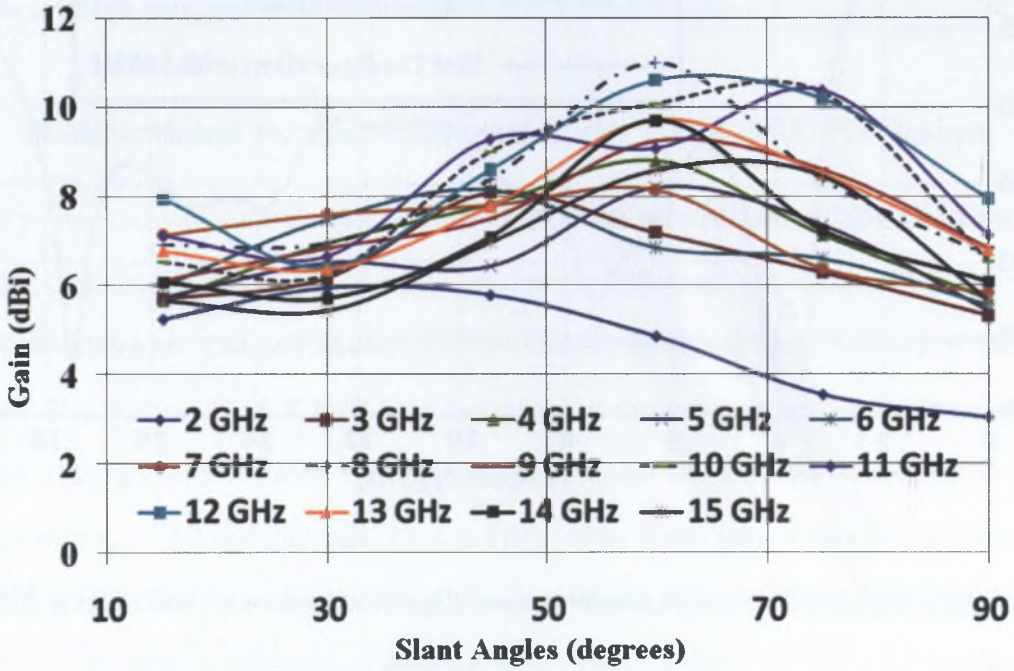


**Figure 6.22:** Variation of gain for different slant angles of the SMSH with frequency as a parameter.

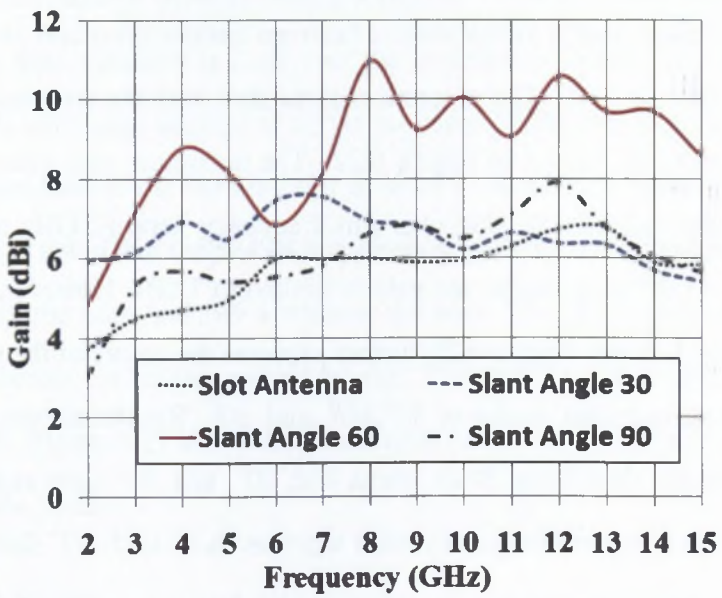


**Figure 6.23:** Variation of gain over entire frequency band with slant angle as a parameter.

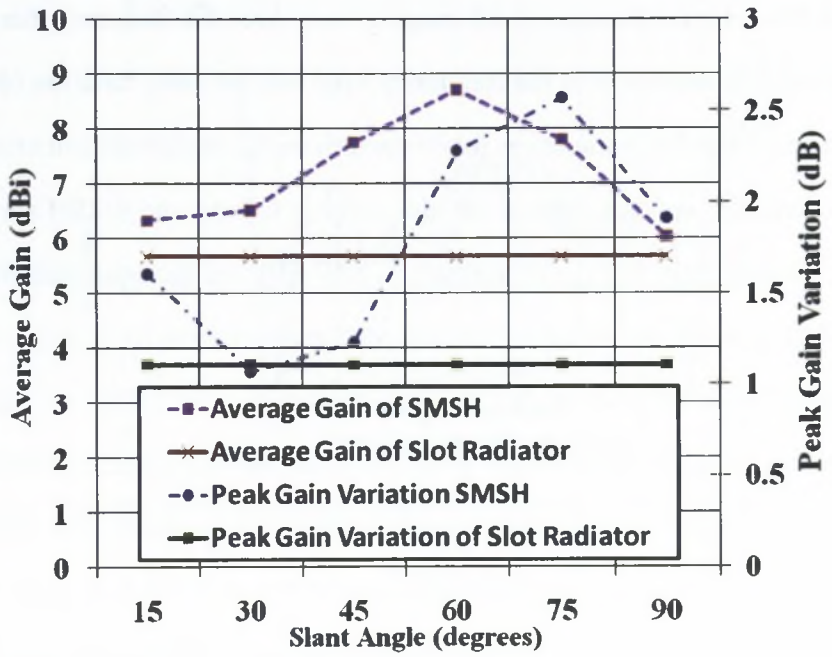


**Figure 6.24:** Variation of the average gain and the peak gain variation of the SMSH and slot radiator with slant angle as a parameter.

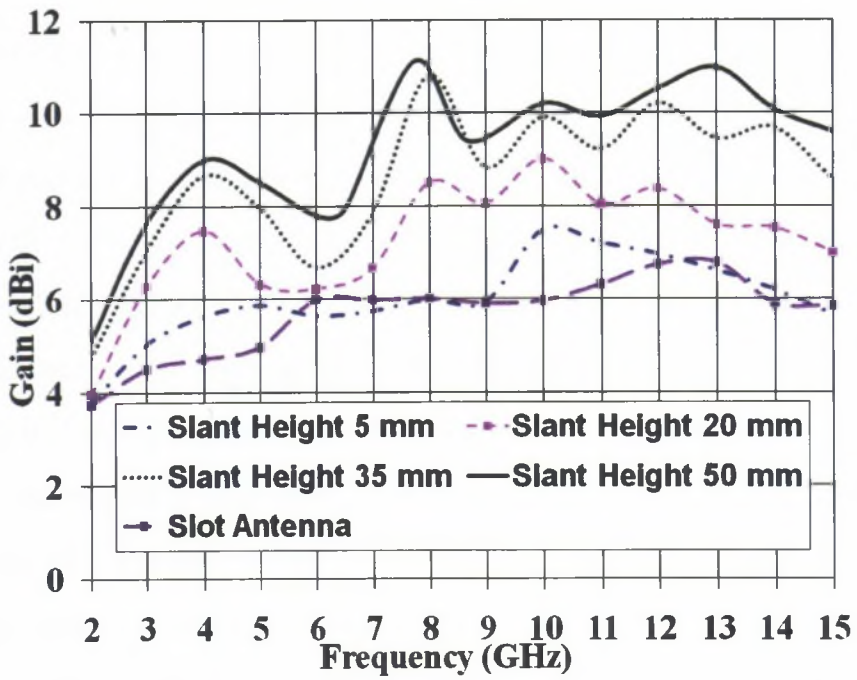


**Figure 6.25:** Variation of the gain with frequency with horn height as a parameter.

The gain of the antenna changes in an irregular way over the frequency band. Therefore, the average gain of the antenna over the frequency band and the peak variation of the gain from the average can be adopted as parameters for characterising the wideband antenna performance. Figure 6.24 presents the average gain of the slot radiator without the SMSH and its peak gain variation. The average gain of the slot radiator is 5.67 dBi and the peak gain variation is 1.1 dB. Figure 6.24 also shows the average gain and peak gain variation for a range of SMSH slant angles. The antenna with $30^0$ slant angle gives smooth gain over the 2 GHz to 15 GHz band with a gain variation of only 1.07 dB, which is even less than the gain variation of the slot radiator without horn. However, the average gain improvement is only 1.04 dB. The antenna with $60^0$ slant angle gives 2.03 dB average gain improvement with a 2.28 dB peak gain variation. The maximum gain improvement is 5.33 dB over the average gain of the bare slot radiator. Further study on the effect of different heights of the horn is carried out with a fixed slant angle. Figure 6.25 shows the variation of gain with the height of the horn as a parameter.

A final design of the SMSH antenna is fabricated with slant angle $\theta = 60^0$ and slant height = 50 mm. The measured reflection coefficient of the slot antenna with and without the SMSH is plotted in Figure 6.26. The very small effect of the SMSH highlighted in the predicted results is verified experimentally. The theoretical impedance bandwidth of 145% matched well with the measured bandwidth of 145%. The measured gain performance of the SMSH is shown in Figure 6.27; the measured peak gain of 10.87 dBi occurs at 8 GHz. The average value of gain is 9.05 dBi with a variation of around 2 dB across the whole impedance bandwidth. The radiation patterns are plotted for elevation and azimuth planes at 3, 6, 8 and 10 GHz in Figure 6.28. The bidirectional nature of the SMSH is clearly seen in the azimuthal plane, while in the elevation plane the antenna patterns are dominated by the slot antenna. The antenna beam is broad at lower frequencies and becomes narrower as frequency goes beyond 8 GHz. Back-lobe radiations are consistent from the antenna. The next section will demonstrate a unidirectional configuration of SMSH that enhances the gain while maintaining the impedance bandwidth.

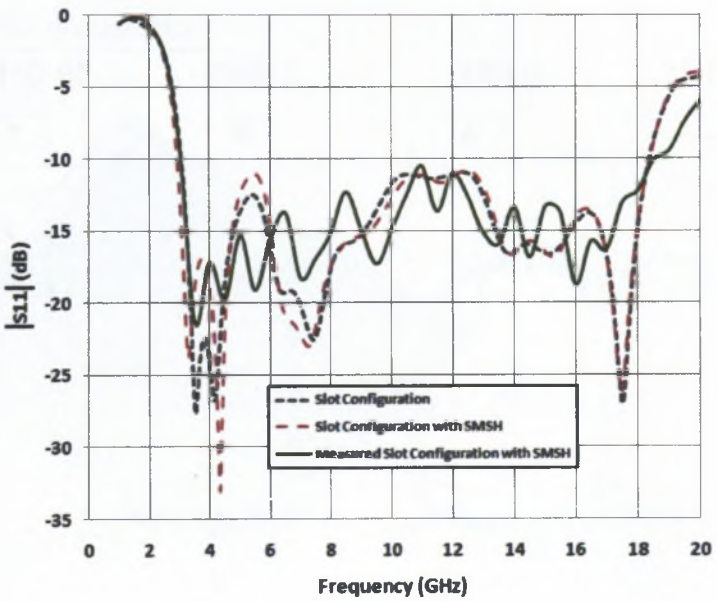


**Figure 6.26:** Measured and predicted reflection coefficient of SMSH horn.

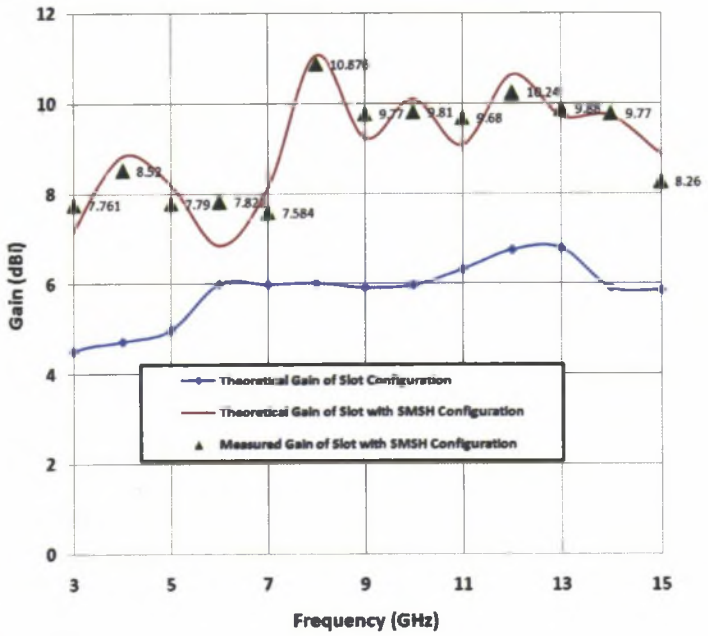


**Figure 6.27:** Measured and predicted gain versus frequency, for bidirectional SMSH.

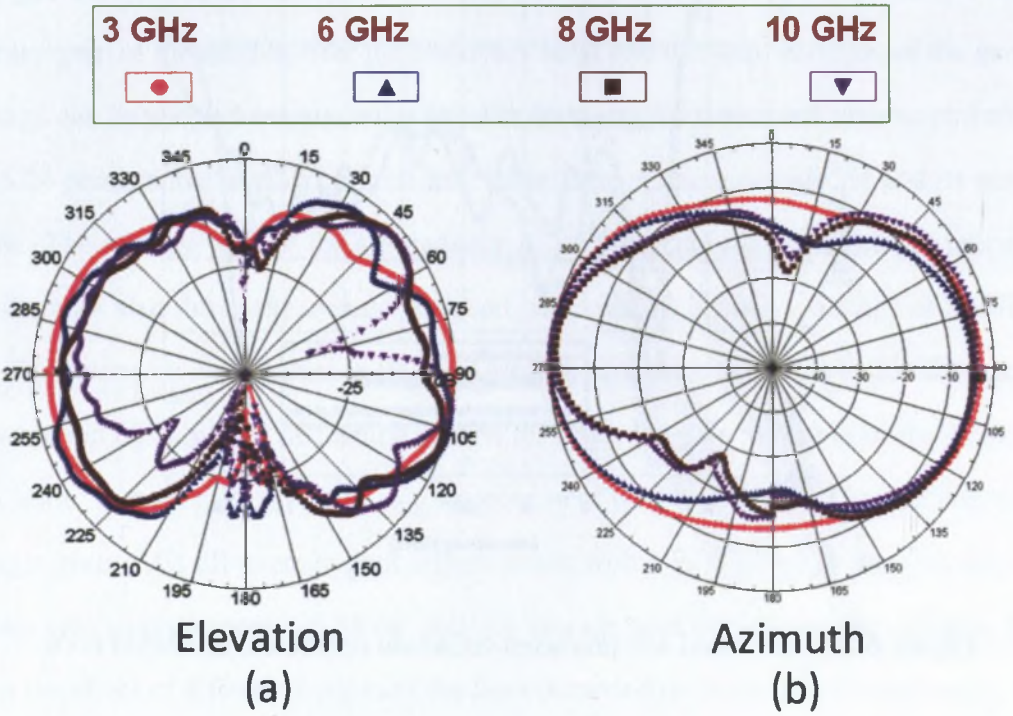


**Figure 6.28:** Measured radiation patterns of bidirectional SMSH at 3, 6, 8 and 10 GHz (a) Elevation plane (b) Azimuth Plane.

## 6.5 High-Gain Unidirectional SMSH

Previously, in section 6.3, a complete study of optimising a short horn was carried out. Based on that knowledge, a high-gain compact short horn antenna with unidirectional radiation is proposed in this section. Figure 6.29 shows the schematic of the antenna design. To excite the short horn, a simple square-slot antenna is chosen for the same reason as described in the previous section. This concept is not limited to this particular slot antenna; designers can use various other slot antennas available in the literature. The performance of the short horn with several microstrip-fed and CPW-fed slot configurations is tested theoretically. In the design process Teflon spacers are used to mount the slot antenna inside the short horn and a small hole in one of the walls of the short horn is made to connect a semi-rigid coaxial cable to the

microstrip feed of the slot antenna.

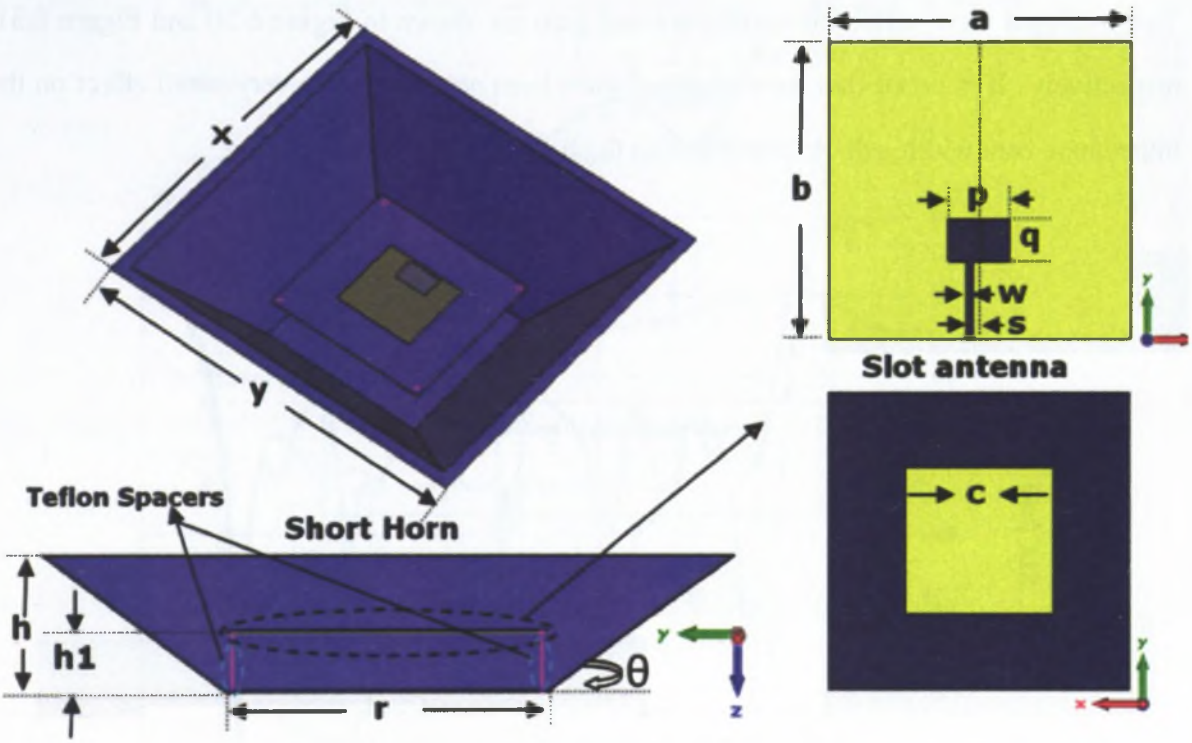


**Figure 6.29:** Compact high-gain unidirectional short horn.

The overall size of the slot antenna is $a = b = 63$ mm. The impedance bandwidth of the slot radiator extends from 2.9 GHz to 18.38 GHz and the average predicted gain is 4 dBi. The gain variation is $\pm 1$ dB over the impedance bandwidth. An optimised short horn with slant angle of $60^0$ is designed to enhance the directivity and gain. The square base of the horn is fixed at $r = 63$ mm. The horn aperture is $x = y = 133$ mm. Its height h was varied from 5 mm to 50 mm to select the optimum gain and compactness, which occurs when the height was 35 mm. The slot antenna is mounted at height $h1 = 15$ mm. The taper cavity formed because of the slant angle of the horn under the slot antenna is capable of reducing the back reflection and providing good gain in the main beam direction.

### 6.5.1 Unidirectional SMSH, Results and Discussions

The predicted input reflection coefficient and gain are shown in Figure 6.30 and Figure 6.31, respectively. It is noted that the optimised short horn structure has a very small effect on the impedance bandwidth, which is 145% with the horn and 149% without it.

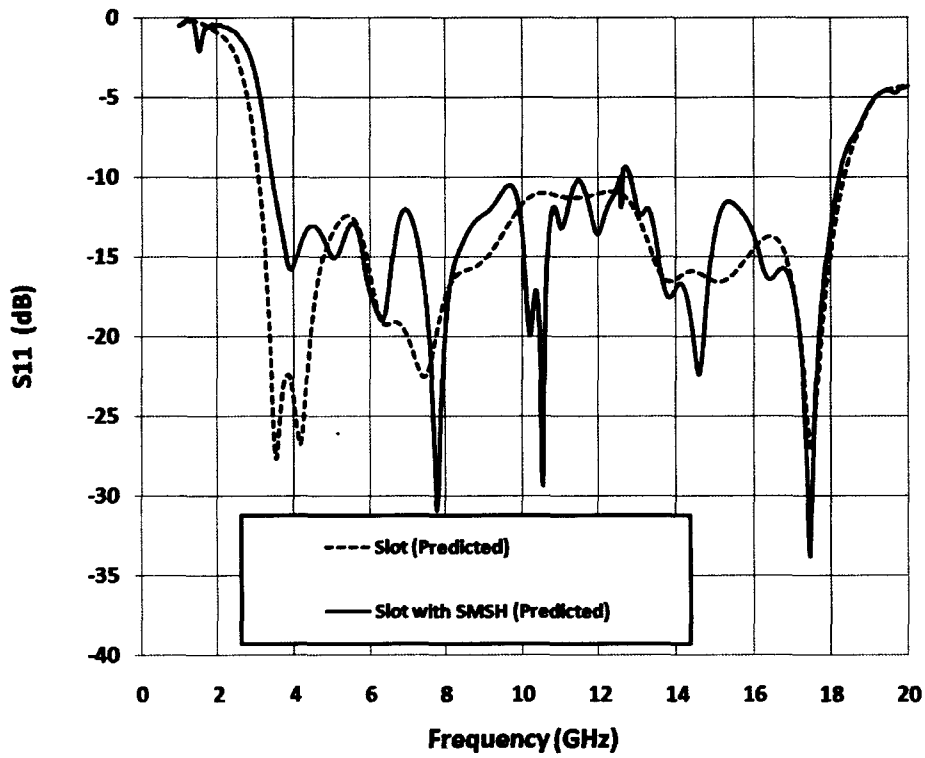


**Figure 6.30:** Predicted reflection coefficient of the slot antenna with & without the SMSH.

The gain tends to increase with the horn height and saturates for heights around 50 mm. The peak gain achieved with the unidirectional short horn is 14.53 dBi. The gain of the antenna changes in an irregular way over the frequency band. The designed antenna with a slant angle of $60^0$ gives 11.60 dBi average gain which shows an improvement of around 6 dB, with a 3 dB peak gain variation as compared to the reference slot radiator.

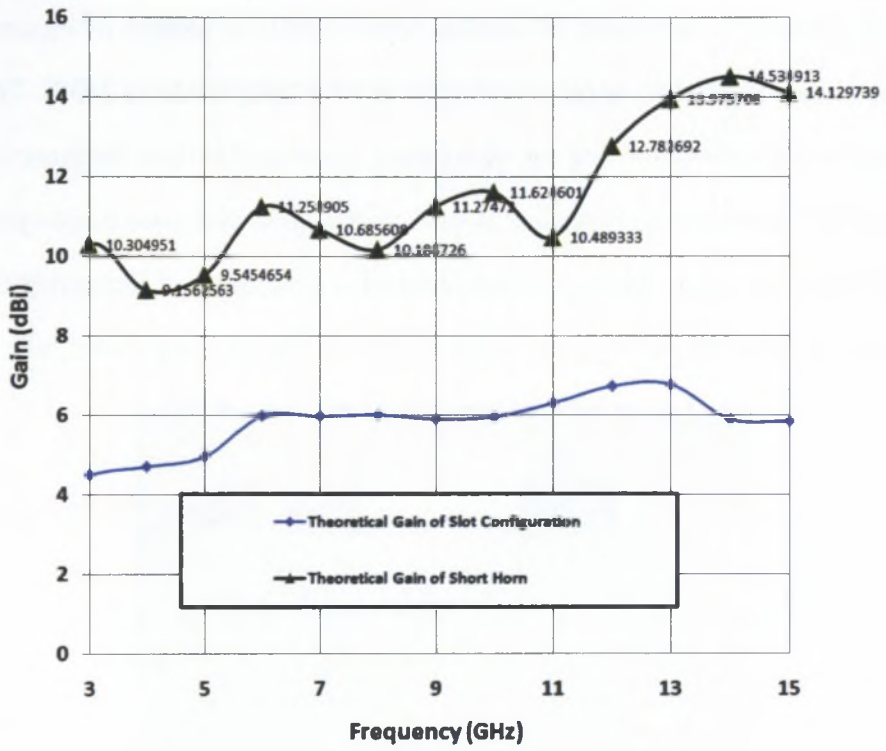


**Figure 6.31:** Predicted gain of two antennas.

**Table 6.2:** Gain comparison of unidirectional SMSH with slot antenna over UWB frequency range

| UWB Band | 3.1 GHz to 5.1 GHz | 5.8 GHz to 10.6 GHz | 3.1 GHz to 10.6 GHz |
|---|---|---|---|
| Peak Gain | 10.30 dBi | 11.62 dBi | 11.62 dBi |
| Avg. Gain | 9.66 dBi | 11 dBi | 10.5 dBi |
| Variation | ±0.64 dB | ±0.62 dB | ±1.1 dB |

In order to make it more favourable for FCC compliance, the gain enhancement for lower and upper UWB bands is also studied. A complete gain study across the UWB band is given in Table 6.2. For the lower UWB band of 2.05 GHz bandwidth (3.1 to 5.1 GHz) the average gain is 9.66 dBi, while the upper UWB band of 4.775 GHz bandwidth (5.825 to 10.6 GHz) shows an average gain of 10.9 dBi. Figure 6.32 and Figure 6.33 show the hardware profile of the antenna.

The measured reflection coefficient of unidirectional SMSH is plotted in Figure 6.34. The measured impedance bandwidth is from 2.90 GHz to 17.8 GHz, which is 143%. The measured radiation patterns in the elevation and azimuth planes are plotted at three frequencies in Figures 6.35, 6.36 and 6.37. Antenna performance is quite satisfactory with good beam symmetry up to 6 GHz, after which the beam starts to squint. There is a possibility of improving the design to obtain more stable radiation patterns and phase centre, but that is not pursued here.

**Figure 6.32:** Hardware profile of the short horn antenna.

**Figure 6.33:** Hardware profile of short horn and commercial dual-ridge horn antennas.

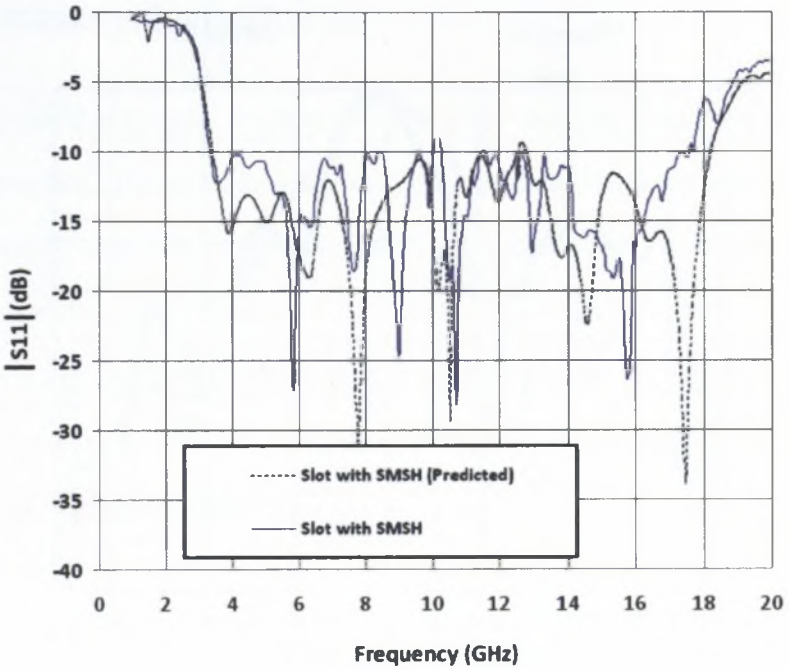


**Figure 6.34:** Measured and predicted reflection coefficient of the unidirectional SMSH.

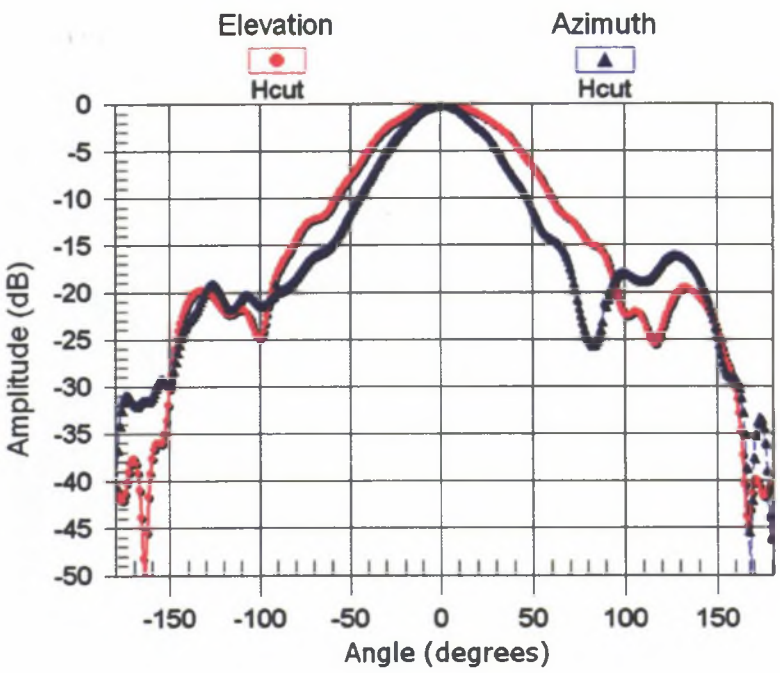


**Figure 6.35:** Measured elevation and azimuth radiation patterns at 3 GHz.

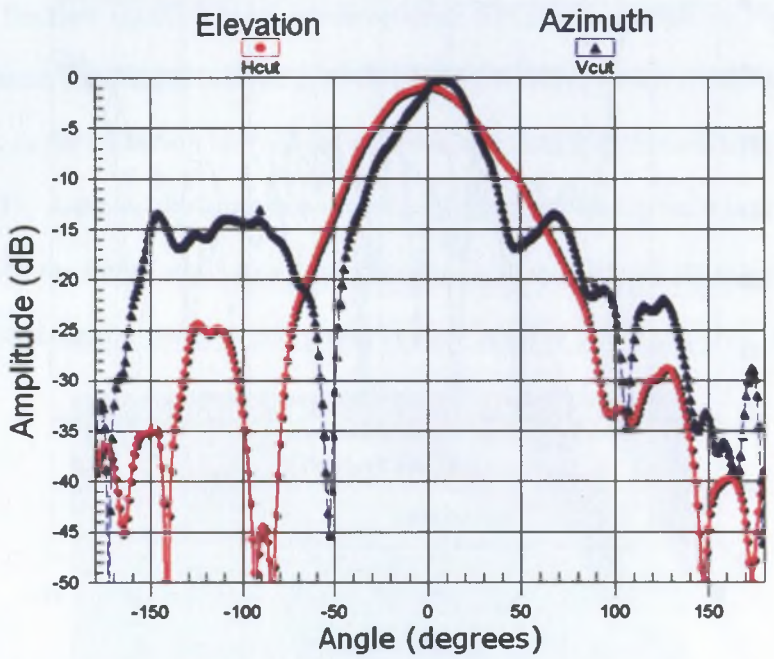


**Figure 6.36:** Measured elevation and azimuth radiation patterns at 6 GHz.

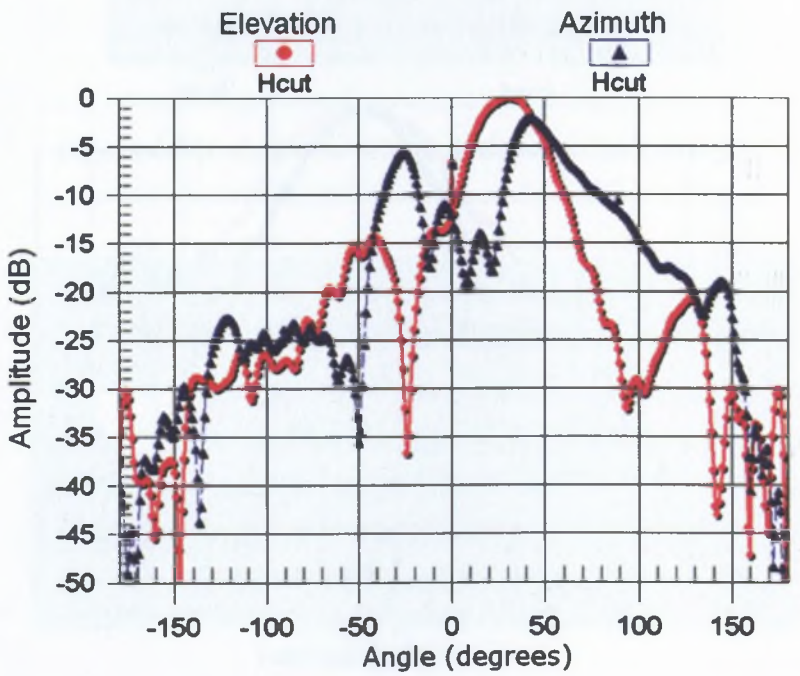


**Figure 6.37:** Measured elevation and azimuth radiation patterns at 8 GHz.

## 6.6 Summary/Conclusions

A CPW-fed printed semicircular slot antenna with a combined linear/stepped impedance transformer is presented. Broad beam coverage and a nearly flat experimental gain of 3.5 dBi $\pm$ 1 dB are achieved over the entire FCC UWB from 3.1 GHz to 10.6 GHz. It was shown that this PSSA design has a large measured impedance bandwidth of 126 % (3.1 GHz to 13.8 GHz) with minimal pulse dispersion. The results presented confirm the suitability of the antenna design for UWB systems. Details of the proposed antenna are described and both theoretical and experimental results are presented.

With the above mentioned semicircular slot antenna employed as UWB radiator, a short, two-plate horn is mounted on the surface to enhance the gain over the entire UWB bandwidth. Theoretical and experimental investigations have been conducted to verify the effectiveness of a two-plate short horn as a means for gain enhancement. Experimental results indicate a large impedance bandwidth from 2.86 GHz to 11.6 GHz and approximately 3 dB gain enhancement across the band. This design has a relatively high gain over the entire FCC UWB band and its gain variation over the band is still acceptable.

The gain enhancement of a slot antenna integrated with a surface-mounted short horn (SMSH) is investigated. Two different configurations of SMSH are presented. The first configuration gives bidirectional radiation patterns because the slot is mounted at the base of the short horn with no conductor backing. The peak gain of the design is 11 dBi and the gain improvement over the average gain of the corresponding bare slot radiator is up to 2.03 dB. The antenna has a 10 dB return loss bandwidth of 145%, 2.9 GHz to 18.38 GHz. Total height is only 35 mm or $0.35\lambda_0$ and $0.93\lambda_0$ at the lower band-edge frequency 3 GHz and at the centre frequency 8.0 GHz respectively. The second design is a unidirectional SMSH, which reduces the back lobe of the previous design by mounting the slot inside the horn. The slant angle of the horn forms a tapered backing cavity, which eliminates the back lobe. The unidirectional nature of the horn

increases the peak gain to 14.53 dBi while the measured bandwidth is maintained at 143%. Compared to the physical lengths of 148 mm and 119 mm for some typical commercial horns (*Model WBH2-18* and *Model WBH1-18S*) [70], the short unidirectional horn has an aperture dimension of 93 $\times$ 93 mm with a physical length of 35 mm. This is a significant reduction in physical length compared to the commercial designs. The peak gain of those commercial horns are in the range of 12 dBi to 14 dBi with impedance bandwidth from 1 GHz to 18 GHz for VSWR less than 2.5:1 and an approximate weight of around 0.8 kg. The proposed horn has a peak gain of 14.53 dBi with an impedance bandwidth of 2.8 GHz to 18 GHz for VSWR less than 2:1 and weighing roughly 0.1 kg. The power-handling capabilities of the proposed horn is less than for the commercial horn because of the microstrip nature of the feed. The radiation patterns of the commercial horns are better above 8 GHz, compared to the SMSH.

# Chapter 7

# Conclusions and Future Work

## 7.1 Conclusions

This thesis addresses the problem of variable gain in printed ultra-wideband antennas. The gain of a printed monopole antenna is low at lower frequencies of FCC UWB band and increases significantly with frequency. In this thesis several antennas with high and nearly constant gain have been presented. Some also have broad radiation patterns over the UWB band. The main challenges addressed in this thesis are:

- The radiation pattern varies with frequency and causes angular variation of peak gain;
- Look-angle dispersion and drop in the signal strength occurs in line-of-sight conditions because of a significant variation of the gain in the main beam direction;
- Losing close to half of the radiated power because of the bidirectional radiation of antennas, and the need of printed reflector to direct that in the main beam direction;
- Lack of ultra-wideband (110% bandwidth) reflectors with correct reflection phase;
- Effect due to near-field interactions and mounting of antennas close to metallic planes;

- The need for compact wideband high-gain antennas with low-profile and light weight for GPR applications.

The gain variations of printed monopole antennas were investigated first and situations were identified where the minimum variation in gain is desirable in UWB systems. A concept of proximity-coupled surface-wave gain enhancement was proposed for printed antennas. This concept enhanced the gain in the lower frequency region of the UWB band. The concept was tested with MS-fed and CPW-fed printed circular monopole antennas. The designed antenna had twin-slot radiators excited through proximity coupling. These slot radiators were mounted on the substrate with a printed monopole, which helped in enhancing the gain with minimum variation across the impedance bandwidth of more than 8.14 GHz (3.86 GHz to 12 GHz). An average gain of 5.5 dBi $\pm$ 1.5 dB was achieved for a MS-fed PCMA while a maximum gain enhancement of 2.5 dB was achieved around 7 GHz for a CPW-fed PCMA. The gain across the whole band is 6 dBi $\pm$ 2 dB. This is a significant enhancement compared to the conventional CPW-fed PCMA that has a gain of 4 dBi $\pm$ 2 dB. The proposed solution of proximity coupling was incorporated with an array of cavity slots excited with proximity coupling. These cavities help in enhancing the average gain, while the improvement in the higher UWB band is 2 dB compared to the twin-slot-excited MS-fed PCMA.

To enhance LOS UWB communication, a new class of short TEM horn antennas fed by printed monopoles was proposed. These designed antennas have ultra-wide bandwidth and nearly constant and high gain over the operating bandwidth. These antennas reduces the TEM length from $10\lambda$ to about $\lambda$ and in addition avoid the need of a UWB balun, which is usually required to feed a conventional balanced TEM horn from a coaxial cable. Three different configurations of short surface-mounted TEM horns were presented. A complete field analysis was presented to illustrate the TEM nature of the fields in the designed antennas. A prototype antenna designed to demonstrate this concept had measured gains in the range of 5.0 dBi $\pm$ 0.5 dB from 3 GHz to 12 GHz. This method can be applied to other types of printed monopole anten-

nas to further improve the performance of UWB antennas. In addition, a new surface-integrated short TEM horn, fabricated on the same substrate as a printed monopole, was presented. This horn is fed by a CPW transmission line and can be integrated directly to a printed-circuit board.

The above-mentioned antennas have semi-directional behaviour. A directional antenna can further enhance the performance of a UWB communication link. An appropriately designed UWB reflector was presented for this purpose. When used in conjunction with UWB printed antennas, it provides the advantage of directionality and shielding from nearby metallic objects that can reduce the antenna bandwidth. The concept of periodic structures and their application to achieve in-phase reflection characteristics was explained in detail. To prove the concept, the designs of two different reflectors (one with a dual layer and the other with four layers) were presented. These reflectors are based on FSS, which are preferred candidates for printed antennas as compared to the other periodic structure like EBGs discussed in the thesis. The performance of the designed reflector screens was first evaluated theoretically and then experimentally with a UWB slot antenna. An extensive parametric study was conducted. Normal and oblique incidence performance of the reflectors were analysed. When the low-profile dual-layer reflector is combined with a UWB slot antenna it achieves an impedance bandwidth of 122% and an average gain of around 8 dBi over the whole UWB frequency band. The other four-layer reflector has a very small effect on the impedance bandwidth of the slot configuration which is 145% (for return loss $< 8$ dB) and 120% (for return loss $< 10$ dB). A peak gain of around 9.3 dBi was achieved with the four-layer FSS. In addition to the gain enhancement, the other most significant achievement was the improvement of gain flatness across the impedance bandwidth. The predicted variation in the gain is only $\pm 0.5$ dB across this 145% bandwidth. This flatness was achieved by controlling the periodicity of the FSS layers.

In addition to the FCC-approved UWB systems, some other traditional systems (like GPR) were also considered in the thesis. The conventional slot and bow-tie antenna configurations presented in the literature were explored first and based on the the concept of bow-tie antenna

a compact CPW-fed printed semicircular slot antenna (PSSA) was introduced. Furthermore, a short two-plate horn was mounted on top of the PSSA for further enhancement of gain. In addition a compact four-plate short bidirectional and unidirectional compact horn were also presented. These horns are capable of producing the high gain with an impedance bandwidth of 145%. A peak gain of around 14.3 dBi with the unidirectional horn was achieved while the bidirectional short horn gives a peak gain of 10.8 dBi. The effectiveness of the design and the preliminary results of the short four-plate horn have shown their potential in UWB systems.

All the designed antennas were tested as standalone products and using a finite set of ground planes. The effect of external large ground planes provided by the chassis, laptop screens and other commercial products was beyond the scope of studies carried out in this research. Standard feed cables were used and the feeding arrangement was along the $\pm$ Z direction of the antenna. The radiation patterns of printed monopoles typically have a null in $\pm$ Z direction (if XY plane is the azimuthal plane), which reduces the effect of the cable.

A brief summary of the various antennas proposed in this thesis is given in Table 7.1. A PCMA is also listed in the table for reference purpose.

**Table 7.1:** Comparisons of various antennas proposed in this thesis

| No. | Type | $f_L$ GHz (10 dB RL) | $f_H$ GHz (10 dB RL) | BW ($f_H - f_L$) (10 dB RL) | Avg. Gain and Gain variation with impedance bandwidth | Size ($X \times Y \times Z$) (Z height of the antenna) (mm) |
|---|---|---|---|---|---|---|
| **1** | PCMA [4] | 2.76 | 9.78 | 7.02 | 3.5 ± 3 dB | 50 × 42 × 1.5 |
| **2** | SW-PC-PCMA [99] | 4.00 | 10.0 | 6.0 | 5.0 ± 1 dB | 50 × 42 × 6.2 |
| **3** | Array S-PCMA | 4.00 | 10.0 | 6.0 | 6.5 ± 0.8dB (flat gain) 7.5 ± 1.1 dB (high gain) | 50 × 174 × 6.2 |
| **4** | GE-LPA [138] | 3.15 | 15.0 | 11.85 | 5.0 ± 1 dB | 50 × 42 × 6.2 |
| **5** | TP-SMS Horn [139] | 2.75 | 10.14 | 7.39 | 5.0 ± 0.5 dB | 50 × 70 × 45 |
| **6** | SMS-TEM Horn | 2.6 | 12.36 | 9.76 | 5.5 ± 1.2 dB | 50 × 42 × 45 |
| **7** | SIS-TEM Horn [140] | 2.52 | 15 | 12.48 | 5.5 ± 1.1 dB | 40 × 40 × 45 |
| **8** | SIS-TEM Horn with reflec-tor [140] | 2.86 | 15 | 12.14 | 6.5 ± 1.1 dB | 40 × 40 × 70 |

| No. | Type | $f_L$ GHz (10 dB RL) | $f_H$ GHz (10 dB RL) | BW ($f_H - f_L$) (10 dB RL) | Avg. Gain and Gain variation with impedance bandwidth | Size ($X \times Y \times Z$) (Z height of the antenna) (mm) |
|---|---|---|---|---|---|---|
| **9** | Dual-layer FSS reflector with slot antenna [141] | 3.15 | 12.5 | 9.35 | $8.0 \pm 1.8$ dB | $110 \times 110 \times 10.3$ |
| **10** | Four-layer FSS Reflector with slot antenna [142] | 2.86 | 18.0 | 15.14 | $9.3 \pm 0.5$ dB | $110 \times 110 \times 18.5$ |
| **11** | SSA [143], [144] | 3.00 | 11.6 | 8.6 | $3.5 \pm 1$ dB | $30 \times 60 \times 1.6$ |
| **12** | SSA with TEM horn [145] | 2.99 | 11.6 | 8.61 | $6.0 \pm 1$ dB | $30 \times 60 \times 46.6$ |
| **13** | High Gain Unidirectional SMSH [146] | 2.86 | 18 | 15.14 | $11.62 \pm 1.1$ dB | $93 \times 93 \times 35$ |

## 7.2 Future Work

The results presented in this dissertation lead to many interesting open questions related to high-gain antenna design for UWB applications. Some directions for future research are as follows.

1. The concept of proximity coupling needs to be investigated more and can provide a useful control of gain over a desired band.

2. The short TEM horn can be integrated with a monopole antenna that has a stable radiation pattern to further enhance the radiation characteristics.

3. Controlling the phase centre of a short horn is another interesting task that needs attention in the future.

4. UWB FCC Compliance study of the short horn, which is presented in Chapter 6, is an option for future work.

5. FSS reflectors presented in Chapter 5 lead to several interesting antenna configurations, which are yet to be explored.

6. A single-layer FSS with a 110% bandwidth is not yet available. If it is possible, that would be a good alternative as a reflector design for printed UWB antennas.

7. FSSs may be used further to control the gain and bandwidth over a certain frequency band and possibly to filter WiFi and (WLAN) HIPERLAN signals.

8. One may attempt to use multi-mode or multi-layered horns to provide further enhancement in the gain.

# Appendix A

# Abbreviations

| | |
|---|---|
| UWB | Ultra Wideband |
| FCC | Federal Communication Commission |
| CEPT | Conference of Postal and Telecommunications |
| RF | Radio Frequency |
| AC | Alternating Current |
| DC | Direct Current |
| dB | Decibels |
| dBi | Decibels Isotropic |
| SNR | Signal to Noise Ratio |
| PSD | Power Spectral Density |
| EIRP | Effective Isotropic Radiated Power |
| DS-UWB | Direct Spread-spectrum UWB |
| MB-OFDM | Multiband Orthogonal Frequency Division Multiplex |
| LOS | Line of Sight |
| TEM | Transverse Electromagnetic |
| GPR | Ground Penetrating Radar |

| | |
|---|---|
| AMC | Artificial Magnetic Conductor |
| FSS | Frequency Selective Surface |
| FSS | Perfect Magnetic Conductor |
| PRS | Partial Reflecting Surfaces |
| TE | Transverse Electric |
| TM | Transverse Magnetic |
| RL | Returnloss |
| SSA | Semicircular Slot Antenna |
| BW | Bandwidth |
| DARPA | Defence Advance Research Project Agency |
| WBAN | Wireless Body Area Network |
| MS | Microstrip |
| CPW | Coplanar Waveguide |
| PCMA | Printed Circular Monopole Antenna |
| RCS | Radar Cross Section |
| QPSK | Quadrature Phase Shift Keying |
| DCM | Dual-carrier Modulation |
| SW-PC | Surface Wave and Proximity Coupled |
| GE-LPA | Gain Enhanced Low Profile Antenna |
| TP-SMS | Two-Plate Surface Mounted Short |
| SMS-TEM | Surface Mounted Short-TEM |
| SIS-TEM | Surface Integrated Short-TEM |
| HG-SMSH | High Gain Surface Mounted Short Horn |

# Bibliography


[1] [Online]. Available: (Comprehensive-UWB-product-testing-Part-2):http://www.eetimes.com/

[2] B. Allen, M. Dohler, E. E. Okon, W. Q. Malik, A. K. Brown, and D. J. Edwards, *Ultra-Wideband Antennas and Propagation for Communication, Radar and Imaging*. Weily Sons, 2007.

[3] C. Reig, E. Navarro, and V. Such, "Fdtd analysis of e-sectoral horn antennas for broadband applications," *Antennas and Propagation, IEEE Transactions on*, vol. 45, no. 10, pp. 1484 –1487, oct 1997.

[4] J. Liang, C. Chiau, X. Chen, and C. Parini, "Study of a printed circular disc monopole antenna for uwb systems," *Antennas and Propagation, IEEE Transactions on*, vol. 53, no. 11, pp. 3500 – 3504, nov. 2005.

[5] J. Liang, L. Guo, C. Chiau, and X. Chen, "Cpw-fed circular disc monopole antenna for uwb applications," in *Antenna Technology: Small Antennas and Novel Metamaterials, 2005. IWAT 2005. IEEE International Workshop on*, march 2005, pp. 505 – 508.

[6] F. Mlinarsky and J. Ziegler. (2007, December) Comprehensive uwb product testing: Part 2.

[7] (2010, April) Uwb: An old technology shakes up the world of wireless. [Online]. Available: http://web.mit.edu/deshpandecenter/downloads/documents/

[8] "Revision of part 15 of the commissions rules regarding ultra-wideband transmission systems," FCC, Washington, D.C. 20554, ET Docket 98-153 FCC 02-48, April April 2002.

[9] OFCOM, "Ultra wideband," Office of Communication, UK,, Tech. Rep., 2005 September.

[10] H. Schantz. Early radio: Narrow band in conception uwb in practice. [Online]. Available: http://www.aetherczar.com/

[11] [Online]. Available: http://www.ultrawidebandplanet.com/

[12] *Standard ECMA-368: High Rate Ultra Wideband PHY and MAC Standard*, Wi-Media, December 2008. [Online]. Available: http://www.wimedia.org/en/specs.asp?id=specs

[13] N. Agrawall, G. Kumar, and K. Ray, "Wide-band planar monopole antennas," *Antennas and Propagation, IEEE Transactions on*, vol. 46, no. 2, pp. 294 –295, feb 1998.

[14] M. Ammann, "Improved pattern stability for monopole antennas with ultrawideband impedance characteristics," in *Antennas and Propagation Society International Symposium, 2003. IEEE*, vol. 1, june 2003, pp. 818 – 821 vol.1.

[15] M. Ammann and Z. N. Chen, "A wide-band shorted planar monopole with bevel," *Antennas and Propagation, IEEE Transactions on*, vol. 51, no. 4, pp. 901 – 903, april 2003.

[16] K.-L. Wong, C.-H. Wu, and S.-W. Su, "Ultrawide-band square planar metal-plate monopole antenna with a trident-shaped feeding strip," *Antennas and Propagation, IEEE Transactions on*, vol. 53, no. 4, pp. 1262 – 1269, april 2005.

[17] S.-Y. Suh, W. Stutzman, and W. Davis, "A new ultrawideband printed monopole antenna: the planar inverted cone antenna (pica)," *Antennas and Propagation, IEEE Transactions on*, vol. 52, no. 5, pp. 1361 – 1364, may 2004.

[18] Z. Chen, M. Ammann, M. Chia, and T. See, "Annular planar monopole antennas," *Microwaves, Antennas and Propagation, IEE Proceedings* -, vol. 149, no. 4, pp. 200 – 203, aug 2002.

[19] ——, "Circular annular planar monopoles with em coupling," *Microwaves, Antennas and Propagation, IEE Proceedings* -, vol. 150, no. 4, pp. 269 – 273, aug. 2003.

[20] K.-L. Lau, P. Li, and K.-M. Luk, "A monopolar patch antenna with very wide impedance bandwidth," *Antennas and Propagation, IEEE Transactions on*, vol. 53, no. 3, pp. 1004 – 1010, march 2005.

[21] K.-H. Kim, J.-U. Kim, and S.-O. Park, "An ultrawide-band double discone antenna with the tapered cylindrical wires," *Antennas and Propagation, IEEE Transactions on*, vol. 53, no. 10, pp. 3403 – 3406, oct. 2005.

[22] S. Palud, F. Colombel, M. Himdi, and C. Le Meins, "A novel broadband eighth-wave conical antenna," *Antennas and Propagation, IEEE Transactions on*, vol. 56, no. 7, pp. 2112 –2116, july 2008.

[23] J. Evans and M. Amunann, "Planar trapezoidal and pentagonal monopoles with impedance bandwidths in excess of 10:1," in *Antennas and Propagation Society International Symposium, 1999. IEEE*, vol. 3, aug 1999, pp. 1558 –1561 vol.3.

[24] Z. N. Chen, "Broadband roll monopole," *Antennas and Propagation, IEEE Transactions on*, vol. 51, no. 11, pp. 3175 – 3177, nov. 2003.

[25] ——, "Novel bi-arm rolled monopole for uwb applications," *Antennas and Propagation, IEEE Transactions on*, vol. 53, no. 2, pp. 672 – 677, feb. 2005.

[26] C.-J. Lee, C. Caloz, K. Leong, S.-M. Han, and T. Itoh, "A planar broadband antenna for uwb pulse transmission," in *Microwave Conference, 2004. 34th European*, vol. 3, oct. 2004, pp. 1329 –1331.

[27] K.-L. Wong, T.-C. Tseng, and P. L. Teng, "Low-profile ultrawideband antenna for mobile phone applications," *Microwave and Optical Technology Letters*, vol. 43, 2004.

[28] J. Liang, L. Guo, C. Chiau, X. Chen, and C. Parini, "Study of cpw-fed circular disc monopole antenna for ultra wideband applications," *Microwaves, Antennas and Propagation, IEE Proceedings* -, pp. 520 – 526, dec. 2005.

[29] Q. Wu, R. Jin, J. Geng, and M. Ding, "Printed omni-directional uwb monopole antenna with very compact size," *IEEE Trans. on Antennas and Propag.*, vol. 56, pp. 896 – 899, 2008.

[30] J. Jung, W. Choi, and J. Choi, "A small wideband microstrip-fed monopole antenna," *IEEE Microwave and Wireless Component Letters*, vol. 15, pp. 703 – 705, 2005.

[31] C. Y. Hong, C. W. Ling, I. Y. Tarn, and S. J. Chung, "Design of a planar ultrawideband antenna with a new band-notch structure," *IEEE Transactions on Antennas and Propag.,*, vol. 55, pp. 3391 – 3396, 2007.

[32] Y. J. Cho, K. H. Kim, D. H. Choi, S. S. Lee, and S. O. Park, "A miniature uwb planar monopole antenna with 5-ghz band-rejection filter and the time-domain characteristics," *IEEE Transactions on Antennas and Propag*, vol. 54, pp. 1453 – 1460, 2006.

[33] K. Ray and Y. Ranga, "Ultrawideband printed elliptical monopole antennas," *Antennas and Propagation, IEEE Transactions on*, vol. 55, no. 4, pp. 1189 –1192, april 2007.

[34] Z. Shunshi, L. Jian-jun, D. Cheng-zhu, and X. Ling-long, "Swb planar antenna technology," in *Microwave Conference, 2008 China-Japan Joint*, sept. 2008, pp. 139 –143.

[35] L. N. Brillouin, "Broadband band antenna," US Patent 2,454,766, November, 1948.

[36] H. Schantz, *The Art and Science of Ultrawideband Antennas*. ARTECH HOUSE, 2005.

[37] W.-L. Chen, G.-M. Wang, and C.-X. Zhang, "Bandwidth enhancement of a microstripline-fed printed wide-slot antenna with a fractal-shaped slot," *Antennas and Propagation, IEEE Transactions on*, vol. 57, no. 7, pp. 2176 –2179, july 2009.

[38] J.-Y. Jan and J.-W. Su, "Bandwidth enhancement of a printed wide-slot antenna with a rotated slot," *Antennas and Propagation, IEEE Transactions on*, vol. 53, no. 6, pp. 2111 – 2114, june 2005.

[39] W. Tam, "Microstripline-fed cylindrical slot antennas," *Antennas and Propagation, IEEE Transactions on*, vol. 46, no. 10, pp. 1587 –1589, oct 1998.

[40] S.-W. Qu, C. Ruan, and B.-Z. Wang, "Bandwidth enhancement of wide-slot antenna fed by cpw and microstrip line," *Antennas and Wireless Propagation Letters, IEEE*, vol. 5, no. 1, pp. 15 –17, dec. 2006.

[41] E. Soliman, S. Brebels, P. Delmotte, G. Vandenbosch, and E. Beyne, "Bow-tie slot antenna fed by cpw," *Electronics Letters*, vol. 35, no. 7, pp. 514 –515, apr 1999.

[42] C.-H. Lee, S.-Y. Chen, and P. Hsu, "Compact modified bow-tie slot antenna fed by cpw for ultra-wideband applications," in *Antennas and Propagation Society International Symposium, 2009. APSURSI '09. IEEE*, june 2009, pp. 1 –4.

[43] J. Yeo, Y. Lee, and R. Mittra, "Wideband slot antennas for wireless communications," *Microwaves, Antennas and Propagation, IEE Proceedings* -, vol. 151, no. 4, pp. 351 – 355, aug. 2004.

[44] C.-Y. Huang and D.-Y. Lin, "Cpw-fed bow-tie slot antenna for ultra-wideband communications," *Electronics Letters*, vol. 42, no. 19, pp. 1073 – 1074, sept. 2006.

[45] A. Eldek, A. Elsherbeni, and C. Smith, "Wideband bow-tie slot antenna with tuning stubs," in *Radar Conference, 2004. Proceedings of the IEEE*, april 2004, pp. 583 – 588.

[46] E. Angelopoulos, A. Anastopoulos, C. Githonas, and D. Kaklamani, "A modified bow-tie slot antenna fed by a cpw-to-cpw transition loaded with inductively coupled slots for ultra wide-band applications," in *Antenna Technology: Small Antennas and Novel Metamaterials, 2005. IWAT 2005. IEEE International Workshop on*, march 2005, pp. 513 – 516.

[47] E. Altshuler, "The traveling-wave linear antenna," *Antennas and Propagation, IRE Transactions on*, vol. 9, no. 4, pp. 324 –329, july 1961.

[48] T. Wu and R. W. P. King, "The cylindrical antenna with nonreflecting resistive loading," *Antennas and Propagation, IEEE Transactions on*, vol. 13, no. 3, pp. 369 – 373, may 1965.

[49] T. Montoya and G. Smith, "Resistively-loaded vee antennas for short-pulse ground penetrating radar," in *Antennas and Propagation Society International Symposium, 1996. AP-S. Digest*, vol. 3, jul 1996, pp. 2068 –2071 vol.3.

[50] K. Kim and J. Scott, W.R., "Improved resistively-loaded vee dipole for ground-penetrating radar applications," in *Antennas and Propagation Society International Symposium, 2004. IEEE*, vol. 3, june 2004, pp. 2548 – 2551 Vol.3.

[51] R. Nilavalan, G. Hilton, and R. Benjamin, "Wideband printed bowtie antenna element development for post reception synthetic focusing surface penetrating radar," *Electronics Letters*, vol. 35, no. 20, pp. 1771 –1772, sep 1999.

[52] K. Shlager, G. Smith, and J. Maloney, "Optimization of bow-tie antennas for pulse radiation," *Antennas and Propagation, IEEE Transactions on*, vol. 42, no. 7, pp. 975 –982, jul 1994.

[53] A. Lestari, A. Yarovoy, and L. Ligthart, "Rc-loaded bow-tie antenna for improved pulse radiation," *Antennas and Propagation, IEEE Transactions on*, vol. 52, no. 10, pp. 2555 – 2563, oct. 2004.

[54] K. Schlager, G. Smith, and J. Maloney, "Tem horn antenna for pulse radiation: an improved design," *Microwave and Optical Technology Letters*, vol. 12, pp. 86 – 90, 1996.

[55] K. Chung, S. Pyun, and J. Choi, "Design of an ultrawide-band tem horn antenna with a microstrip-type balun," *Antennas and Propagation, IEEE Transactions on*, vol. 53, no. 10, pp. 3410 – 3413, oct. 2005.

[56] Y. Xia and Z. Duan, "Compact cpw-fed dual ellipses antenna for ultra-wideband system," *Electronics Letters*, vol. 44, no. 9, p. 567, 24 2008.

[57] H. Schantz, "Introduction to ultra-wideband antennas," in *Ultra Wideband Systems and Technologies, 2003 IEEE Conference on*, nov. 2003, pp. 1 – 9.

[58] H. Friis, "A note on a simple transmission formula," *Proceedings of the IRE*, vol. 34, pp. 254 – 256, 1946.

[59] R. Rojas and K. Lee, "Control of surface waves in planar printed antennas," in *Antennas and Propagation Society International Symposium, 1998. IEEE*, vol. 3, jun 1998, pp. 1566 –1569 vol.3.

[60] ——, "Surface wave control using nonperiodic parasitic strips in printed antennas," *Microwaves, Antennas and Propagation, IEE Proceedings* -, vol. 148, no. 1, pp. 25 –28, 2001.

[61] H. Hertz, *The Forces of Electrical Oscillations Treated According to Maxwells Theory, Weidemanns Ann. 36, 1 (1889); reprinted in chap. 9 of H. Hertz, Electric Waves (Dover, New York, 1962). A translation by O. Lodge appeared in Nature 39, 402 (1889),*, 1889.

[62] C. A. Balanis, *Antenna Theory Analysis and Design.* Harper and Row, 1982.

[63] W. Malik, D. Edwards, and C. Stevens, "Angular-spectral antenna effects in ultra-wideband communications links," *Communications, IEE Proceedings-*, vol. 153, no. 1, pp. 99 – 106, feb. 2006.

[64] D.-H. Kwon, "Effect of antenna gain and group delay variations on pulse-preserving capabilities of ultrawideband antennas," *Antennas and Propagation, IEEE Transactions on*, vol. 54, no. 8, pp. 2208 –2215, aug. 2006.

[65] S. Cohn, "Properties of ridge wave guide," *Proceedings of the IRE*, vol. 35, no. 8, pp. 783 – 788, aug. 1947.

[66] J. Kerr, "Short axial length broad-band horns," *Antennas and Propagation, IEEE Transactions on*, vol. 21, no. 5, pp. 710 – 714, sep 1973.

[67] K. L. Walton and V. C. Sundberg, "Broadband ridged horn design," *Microwave Journal*, pp. 96–101, 1964.

[68] C. Bruns, P. Leuchtmann, and R. Vahldieck, "Analysis and simulation of a 1-18-ghz broadband double-ridged horn antenna," *Electromagnetic Compatibility, IEEE Transactions on*, vol. 45, no. 1, pp. 55 – 60, feb 2003.

[69] V. Rodriguez, "Newbroadband emc double-ridged guide horn antenna," *R.F. Design*, p. 4447, May 2004.

[70] [Online]. Available: www.q-par.com/products/horn-antennas

[71] A. Rahman, A. Verma, and A. Omar, "High gain wideband compact microstrip antenna with quasi-planar surface mount horn," in *Microwave Symposium Digest, 2003 IEEE MTT-S International*, vol. 1, june 2003, pp. 571 – 574 vol.1.

[72] ——, "High gain microstrip antenna element and array low and high permittivity substrate," in *Wireless Technology, 2005. The European Conference on*, oct. 2005, pp. 487 –489.

[73] Nasimuddin and K. Esselle, "Antennas with dielectric resonators and surface mounted short horns for high gain and large bandwidth," *Microwaves, Antennas Propagation, IET*, vol. 1, no. 3, pp. 723 –728, june 2007.

[74] ——, "A low-profile compact microwave antenna with high gain and wide bandwidth," *Antennas and Propagation, IEEE Transactions on*, vol. 55, no. 6, pp. 1880 –1883, june 2007.

[75] ——, "High-gain wideband circularly polarized stacked microstrip antennas with single microstrip feeds and short horns," in *Antennas and Propagation Society International Symposium, 2007 IEEE*, june 2007, pp. 737 –740.

[76] Nasimuddin, K. Esselle, and A. Verma, "Wideband high-gain circularly polarized stacked microstrip antennas with an optimized c-type feed and a short horn," *Antennas and Propagation, IEEE Transactions on*, vol. 56, no. 2, pp. 578 –581, feb. 2008.

[77] D. Manteuffel, T.-A. Ould-Mohamed, and J. Romme, "Impact of integration in consumer electronics on the performance of mb-ofdm uwb," in *Electromagnetics in Advanced Applications, 2007. ICEAA 2007. International Conference on*, sept. 2007, pp. 911 –914.

[78] D. Sievenpiper, "High-impedance electromagnetic surfaces," Ph.D. dissertation, UCLA, 1999.

[79] N. Engheta and R. W. Ziolkowski, *Electromagnetic Metamaterials: Physics and Engineering Explorations*. Wiley-IEEE Press, July 2006.

[80] B. A. Munk, *Frequency Selective Surfaces: Theory and Design*. Wiley-Interscience, 1 edition (April 2000).

[81] Y. Erdemli, K. Sertel, R. Gilbert, D. Wright, and J. Volakis, "Frequency-selective surfaces to enhance performance of broad-band reconfigurable arrays," *Antennas and Propagation, IEEE Transactions on*, vol. 50, no. 12, pp. 1716 – 1724, dec 2002.

[82] M. Pasian, S. Monni, A. Neto, M. Ettorre, and G. Gerini, "Frequency selective surfaces for extended bandwidth backing reflector functions," *Antennas and Propagation, IEEE Transactions on*, vol. 58, no. 1, pp. 43 –50, jan. 2010.

[83] R. Cruz, A. D'Assunao, and P. da F Silva, "A new fss design proposal for uwb applications," in *Antenna Technology (iWAT), 2010 International Workshop on*, march 2010, pp. 1 –4.

[84] H. Schantz, "A brief history of uwb antennas," in *Ultra Wideband Systems and Technologies, 2003 IEEE Conference on*, nov. 2003, pp. 209 – 213.

[85] W. Malik, C. Stevens, and D. Edwards, "Synthetic aperture analysis of multipath propagation in the ultra-wideband communications channel," in *Signal Processing Advances in Wireless Communications, 2005 IEEE 6th Workshop on*, june 2005, pp. 375 – 379.

[86] Q. Spencer, B. Jeffs, M. Jensen, and A. Swindlehurst, "Modeling the statistical time and angle of arrival characteristics of an indoor multipath channel," *Selected Areas in Communications, IEEE Journal on*, vol. 18, no. 3, pp. 347 –360, mar 2000.

[87] C.-C. Chong, C.-M. Tan, D. Laurenson, S. McLaughlin, M. Beach, and A. Nix, "A new statistical wideband spatio-temporal channel model for 5-ghz band wlan systems," *Se-*

*lected Areas in Communications, IEEE Journal on*, vol. 21, no. 2, pp. 139 – 150, feb 2003.

[88] *MB-OFDM Physical Layer Proposal for IEEE 802.15Task Group 3a*, Mar. 2004, IEEE P802.15 Std. P802.15-03/268r3.

[89] R. Fisher, R. Kohno, M. McLaughlin, and M. Welbourn, "Ds-uwb physical layer submission to ieee 802.15 task group 3a," IEEE P802.15, Tech. Rep., Jan. 2005,.

[90] K. Ray, Y. Ranga, and P. Gabhale, "Printed square monopole antenna with semicircular base for ultra-wide bandwidth," *Electronics Letters*, vol. 43, no. 5, pp. 13 –14, 1 2007.

[91] K. Ray and Y. Ranga, "Ultra-wideband printed modified triangular monopole antenna," *Electronics Letters*, vol. 42, no. 19, pp. 1081 – 1082, sept. 2006.

[92] X. N. Low, Z. N. Chen, and T. See, "A uwb dipole antenna with enhanced impedance and gain performance," *Antennas and Propagation, IEEE Transactions on*, vol. 57, no. 10, pp. 2959 –2966, oct. 2009.

[93] A. Alipour and H. Hassani, "A novel omni-directional uwb monopole antenna," *Antennas and Propagation, IEEE Transactions on*, vol. 56, no. 12, pp. 3854 –3857, dec. 2008.

[94] M. Klemm, I. Kovacs, G. Pedersen, and G. Troster, "Comparison of directlional and omnl-directlonal uwb antennas for wireless body area network applications," in *Applied Electromagnetics and Communications, 2005. ICECom 2005. 18th International Conference on*, oct. 2005, pp. 1 –4.

[95] J. Ge and W. Yanagisawa, "A novel compact ultrawideband antenna," *Antennas and Propagation, IEEE Transactions on*, vol. 57, no. 2, pp. 318 –323, feb. 2009.

[96] Z.-A. Zheng and Q.-X. Chu, "Cpw-fed ultra-wideband antenna with compact size," *Electronics Letters*, vol. 45, no. 12, pp. 593 –594, 4 2009.

[97] *CST Microwave Studio, www.cst.com.*

[98] Z. N. Chen, X. H. Wu, H. F. Li, N. Yang, and M. Chia, "Considerations for source pulses and antennas in uwb radio systems," *Antennas and Propagation, IEEE Transactions on*, vol. 52, no. 7, pp. 1739 – 1748, july 2004.

[99] Y. Ranga, K. P. Esselle, A. R. Weily, and A. K. Verma, "A printed antenna with constant gain over a wide bandwidth for ultra-wideband applications," *Microwave and Optical Technology Letters*, vol. 54, p. 1261 1264, 2010.

[100] G. Stickley, I. Longstaff, and M. Radcliffe, "Synthetic aperture radar for the detection of shallow buried objects," in *The Detection of Abandoned Land Mines: A Humanitarian Imperative Seeking a Technical Solution, EUREL International Conference on (Conf. Publ. No. 431)*, oct 1996, pp. 160 –163.

[101] S. Vitebskiy, L. Carin, M. Ressler, and F. Le, "Ultra-wideband, short-pulse ground-penetrating radar: simulation and measurement," *Geoscience and Remote Sensing, IEEE Transactions on*, vol. 35, no. 3, pp. 762 –772, may 1997.

[102] E. Zaikov, J. Sachs, M. Aftanas, and J. Rovnakova, "Detection of trapped people by uwb radar," *Microwave Conference (GeMIC), 2008 German*, pp. 1 –4, march 2008.

[103] Micropower impulse radar. [Online]. Available: https://www.llnl.gov/str/pdfs/01_96.2.pdf

[104] S. Hantscher, A. Reisenzahn, and C. Diskus, "An uwb wall scanner based on a shape estimating sar algorithm," in *Microwave Symposium, 2007. IEEE/MTT-S International*, june 2007, pp. 1463 –1466.

[105] J. Huettner, R. Gierlich, A. Ziroff, and R. Weigel, "A low cost ultra-wide-band pulse radar in a guided wave gauging application," in *Radar Conference, 2009. EuRAD 2009. European*, 30 2009-oct. 2 2009, pp. 101 –104.

[106] G. Bosch GmbH, Gerlingen. (2009) Wall scanner. http://www.wallscanner.com.

[107] X. Li, E. Bond, B. Van Veen, and S. Hagness, "An overview of ultra-wideband microwave imaging via space-time beamforming for early-stage breast-cancer detection," *Antennas and Propagation Magazine, IEEE*, vol. 47, no. 1, pp. 19 – 34, feb 2005.

[108] M. Klemm, I. Craddock, J. Leendertz, A. Preece, and R. Benjamin, "Radar-based breast cancer detection using a hemispherical antenna array," *Antennas and Propagation, IEEE Transactions on*, vol. 57, no. 6, pp. 1692 –1704, june 2009.

[109] E. Staderini, "Uwb radars in medicine," *Aerospace and Electronic Systems Magazine, IEEE*, vol. 17, no. 1, pp. 13 –18, jan 2002.

[110] M. Leib, W. Menzel, B. Schleicher, and H. Schumacher, "Vital signs monitoring with a uwb radar based on a correlation receiver," in *Antennas and Propagation (EuCAP), 2010 Proceedings of the Fourth European Conference on*, april 2010, pp. 1 –5.

[111] F. Thiel, M. Hein, U. Schwarz, J. Sachs, and F. Seifert, "Fusion of magnetic resonance imaging and ultra-wideband-radar for biomedical applications," in *Ultra-Wideband, 2008. ICUWB 2008. IEEE International Conference on*, vol. 1, sept. 2008, pp. 97 –100.

[112] M. Win and R. Scholtz, "On the robustness of ultra-wide bandwidth signals in dense multipath environments," *Communications Letters, IEEE*, vol. 2, no. 2, pp. 51 –53, feb 1998.

[113] R.-M. Cramer, R. Scholtz, and M. Win, "Evaluation of an ultra-wide-band propagation channel," *Antennas and Propagation, IEEE Transactions on*, vol. 50, no. 5, pp. 561 –570, may 2002.

[114] M. Win, R. Scholtz, and M. Barnes, "Ultra-wide bandwidth signal propagation for indoor wireless communications," in *Communications, 1997. ICC 97 Montreal, 'Towards the Knowledge Millennium'. 1997 IEEE International Conference on*, vol. 1, jun 1997, pp. 56 –60 vol.1.

[115] R. Martens, E. Safin, and D. Manteuffel, "On the relation between the element correlation of antennas on small terminals and the characteristic modes of the chassis," in *Antennas and Propagation Conference (LAPC), 2010 Loughborough*, nov. 2010, pp. 457 –460.

[116] I. Makris, D. Manteuffel, R. Seager, and J. Vardaxoglou, "Modified designs for uwb planar monopole antennas," in *Antennas and Propagation Conference, 2007. LAPC 2007. Loughborough*, april 2007, pp. 249 –252.

[117] I. Makris, D. Manteuffel, and R. Seager, "Miniaturized reconfigurable uwb antennas for the integration into consumer electronic products," in *Antennas and Propagation, 2007. EuCAP 2007. The Second European Conference on*, nov. 2007, pp. 1 –6.

[118] Li-Chung, T. Chang, and W. Burnside, "An ultrawide-bandwidth tapered resistive tem horn antenna," *Antennas and Propagation, IEEE Transactions on*, vol. 48, no. 12, pp. 1848 –1857, dec 2000.

[119] A. Ameri, G. Kompa, and A. Bangert, "Study about tem horn size reduction for ultra-wideband radar application," in *Microwave Conference (GeMIC), 2011 German*, march 2011, pp. 1 –4.

[120] R. Lee and G. Smith, "A design study for the basic tem horn antenna," *Antennas and Propagation Magazine, IEEE*, vol. 46, no. 1, pp. 86 – 92, feb 2004.

[121] A. Lai, A. Sinopoli, and W. Burnside, "A novel antenna for ultra-wide-band applications," *Antennas and Propagation, IEEE Transactions on*, vol. 40, no. 7, pp. 755 –760, jul 1992.

[122] M. Sironen, Y. Qian, and T. Itoh, "A 60 ghz conical horn antenna excited with quasi-yagi antenna," in *Microwave Symposium Digest, 2001 IEEE MTT-S International*, vol. 1, 2001, pp. 547 –550 vol.1.

[123] X. Li, S. Davis, S. Hagness, D. van der Weide, and B. Van Veen, "Microwave imaging via space-time beamforming: experimental investigation of tumor detection in multilayer breast phantoms," *Microwave Theory and Techniques, IEEE Transactions on*, vol. 52, no. 8, pp. 1856 – 1865, aug. 2004.

[124] A. Sibille, S. Bories, R. D'Errico, and C. Roblin, "Uwb antenna performance evaluation from the communication system point of view," in *Wireless Communication Systems, 2006. ISWCS '06. 3rd International Symposium on*, sept. 2006, pp. 417 –422.

[125] R. D'Errico, H. Ghannoum, C. Roblin, and A. Sibille, "Small semi directional antenna for uwb terminal applications," in *Antennas and Propagation, 2006. EuCAP 2006. First European Conference on*, nov. 2006, pp. 1 –6.

[126] H. Ghannoum, S. Bories, and R. D'Errico, "Small-size uwb planar antenna and its behaviour in wban/wpan applications," in *Ultra Wideband Systems, Technologies and Applications, 2006. The Institution of Engineering and Technology Seminar on*, april 2006, pp. 221 –225.

[127] C. Roblin and M. A. Yousuf, "Statistical models of wideband and uwb omni-directional antennas based on a parametric modelling," in *Antennas and Propagation (EuCAP), 2010 Proceedings of the Fourth European Conference on*, april 2010, pp. 1 –5.

[128] X. Qing, Z. N. Chen, and M. Yan Wah Chia, "Network approach to uwb antenna transfer functions characterization," in *Microwave Conference, 2005 European*, vol. 3, oct. 2005, p. 4 pp.

[129] W. Dullaert, G. Adamiuk, and H. Rogier, "Compression of measured 2d uwb antenna transfer functions," *Electronics Letters*, vol. 46, no. 8, pp. 552 –553, 15 2010.

[130] S.-S. Zhong, X.-L. Liang, and W. Wang, "Compact elliptical monopole antenna with impedance bandwidth in excess of 21:1," *Antennas and Propagation, IEEE Transactions on*, vol. 55, no. 11, pp. 3082 –3085, nov. 2007.

[131] L. Moustafa and . p. . d. Bernard Jecko vol. 2010, Article ID 139069, "Design and realization of a wide-band ebg antenna based on fss and operating in the ku-band," *International Journal of Antennas and Propagation*, p. 8 pages, 2010.

[132] L. Moustafa, B. Jecko, M. Thevenot, T. Monediere, and R. Gonzalo, "Ebg antenna performance enhancement using conducting element fss," in *Antennas and Propagation, 2007. EuCAP 2007. The Second European Conference on*, nov. 2007, pp. 1 –4.

[133] J. Romeu and Y. Rahmat-Samii, "Fractal fss: a novel dual-band frequency selective surface," *Antennas and Propagation, IEEE Transactions on*, vol. 48, no. 7, pp. 1097 –1105, jul 2000.

[134] A. Chuprin, E. Parker, and J. Batchelor, "Resonant frequencies of open and closed loop frequency selective surface arrays," *Electronics Letters*, vol. 36, no. 19, pp. 1601 –1603, sep 2000.

[135] H.-D. Chen, J.-S. Chen, and J.-N. Li, "Ultra-wideband square-slot antenna," *Microwave and Optical Technology Letters*, vol. 48, no. 3, pp. 500–502, 2006. [Online]. Available: http://dx.doi.org/10.1002/mop.21391

[136] W. Sun and C. Balanis, "Analysis and design of quadruple-ridged waveguides," *Microwave Theory and Techniques, IEEE Transactions on*, vol. 42, no. 12, pp. 2201 –2207, dec 1994.

[137] R. Dehdasht-Heydari, H. R. Hassani, and A. R. Mallahzadeh, "Quad-ridged horn antenna for uwb applications," *Progress In Electromagnetics Research, PIER*, vol. 79, pp. 23 – 38, 2008.

[138] Y. Ranga, K. Esselle, and A. Weily, "A simple thin antenna with an enhanced gain for mb-ofdm uwb systems," in *Signal Processing and Communication Systems (ICSPCS), 2010 4th International Conference on*, dec. 2010, pp. 1 –4.

[139] Y. Ranga, A. Verma, and K. Esselle, "Planar-monopole-fed, surface-mounted quasi-tem horn antenna for uwb systems," *Antennas and Propagation, IEEE Transactions on*, vol. 58, no. 7, pp. 2436 –2439, july 2010.

[140] Y. Ranga, A. Verma, K. Esselle, and A. Weily, "A gain-enhanced semicircular disc antenna with a quasi-planar surface-mounted short tem horn," in *Wireless Technology Conference (EuWIT), 2010 European*, sept. 2010, pp. 177 –180.

[141] Y. Ranga, L. Matekovits, K. Esselle, and A. Weily, "Multioctave frequency selective surface reflector for ultrawideband antennas," *Antennas and Wireless Propagation Letters, IEEE*, vol. 10, pp. 219 –222, 2011.

[142] ——, "Multilayer frequency-selective-surface reflector for constant gain over ultra wideband," in *Antennas and Propagation (EUCAP), Proceedings of the 5th European Conference on*, april 2011, pp. 332 –334.

[143] Y. Ranga and K. Esselle, "Cpw-fed semicircular slot antenna for uwb pcb applications," in *Antennas and Propagation Society International Symposium, 2009. APSURSI '09. IEEE*, june 2009, pp. 1 –4.

[144] Y. Ranga, K. P. Esselle, and A. R. Weily, "Compact ultra-wideband cpw-fed printed semicircular slot antenna," *Microwave and Optical Technology Letters*, vol. 52, p. 2367 2372, 2010.

[145] Y. Ranga, K. Esselle, A. Weily, and A. Verma, "A compact antenna with high gain for ultra wide band systems," in *Microwave Conference, 2009. EuMC 2009. European*, 29 2009-oct. 1 2009, pp. 85 –88.

[146] ——, "Compact high-gain short-horn antenna for uwb applications," in *Antennas and Propagation (EUCAP), Proceedings of the 5th European Conference on*, april 2011, pp. 1511 –1513.

[147] M. J. Ammann, "Square planar monopole antenna," in *In Proc. Inst. Elect.Eng. Nat. Conf. Antennas Propag*, 1999, p. 3740.

[148] J. M. Bell, M. F. Iskander, and J. J. Lee, "Ultrawideband hybrid ebg/ferrite ground plane for low-profile array antennas," *Antennas and Propagation, IEEE Transactions on*, vol. 55, no. 1, pp. 4 –12, jan. 2007.

[149] Z. Chen, M. Chia, and M. Ammann, "Optimization and comparison of broadband monopoles," *Microwaves, Antennas and Propagation, IEE Proceedings* -, vol. 150, no. 6, pp. 429 – 435, dec 2003.

[150] Z. N. Chen, "Uwb antennas: Design and application," in *Information, Communications Signal Processing, 2007 6th International Conference on*, dec. 2007, pp. 1 –5.

[151] J. Foerster and Q. Li, "Channel modeling sub-committee report draft," IEEE P802.15 Working Group for Wireless Personal Area Networks (WPANs), Tech. Rep., 4 September, 2002.

[152] R. Fontana, E. Richley, A. Marzullo, L. Beard, R. Mulloy, and E. Knight, "An ultra wideband radar for micro air vehicle applications," in *Ultra Wideband Systems and Technologies, 2002. Digest of Papers. 2002 IEEE Conference on*, 2002, pp. 187 – 191.

[153] S. Honda, M. Ito, H. Seki, , and Y. Jinbo, "A disk monopole antenna with 1:8 impedance bandwdith and omnidirectional radiation pattern," in *Proceeding of ISAP, Sapporo, Japan*, 1992.

[154] I. Immoreev, "Practical applications of uwb technology," *Aerospace and Electronic Systems Magazine, IEEE*, vol. 25, no. 2, pp. 36 –42, feb. 2010.

[155] J. Lee, S. Livingston, R. Koenig, D. Nagata, and L. Lai, "Compact light weight uhf arrays using long slot apertures," *Antennas and Propagation, IEEE Transactions on*, vol. 54, no. 7, pp. 2009 – 2015, july 2006.

[156] Z. Li and Y. Rahmat-Samii, "Pbg, pmc and pec ground planes: a case study of dipole antennas," in *Antennas and Propagation Society International Symposium, 2000. IEEE*, vol. 2, 2000, pp. 674 –677 vol.2.

[157] T. Liu, W. Zhang, M. Zhang, and K. Tsang, "Low profile spiral antenna with pbg substrate," *Electronics Letters*, vol. 36, no. 9, pp. 779 –780, apr 2000.

[158] J. McLean, R. Sutton, A. Medina, H. Foltz, and J. Li, "The experimental characterization of uwb antennas via frequency-domain measurements," *Antennas and Propagation Magazine, IEEE*, vol. 49, no. 6, pp. 192 –202, dec. 2007.

[159] T. Montoya and G. Smith, "A study of pulse radiation from several broad-band loaded monopoles," *Antennas and Propagation, IEEE Transactions on*, vol. 44, no. 8, pp. 1172 –1182, aug 1996.

[160] J. Park, C.-C. Chang, Y. Qian, and T. Itoh, "An improved low-profile cavity-backed slot antenna loaded with 2d uc-pbg reflector," in *Antennas and Propagation Society International Symposium, 2001. IEEE*, vol. 4, 2001, pp. 194 –197 vol.4.

[161] Y. Ranga, A. Verma, K. Esselle, and A. Weily, "Gain enhancement of uwb slot with the use of surface mounted short horn," in *Antennas and Propagation Society International Symposium (APSURSI), 2010 IEEE*, july 2010, pp. 1 –4.

[162] K. Ray, "Design aspects of printed monopole antennas for ultra-wide band applications," *International Journal of Antennas and Propagation*, pp. Article ID 713 858, 8 pages, 2008.

[163] K. Ray and Y. Ranga, "Printed rectangular monopole antennas," in *Antennas and Propagation Society International Symposium 2006, IEEE*, july 2006, pp. 1693 –1696.

[164] K. Ray and S. Tiwari, "Ultra wideband printed hexagonal monopole antennas," *Microwaves, Antennas Propagation, IET*, vol. 4, no. 4, pp. 437 –445, april 2010.

[165] J. H. Reed, *An Introduction to Ultra Wideband Communication Systems*. Prentice Hall, April 15, 2005.

[166] H. Schantz, "Dispersion and uwb antennas," in *Ultra Wideband Systems, 2004. Joint with Conference on Ultrawideband Systems and Technologies. Joint UWBST IWUWBS. 2004 International Workshop on*, may 2004, pp. 161 – 165.

[167] ——, "Uwb magnetic antennas," in *Antennas and Propagation Society International Symposium, 2003. IEEE*, vol. 3, june 2003, pp. 604 – 607 vol.3.

[168] ——, "A brief history of uwb antennas," in *Ultra Wideband Systems and Technologies, 2003 IEEE Conference on*, nov. 2003, pp. 209 – 213.

[169] J. Timmermann, D. Manteuffel, and W. Wiesbeck, "Simulation of the impact of antennas and indoor channels on uwb transmission by ray tracing and measured antenna patterns," in *Ultra-Wideband, 2007. ICUWB 2007. IEEE International Conference on*, sept. 2007, pp. 194 –197.

[170] F. Yang and Y. Rahmat-Samii, "Reflection phase characterizations of the ebg ground plane for low profile wire antenna applications," *Antennas and Propagation, IEEE Transactions on*, vol. 51, no. 10, pp. 2691 – 2703, oct. 2003.